# Microscopic modeling of the yield curve

Victor Le Coz

▶ **To cite this version:**

Victor Le Coz. Microscopic modeling of the yield curve. Mathematical Physics [math-ph]. Institut Polytechnique de Paris, 2024. English. NNT : 2024IPPAX096 . tel-04952448

**HAL Id: tel-04952448**

**https://theses.hal.science/tel-04952448v1**

Submitted on 17 Feb 2025

**HAL** is a multi-disciplinary open access archive for the deposit and dissemination of scientific research documents, whether they are published or not. The documents may come from teaching and research institutions in France or abroad, or from public or private research centers.

L'archive ouverte pluridisciplinaire **HAL**, est destinée au dépôt et à la diffusion de documents scientifiques de niveau recherche, publiés ou non, émanant des établissements d'enseignement et de recherche français ou étrangers, des laboratoires publics ou privés.

INSTITUT POLYTECHNIQUE DE PARIS

NNT : 2024IPPAX096

Thèse de doctorat

ÉCOLE POLYTECHNIQUE

IP PARIS

# Microscopic modeling of the yield curve

Thèse de doctorat de l'Institut Polytechnique de Paris
préparée à l'École polytechnique

École doctorale n°626 Ecole doctorale de l'Institut Polytechnique de Paris (EDIPP)
Spécialité de doctorat : Sciences économiques

Thèse présentée et soutenue à Palaiseau, le 21 Novembre 2024, par

**VICTOR LE COZ**

Composition du Jury :

| | |
|---|---|
| Charles-Albert Lehalle<br>Ecole polytechnique | Président du jury |
| Aurélien Alfonsi<br>Ecole Nationale des Ponts et Chaussées | Rapporteur |
| Thomas Lux<br>Kiel University | Rapporteur |
| Sandrine Jacob-Leal<br>ICN Business School | Examinatrice |
| Michael Benzaquen<br>CNRS & Ecole polytechnique | Directeur de thèse |
| Damien Challet<br>CentraleSupélec | Co-directeur de thèse |
| Bertrand Hassani<br>Quant AI Lab | Co-encadrant |
| Iacopo Mastromateo<br>Capital Fund Management | Invité |

*À Laure*

## Remerciements

J'aimerais commencer par exprimer ma plus profonde gratitude à mes deux directeurs de thèse, Michael Benzaquen et Damien Challet. En acceptant de diriger ma thèse, ils m'ont permis d'embrasser une nouvelle carrière, dont je n'avais pas soupçonné, à la fin de mes études, qu'elle me conviendrait mieux que tous les autres métiers que j'ai pu exercer. Leur savoir, leur absolue bienveillance, leur inconditionnel soutien, et la grisante liberté avec laquelle ils m'ont laissé conduire mes recherches, ont rendu ces trois années totalement exceptionnelles. Mais cette histoire ne se serait jamais écrite sans la passion pour la recherche et le talent entrepreneurial de Bertrand Hassani, qui a accepté de financer ce projet par l'intermédiaire de l'entreprise qu'il venait de fonder, Quant AI Lab. Cette thèse doit beaucoup à la confiance et à la liberté qui m'ont été accordées par ses équipes, en particulier par Julien Doutrémépuich, dès le tout début de mes recherches.

J'ai aussi eu le privilège de collaborer avec Iacopo Mastromatteo et Jean-Philippe Bouchaud qui ont bouleversé ma manière de penser les mathématiques financières. Leurs intuitions fulgurantes et leurs connaissances encyclopédiques sont à l'origine de beaucoup des résultats présentés ici.

Je remercie aussi les membres de mon jury de doctorat Aurelien Alfonsi, Thomas Lux, Charles-Albert Lehalle, et Sandrine Jacob-Leal. *I am particularly grateful to Aurelien Alfonsi and Thomas Lux for agreeing to assume the roles of referee. I also would like to thank Thibaut de Roquemaurel and Stefano Corradin for participating in my midterm PhD committee and for their advice.*

Parmi les nombreux collègues ou amis rencontrés ces dernières années, beaucoup ont contribué directement ou indirectement à ce projet de recherche. Dans la phase de construction du sujet, William De Vijlder et Jean-Michel Ly m'ont fait prendre conscience respectivement, des limites de la théorie macroéconomique et des modèles de taux. La virtuosité de David Kas dans mise en œuvre d'une version très préliminaire du modèle d'agent m'a permis d'en identifier les limites. L'aide de Nolwenn Allaire dans l'analyse des données des marchés monétaires m'a permis d'élaborer des solutions à ces problèmes. Cette thèse doit aussi beaucoup à l'intime compréhension de la microstructure des marchés de Mehdi Thomas et Natasha Hey, aux conseils de Samy Lakhal dans la construction de champs aléatoires, et à la pédagogie de Ruben Zakine devant mes lacunes en physique. Je remercie aussi Tomas Espana pour sa motivation et son énergie pétillante durant son stage et Matteo Smerlak pour ses brillantes intuitions.

Je souhaiterais ensuite remercier tous les membres de la chaire EconophysiX et du LadHyX qui m'ont accompagné ces trois années. Je remercie également les équipes de CFM qui se sont toujours montrées patientes et bienveillantes dans le partage de leurs données et outils. *Notably, I am grateful to Emmanuel Serie and Stephen Hardiman for their assistance in the use of high-performance computing*

*tools.*

Un grand merci aux relecteurs de ce manuscrit qui m'ont été d'une aide précieuse: Damien, Michael, Swann, et Natasha.

J'ai une pensée pour les chercheurs, écrivains, journalistes et économistes de mon entourage qui m'ont poussé dans cette voie de l'investigation: Jerome, Corentin, Yvane, Clement, Stéphane. Et à Félix, qui hésite encore à prendre cette direction.

Je remercie enfin mes parents, dont je suis redevenu l'enfant lors de mes nombreux séjours prolongés en Bretagne ces dernières années, me permettant ainsi de reprendre des études interrompues trop tôt. La passion épistémologique de ma mère et l'enthousiasme de mon père pour les démonstrations géométriques sont probablement à l'origine de mon goût pour la recherche. Merci aussi à Paul et à Mathilde.

Je dédie ce manuscrit à Laure, qui m'a soutenu, rassuré, et guidé avec espièglerie et sagesse à chaque étape de cette aventure. Merci pour toutes ces années à mes côtés et pour toutes celles qui nous attendent.

# Foreword

In 2018, while working as an internal auditor, I was assigned to review the interest rate derivative pricing models used by a large financial institution. During my interviews with quantitative researchers and traders, I encountered a striking paradox: despite their high dependence on these models, practitioners did not believe in the core assumption of these models, i.e., the existence of a short rate from which agents' expectations produce long-term rates. The traders and researchers of this financial institution considered that the actual path of the short-term rate bore little relation to long-term rates.

Earlier in my career, while designing stress-testing models for the European Central Bank, I encountered another fundamental issue: these models, which were supposed to anticipate major financial crises, did not account for interactions among agents. Instead, they focused solely on modeling the individual balance sheets of banks.

During the COronaVIrus Disease of 2019 (COVID-19) crisis, as I reflected on these issues, I learned about the "EconophysiX" chair, which aimed to tackle such questions through unorthodox approaches. I reached out to Michael Benzaquen to propose a research project addressing these challenges. I had been away from academia for nearly a decade. However, Michael, along with Damien Challet, encouraged me to develop a full-fledged Ph.D. project. After nearly another year of work, the idea of designing an agent-based model of the interest rate curve came to fruition. This model would combine heterogeneous bank interactions that influence the short-term rate with statistical physics tools (initially inspired by spin-glass theory) to describe the propagation of information along the yield curve. My meeting with Bertrand Hassani, who had recently founded a new company, Quant AI Lab, finally made it possible to secure funding for this thesis.

The past three years have been the most exciting and fulfilling of my professional career. Trained in applied mathematics, I discovered the remarkably intuitive approach physicists use in their work. I was particularly fortunate to collaborate with Iacopo Mastromatteo and Jean-Philippe Bouchaud, from whom I learned that even the most abstract mathematical concepts can be approached from an intuitive perspective.

This manuscript is not presented as a typical work in Monetary Economics or Quantitative Finance, despite addressing key questions in these fields, such as monetary transmission mechanisms and yield curve modeling. Instead, I have chosen to adopt the lighter notation of physics and to present results not as formal theorems but as intuitive mechanisms.

## List of publications

Le Coz et al. (2024a) **L. C. V.**, Allaire N., Benzaquen, M., Challet, D. (2024) "Stylized facts in money markets: an empirical analysis of the eurozone data." *Under review*, arXiv:2410.16021

Le Coz et al. (2024b) **L. C. V.**, Benzaquen, M., Challet, D. (2024) "A minimal model of money creation under regulatory constraints." *Under review*, arXiv:2410.18145

Le Coz et al. (2024d) **L. C. V.**, Mastromatteo I., Challet D., Benzaquen M. (2024) "When is cross impact relevant?" *Quantitative Finance* 10.1080/14697688.2024.2302827

Le Coz and Bouchaud (2024) **L. C. V.**, Bouchaud J.-P. (2024) "Revisiting Elastic String Models of Forward Interest Rates." *Quantitative Finance* 10.1080/14697688.2024.2401450

Le Coz et al. (2024c) **L. C. V.**, Mastromatteo I., Benzaquen, M. (2024) "How does liquidity shape the interest rate curve?" *Under review*, arXiv:2409.12282

# Contents

# Part I

# Motivation and background

# Introduction

*There are many open issues regarding the interplay between the yield curve and monetary policy that require further research in my view. [...]. First on the list should be a better understanding of the role of term premiums in macroeconomic models [...]. Second is an improved modelling of long-term trends.*

Philip Lane, speech at the Department of Economics at University College London, 2020

## Motivation

Interest rates serve both as indicators of an economy's state, influenced by central bank policy and the behavior of economic agents, and as major determinants of its evolution, influencing the decisions of these agents. Consequently, interest rates are considered to be one of the key state variables in macroeconomic theory, linking money creation to economic growth.

In any given economy, a variety of interest rates coexist, differentiated by the maturity and credit risk associated with the corresponding loans. This thesis focuses on the collection of risk-free interest rates of different maturities, commonly referred to as the "yield curve", while the study of credit risk falls outside its scope. Some fundamental questions arise: what is the interplay between each of the points of this curve? In particular, what is the relationship between the short-term and long-term ends of the yield curve? These questions are closely related to the broader inquiry in Monetary Economics regarding the transmission of monetary policy to the real economy through the bank lending channel. From this perspective, monetary policy primarily influences the nominal short-term interest rate, which, in turn, affects the rates and volumes of bank lending to firms and households. Since banks use long-term rates to set their lending rates, understanding the mechanisms that determine these long-term rates is essential to understand this transmission channel. One could argue that non-conventional monetary policies now aim to directly set the level of long-term rates through the purchase of safe assets. However, in July 2024, the total asset size of the banking

sector was three times larger than the consolidated balance sheets of all central banks[1], indicating that banks remain the main actors in the money creation process.

To address these questions, we must define the components of the yield curve more precisely, as their price formation mechanisms vary significantly with the maturity. On one hand, the short end of the interest rate curve, particularly the overnight interbank lending market, is largely unobservable. On the other hand, long-term rates, such as those with a 10-year maturity, are determined primarily in the interest rate swap markets, where trading occurs on electronic platforms that allow all participants to submit quotes directly, similar to the operation of stock exchanges. Despite their differences, these markets are strongly interconnected. The ultimate underlying factor in the interest rate swap market is the weighted average of overnight interbank rates, such as the Secured Overnight Financing Rate (Secured Overnight Funding Rate (SOFR)) in the U.S. or the Euro Short-Term Rate (Euro Short-Term Rate (ESTR)) in the Eurozone.

Early models of the yield curve posited that long-term rates are simply the average of market participants' expectations of future overnight interbank rates. However, empirical evidence has shown that long-term rates are typically higher than the predictions of these models. This discrepancy was addressed by adjusting the weighting used to average short-term rates through the introduction of a risk-neutral probability measure. The micro-foundations of this mathematical tool suggest that either agents frequently change preferences or consistently misjudge future inflation, both of which are unconvincing.

Given that the influence of short-term rates on long-term rates appears to be more complex than anticipated, it is worth considering the reverse: how do long-term rates affect the shortest maturities of the interest rate curve? One might argue that, fundamentally, the level of the long-term interest rate swap market influences credit demand, which in turn impacts payment flows within the banking system and ultimately the interbank rate. However, this overnight rate is constrained by the corridor defined by central bank policy rates, specifically, the rate paid on cash reserves and the central bank's last resort borrowing rate. Thus, the feedback from long-term rates to interbank markets is likely limited. Nevertheless, could maturities longer than those directly influenced by the central bank (i.e., those greater than a couple of weeks) be affected by long-term rates?

This thesis aims to develop a micro-founded theory of the yield curve that addresses these questions. We focus on the processes that influence bank loan rates: long-term rate hedging through forward rate agreements and refinancing in the repurchase agreement (repo) market. Given their significant market power in

[1] According to the ECB Data Portal `https://data.ecb.europa.eu/publications/money-credit-and-banking/3031820`

most economies, banks directly set borrowing rates for the majority of firms and households. Thus, studying the benchmark risk-free short- and long-term rates used by these financial institutions is crucial for understanding the mechanisms of monetary policy transmission. We will build models of these markets using agents and statistical physics tools.

## Thesis layout

This thesis is organized into three parts. The first part, "Motivation and Background," sets the stage by reviewing existing literature and describing the microstructure of the markets that compose the yield curve. Chapter 1 presents some essential definitions and explores the economic factors influencing the yield curve, including the roles of central bank policies and other economic agents. It also examines various theoretical models, such as expectation theory, arbitrage-free models, and macroeconomic frameworks. Chapter 2 shifts focus to the microstructure of the markets that compose the yield curve, particularly the interbank, swap, and sovereign bond markets. It describes the actors and microeconomic mechanisms that influence the yield curve.

The second part, "Money Creation in the Repo Market," introduces a microfounded model of money creation that successfully replicates the recently established stylized facts within interbank lending markets. We begin by offering straightforward accounting and regulatory explanations for these empirical facts in chapter 3. Then, in chapter 4, we present a minimal agent-based model that accurately reproduces all these stylized facts.

The final part, "Liquidity Flows on the Interest Rate Curve," explores the intricate relationship between liquidity and the behavior of the interest rate curve. This section begins with a detailed examination of the phenomenology of the yield curve in chapter 5, exploring the stylized facts associated with it. It then transitions into an in-depth analysis of cross-impact modeling in chapter 6, establishing a new stylized fact about the yield curve. Chapter 7 then develops a field theory that accurately reproduces the correlation structure of the yield curve. The final chapter 8 interprets this model as a cross-impact model, reproducing all the stylized facts previously established.

This thesis concludes with a summary of the findings and suggestions for future research directions.

Key results and messages are summarized at the end of each chapter, while detailed calculations are provided in dedicated appendices at the end of the manuscript. A table of notation is included at the end of the chapters6, 7, and 8 and a list of acronyms is presented before the appendices.

# Chapter 1

# Literature review

*There is a certain rate of interest on loans which is neutral in respect to commodity prices, and tends neither to raise nor to lower them.*

Knut Wicksell, 1898

Modeling interest rates is essential in a wide array of research fields, including Monetary Economics, Macroeconomics, Quantitative Finance, and Risk Management. To situate our contribution within the existing literature, this chapter provides an overview of the mechanisms and models that describe the yield curve.

Here, we broadly define the interest rate curve as the market reference rates across various maturities within a given economy. For example, in the euro area, the interest rate curve comprises (i) central bank rates, (ii) short-term interbank and money market rates (notably repo rates ranging from one day to one year), (iii) forward and swap rates for longer maturities (typically from a few months to 30 years) indexed to these instruments, and (iv) sovereign bond yields, provided these bonds do not carry significant credit risk.

After introducing the notation and definitions used throughout the chapter, we examine the factors that influence the level of the yield curve. We then review the insights and limitations of the two primary classes of interest rate models: the arbitrage-free framework and macroeconomic models. The chapter concludes with dedicated sections on agent-based models of the yield curve and the interbank market.

## 1.1 Notations and definitions

We recall here the usual definitions of a zero-coupon bond, a forward rate, and the instantaneous rate, using the typical compounding approaches.

**1.1.0.0.1 Zero-coupon Bond.** Let $P(t,T)$ represent the price at time $t$ of a zero-coupon bond maturing at $T$. This bond pays one unit of currency at maturity $T$ without any intermediate coupon.

**1.1.0.0.2 Forward Rate.** Consider time $t$ and two future times, $S$ and $T$, where $t < S < T$. The forward rate, a risk-free interest rate for the period $[S,T]$, is derived from zero-coupon bonds. By selling a zero-coupon bond maturing at $S$ for $P(t,S)$ euros and purchasing $\frac{P(t,S)}{P(t,T)}$ units of a bond maturing at $T$, we establish a contract that costs nothing at $t$, pays one unit of currency at $S$, and yields $\frac{P(t,S)}{P(t,T)}$ euros at $T$. This setup leads to a deterministic rate of return, with the continuously compounded forward rate $f(t,S,T)$ given by:

$$e^{f(t,S,T)(T-S)} := \frac{P(t,S)}{P(t,T)}, \tag{1.1}$$

solving to:

$$f(t,S,T) := -\frac{\log P(t,T) - \log P(t,S)}{T-S}. \tag{1.2}$$

We also note $y(t,T) = -\frac{ln(P(t,T))}{T-t} = f(t,t,T)$ the continuously compounded yield of the zero-coupon bond.

Furthemore, the simply compounded forward rate $F$ at time $t$, between the times $S$ and $T$, is defined by

$$1 + (T-S)F(t,S,T) = \frac{P(t,S)}{P(t,T)}, \tag{1.3}$$

solving to:

$$F(t,S,T) = \frac{1}{T-S}\left(\frac{P(t,S)}{P(t,T)} - 1\right). \tag{1.4}$$

As discussed in chapter 2, certain forward rates are quoted on organized markets in the form of listed products known as "Futures." These products are available in both the eurozone and the United States of America (U.S.) for a series of equally spaced maturities $T_i$. Using Eq. (1.3), one can readily compute the zero-coupon bond curve implied by the market. Section 2.2.1 provides a more detailed procedure for deriving zero-coupon prices from swap rates, which is more complex.

Following the 2008's Great Financial Crisis ("Great Financial Crisis (GFC)" hereafter), interbank rates for maturities beyond overnight are no longer considered risk-free due to the emergence of counterparty credit risk among banks

(Grbac and Runggaldier, 2015). In other words, Eq. (1.4) can only be used to derive the zero-coupon bond that reflects the risk-free rate when based on forward rate contracts linked to the overnight interbank rate, where counterparty risk remains limited. This paradigm shift is often referred to as the "multicurve hypothesis," as it enables the definition of different zero-coupon bond curves that incorporate varying levels of credit risk, corresponding to different maturities (typically overnight, one month, three months, or six months) of the underlying rate of Futures contracts.

**1.1.0.0.3 Instantaneous Forward Rate.** As $S$ approaches $T$, the limit of $f(t, S, T)$ defines the instantaneous forward rate $f(t, T)$:

$$f(t,T) = -\frac{\partial \log P(t,T)}{\partial T}, \tag{1.5}$$

The collection of these rates for various $T$ forms the Forward Rate Curve (Forward Rate Curve (FRC)). In the following sections, we often define the instantaneous forward rate $f(t, \theta)$ in terms of the time-to-maturity or "tenor" $\theta = T - t$. This dimension $\theta$ is often referred to as the "space" dimension, as opposed to the time dimension $t$.

**1.1.0.0.4 Short rate.** We define the short rate as the value of the instantaneous forward rate at $t$ of maturity $T$ in the case where $t = T$:

$$r(t) = f(t,t) \tag{1.6}$$

The short rate can thus be interpreted as the risk-free rate of interest, contracted at $t$ over the infinitesimal interval $[t, t + \mathrm{d}t]$.

## 1.2 Economic factors influencing the yield curve

In this first section we review the factors influencing the fundamental level of the interest rate curve, particularly the influence of central banks and other economic agents. We also study the effects of the interest rate curve on bank activities.

### 1.2.1 Influence of central banks monetary policy

Within macroeconomic theory, monetary policy exerts its influence on the economy through various channels, most of which depend on the interest rate curve as the primary transmission mechanism. Consequently, central banks have developed a range of instruments specifically designed to shape the yield curve. After outlining the main channels of monetary policy and the instruments employed by

central banks, we will discuss how these tools influence the fundamental level of the yield curve.

#### 1.2.1.1 Channels of monetary policy transmission

The traditional "interest rate channel" posits that monetary policy directly influences real interest rates (defined in section 1.2.2.2), thereby affecting investments and consumer durable expenditures. Beyond this view, monetary policy transmission channels are nowadays categorized into two main groups: (i) those related to changes in credit activity, commonly referred to as the "credit view", and (ii) those related to changes in other asset prices, known as "other asset price effects". As summarized by Mishkin (2013), the following transmission channels are typically identified:

- Within the credit view:
  - the **bank lending channel**, which suggests that monetary policy primarily impacts the nominal short-term interest rate and liquidity in the interbank market, influencing the rates and volumes of bank lending to firms and households;
  - the **balance sheet channel** and **cash flow channel**, which argue that lower real interest rates increase lending by improving firms' net worth and cash flows net of nominal interest rates, thereby reducing credit risk for lenders;
  - the **unanticipated price level channel**, which asserts that monetary policy affects the general price level, leading to decreased labor costs if inflation is unanticipated by households and an increase in firms' real net worth by reducing the real value of nominally fixed liabilities;
  - the **household liquidity effect**, which posits that lower real interest rates increase stock prices, improving household balance sheet liquidity, and that lower nominal rates increase household net cash flows, both of which boost consumer durable expenditures and housing investments.
- Within the other asset price effects:
  - **exchange rate effects on net exports**, which occur as monetary easing leads to currency depreciation, thereby boosting net exports and aggregate demand;
  - **Tobin's q theory** (Tobin, 1969; Hayashi, 1982), which posits that monetary policy influences stock prices, thereby affecting investment decisions as asset valuations become more sensitive to capital costs when nominal rates decline;

– **wealth effects**, which suggest that higher stock prices increase consumers' lifetime resources, following the "life-cycle hypothesis of saving" (Modigliani and Brumberg, 1955; 1980) or the "permanent income hypothesis" (Friedman, 1957), leading to higher consumption of non-durable goods and services.

It is important to note that the global decline in traditional bank lending, as highlighted by Mishkin (2013), has reduced the prominence of the bank lending channel relative to other channels. Since the 1960s, particularly in the U.S., the process of "disintermediation" has redirected deposits from savers directly to borrowers, bypassing banks. However, the importance of the bank lending channel was revisited following the GFC, as the weakness of the banking sector significantly impacted economic output.

The GFC also spurred the development of unconventional monetary policy instruments in advanced economies, which are discussed in the following section.

#### 1.2.1.2 Monetary policy instruments

Currently, monetary policy in advanced economies relies on three primary instruments, each playing a key role in shaping the interest rate curve:

- setting the short-term nominal rate for commercial bank funding and the remuneration of reserves (see chapter 2);
- Asset Purchase Programs (APP) aimed at lowering long-term interest rates by acquiring high-quality (investment-grade) sovereign and corporate bonds (or even equities in Japan) in secondary markets;
- forward guidance communication to influence market expectations regarding the future path of central bank policy.

Although short-term nominal rates primarily influence the shortest maturities of the interest rate curve, asset purchase programs have a more pronounced effect on long-term rates. The following sections review the literature on the influence of short-term monetary policy rates and other monetary policy instruments on the interest rate curve.

#### 1.2.1.3 Effects of short term monetary policy rate

Within advanced economies, the central bank's short-term monetary policy rate is closely linked to the shortest point on the interest rate curve: the overnight interbank rate. For such short maturities, banks have the option to borrow either on the interbank market or directly from the central bank, which prevents the

interbank rate from deviating significantly from the central bank rate. Several modeling attempts have been made to capture the dynamics of this overnight rate, many of which utilize network theory to replicate its key stylized facts (see section 1.7). The longer maturities of the interest rate curve, however, are primarily determined in the derivatives, swap, and Futures markets or in the bond market (see chapter 2). Consequently, the transmission of central bank rates to long-term rates is not always straightforward or guaranteed.

Numerous studies have documented substantial effects of central bank rates on long-term rates (Culbertson, 1957; Sargent, 1972; 1979; Shiller, 1979; Singleton, 1980; Shiller, 1981; Shiller et al., 1983; Rudebusch, 1995; Fuhrer, 1996; Ayuso et al., 1997; Cochrane and Piazzesi, 2002; Gürkaynak et al., 2005; Hanson and Stein, 2015; Brooks et al., 2018; Hanson et al., 2021). Yet, these effects are often stronger than those predicted by standard theories linking short-term and long-term rates. Notably, the Dynamic Stochastic General Equilibrium (hereafter referred to as Dynamic Stochastic General Equilibrium (DSGE)) framework, a mainstay in macroeconomic modeling (see section 1.4), predicts lower sensitivities of long-term rates to short-term rates than are empirically observed (see section 1.4). The expectation and arbitrage-free theories, which share the same foundational assumptions, also exhibit inconsistencies in this regard (see section 1.3).

Among these models, Piazzesi (2005) proposed an extended affine term structure model (see section 1.3.2.1) that explicitly incorporates the reaction of the interest rate curve to monetary policy shocks. In this model, long-term and short-term rates are interrelated, with long-term yields expressed as functions of (i) the U.S. Federal funds rate (i.e., the central bank refinancing rate), (ii) the spread between the short-term rate and the Federal funds rate, and (iii) other macroeconomic factors. Furthermore, the U.S. Federal funds rate is modeled as a pure jump process with intensities dependent on macroeconomic conditions. The calibrated sensitivity of these jumps to macroeconomic factors is significant and positive. Since the characteristic half-life of these factors typically exceeds one year, they induce positive autocorrelation in the Federal funds rate, reproducing the observed central bank policy better than the Taylor rule (Taylor, 1993). In addition, this model successfully explains the strong response of long-term yields to monetary policy shocks, as macroeconomic shocks to the central bank dissipate slowly under the risk-neutral measure. It also effectively models the humped shape of the yield curve volatility (see chapter 5).

Similarly, Renne (2017) applied the arbitrage-free theory to develop a model of the interest swap market that incorporates discrete changes in central bank policy rates and a spread to the short-term rate. The study demonstrates that the shape of the yield curve is closely related to the monetary policy phase, be it easing, status quo, or tightening.

We will see, however, that this type of models, developed within the arbitrage-

free framework are generally misspecified (see section 1.3.2.1).

#### 1.2.1.4 Effects of other monetary policy instruments

Gagnon et al. (2011), Krishnamurthy and Vissing-Jorgensen (2011), and Li and Wei (2013) demonstrate the significant effects of the Federal Reserve's Large-Scale APPS on yields. In chapter 7 we show that APPs in the U.S. strongly modifies the parameters of an elastic string model. During such an event, the line tension parameter, defining the strength of the relationship between different maturities of the FRC becomes significantly lower. We also model in chapter 4 the effect of an APP on the interbank market network structure. Furthermore, in chapter 4 we show that an APP reduces the volumes of transactions on the interbank secured markets and increases excess liquidity.

### 1.2.2 Influence of the other economic agents

#### 1.2.2.1 In the short run: supply and demand for credit

In the short term, the factors that influence the yield curve are primarily related to transaction flows. For short-term interest rates, these flows are mainly payments among economic agents that generate liquidity shocks in the banking system, as described in the model by Poole (1968) (see section 1.7 for a detailed review of interbank market models). The rest of the yield curve is shaped by credit demand for loans and bonds, and the activity in derivative markets serving as hedging instruments for these contracts (see chapter 2 for an overview of banks' risk management practices).

Empirical studies have shown that fluctuations in bond supply and demand can significantly influence changes in the sovereign bond yield curve beyond what is explained by traditional macroeconomic variables such as expected short-term interest rates and inflation (see the following section). For example, Greenwood and Vayanos (2014), Krishnamurthy and Vissing-Jorgensen (2012), and Hamilton and Wu (2012) empirically observe a strong relationship between the supply of U.S. sovereign bonds by maturity and their yields. Furthermore, Hu et al. (2013) identify a noise component in Treasury yields linked to arbitrage activities among Treasury securities. These findings have led some researchers to explore "preferred habitat" models (see section 1.6), which emphasize how the term structure is influenced by the interaction between investors with specific maturity preferences.

Moreover, some studies suggest that price formation in sovereign bond markets occurs primarily in the Futures market rather than in the cash market (Pelizzon et al., 2014). In particular, these studies highlight that limits to arbitrage are substantial even in the most liquid European markets, as the basis between the cash and Futures markets can deviate from its equilibrium level for several consecutive

days. These results align with the findings presented in chapter 6 where we show that price formation occurs among the most liquid assets of the Futures market.

#### 1.2.2.2 In the long run: factors influencing the natural rate

Noticing that banks create purchasing power (see chapter 2), Wicksell (1898) introduced the concept of the natural rate, $r_e^*$, as the real rate (further defined below) that equates the bank loan rate with the capital rate (i.e., the rate that balances the supply and demand for real capital goods). Ramsey (1928) provided a structural micro-foundation for the natural rate, which was later expanded by Cass (1965) and Koopmans (1963). This approach endogenously defines optimal consumption and savings over time, in contrast to the Solow (1956) and Swan (1956) growth models, which consider savings decisions as exogenous. In the Ramsey-Cass-Koopmans model, the optimal savings condition yields a balanced growth relationship between the real interest rate, $r_e^*$, agents' preferences, and population growth:

$$r_e^* = \frac{1}{\sigma(c)}\mu_c + \mu_N + \delta, \tag{1.7}$$

where $\mu_c$ is the growth rate of consumption per capita (influenced by technological change), $\mu_N$ is the rate of population growth, $\delta$ is the rate of time preference (the discount rate for future utility), and $\sigma(c)$ is the elasticity of intertemporal substitution in the utility function of consumption $U(c)$, defined as:

$$\sigma(c) := -\frac{\mathrm{d}\ln c}{\mathrm{d}\ln U'(c)}. \tag{1.8}$$

In Eq (1.7), the real interest rate $r_e$ can be related, in the long-run equilibrium, to the nominal interest rate $r$ —the focus of this thesis— via the Fisher equation (Fisher, 1907):

$$r(t) = r_e(t) + \pi(t), \tag{1.9}$$

where $\pi(t)$ is the inflation rate. In the traditional view, the real rate converges to the natural rate (defined by agents' preferences), while the money supply governs inflation, making the nominal rate a function of these two equilibria. However, the "Neo-Fisherism" perspective posits that the central bank controls the nominal rate causing the inflation rate to adjust to the difference between the nominal and natural rates.

Wicksell's concept was integrated into modern macroeconomic theory by Woodford (2003), who defined $r_e^*$ as the real rate necessary to maintain aggregate demand equal to output in a hypothetical economy with full price flexibility, consistent with the DSGE framework (see section 1.4). Following this approach, several

authors have modeled the natural rate as the real interest rate that would prevail if all prices were flexible in a DSGE framework (Neiss and Nelson, 2001; Andrés et al., 2009; Cúrdia et al., 2015).

An alternative approach to defining and measuring the natural rate of interest was proposed by Laubach and Williams (2003). They conceptualized the natural rate as the real short-term interest rate that closes the output gap, where the potential output is the level that ensures stable inflation (Bomfim, 1997). In this framework, the natural rate corresponds to the intercept of the Taylor rule (Taylor, 1993), which links the inflation gap and the output gap to the nominal rate. Using this methodology, studies by Mésonnier and Renne (2007), Laubach and Williams (2016), and Holston et al. (2017) have shown that the estimated natural rate of interest has declined sharply in western economies since the GFC.

All these models share a significant limitation: they assume that the representative agent lives indefinitely. To address this, another class of models, known as Overlapping Generations (OLG) models, was introduced by Samuelson (1958), Diamond (1965), and Blanchard (1985). These models explicitly account for the life-cycle behavior of agents who are born, age, and eventually die. As noted in Brand et al. (2018), demographic changes in OLG models influence the equilibrium rate, $r_e^*$. The OLG literature identifies three main channels through which demographic transitions affect $r_e^*$:

1. **Reduced labor input**: a shrinking labor force increases capital per worker, which lowers the marginal product of capital and $r_e^*$, similar to a sustained drop in productivity growth.

2. **Increased life expectancy**: longer life expectancies drive people to save more for retirement, decreasing $r_e^*$.

3. **Growing proportion of dissavers**: as the population ages, a larger share of individuals spend more than they save, reducing capital supply and putting upward pressure on $r_e^*$.

Overall, most studies find that aging tends to lower $r_e^*$, with the impact of increased life expectancy generally outweighing the effect of increased dissaving by the elderly. For example, using the approach pioneered by Auerbach and Kotlikoff (1987), Bielecki et al. (2018) developed an OLG model to quantify the effects of demographic changes on the natural rate of interest, attributing much of the secular decline in the natural rate since the 1980s to aging.

In this thesis, we adopt the view of some authors (Black, 1986; Summers, 1986; Poterba and Summers, 1988; Bouchaud and Potters, 2003; Bouchaud et al., 2017) that the prices formed within financial markets can diverge from their fundamentals for very long periods (see also section 1.5 regarding the tests of the

efficient market hypothesis). Hence, we focus our study of the yield curve on the supply and demand market mechanisms leading to the formation of prices.

### 1.2.3 Influence of the rate environment on bank lending activity

Since the seminal work of Bernanke and Blinder (1988), which suggested that monetary policy impulses influence loan supply by affecting banks' access to liquidity, understanding the role of banks as loan suppliers has become a central focus in the literature on monetary policy transmission. The yield curve affects banks through three primary mechanisms: short-term liquidity funding, setting of lending rates, and long-term changes in bank activities.

Banks with weaker balance sheets are less able to shield their lending activities from monetary shocks, as they face greater difficulties in accessing funding. For instance, Kashyap and Stein (1994) linked banks' responses to monetary policy to their size, while Kishan and Opiela (2000) identified capitalization as a significant factor in the lending channel. Altunbas et al. (2010) extended this analysis by highlighting the impact of banks' credit risk from the perspective of investors. More recently, with regard to the euro area, Cantero-Saiz et al. (2014), 2021 emphasized the role of sovereign risk in bank lending. These findings underscore the importance of modeling individual banks' balance sheets to fully understand the dynamics of the yield curve, as explored in chapter 4.

The effect of the interest rate curve on banks' lending rates is notably influenced by the price elasticity of credit demand and sight deposit supply. When these elasticities are low, banks may maintain high loan rates and reduce deposit rates to preserve their margins in a low-interest-rate environment. Borio (1995) explains that the response of lending rates to changes in market rates, which can take from one month to several years, depends on (i) the degree of banks' monopoly power, (ii) customer aversion to variable interest rates, and (iii) the volatility of market and policy rates. Gambacorta and Iannotti (2007) observed banks update their lending rates slower when market rates decrease than when they increase. In this thesis, we focus on modeling the market rates defined in bond and derivative markets. Although these rates directly influence banks' lending rates (see chapter 2), we do not consider the variability of bank interest rate margins, which would be required to model actual lending rates to the real economy.

Additionally, the prolonged low-interest-rate environment has impacted banks' intermediation activities in the European Union (E.U.) and the U.S. Brei et al. (2020) observed that low-interest rates lead banks to (i) shift their activities from interest-generating to fee-related services (see Baumol (1959) for the first models of "sales maximization"), (ii) adjust their funding structure away from short-term market funding toward deposits, and (iii) reduce their solvency ratios. Moreover, when funding costs are low and liquidity is abundant, banks have less incentive

to pursue liquidity and funding through securitization (Pescatori et al., 2016). Low rates may also encourage increased risk-taking in new loans, as argued by Maddaloni and Peydro (2011), Borio and Zhu (2012), and Jiménez et al. (2014).

We have seen in this section that central banks, investors, and households exert a significant influence on the yield curve, although on different time scales. We have also described the feedback effect of yield levels on banking activities. In the next section, we introduce the most commonly used modeling framework for the yield curve, which assumes the existence of a single representative agent. These approaches primarily focus on the notion that long-term rates reflect expectations of future short-term rates.

## 1.3 From the expectation theory to arbitrage free models

### 1.3.1 Expectation theory

The evolution of the relationship between short-term and long-term interest rates has been shaped by various economic theories and empirical observations. Fisher (1930) laid the foundation for the term structure expectation theory, linking short- and long-term rates under conditions of perfect foresight. However, Fisher also highlighted the influence of institutional factors, noting that real-world complexities often render precise theoretical formulations inapplicable. Riefler (1930) reinforced Fisher's findings, revealing a general alignment in the direction and timing of movements between short-term and long-term yields using data from the 1920s. Keynes (1930) initially endorsed this view using British data to argue that changes in short-term rates, driven by central bank actions, effectively influenced long-term rates, making monetary policy effective through this channel. However, Keynes (1936) revised this position in response to the stubbornly high long-term rates of the 1930s. He proposed that long-term interest rates were more a product of conventional beliefs and psychological factors, emphasizing the role of expectations about future rates.

Based on these macroeconomic perspectives, the expectation theory of the term structure, developed by Lutz (1940) and Hicks (1946), assumes market efficiency and rational agents to derive long-term interest rates as the average of expected future short-term rates $(r(s))_{s\geq 0}$ plus a liquidity term premium $\Phi(T-t)$. This liquidity premium accounts for the ease of buying or selling a bond with time-to-maturity $T-t$, but not for interest rate risk (i.e., the risk of short-term rate fluctuations). Formally, in this framework, the continuously compounded yield to maturity $y(t,T) = -\frac{\ln P(t,T)}{T-t}$ associated with the price of a zero-coupon bond

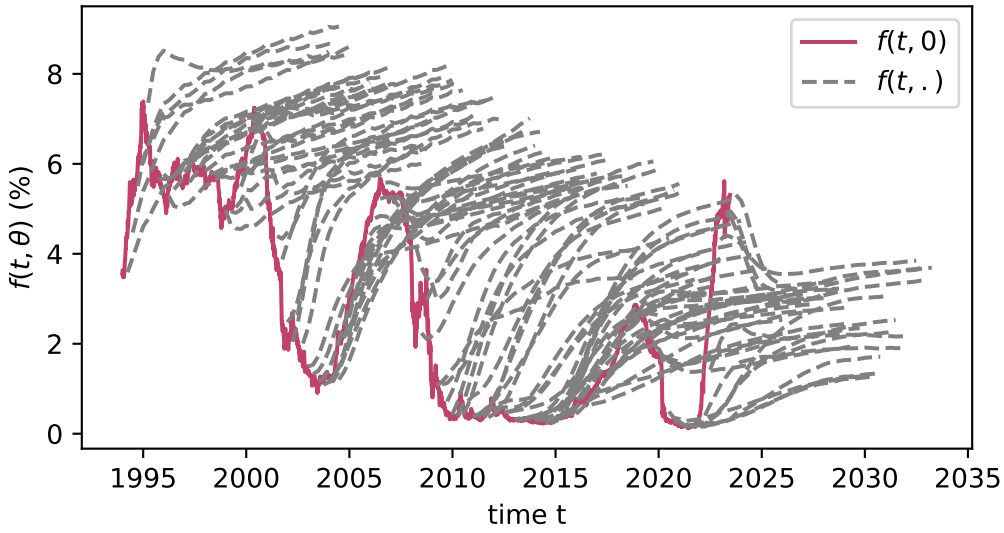


**Figure 1.1:** Historical time series of the mid-price at time $t$, $f(t, t+\theta)$, of a 3-month SOFR Futures contract maturing at $t+\theta$. The SOFR Futures dataset comprises daily historical variations from 1994 to 2023, covering maturities from 3 months to 117 months.

$P(t,T)$ maturing at $T$ is given by:

$$y(t,T) = \frac{1}{T-t}\mathbb{E}_t^{\mathbb{P}}\left[\int_t^T r(s)\mathrm{d}s\right] + \Phi(T-t), \tag{1.10}$$

where $\mathbb{E}_t^{\mathbb{P}}[.]$ denotes the mathematical expectation, conditional to the information available at $t$, under the historical probability $\mathbb{P}$. The limitations of this theory become evident when the short-term rate process $(r(s))_{s\geq 0}$ is an Itô process with no drift, $\mathrm{d}r(s) = \sigma(s)\mathrm{d}W(s)$, where $W(s)$ is a Brownian motion. In this case, the yield curve without a liquidity premium would have a zero slope:

$$y(t,T) = \frac{1}{T-t}\mathbb{E}_t^{\mathbb{P}}\left[\int_t^T r(t) + \left(\int_t^s \sigma(u,\omega)\mathrm{d}W(u)\right)\mathrm{d}s\right] = r(t). \tag{1.11}$$

A further issue, first identified by Shiller et al. (1983), is that even when the short rate exhibits a trend, this theory is inconsistent with empirical data. For instance, Fig. 1.1 shows that the rate $f(t, t+\theta)$ of Secured Overnight Funding Rate (SOFR) Futures for 3-month contracts do not consistently predict the path of the spot rates $f(t, 0)$. Notably, apart from the period from 2021 to 2023, the forward rate tends to be systematically higher than the actual short-term rate path.

Furthermore, evidence from Culbertson (1957), Sargent (1972), 1979, Shiller (1979), Singleton (1980), Shiller (1981), Shiller et al. (1983), Cochrane and Piazzesi (2002), Gürkaynak et al. (2005), Hanson and Stein (2015), Brooks et al. (2018), and Hanson et al. (2021) shows that the volatility and sensitivity of long-term rates to short-term rate exceed predictions from the expectation theory (see also section 1.4.1).

To better align with empirical data, the expectation theory was modified by introducing an alternative weighting scheme for averaging future short-term rates. Mathematically, this is achieved by defining a so-called "risk-neutral" probability measure (see section 1.3.2), ensuring that Eq. (1.10) remains valid when using an expectation operator defined under this new measure.

### 1.3.2 Arbitrage-free models of the interest rate curve

A large body of literature on derivative pricing has emerged since the 1970s, following the work of Black and Scholes (1973), who proposed a closed-form formula for the pricing of European options under the arbitrage-free assumption (or equivalently, the efficient market hypothesis). This theory posits that, after adjusting for volatility, each financial asset has the same return, commonly referred to as the "Sharpe ratio" (Sharpe, 1964). The Sharpe ratio enables the definition of a new probability measure, the "risk-neutral" measure, under which the return on all risky assets equals the risk-free rate.

In the context of interest rate products, the arbitrage approach models the stochastic evolution of one or more interest rates and subsequently derives the prices of all contingent claims by ensuring that no arbitrage opportunities exist within the economy. A refinement of this approach involves either modeling the initial yield curve and its subsequent movements, as proposed by Ho and Lee (1986), or examining shifts in forward rates, as in the framework developed by Heath et al. (1992) (further detailed below), both while maintaining arbitrage-free conditions.

In its most common form, the continuous-time arbitrage theory considers an infinite set of derivatives, specifically zero-coupon bonds of various maturities, all anchored by a single underlying non-risky asset, typically the risk-free asset (Brennan and Schwartz, 1977; Vasicek, 1977; Björk, 1998). This risk-free asset can be conceptualized as the shortest maturity rate, usually set by the central bank. As Björk (1998) explains, this market is inherently incomplete, involving one or more diffusion factors for risk-free assets while there is no risky asset. However, the absence of arbitrage establishes a relationship among zero-coupon bonds, allowing the determination of bond prices across all maturities. Within this framework, the market price of risk, which facilitates the transition from historical to risk-neutral probability, is determined by market participants based on their preferences, as

observed in market prices (see section 1.3.2.3).

An important feature of this framework is that, under the risk-neutral measure, differences in the values of zero-coupon bonds with different maturities are solely explained by changes in the expected future risk-free rate, meaning there is no risk premium for duration risk. In contrast, under the historical probability measure, each zero-coupon bond is driven by its own drift and volatility, with the constraint that all market prices of risk are equal, allowing for the derivation of a non-zero term premium (see section 1.3.2.2).

Formally, if $P(t,T)$ and $P(t,S)$ denote the prices at time $t$ of two zero-coupon bonds maturing at $T$ and $S$, respectively, and $W^{\mathbb{P}}$ represents the Brownian motion driving the diffusion of the instantaneous risk-free rate $r(t)$, then the dynamics under the historical probability $\mathbb{P}$ of these bonds are given by:

$$\frac{\mathrm{d}P(t,T)}{P(t,T)} = \alpha_T(t)\mathrm{d}t + \sigma_T(t)\mathrm{d}W^{\mathbb{P}}(t), \tag{1.12}$$

$$\frac{\mathrm{d}P(t,S)}{P(t,S)} = \alpha_S(t)\mathrm{d}t + \sigma_S(t)\mathrm{d}W^{\mathbb{P}}(t), \tag{1.13}$$

where $\alpha_T(t)$, $\sigma_T(t)$ and $\alpha_S(t)$, $\sigma_S(t)$ are time-dependent (and possibly stochastic) parameters representing the drift and volatility of the zero-coupon bonds maturing at $T$ and $S$, respectively. Under the risk-neutral probability $\mathbb{Q}$, the dynamics of these bonds are given by:

$$\frac{\mathrm{d}P(t,T)}{P(t,T)} = r(t)\mathrm{d}t + \sigma_T(t)\mathrm{d}W^{\mathbb{Q}}(t), \tag{1.14}$$

$$\frac{\mathrm{d}P(t,S)}{P(t,S)} = r(t)\mathrm{d}t + \sigma_S(t)\mathrm{d}W^{\mathbb{Q}}(t), \tag{1.15}$$

where $W^{\mathbb{Q}}$ is the Brownian motion driving the diffusion of the instantaneous short rate $r(t)$ under the risk-neutral probability $\mathbb{Q}$, defined by its Radon-Nikodym derivative with respect to $\mathbb{P}$:

$$\left.\frac{\mathrm{d}\mathbb{Q}}{\mathrm{d}\mathbb{P}}\right|_t = \exp\left(\int_0^t \frac{r(s)-\alpha_T(s)}{\sigma_T(s)}\mathrm{d}W^{\mathbb{P}}(s) - \int_0^t \frac{1}{2}\left(\frac{r(s)-\alpha_T(s)}{\sigma_T(s)}\right)^2 \mathrm{d}s\right). \tag{1.16}$$

The absence of arbitrage in the term structure of zero-coupon bonds ensures the existence of a stochastic process $(\lambda(s))_{s\geq 0}$ such that (Björk, 1998):

$$\forall(s,T,S),\ \frac{r(s)-\alpha_T(s)}{\sigma_T(s)} = \frac{r(s)-\alpha_S(s)}{\sigma_S(s)} = -\lambda(s). \tag{1.17}$$

This process $(\lambda(s))_{s\geq 0}$ is known as the "market price of risk," representing the compensation for bearing interest rate risk when purchasing a zero-coupon bond.

Assuming the zero-coupon bond price $P(t,T)$ is a sufficiently smooth function of the instantaneous short rate $r(t)$, we can apply Itô's lemma to derive the stochastic differential equation satisfied by the zero-coupon bond price:

$$\mathrm{d}P(t,T) = \left(\frac{\partial P}{\partial t}(t,T) + \mu_r(t)\frac{\partial P}{\partial r}(t,T) + \frac{1}{2}\sigma_r^2(t)\frac{\partial^2 P}{\partial r^2}(t,T)\right)\mathrm{d}t + \sigma_r(t)\frac{\partial P}{\partial r}(t,T)\mathrm{d}W^{\mathbb{P}}(t), \tag{1.18}$$

where $\mu_r(t)$ and $\sigma_r(t)$ are, respectively, the drift and volatility functions in the diffusion equation of $r(t)$ under the historical probability. Identifying the drift and volatility terms in Eqs. (1.12) and (1.18) yields the stochastic differential equation governing the price of the zero-coupon bond, known as the "term structure equation" (Björk, 1998):

$$\begin{cases} \frac{\partial P}{\partial t}(t,T) + (\mu_r(t) - \lambda_t\sigma_r(t))\frac{\partial P}{\partial r}(t,T) + \frac{1}{2}\sigma_r^2(t)\frac{\partial^2 P}{\partial r^2}(t,T) - r(t)P(t,T) = 0, \\ P(T,T) = 1, \end{cases} \tag{1.19}$$

This equation is equivalent, by the Feynman-Kac theorem, to the pricing formula for the zero-coupon bond within the arbitrage-free theory:

$$\begin{cases} P(t,T) = \mathbb{E}_t^{\mathbb{Q}}\left[\exp\left(-\int_t^T r(s)\mathrm{d}s\right)\right], \\ \mathrm{d}r(t) = (\mu_r(t) - \lambda(t)\sigma_r(t))\mathrm{d}t + \sigma_r(t)\mathrm{d}W^{\mathbb{Q}}(t). \end{cases} \tag{1.20}$$

A similar formula can be derived in the more general case where the diffusion of the risk-free rate is driven by a $d$-dimensional Brownian motion. In this scenario, the valuation of zero-coupon bonds enables the pricing of all derivative instruments, including Futures contracts (see section 1.1). However, a significant limitation of this framework is that it requires the correlation matrix of any $k+d$ forward rates to be singular when the model is driven by $d$ factors (Goldstein, 2000). This stipulation conflicts with empirical observations (see chapter 5). Consequently, models defined within this framework are often misspecified, as will be discussed in the next section.

Under the assumption of a deterministic instantaneous risk-free rate $r(t)$, the price of a zero-coupon bond simplifies to $P(t,T) = \exp\left(-\int_t^T r(s)\mathrm{d}s\right)$, so the dynamic equation for the bond price becomes:

$$\mathrm{d}P(t,T) = -r(t)P(t,T)\mathrm{d}t, \tag{1.21}$$

under the historical probability measure. In this scenario, the market price of risk is zero, and the probability measures $\mathbb{P}$ and $\mathbb{Q}$ coincide. This corresponds to the expectation hypothesis framework, which is known to be incompatible with

empirical data (see section 1.3.1). In contrast, as we will demonstrate in the following section, the arbitrage-free theory of the interest rate curve can generate non-zero term premiums.

#### 1.3.2.1 Affine term structure models

One of the most commonly used classes of arbitrage-free models of the term structure are the so-called "affine term structure models". These models assume the following form for the price of a zero-coupon bond:

$$P(t,T) = \exp\left(A(t,T) - B(t,T)r(t)\right), \tag{1.22}$$

where $A(t,T)$ and $B(t,T)$ are two deterministic time-dependent functions such that $A(T,T) = B(T,T) = 0$. In this framework, it is generally further assumed that the risk-free rate is driven by $d$ diffusion factors, modeled through a Markovian and time-homogeneous hidden state variable $x(t)$ (Piazzesi, 2010):

$$\begin{cases} r(t) = \delta_0 + \delta_1^\top x(t), \\ \mathrm{d}x(t) = k(\bar{x} - x(t))\mathrm{d}t + \Sigma x(t)\mathrm{d}W^{\mathbb{Q},d}(t), \end{cases} \tag{1.23}$$

where $\delta_0$ and $k$ are calibration parameters, $\delta_1$ and $\bar{x}$ are parameter vectors, $\Sigma$ is a diagonal matrix of parameters, and $W^{\mathbb{Q},d}(t)$ is a brownian motion of dimension $d$.

Although arbitrage-free models in the financial industry are typically calibrated using current market prices from derivatives, these models can also be estimated using more common inference techniques on historical data. In particular, affine term structure models can be calibrated using maximum likelihood approaches on historical time series. The maximum likelihood method aims to maximize the probability of a given set of parameters $\Theta$ based on $n$ observed realizations $\tilde{x}(t_{i\in[\![1,n]\!]})$ of the state variable process $(x(t))_{t\geq 0}$. This is equivalent, by Bayes' theorem, to maximizing the following loss function over the set of parameters $\mathbf{p}$:

$$L(\theta) = \mathbb{P}\left[x(t_1) = \tilde{x}(t_1), \ldots, x(t_n) = \tilde{x}(t_n)|\mathbf{p}\right]\mathbb{P}\left[\mathbf{p}\right]. \tag{1.24}$$

Thanks to the Markovianity and time-homogeneity of the state variable process $(x(t))_{t\geq 0}$, it is possible to reformulate the joint probability of the state vector path as:

$$\begin{aligned} &\mathbb{P}\left[x(t_1) = \tilde{x}(t_1), \ldots, x(t_n) = \tilde{x}(t_n)\right] \\ &\qquad = \prod_{i=2}^{n} \mathbb{P}\left[x(t_i) = \tilde{x}(t_i)|x(t_{i-1}) = \tilde{x}(t_{i-1})\right]\mathbb{P}\left[x(t_1) = \tilde{x}(t_1)\right], \\ &\qquad = \prod_{i=2}^{n} f_x(\tilde{x}(t_i)|\tilde{x}(t_{i-1}))f_x(\tilde{x}(t_1)), \end{aligned}$$

where $f_x(\tilde{x}(t_i)|\tilde{x}(t_{i-1}))$ is the transition density of the state variable $x$. Finally, the joint probability density of the observed historical yield time series $f_y(\tilde{y}(t+1)|\tilde{y}(t))$ can be expressed as a function of the density of the state vector $f_x(\tilde{x}(t+1)|\tilde{x}(t))$ via a change of variables:

$$f_y(\tilde{y}(t)|\tilde{y}(t-1)) = f_x(\tilde{x}(t)|\tilde{x}(t-1)) \left| \frac{\mathrm{d}x(t)}{\mathrm{d}y(t)} \right|, \tag{1.25}$$

where $\left| \frac{\mathrm{d}x(t)}{\mathrm{d}y(t)} \right|$ is the determinant of the Jacobian matrix of the function relating the state vector to the observed yield, as defined by the model.

Therefore, the estimation of the model parameters in Eq. (1.23) can be conducted using the time series of zero-coupon yields $y(t,T)$ (for e.g., implied from swap rates, see section 2.2.1). However, this class of models typically generates a so-called "stochastic singularity" (Piazzesi, 2010): since the number of maturities $T$ is infinite, but there are only $d$ diffusion factors, the model can be rejected if the historical observations include $d+1$ yields of different maturities. This issue can be overcome by assuming that the yields of different maturities are observed with some measurement errors, so the calibrated model becomes:

$$\begin{cases} y(t,\theta) = A'(\theta) + B'(\theta)^\top x(t) + \epsilon(t,\theta), \\ \mathrm{d}x(t) = k^*(\bar{x}^* - x(t))\mathrm{d}t + \Sigma x(t)\mathrm{d}W^{\mathbb{Q},d}(t), \end{cases} \tag{1.26}$$

where $\theta = T - t$ is the time-to-maturity, $A'(\theta)$ and $B'(\theta)$ are functions defined by the parameters of the model, and $\epsilon(t,\theta)$ represents residuals accounting for measurement errors, assumed to be independent across time.

However, as explained by Duffie and Singleton (1997), Dai and Singleton (2000), Piazzesi (2005), and Hamilton and Wu (2014), the measurement errors $\epsilon(t,\theta)$ generated by affine term structure models are typically highly auto-correlated (up to 90% at one day). While Duffie and Singleton (1997) address this issue by assuming that errors follow AR(1) processes, Hamilton and Wu (2014) suggest that these errors actually include additional explanatory factors such as liquidity premiums. Nonetheless, as Piazzesi (2010) notes: "*Auto-correlation in measurement errors is worrisome because it suggests that these errors might have in fact nothing to do with measurement issues but with omitted state variables or functional form assumptions. [...] Much more research is needed in this direction.*"

#### 1.3.2.2 Term premiums within the arbitrage free framework

As mentioned above, arbitrage-free models generate term premiums under the historical probability, even when the risk-free rate has no drift. Notably, the U.S. Federal Reserve employs a three-factor affine term structure model to derive the term premiums implied by the market prices of U.S. sovereign bonds (Kim and

Wright, 2005). They define the term premium $\phi(T)$ as the difference between the current risk-neutral yield of the zero-coupon bond, $y(0,T)$, and the average expected value of the risk-free rate under the historical probability (i.e., the definition of $y(0,T)$ within the expectation theory[2], see section 1.3.1):

$$\phi(T) = -\frac{\ln P(0,T)}{T} - \frac{1}{T}\int_0^T \mathbb{E}^{\mathbb{P}}\left[r(t)\right] \mathrm{d}t. \tag{1.27}$$

This model allows the authors to disentangle the effects of changes in long-term rates related to the market price of risk (i.e., agents' preferences, see next section) from changes in agents' expectations regarding the future path of the short-term rate $r(t)$.

The model is calibrated using a maximum likelihood approach (see section 1.3.2.1) on historical observations of the zero-coupon yields derived from U.S. sovereign bonds. However, as shown by Kim and Orphanides (2012), in a term structure sample spanning 5 to 15 years, an insufficient number of mean reversions may be observed to accurately estimate the drift (i.e., the market price of risk) of the hidden state variable $r(t)$. Therefore, Kim and Wright (2005) also incorporate survey forecasts of the future short-term rate to infer the expected path of $r(t)$. In the following years, this model was extended to four diffusion factors by Cochrane and Piazzesi (2009), obtaining similar results. Finally, in the affine term structure approach proposed by Renne (2017), time-varying term premiums are derived by expressing bond prices as functions of central bank rates and their associated spreads to the short term (see section 1.2.1.3).

#### 1.3.2.3 Micro-foundations of arbitrage free yield curve models

Equilibrium models, developed, among others, by Cox et al. (1981), 1985a, b, Longstaff and Schwartz (1992), Duffie (2001), Kim and Wright (2005), and Piazzesi (2010) generally assume the stochastic evolution of one or more exogenous state variables and the existence of a representative investor. Unlike the arbitrage approach, these models derive the term structure of interest rates directly from the equilibrium conditions within the economy, taking into account both the supply and demand for bonds. Ultimately, these models arrive at a diffusion equation for the price of zero-coupon bonds that is consistent with the arbitrage-free framework. The key advantage of the equilibrium approach over the arbitrage approach is its endogenous determination of the functional forms of term premiums (i.e., the market prices of risk).

[2]The actual expression for the second term in Eq. (1.27) should be $-\frac{1}{T}\ln\left(\mathbb{E}_t^{\mathbb{P}}\left[\exp\left(-\int_0^T r(s)\mathrm{d}s\right)\right]\right)$, which is lower than $-\frac{1}{T}\mathbb{E}_t^{\mathbb{P}}\left[\int_0^T r(s)\mathrm{d}s\right]$ by Jensen's inequality. Thus, these term premiums include the effect of the convexity of the relationship between bond prices and yields.

A straightforward way to reconcile the equilibrium approach with the arbitrage-free framework is by deriving the price of a zero-coupon bond based on the optimization of the utility function of a representative agent. For instance, in the DSGE framework (see section 1.4), the so-called "Euler equation" can be expressed as:

$$\frac{P(t,T)}{\exp\left(\int_0^t \delta(s)\mathrm{d}s\right)}\frac{U'(c(t))}{p(t)} = \mathbb{E}_t^{\mathbb{P}}\left[\frac{1}{\exp\left(\int_0^T \delta(s)\mathrm{d}s\right)}\frac{U'(c(T))}{p(T)}\right], \tag{1.28}$$

where $\delta(s)$ represents the instantaneous rate of time preference – the discount rate for future utility –, $U'(c(T))$ is the marginal utility of consumption, $c(t)$ is consumption at time $t$, and $p(t)$ denotes the general price level. In the arbitrage-free framework, rewriting Eq. (1.20) under the historical probability gives:

$$\frac{P(t,T)}{\exp\left(\int_0^t r(s)\mathrm{d}s\right)}\left.\frac{\mathrm{d}\mathbb{Q}}{\mathrm{d}\mathbb{P}}\right|_t = \mathbb{E}_t^{\mathbb{P}}\left[\frac{1}{\exp\left(\int_0^T r(s)\mathrm{d}s\right)}\left.\frac{\mathrm{d}\mathbb{Q}}{\mathrm{d}\mathbb{P}}\right|_T\right]. \tag{1.29}$$

By comparing Eq. (1.28) and Eq. (1.29), we can identify the stochastic instantaneous risk-free rate $r(s)$ with the instantaneous rate of time preference $\delta(s)$, and the Radon-Nikodym derivatives of the risk-neutral probability as:

$$\left.\frac{\mathrm{d}\mathbb{Q}}{\mathrm{d}\mathbb{P}}\right|_t = \mathbb{E}_t^{\mathbb{P}}\left[\frac{U'(c_T)}{p(T)}\right]. \tag{1.30}$$

Thus, in the arbitrage-free framework, the existence of risk premiums (i.e., the market price of risk $\lambda$) observed in Fig. 1.1 can be attributed to either (i) a systematic estimation by economic agents that inflation will rise in the coming years or (ii) constant shifts in these agents' preferences, both of which are not entirely convincing explanations (see Bouchaud and Potters (2003) for more detailed critique).

#### 1.3.2.4 Excess volatility in the arbitrage free theory

In its most common form, the arbitrage-free theory of the term structure assumes the existence of an instantaneous risk-free rate, much like the expectation theory. However, even with the introduction of a risk neutral probability measure to account for variations in investor preferences, the theory does not solve the so-called long-term rates "excess volatility puzzle" (Giglio and Kelly, 2018; d'Arienzo, 2020; Hanson et al., 2021): the volatility of long-term rates is higher than predicted by these models. Specifically, Giglio and Kelly (2018) assume, in a discretized

framework, that the instantaneous short-term rate follows an AR(1) process under the risk-neutral probability $\mathbb{Q}$:

$$r(t+1) = r(0) + \rho r(t) + \epsilon(t), \tag{1.31}$$

where $t$ is in days, the residuals $\epsilon(t)$ are normally distributed and homoskedastic[3], and $\rho < 1$. This process can be viewed as a discretized version of a mean-reverting Ornstein-Uhlenbeck process (Uhlenbeck and Ornstein, 1930), so it includes a market price of risk similarly to Eq. (1.20). Giglio and Kelly (2018) express the yield of a zero-coupon bond maturing in $\theta$ days under the risk-neutral measure as a function of the price of the zero-coupon bond maturing tomorrow:

$$y(t, t+\theta) \approx \frac{1}{\theta}\mathbb{E}_t^{\mathbb{Q}}\left[\sum_{i=1}^{\theta} r(t+i)\right] = r(0) + \beta(\theta)y(t, t+1), \tag{1.32}$$

where $\beta(\theta) = \frac{1}{\theta}\frac{1-\rho^\theta}{1-\rho}$ represents the sensitivity of the zero-coupon bond of maturity $\theta$ to the shortest-maturity yield. Although this sensitivity theoretically converges to zero as the time-to-maturity $\theta$ increases, the empirical coefficients of the regression of long-term yields on the shortest-maturity yield increase more rapidly than predicted by the model, leading the authors to conclude an excess volatility and excess sensitivity of long-term yields to the short-term rate.

However, according to our tests, the high temporal autocorrelation of zero-coupon bond yields (see section 1.3.2.1) results in highly correlated residuals when regressing $y(t, t+\theta)$ on $y(t, t+1)$, thereby invalidating the model of Eq. (1.32). Hence, we can actually conclude that the econometric version of the arbitrage-free framework is misspecified, but it does not confirm an excess volatility puzzle.

It is possible to partially overcome the "stochastic singularity" of the arbitrage-free framework by assuming that each instantaneous forward rate $f(t, T)$ of maturity $T$ solves its own stochastic differential equation, as described in the next section (see section 1.3.2).

#### 1.3.2.5 Current industry practice: the HJM framework

The Heath-Jarrow-Morton (HJM) framework has become the industry standard (Heath et al., 1992; Hughston, 1996). Within this framework, the dynamics of the FRC (i.e., the collection of the instantaneous forward rates $f(t, \theta)$, see section 1.1) is described by Itô processes driven by a $d$-dimensional Brownian motion. Consequently, bond prices for each tenor $\theta$ are regarded not as financial derivatives of the risk-free rate $f(t, 0)$ but as individual risky assets, leading to a possibly

[3]The authors also analyze a heteroskedastic model, finding that it has a limited impact on excess volatility.

infinite number of such assets. The finite number $d$ of diffusion factors introduces the potential for arbitrage opportunities among bond prices (Björk, 2019). Thus, conditions are established on the drift components of instantaneous forward rate processes to ensure arbitrage-free pricing of zero-coupon bonds. This framework rests only on two fundamental assumptions: the continuity of sample paths of forward rate processes and the finite number of Brownian motions driving these processes.

Similarly to the models based on the diffusion of a single risk-free rate, a limitation of the HJM framework is its stipulation that for any integer $k$, the correlation matrix of $k+d$ instantaneous forward rates must be singular when the model employs $d$ factors, contradicting empirical results (see chapter 5)

This limitation also complicates the calibration of the HJM framework when attempting to fit the model to historical market prices. Similarly to affine term structure models, such calibration requires the addition of a residual noise to account for measurement errors. For example, De Jong and Santa-Clara (1999) attempted to fit zero-coupon bond yields derived from swap data using a two-factor model within the HJM framework. Using a maximum likelihood approach, they calibrated the following expression:

$$y(t, t+\theta) = A(\theta) + B(\theta)\psi(t) + \epsilon(t, \theta), \tag{1.33}$$

where $A(\theta)$ and $B(\theta)$ are functions of the time-to-maturity $\theta$ to be fitted, $\psi(t)$ is a state parameter based on the dynamics of the instantaneous forward rate, and $\epsilon(t, \theta)$ represents the measurement error. Unfortunately, but perhaps expected, these measurement errors exhibit high autocorrelation (up to 90% at one day).

The serial autocorrelation of these measurement errors is significantly lower, around 16%, when fitting such a model directly to Futures prices (Bhar and Chiarella, 2011). In such an approach, it is crucial to recognize the formal difference between the simply-compounded yield $F(t, S, T)$ associated with Futures prices, defined by (see section 1.1):

$$\frac{1}{1 + F(t, S, T)(S - T)} = \frac{P(t, T)}{P(t, S)}, \tag{1.34}$$

and the instantaneous forward rate $f(t, T)$ modeled within the HJM framework (Bhar and Chiarella, 2011). Specifically, a maturity bias arises because the limit $S \to T$ is not quoted in financial markets, and a convexity bias exists because $f(t, S, T)$ is a continuously compounded rate defined by (see section 1.1):

$$\exp\left(-f(t, S, T)(T - S)\right) = \frac{P(t, T)}{P(t, S)}. \tag{1.35}$$

Bhar and Chiarella (2011) observed that these biases are non-negligible and proposed treating Futures contracts as derivative instruments written on the instantaneous forward rates. This approach led to the derivation of a full-information maximum likelihood estimator for observable Futures prices. The authors obtained a diffusion equation for Futures prices of the form:

$$\frac{\mathrm{d}F(t,S,T)}{F(t,S,T)} = \Sigma(S,T)\mathrm{d}W^{\mathbb{Q},d} + \epsilon(S,T), \tag{1.36}$$

where $\epsilon(S,T)$ accounts for measurement errors, and $\Sigma(S,T)$ is a $d \times d$ matrix. In this equation, measurement errors are proportional to the relative variations of Futures prices, which are known to be temporally uncorrelated. Therefore, this calibration is less misspecified than a calibration on zero-coupon bond yields, where measurement errors are proportional to the yields (see Eq. (1.36)).

To avoid misspecification entirely, the HJM framework can be extended to define as many diffusion factors as the number of existing Futures. This approach, often referred to as a LIBOR Market Model (LMM), then requires the calibration of a large number of parameters. In practice, the financial industry typically calibrates HJM models using risk-neutral prices of derivative instruments which are highly sensitive to the parameters of the model, thus avoiding the need for defining measurement errors.

An other major limitation of the HJM framework, noticed by Bouchaud and Potters (2003), is its stipulation, to ensure absence of arbitrage, that the drift of the forward rate reads, under the historical probability,

$$\mu_f(t,\theta) := \sigma_f(t,\theta)\left(\int_0^\theta \mathrm{d}\theta' \sigma_f(t,\theta') - \lambda(t)\right), \tag{1.37}$$

where $\sigma_f(t,\theta)$ is the volatility of the forward rate process and $\lambda(t)$ is the market price of risk. Bouchaud and Potters (2003) observe that under the reasonable assumption of a stationary volatility and market price of risk (i.e., $\lambda(t) = \lambda$ and $\sigma_f(t,\theta) = \sigma_f(\theta)$), the empirical average of the forward rate over an interval $\mathcal{I} \gg \theta$ is given by:

$$\langle f(t,\theta) - f(t,0)\rangle|_\lambda \approx \lambda \int_0^\theta \sigma_f(u)\mathrm{d}u - \theta\sigma_f(\Theta) + O\left(\frac{\theta^2\sigma_f(\Theta)}{\mathcal{I}}\right), \tag{1.38}$$

where $\Theta$ is the maximum available maturity of the FRC. The authors deduce that this contribution is negative (when $\lambda > 0$) for some initial region of the FRC if, as empirically found, $\sigma_f(\theta) > \sigma_f(0)$ for all $\theta$ (see section 1.3.2.4). Unfortunately, the actual shape of the average empirical FRC is very different (see section 5) from the one prescribed by Eq. (1.38).

In fact, to address this issue, some authors (Moraleda and Vorst, 1997) proposed non-stationary volatility functions $\sigma_f(t, \theta)$ to fit the humped volatility of the term structure (see chapter 5). We show in chapter 7 that an elastic string model allows us to reproduce the full volatility structure of the FRC, while being stationary.

## 1.4 Macroeconomic models

Interest rates are viewed in macroeconomics as a critical state parameter that links money creation to economic growth. Since the publication of *The General Theory of Employment, Interest, and Money* by Keynes in 1936, and its formalization within the IS-LM (Investment-Savings, Liquidity-Money) model the following year by Hicks (1937), the monetary policy transmission mechanism has primarily been understood through the interest rate channel. This perspective assumes that the central bank can set the real interest rate, which then influences investment, spending, and aggregate demand.

This modeling approach evolved in the 1950s into the commonly accepted "neoclassical synthesis", which posits that prices are flexible in the long run, causing the output gap to revert to equilibrium after a shock. Consequently, the "unanticipated price level channel" (Mishkin, 2013) became the main transmission mechanism of monetary policy. In the long run, according to the classical view, an expansionary monetary policy generates inflation, leading economic agents to raise their inflation expectations and, eventually, their wage demands. The neoclassical synthesis perspective hinges on the temporary differences between anticipated and realized inflation. As economists sought microfoundations for the Phillips curve linking inflation with unemployment (Phillips, 1958), they proposed several constraints on price flexibility to explain the short-term effects of monetary expansion driven by inflationary surprises. For example, the "advance fixing of nominal wages" and the related concept of "misperceptions", introduced by Friedman (1968) and further developed by Lucas (1973), suggest that when wages cannot immediately adjust to inflation (or producers misinterpret inflation), real labor costs decrease during an inflationary surprise, thereby boosting employment and production.

The neoclassical synthesis was later extended by the New Keynesian (hereafter referred to as New Keynesian (NK)) economic theory, particularly through the development of the NK DSGE modeling framework (see section 1.4), as developed by Rotemberg (1982) and Calvo (1983), among others. In these models, the output gap is a function of the private sector's expectations regarding the future path of the short-term real interest rate, which also determines the long-term rate in the arbitrage-free theory (under a "risk-neutral" probability measure, see section

1.3.2). Consequently, by setting the short-term real interest rate, the central bank influences the private sector expectations of the long-term rate, which is directly linked to the output gap in this framework. Formally, in these models, the interest rate primarily affects the arbitrage decisions of households between consumption and saving, rather than firms' investment or any other monetary policy channels described in section 1.2.1.

In the following years, a vast diversity of modeling approaches flourished within the NK DSGE framework, trying to address some of the identified issues of this class of models. In particular, one can mention the attempts to include some backward-looking decision making by agents when resetting their prices to better fit empirical data that demonstrate the persistence of inflation (Fuhrer and Moore, 1995; Roberts, 1997; 1998; Galí and Gertler, 1999).

### 1.4.1 Excess sensitivity puzzle in macroeconomic models

Within the standard DSGE framework, short-term interest rates are expected to quickly return to a deterministic steady state following a macroeconomic or monetary policy shock. Consequently, one would anticipate only a limited response from long-term interest rates to these disturbances. However, empirical evidence suggests that long-term rates are far more sensitive to new information than DSGE models predict (Rudebusch, 1995; Fuhrer, 1996; Gürkaynak et al., 2005; Hanson and Stein, 2015). For instance, Gürkaynak et al. (2005) analyzed the sensitivity of long-term interest rates (derived from U.S. sovereign bonds) to economic news and monetary policy surprises, finding that long-term rates are significantly more responsive to such news than the NK DSGE framework predicts.[4] Moreover, while monetary policy surprises typically cause short-term interest rates to move in the expected direction, forward rates at longer horizons often move in the opposite direction—i.e., a surprise policy tightening can lead to a decline in long-term forward rates. Gürkaynak et al. (2005) suggests that this strong sensitivity of long-term nominal rates to short-term rates could be consistent with the expectations hypothesis only if long-run inflation expectations are unanchored and continuously updated (see Eq (1.28) in section 1.3.2.3).

Beechey (2006) addresses the excess sensitivity puzzle within the DSGE framework by hypothesizing that the central bank's inflation target is not explicitly communicated, and macroeconomic shocks are imperfectly observed. As a result, bond markets infer the inflation target from noisy signals, leading to increased sensitivity of long-term inflation expectations to transitory shocks. This mecha-

[4]The authors tested two types of DSGE models: (i) a model generating a forward-looking Phillips curve (Clarida et al., 2000); and (ii) a backward-looking version of this model proposed by Rudebusch (2001). As previously noted, the persistence of inflation in empirical data tends to invalidate forward-looking DSGE models.

nism amplifies the response of long-term interest rates to monetary policy actions and inflation surprises.

Hanson and Stein (2015) propose two potential explanations for this excess sensitivity: either monetary policy (i) influences expected future real rates at very distant horizons (see the model by Piazzesi (2005) in section 1.2.1.3), which contradicts the rational expectations hypothesis, or (ii) affects the term premium on long-term bonds, implying that the observed effect on forward rates should mean-revert over time. Hanson and Stein (2015) observe such overreactions of long-term rates, as discussed in section 1.5. They suggest that these effects can be reproduced using an agent-based model with two types of investors trading at different time scales (see section 1.6).

### 1.4.2 DSGE models including bank agents or an interbank market

Another significant improvement in yield modeling is the integration of a more sophisticated banking system within the DSGE framework (Boissay et al., 2016; Jakab and Kumhof, 2018; Gertler et al., 2020; Coimbra and Rey, 2024). Although these extensions were developed in response to the GFC, addressing the need for a more realistic representation of the financial sector (Benner, 2013; Fagiolo and Roventini, 2016), they also enhance the micro-foundation of interest rates.

For example, the approach by Boissay et al. (2016), which models endogenous banking crises, incorporates two rates that can be interpreted as short-term (interbank) and long-term (corporate loan) rates. Within this framework, the term premium is related to the marginal product of capital, which aligns with Tobin's q theory (Tobin, 1969). This model is designed to capture the long-term dynamics of credit in both interbank and corporate markets, but it does not fully account for the stylized facts of the interbank network (see section 1.7).

However, many of these models continue to assume that banks function merely as intermediaries of loanable funds, whereas, in reality, banks finance loans through money creation under regulatory constraints (see section 1.7). This limitation has been addressed by Jakab and Kumhof (2018), who proposed an extension of the DSGE framework in which banks are modeled as heterogeneous financial intermediaries. In their model, loans are financed through the ex-nihilo creation of ledger-entry deposits, facilitating payments among non-bank entities. Unfortunately, this model accounts for only a single maturity of the yield curve.

### 1.4.3 Macro-finance models

Lastly, it is worth noting that the field of "macrofinance" has sought to address inconsistencies between asset prices and economic fluctuations (Cochrane, 2017). One major discrepancy is the so-called "equity-premium risk-free rate puzzle"

(Mehra and Prescott, 1985; Hansen and Jagannathan, 1991): the volatility of consumption in the DSGE framework is insufficient to generate the observed equity premium in financial markets, unless an unrealistically high risk-free rate is assumed.

In a recent review, Cochrane (2017) highlights several efforts to solve this puzzle, including the generalization of the marginal utility of consumption —and consequently the risk-free rate— within various frameworks (e.g., consumption habits as proposed by Campbell and Cochrane (1999) or heterogeneous preferences as suggested by Gârleanu and Pedersen (2016)). A notable explanation for the higher equity premium is offered by leverage finance models (Brunnermeier, 2009; He and Krishnamurthy, 2013), where only highly leveraged intermediaries participate in the market and are forced to fire sale assets when the market declines.

Some authors in this field have proposed abandoning the rational expectations hypothesis (Barberis et al., 2015), which is a key assumption leading to the primary puzzle of the yield curve: the excess volatility of long-term rates (see sections 1.3.2.1, 1.3.2.4, and 1.4.1). Although the "Macro-finance" literature has not yet addressed this specific puzzle, numerous studies have tested the validity of the expectations hypothesis, as discussed in the following section.

## 1.5 Overreactions and irrationality

Given that both the arbitrage-free and macroeconomic frameworks rely on the assumption of rational expectations and face the issue of excess volatility, several attempts have been made to test this hypothesis. Early efforts by Shiller et al. (1983) and Mankiw and Summers (1984) to model specific forms of irrational expectations were unsuccessful. Specifically, Shiller et al. (1983) examined whether interest rates reverted to their previous levels following money stock surprises[5] but found no evidence to support such behavior, thus validating the martingale property of forward rates.

In subsequent research, Fama and Bliss (1987) investigated the predictability of 1-year holding period excess returns on bonds, $\log\left(\frac{P(t+1,t+\theta)}{P(t,t+\theta)}\right) - y(t,t+1)$, using forward-spot spreads, approximated as follows:

$$\log\left(\left(\frac{P(t,t+\theta)}{P(t,t+\theta+1)}\right) - y(t,t+1) \approx F(t,t+\theta,t+\theta+1) - y(t,t+1), \quad (1.39)$$

[5]In the 1970s in the U.S., the Federal Reserve published weekly money-stock announcements. The expected money supply was defined as the median forecast of the money stock from the weekly market survey of Money Market Services, published every Tuesday. The money surprise was calculated as the difference between the announced and expected money stock.

where $t$ is the current time in years, $\theta$ is the time-to-maturity in years, and $y(t, t+1)$ is the yield of a 1-year zero-coupon bond, which defines the spot risk-free rate. Within the arbitrage-free framework, one would expect no variation in 1-year holding period excess returns. Indeed, approximating for convexity effects, we have[6]:

$$\begin{aligned}&\log\left(\frac{P(t+1,t+\theta)}{P(t,t+\theta)}\right) - y(t,t+1)\\ &\quad\approx \mathbb{E}_t^{\mathbb{Q}}\left[\int_{t+1}^{t+\theta} r_s \mathrm{d}s - \int_t^{t+\theta} r_s \mathrm{d}s\right] - \mathbb{E}_t^{\mathbb{Q}}\left[\int_t^{t+1} r_s \mathrm{d}s\right] = 0. \end{aligned} \tag{1.40}$$

However, Fama and Bliss (1987) observed significant variations in 1-year holding period excess returns, particularly for medium- to long-term maturities (1 to 5 years), whereas forward rates poorly predict short-term (less than 1 year) interest rate changes, consistent with Shiller et al. (1983). Overreactions of long-term rates to surprises in the Fed funds rate have also been documented by Hanson and Stein (2015) and Das (2002). Notably, Hanson and Stein (2015) reported that increases in long-term forward rates on monetary policy announcement days predict a reversal over the next 12 months, implying non-Markovian dynamics in the yield curve, which contradicts the affine term structure framework's assumptions.

Testing the full-information rational expectations hypothesis is challenging due to the unobservability of the complete information set used by forecasters. However, studies by Coibion and Gorodnichenko (2015), Bordalo et al. (2020), and Wang (2021) have conducted tests on key macroeconomic variables (e.g., inflation, output growth, interest rates, consumption growth) using data from U.S. professional forecasters (e.g., The Livingston Survey, SPF, and Blue Chip) and consumer expectations (e.g., The Michigan Survey of Consumers). Coibion and Gorodnichenko (2015) proposed regressing forecast errors on forecast revisions, where a positive correlation indicates underreaction and a negative correlation indicates overreaction. Using this method, Bordalo et al. (2020) showed that 5- and 10-year U.S. Treasury rate forecasts overreact to new information, while forecasts of the Fed funds rate or 3-month Treasury rates underreact. Building on this, Wang (2021) successfully modeled the observed downward-sloping term structure of misreaction by distorting professional forecasters' subjective perceptions of short rate path.

Finally, while the affine term structure framework assumes exponential discounting $P(0,\theta) = \exp(-r\theta)$ (see section 1.3.2.1), studies in Neuroscience, Behavioral Economics, and Finance (Green et al., 1994; Sozou, 1998; Frederick et

[6]The authors derive this result within the expectation theory under the historical probability. Here, we extend this finding to the arbitrage-free framework where all bond prices are expressed under the risk-neutral probability.

al., 2002; Green and Myerson, 2004; Dasgupta and Maskin, 2005; Thaler, 2005; Farmer and Geanakoplos, 2009; Kim and Zauberman, 2009; Cui, 2011; Ray and Bossaerts, 2011) suggest that agents may use hyperbolic discounting:

$$P(0,\theta) = (1 - \alpha\theta)^{-\beta}. \tag{1.41}$$

We demonstrate in chapter 7 that this form of discounting is crucial for modeling the yield curve.

## 1.6 Agent-based models of the interest rate curve: the preferred-habitat theory

Standard economic theory connects the interest rate for a given maturity $T$ to the willingness of a representative agent to change consumption between times $t$ and $T$, driven by the maximization of a utility function (see section 1.3.2.3). In a different view, the so-called "preferred-habitat" theory, proposed by Culbertson (1957) and Modigliani and Sutch (1966), suggests that certain agents (i.e., investor groups) have a predilection for specific maturities of the yield curve, which in turn affects interest rates based on the demand from these clienteles and the supply of bonds with corresponding maturities. For example, pension funds typically prefer long-term bonds, so an increase in their demand would likely reduce long-term interest rates. In essence, the preferred-habitat view argues that bond market prices are subject to demand and supply pressures from heterogeneous investor preferences.

This modeling approach has been further developed in recent years to address the puzzles of the term structure (Greenwood and Vayanos, 2010; 2014; Hanson, 2014; Hanson and Stein, 2015; Mixon and Tuzun, 2018; Hanson et al., 2021; Vayanos and Vila, 2021). In particular, Hanson and Stein (2015) and Hanson et al. (2021) have proposed models that assume the existence of yield-oriented investors who allocate their portfolios between short- and long-term bonds to maximize their current short-term income, which is crucial for performance reporting. When short-term rates decline, these investors shift towards long-term bonds, creating upward pressure on their prices (and thus lowering yields), which helps explaining the high sensitivity of long-term rates to short-term rate changes (see section 1.3.2.1). These models also account for temporary overreactions of long-term rates to changes in short-term rates (see section 1.5) by introducing two types of investors with different trading horizons: short-term investors who focus on near-term returns and long-term investors who trade less frequently and consider future returns over longer periods. The need for both types of investors to absorb a fixed supply of long-term bonds generates price overreactions.

The model proposed by Mixon and Tuzun (2018) decomposes yield curve shifts into two components: a fundamental value modeled using the Nelson–Siegel framework (Nelson and Siegel, 1987; Diebold and Li, 2006; Diebold et al., 2006; Christensen et al., 2011) and a part generated by price pressure effects resulting from dealer inventories (as defined in chapter 5). This model provides evidence that net dealer Treasury inventories significantly impact the yield curve (see section 1.2.2.1). Finally, d'Arienzo (2020) offers another explanation for the excess volatility of long-term rates, suggesting that it is the result of increasing overreactions to news as the maturities of the bonds lengthen. This occurs because biased investors tend to extrapolate recent changes in short-term rates to long-term rates. The author posits that investors perceive a distorted version of the short rate diffusion, which is more sensitive to current information than standard short rate models would suggest.

Although preferred-habitat theory better reproduces the relationship between short-term and long-term rates, the finite number of agent groups considered prohibits modeling of the entire yield curve. The field theory of the interest rate curve developed in chapters 7 and 8 is connected to these approaches, as it similarly posits that yield variations arise, at least partially, from net trading flows.

Another class of agent-based models focuses on the interbank lending market, where the shortest-term yields are determined. In the next section, we will explore several models that describe these markets.

## 1.7 Agent-based models of the money markets

Several approaches to the modeling of the interbank unsecured markets have been proposed. The influential article of Poole (1968) introduces a model in which the interbank lending network absorbs randomly generated payment shocks, under reserves requirements' constraints. This seminal work has been followed by numerous proposals of network modeling of the interbank market. Recently, Heider et al. (2015) included counterparty risk in the lending network and generated endogenous liquidity hoarding. Bech and Monnet (2016) considered a search-based model that can reproduce the decrease of trading volumes due to a surge in excess reserves, without identifying the initial cause of deposits surpluses. This was later identified by Vari (2020) as the eurozone interbank market fragmentation: banks, depending on their country of location, have different probabilities of default. This fragmentation disrupts the transmission of monetary policy, generating endogenously excess liquidity. Vari (2020) distinguishes two groups: core banks (in Germany and Netherlands) do not use central bank funding but hold excess reserves; peripheral banks (e.g. in Spain and Italy) borrow massively from the central bank to fulfill their needs. Yet, the obtained funding ends up within the

core banks due to payment imbalances. We reproduce the same behavior but we reverse its causality in chapter 4. In our Agent Based Model (ABM), the flow of payment shocks moves deposits from peripheral to core banks, generating liquidity needs in the first ones, and excess liquidity in the others (see Sec. 4.1.7). More recently, the decline of unsecured markets led several authors (Piquard and Salakhova, 2019; De Fiore et al., 2021) to build equilibrium models explaining the substitution effects between secured and unsecured interbank markets. Yet, all these modeling proposals are only able to describe the equilibrium state of the interbank market.

Other authors proposed dynamic models of unsecured interbank markets (Afonso and Lagos, 2015; Lux, 2015; Blasques et al., 2018; Halaj, 2018; Liu et al., 2020). Notably, Blasques et al. (2018) assume profit maximization and risk monitoring cost to generate a sparse core-periphery structure and stable bilateral trading relationships. Lux (2015) obtain the same result using a reinforcement-learning scheme. Liu et al. (2020) proposed an ABM of the interbank network leading to the endogenous formation of a financial network using only individual banks data.

Within ABMs for Macroeconomics, several frameworks include multiple bank agents from which firms can borrow, although they do not allow interactions among banks (Dosi et al., 2010; Cincotti et al., 2012; Dawid et al., 2012; Dosi et al., 2013; Dawid and Gemkow, 2014; Dosi et al., 2015; Dawid et al., 2016; Dosi et al., 2017; Dawid et al., 2018). The modeling of a static interbank lending market is found in some macroeconomic models (Schasfoort et al., 2017; Gurgone et al., 2018; Reissl, 2018; Reale, 2019).

In general, these approaches focus on unsecured markets, which have been largely replaced by secured markets (see chapter 3). Moreover, these models assume the absence of endogenous money creation while this process induces non-centered shocks requiring a specific modeling (Jakab and Kumhof, 2015; 2018). Finally, these frameworks only account for reserves constraints while the introduction of the liquidity regulations significantly modified money markets (see chapter 3). We overcome these limitations in our ABM of the interbank lending market described in chapter 4.

## 1.8 Summary

Within macroeconomic theory, monetary policy exerts its influence on the economy through various channels, most of which depend on the interest rate curve as the primary transmission mechanism. In contrast, in the long run, economic theory assumes a strong influence of consumption growth, population growth, and time preferences on the level of interest rates. However, more recent empirical studies challenge this view by highlighting the significant impact of supply and

demand for credit on the yield curve. Evidence from sovereign bond markets points to substantial yield variations that are driven by transaction flows.

In line with standard economic theory, most yield curve models assume the existence of a rational representative agent who optimizes utility between current and future consumption. However, the calibration of these models using market prices generally shows that they are misspecified. Furthermore, these models often conclude to an excess volatility puzzle: long-term rates are more volatile than predicted by the diffusion of the short-term rate. One approach to address this issue is to model each forward rate individually, as in the Libor Market Model, within the HJM framework. However, this method requires calibrating a large number of parameters and introduces a change in probability with weak microfoundations, as it relies on the unrealistic assumption that agents constantly change their preferences. An alternative approach, first introduced in the macrofinance literature and more recently developed through ABMs, discards the assumption of a rational representative agent. A prominent framework in this regard is the preferred-habitat theory, which posits that different groups of agents have preferred investment maturities. Although this type of model more accurately captures the relationship between short- and long-term rates, the limited number of agent groups restricts its ability to model the entire yield curve.

The shortest maturities of the yield curve have been modeled using agent-based approaches and network theory since the 1960s. However, these models have traditionally focused on unsecured markets, which have become less relevant in western economies after the shift of bank refinancing toward secured lending (see chapter 3). In chapter 4, we propose a minimal model of the secured interbank market.

In order to build alternative approaches that address the limitations identified in existing yield curve models, we begin in chapter 2 by examining the microstructure of the markets that determine interest rate levels in modern economies, focusing on interbank lending, derivatives, and other relevant markets.

## Key takeaways

- In line with standard economic theory, most yield curve models assume the existence of a rational agent optimizing utility between present and future consumption.
- These models, which are generally misspecified, are incompatible with the observed volatility of long-term rates (the excess volatility puzzle).
- Modeling each forward rate separately (HJM framework) requires many parameters and a probability change with weak microfoundations.

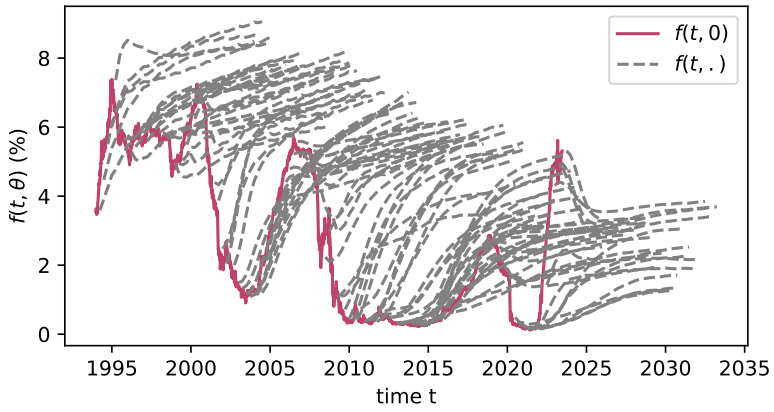


- Alternative approaches in macrofinance and ABM methods abandon the rational agent assumption. Notably, the preferred-habitat theory links short- and long-term rates through investor groups with heterogeneous preferences but does not model the potential infinite number of yield curve maturities.
- Since the 1960s, agent-based and network models have focused on the shortest-maturity rates, but they mainly apply to unsecured markets, which have declined in relevance.

# Chapter 2

# Market microstructure of the yield curve

In this chapter, we present the actors, markets, and microeconomic mechanisms that define the yield curve. We begin by examining the shortest available maturity, the overnight interbank rate, and then analyze the price formation mechanisms of long-term rates in the swap, Futures and bond markets. Throughout this exploration, we will identify the most liquid products influencing each of these markets, guided by the principle that price formation occurs primarily within the most liquid assets (as shown in chapter 6).

## 2.1 The interbank market

Central banks largely control the shortest maturity interest rate in a given economy. However, the interbank lending market provides banks with some leeway in determining the market rate, which ultimately shapes the entire interest rate curve. This price-setting mechanism is directly related to the money creation process, which occurs through credit lending via long-term loans. Subsequently, payment shocks require interbank lending to compensate for the reallocation of liquidity by economic agents. In this section, we detail these processes.

### 2.1.1 Money creation

In western countries, money is created primarily by commercial banks through lending. The production of goods is independent from the money creation process. When a good, such as a car, is ready to be sold, the banking system's role is to create sufficient money to facilitate the transaction. This money creation typically occurs through a process such as issuing a consumer loan (see Fig. 2.1a) for a car

purchase. From an accounting perspective, this operation consists in increasing the assets and liabilities of bank $A$ by the same amount. When the buyer $A$ of the car transfers cash from his bank account to the one of the seller $B$, the balance sheets of banks $A$ and $B$ become unbalanced. The excess cash in bank $B$ is then used to compensate for missing deposits in bank $A$ (see Fig. 2.1b).

In reality, bank $B$ in Fig. 2.1 cannot use all its excess cash to fund bank $A$. Indeed, minimum reserves regulations require banks to deposit a share of the deposits they received at the central bank. This minimum reserve creates an imbalance in the system, which requires the central bank to loan the missing amount of liquidity to bank $A$ (see Fig. 2.2). This yields two types of control parameters for the central bank: the amount and rate of remuneration of the minimal reserves and the amount and interest rate of central bank loans.

Since the GFC, unsecured borrowings have largely been replaced by secured ones (see section 3.1). This shift means that interbank borrowings must now be secured by high-quality assets, typically sovereign bonds. Collateralized loans in the interbank market are known as repurchase agreements ("repos", see also section 3.2). Figure 2.3 illustrates the process of money creation through a repo agreement following the issuance of sovereign debt by the government. This mechanism is central to the ABM of the interbank market developed in chapter 4.

As money is created through bank credit, the repayment of existing loans results in money destruction. Therefore, for the total amount of money to grow, the issuance of new loans must exceed the amount of loans being repaid. However, the quantity of money available is not directly related to inflation because it is used not only for transactions but also as a reserve of value (Serletis, 2007). In the next section, we will explore the market mechanisms that link money creation to the shortest maturity interest rate.

### 2.1.2 The interbank rate

Money creation can only occur if banks can meet their short-term liquidity needs through the interbank market. Since these needs fluctuate, interbank borrowings have historically been contracted with very short maturities, often as short as overnight. As explained in section 3.2, most of the short-term liquidity needs of banks are now funded through callable collateralized loans with infinite maturity. The interest rates on these loans are often floating, with a reference rate based on an overnight average interbank rate, such as the ESTR in the E.U. or the SOFR in the U.S. These reference rates are subject to specific regulations in the E.U. and the U.S. because they serve as anchor points for the entire interest rate curve. As explained in section 2.1.3, the cost of short-term liquidity in the banking system is a key determinant of the long-term cost of money. For example, in the E.U., the E.U. Benchmark Regulation (*Benchmarks Regulation (EU) 2016/1011* 2016)

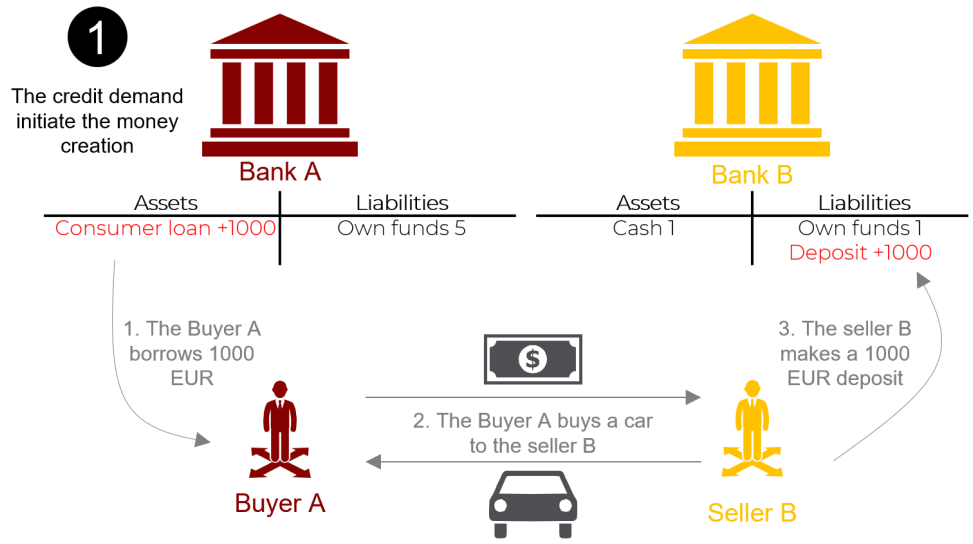


**(a)** Issuance of a consumer loan by the bank of the economic agent $A$ who aims at buying the car constructed by the economic agent $B$.

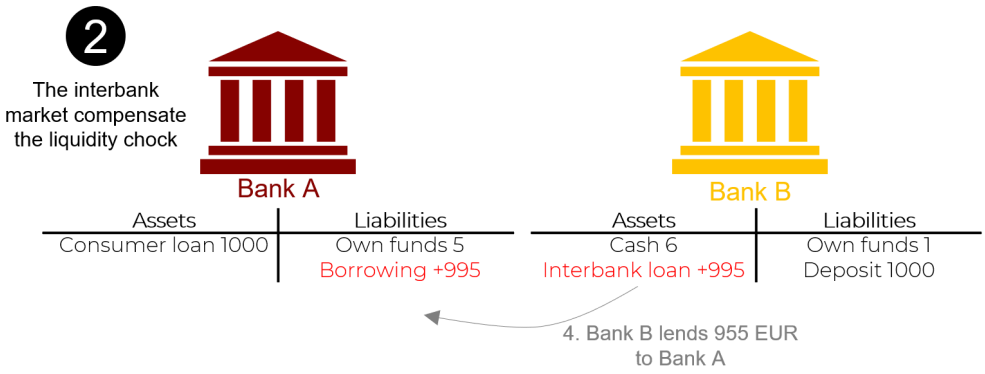


**(b)** The payment of the car generates a liquidity shock from bank $A$ to $B$ which is compensated by an unsecured interbank loan.

**Figure 2.1:** Money creation via unsecured interbank borrowings in absence of a central bank.

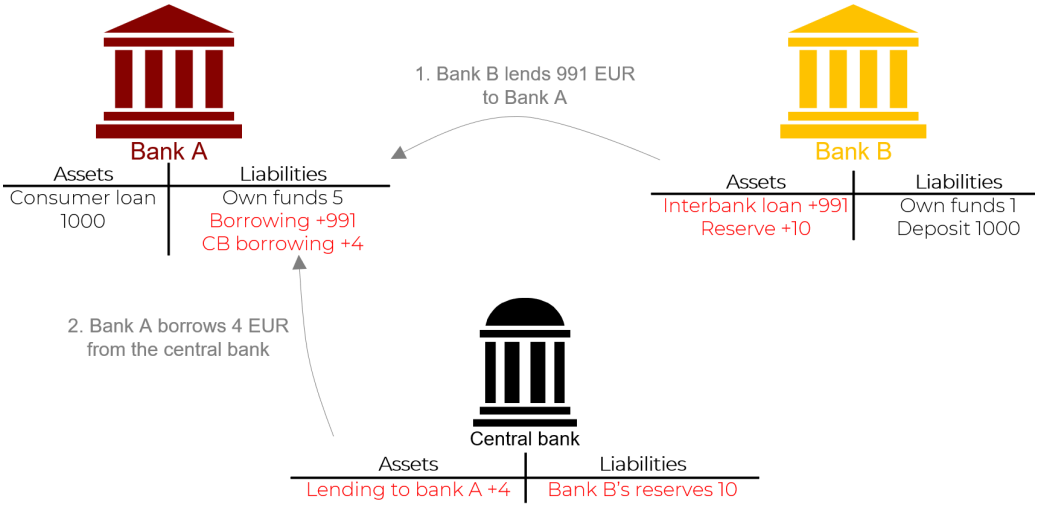


**Figure 2.2:** Money creation via unsecured interbank borrowings with minimum reserve constraints.

requires all interest rate derivatives denominated in euros to be indexed on the ESTR. We present the ESTR and SOFR rates in more detail in the following sections.

#### 2.1.2.1 The ESTR

The Euro Short-Term Rate (ESTR) replaced the Euro Overnight Index Average (Euro OverNight Index Average (EONIA)) as the overnight interest rate benchmark of the E.U. because the latter was not in compliance with the E.U. benchmarks regulation (*Benchmarks Regulation (EU) 2016/1011* 2016). The transition was initiated in 2018, with ESTR officially introduced on 2 October 2019. This benchmark average rate is calculated using euro transactions with financial counterparties defined by the Money Market Statistical Reporting (MMSR) regulation (*MMSR Regulation (EU) 1333/2014* 2014) and reflects the wholesale unsecured euro borrowing costs of banks in the eurozone, in contrast to EONIA that measured interbank lending.

Following the definition presented above, the ESTR rate represents an average overnight borrowing cost of European banks, excluding the deposits from corporate and retail clients. Indeed, even if these later deposits also have an overnight contractual maturity, they are actually very stable over time, so they cannot absorb payment shocks.

However, despite being based on a broader set of transactions, the majority of contributing transactions come from non-bank agents with less bargaining power

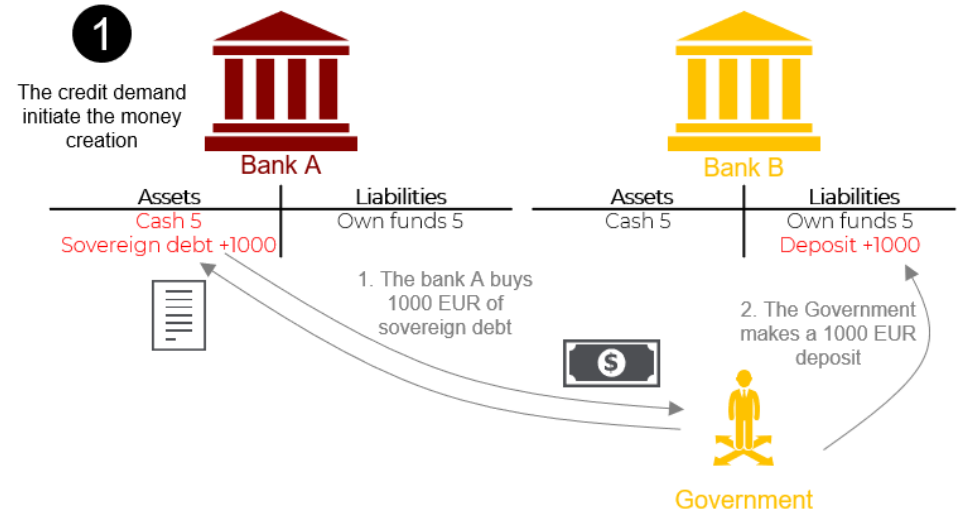


**(a)** Bank $A$ buys a bond issued by the government which deposits the received cash to bank $B$.

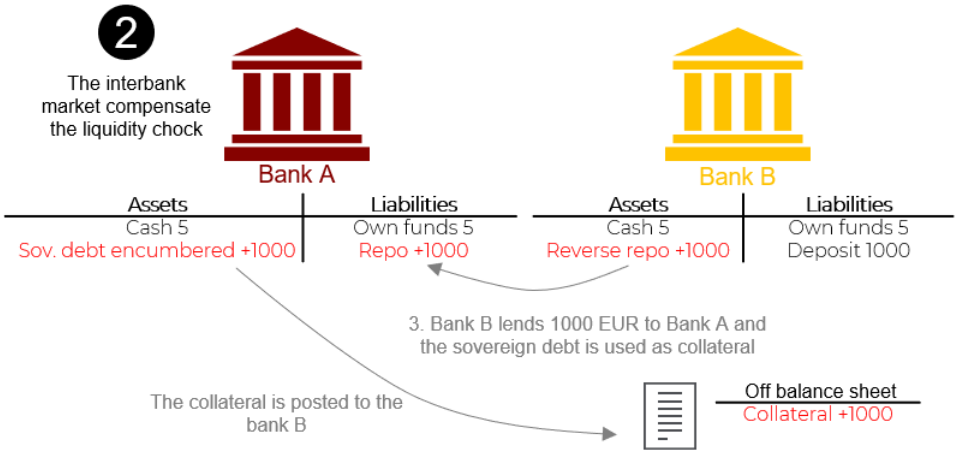


**(b)** The liquidity needs of bank $A$ are fulfilled by a repo aggreement.

**Figure 2.3:** Money creation via secured interbank borrowings in absence of a central bank.

than banks, as they do not have access to central bank funding. This has led to ESTR being set below the ECB's deposit facility rate, highlighting potential limitations in its role as a reliable benchmark rate.

#### 2.1.2.2 The SOFR

The Secured Overnight Funding Rate (SOFR) was introduced as the U.S. overnight interest rate benchmark to replace the London Interbank Offered Rate (LIBOR), which was phased out due to manipulation concerns and a lack of underlying transactions. The transition to SOFR began in 2017, with SOFR officially published by the Federal Reserve Bank of New York on 3 April 2018. Unlike LIBOR, which was based on estimated rates, SOFR is grounded in actual transactions and is calculated using data from the U.S. repo market. This market involves the overnight borrowing and lending of U.S. sovereign bonds, making SOFR a secured rate that reflects the cost of borrowing cash within collateralized contracts. Notably, since SOFR is based on a wide range of transactions secured by high-quality collateral, it is less susceptible to manipulation and more reflective of true market conditions than its predecessor. However, SOFR is highly sensitive to supply and demand dynamics in the repo market, so it can experience high volatility at quarter-end or year-end periods. Despite these challenges, SOFR has become the most used underlying of U.S. dollar-denominated interest rate derivatives.

Part II of this thesis is dedicated to the study of money creation by the banking system through interbank lending. In particular, in chapter 3, we present and reproduce several stylized facts of the European money markets. In chapter 4, we model the money creation process and the absorption of payment shocks by the banking system. Since the overnight interbank rate remains closely tied to central bank rates, our focus in these two chapters is on trading flows rather than prices.

### 2.1.3 Banks' balance sheet

We have seen how short-term liquidity needs of banks define the shortest maturity rates of the yield curve. In this section, we explore how longer-term interest rates are influenced by the way financial institutions manage their balance sheets.

The primary purpose of banks is to create the money necessary for an economy to facilitate the exchange of goods and store value. As discussed previously, this is achieved through the issuance of loans or the purchase of bonds issued by other economic agents. These agents are typically firms that require a few years to organize production before they can repay their debts. In many countries, a significant portion of these loans and bonds have fixed rates set at the time of contract signing. As a result, banks' balance sheets are typically filled with fixed-rate loans recorded as assets. On the liability side, banks receive deposits from

economic agents, which can be at fixed or floating rates depending on the jurisdiction. Additionally, payment shocks are absorbed through interbank borrowings (see section 2.1.1). These two types of liabilities, floating-rate deposits and interbank borrowing, are typically remunerated using the shortest-term rate available, as these products are callable at any time. Figure 2.4 illustrates a typical bank's balance sheet. This balance sheet structure, consisting of long-term fixed-rate loans and short-term floating-rate borrowings, is highly sensitive to increases in the short-term rate, which would raise the bank's funding costs while leaving its revenues unchanged.

As a result, banks' asset and liability management typically involves hedging, at least partially, their interest rate risk through the use of financial derivatives that exchange fixed rates for floating rates, such as interest rate swaps. Consequently, the interest rates of bank loans are set in line with these hedges. Therefore, the formation of long-term interest rates actually takes place in the swap market, which is described in more detail in the next section.

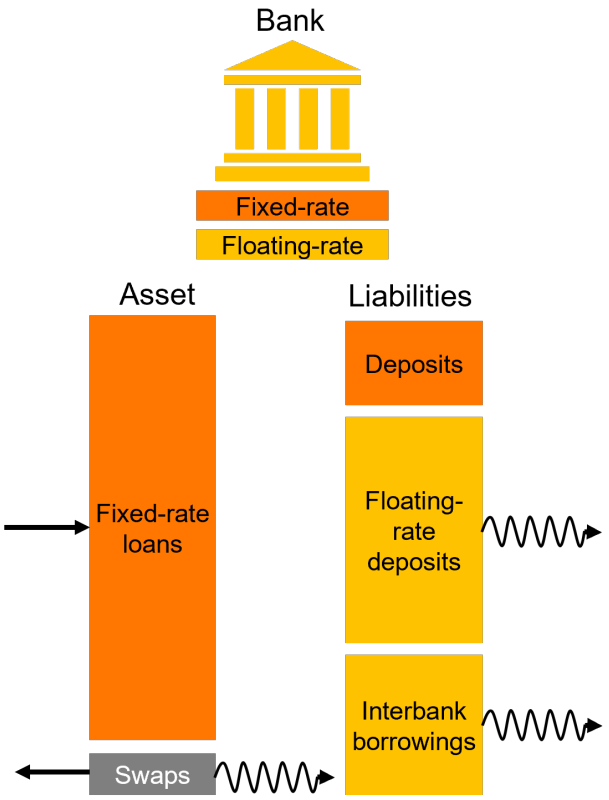


**Figure 2.4:** Typical balance sheet of a bank. Fix-rate flows are represented by a black straight arrow, while floating rate flows are depicted as a curvy black arrow. Similarly, we show fixed and floating rate financial contracts in orange and yellow respectively. Interest rate hedges, typically swaps, are represented in grey. They allow the matching of the floating and fixed rate flows of a bank's balance sheet.

## 2.2 The swap market

A cash-settled interest rate swap with a notional value of $N$, maturity $T$, starting at $T_0 > t$, pays a fixed swap rate $S(t,T)$, in exchange for a floating rate at several future payment dates. As illustrated in Fig. 2.5, such a swap consists of the following two legs:

- **Variable leg**: Pays the forward rate over each future time period $[T_{i-1}^V, T_i^V]$ of length $\delta^V$ (generally 6 months for contracts in euros and 3 months for contracts in dollars) on each date $T_i^V$. The present value at time $t$ of the variable leg is given by,

$$PV^V(t) = N \sum_{i=1}^{m} \delta^V F(t, T_{i-1}^V, T_i^V) P(t, T_i^V), \tag{2.1}$$

  where $m$ is the total number of payment dates for the variable leg, and $\delta^V$ is the fraction of the year for any interest period $[T_{i-1}^V, T_i^V]$.

- **Fixed leg**: Pays the swap rate $S(t,T)$ over each future time period $[T_{i-1}^F, T_i^F]$ of length $\delta^F$ on each date $T_i^F$ (generally annually for contracts in euros and semi-annually for contracts in dollars). The present value at time $t$ of the fixed leg is given by

$$PV^F(t) = N \sum_{i=1}^{n} \delta^F S(t,T) P(t, T_i^F), \tag{2.2}$$

  where $n$ is the total number of payment dates for the fixed leg, and $\delta^F$ is the fraction of the year for any interest period $[T_{i-1}^F, T_i^F]$.

As a result, interest rate swaps can be viewed as a linear combination of forward rate contracts with a short-term maturity of $T_i^V - T_{i-1}^V$. In the U.S., the most common swap rates typically use the SOFR rate compounded over a period of $T_i^V - T_{i-1}^V = 3$ months. We will see that these forward rate contracts are generally more liquid than swaps, and therefore this thesis focuses on the modeling of these products.

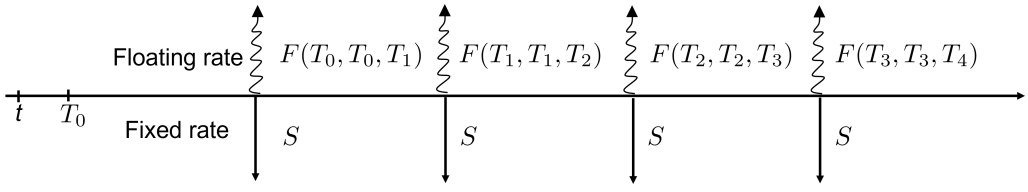


**Figure 2.5:** Fix and floating rates of a cash-settled interest rate swap

### 2.2.1 The interest rate curve implied by swap rates

This thesis aims to micro-found the interest rate curve, so here we present how market participants usually derive the interest rate curve from these instruments. These standard pricing formulas can be found, for example, in Brigo and Mercurio (2006) and Filipovic (2009).

As explained in section 1.1, the forward rate can be expressed as a function of zero-coupon bonds:

$$F(t, T_{i-1}^V, T_i^V) = \frac{1}{\delta^V}\left(\frac{P(t, T_{i-1}^V)}{P(t, T_i^V)} - 1\right). \tag{2.3}$$

If we substitute the forward rate with its definition in Eq. (2.1) the present value of the variable leg becomes:

$$PV^V(t) = N\left[P(t, T_0) - P(t, T_m^V)\right]. \tag{2.4}$$

Hence, the swap rate $S(t,T)$ of maturity $T$ at time $t$ can be expressed as:

$$S(t,T) = \frac{P(t, T_0) - P(t, T_m^V)}{\sum_{i=1}^n \delta^F P(t, T_i^F)}. \tag{2.5}$$

From equation (2.5), it is possible to retrieve the prices of zero-coupon bonds that match the swap rates observable on the market for different maturities. At time $t = T_0$, assuming $\delta^F = 1$, we can express each of the available swap prices as a function of the zero-coupon bonds. For example, the first three swap rates are given by:

$$\begin{aligned}
S(T_0, T_0 + 1Y) &= \frac{1 - P(T_0, T_0 + 1Y)}{P(T_0, T_0 + 1Y)}, \\
S(T_0, T_0 + 2Y) &= \frac{1 - P(T_0, T_0 + 2Y)}{P(T_0, T_0 + 1Y) + P(T_0, T_0 + 2Y)}, \\
S(T_0, T_0 + 3Y) &= \frac{1 - P(T_0, T_0 + 3Y)}{P(T_0, T_0 + 1Y) + P(T_0, T_0 + 2Y) + P(T_0, T_0 + 3Y)}.
\end{aligned} \tag{2.6}$$

Inverting this set of equations yields the zero-coupon bond price as a function of the swap rate with a time-to-maturity of $i$ years:

$$\begin{cases}
P(T_0, T_i^F) &= \frac{1 - \sum_{k=0}^{i-1} S(T_0, T_k^F) P(T_0, T_k^F)}{1 + S(T_0, T_i^F)}, \\
P(T_0, T_1^F) &= \frac{1}{1 + S(T_0, T_1^F)}.
\end{cases}$$

However, only a limited list of maturities is quoted on the swap market. For example, Fig. 2.6 presents the maturities available on the Tradeweb platform

| Quoted maturities | | | | | | | | |
|---|---|---|---|---|---|---|---|---|
| 1 week | 2 weeks | 3 weeks | 1 month | 2 months | 3 months | 4 months | 5 months | 6 months |
| 7 months | 8 months | 9 months | 10 months | 11 months | 1 year | 15 months | 18 months | 21 months |
| 2 years | 3 years | 4 years | 5 years | 6 years | 7 years | 8 years | 9 years | 10 years |
| 11 years | 12 years | 13 years | 14 years | 15 years | 20 years | 25 years | 30 years | 40 years |

**Figure 2.6:** Maturities quoted for ESTR overnight interest rate swaps provided by Tradeweb as of January 2022.

(see section 2.2.2.1) for overnight indexed swaps: Thus, it is necessary to make an assumption regarding the rates between, for example, the 15- and 20-year maturities. The market standard is to assume that the continuously compounded rate $R(t,T)$ associated with the zero-coupon bond $P(t,T) = \exp\left(-R(t,T)(T-t)\right)$ is linear between these maturity dates. In our example, one would estimate the values of $R(t,T_{16}^F)$, $R(t,T_{17}^F)$, $R(t,T_{18}^F)$, and $R(t,T_{19}^F)$ as a function of $R(t,T_{15}^F)$ and $R(t,T_{20}^F)$:

$$
\begin{aligned}
R(t,T_{16}^F) &= R(t,T_{15}^F) + \frac{R(t,T_{20}^F) - R(t,T_{15}^F)}{5}, \\
R(t,T_{17}^F) &= R(t,T_{15}^F) + 2\frac{R(t,T_{20}^F) - R(t,T_{15}^F)}{5}, \\
R(t,T_{18}^F) &= R(t,T_{15}^F) + 3\frac{R(t,T_{20}^F) - R(t,T_{15}^F)}{5}, \\
R(t,T_{19}^F) &= R(t,T_{15}^F) + 4\frac{R(t,T_{20}^F) - R(t,T_{15}^F)}{5}.
\end{aligned}
$$

This approach of interpolating unavailable prices as the average of their neighbors is further developed in chapter 7, where we show that it leads to a dynamical equation that successfully models most of the stylized facts of the interest rate curve (see chapter 5).

### 2.2.2 Structure of the swap market

In order to establish the market mechanisms that define long-term rates, this section describes the formation of prices in the swap market. Although swaps are among the most traded derivatives by volume (ISDA, 2023) due to their importance in the hedging of banks' balance sheets, swap prices are difficult to observe. This is because these products, which are custom made to client needs, are traded over-the-counter (OTC), meaning that trades are conducted directly between two parties without the oversight of an exchange. As a result, the swap market is structured into two distinct segments, further described in this section: (i) the dealer-to-dealer segment and (ii) the dealer-to-client segment. The dealer-to-dealer segment facilitates the hedging and pricing of swaps by market

makers (i.e., firms that provide liquidity by continuously quoting prices), while the dealer-to-client segment ensures access to these products for other economic agents.

#### 2.2.2.1 The dealer-to-client swap market

The risk management functions of banks use the dealer-to-client market to hedge the interest rate risk arising from their money creation activities. In both the E.U. and the U.S., the dealer-to-client swap market operates primarily through two electronic platforms: (i) Bloomberg and (ii) Tradeweb. These platforms aggregate the continuously streamed prices from all available market makers. Unlike an order book, the bid and ask prices are displayed alongside the names of the dealers and are available for a fixed maximum volume (see Fig. 2.7). Clients can select a dealer on these platforms and request a formal quote for the notional amount they need. As the notional amount increases, the fees charged by the dealer also rise, resulting in a wider bid-ask spread. Therefore, the prices streamed by swap dealers on these platforms, unlike those in the order book of the dealer-to-dealer segment, are not considered as "firm" prices.

| Quotes (e.g. TradeWeb) | | | | |
|---|---|---|---|---|
| Dealer | Bid | | Ask | |
| | Volume | Rate (%) | Volume | Rate (%) |
| Goldman Sax | € 1,000.00 | 0.99 | € 1,000.00 | 1.01 |
| BNP Paribas | € 50,000.00 | 0.98 | € 50,000.00 | 1.02 |
| City Group | € 80,000.00 | 0.96 | € 80,000.00 | 1.03 |

**Figure 2.7:** Example of the trading quotes available on a dealer-to-client electronic platform. Sources: Tradeweb, swap dealers.

Therefore, in the dealer-to-client market, prices are primarily set by market makers, although they must adjust to the supply and demand from clients. These prices are determined by the market makers based on the dealer-to-dealer market, which is presented in the following section.

#### 2.2.2.2 The dealer-to-dealer swap market

The dealer-to-dealer swap market relies on the brokerage activities of four main swap brokers: (i) ICAP, (ii) BGC Partners, (iii) Tradition, and (iv) Tullet. These brokers facilitate the setup of swap contracts between swap market makers in the euro market. According to my interviews with these actors, a large share of these transactions are still conducted through voice orders from market makers to the

swap brokers. The broker then manually matches the bids and asks provided by the various market makers using its services.

In the last decade, to enhance the liquidity of the swap markets, three of the previously mentioned brokers, namely ICAP, BGC, and Tradition, have set up electronic platforms allowing the automated trading of swaps in the major currencies (i.e. euro and U.S. dollars). These platform encourage (via fees discounts notably) their market makers commercial partners to "stream" continuously their prices (i.e. provide the broker with bid and ask prices they agree to trade at, along with the corresponding volumes) in order to allow the building of an order book that is made available to all market participants. However, the key difference between this order book and a traditional Limit Order Book (Limit Order Book (LOB), see section 2.3 for a detailed definition of the microstructure of these organized markets) is that streamed prices are not limit orders waiting to be executed. Instead, they represent a commitment to enter into an OTC contract at the displayed prices, within the limits of the displayed volume.

| Order book (e.g. ICAP) | | | |
|---|---|---|---|
| Bid | | Ask | |
| Volume | Rate (%) | Volume | Rate (%) |
| € 1,000.00 | 0.99 | € 1,000.00 | 1.01 |
| € 50,000.00 | 0.98 | € 50,000.00 | 1.02 |
| € 80,000.00 | 0.96 | € 80,000.00 | 1.03 |

**Figure 2.8:** Example of the order book available on a dealer to dealer electronic platform, sources: ICAP, Swap dealers.

However, following significant monetary policy events, it often happens that none of the swap dealers agrees to stream prices for a few days, leaving the broker "indicative prices" as the only available price information. These indicative prices are derived not only from observed swap transactions but also from various other market information. According to my interviews with swap brokers, the typical pricing methodology for an interest rate swap denominated in euros, in the absence of streamed prices, relies on different information depending on the product's maturity.

- Futures on the ESTR and 3-month Euro Interbank Offered Rate (EURIBOR) (Euro Interbank Offered Rate[7]) are quoted on LOBs (on Euronext-ICE) for maturities up to 2 years and 6 years, respectively. Thus, the indicative price of short-maturity swaps (typically less than three years) is set

[7]EURIBOR is a other benchmark rate in euro defined by the interbank lending rates with a 3-months maturity

consistently with the zero-coupon curves derived from these products.

- Futures on German sovereign bonds with maturities of 1 year, 2 years, 5 years, and 10 years are quoted on LOBs (on Eurex). Swaps with maturities longer than 3 years are priced using the rates of these products, with a spread manually updated several times a day, based on streamed prices and observed transactions of Gadget products (i.e., derivatives exchanging a sovereign rate for a swap rate).

The swap rates for maturities not covered by the Futures on sovereign bonds or the ESTR and EURIBOR Futures are estimated using the closest available maturities plus a spread manually updated from the streamed prices and observed transactions.

According to my interviews, the continuously quoted indicative prices from swap brokers are used by swap dealers to price their interest rate swaps, in conjunction with the market prices of the listed Futures mentioned above.

Overall, swap rates are determined using information from more liquid related products, such as Futures contracts on sovereign bonds and interbank rates, both of which are quoted within limit order books, as presented in the next section.

## 2.3 Futures and sovereign bonds markets

A LOB is a record of all outstanding limit orders in a market, organized by price level. A limit order is an instruction from a trader to buy or sell a specific quantity of an asset at a specified price or better. Limit orders remain in the LOB until they are matched with a corresponding order or canceled by the trader. These orders contribute to the market's liquidity, as they are available for other traders to execute against. In contrast, a market order is an instruction to buy or sell an asset immediately at the best available price according to the existing limit orders. Traders who place limit orders are known as liquidity providers because they add liquidity to the market by offering assets for sale or purchase at specific prices. Conversely, traders who place market orders are known as liquidity takers because they consume the liquidity provided by limit orders. Orders in the LOB are executed according to price-time priority, meaning that orders with better prices are executed first, and among orders at the same price, those submitted earlier are prioritized.

Futures contracts on sovereign bonds and interbank rates are quoted on LOBs. Therefore, unlike swap rates, their prices are perfectly observable. In the following two sections, we present the interbank rate Futures and sovereign bond markets.

### 2.3.1 Interbank rate Futures

In the E.U., Futures contracts on overnight and 3-month interbank rates are currently quoted on the ICE Futures Europe marketplace. The following money market Futures contracts are available:

1. Futures contracts on the 1-month accrued ESTR rate, with maturities ranging from 1 to 24 months;

2. Futures contracts on the 3-month EURIBOR rate, with maturities ranging from 3 to 72 months.

In the U.S., Futures contracts on the SOFR, are currently quoted on the CME Group's exchange. The following SOFR Futures contracts are available:

1. Futures contracts on the 1-month SOFR rate, with maturities ranging from 1 to 24 months;

2. Futures contracts on the 3-month SOFR rate, with maturities ranging from 3 to 120 months.

Among these liquid products, the Futures on the 3-month SOFR are available across the largest range of maturities. Therefore, we model the dynamics of these prices in chapter 7.

### 2.3.2 Sovereign bond market

While swap markets represent the risk-free borrowing cost for the private sector, a complementary risk-free rate can be derived from the prices of the highest-quality sovereign bonds, representing the borrowing cost of the public sector.

#### 2.3.2.1 The cash market

The cash sovereign bond market is segmented into two distinct categories: the *primary market* and the *secondary market*:

- The primary market, often referred to as the "new issues" market, is where transactions occur directly between bond issuers and bond buyers. In this market, brand-new debt securities are created and offered to the public for the first time.

- The secondary market involves the buying and selling of securities that have already been issued in the primary market. Investors can purchase these bonds from a broker, who acts as an intermediary between the buying and selling parties.

In the Euro area, German government bonds are used as the reference risk-free rate, as most market participants consider Germany's debt to be free of counterparty credit risk. The spread between the euro Overnight Indexed Swap (OIS), which is effectively risk-free due to clearing with a nil threshold and daily margining, and German sovereign bonds of the same maturity can be defined as the difference between (i) the supply and demand for German debt, largely influenced by the ECB's asset purchase program, and (ii) the actual risk-free interest rate in euros. Secondary markets for German sovereign bonds are quoted on the MTS marketplace.

The U.S. Treasury market is one of the largest and most liquid bond markets in the world. In particular, U.S. Treasury bonds are actively traded on the secondary market. This market is segmented into a dealer-to-dealer market, where market makers hedge their positions, and a dealer-to-customer market, where dealers buy securities from and sell securities to a variety of clients. Unlike the swap market, most interdealer cash trading takes place on electronic platforms provided by brokers operating LOBs (Chaboud et al., 2022).

#### 2.3.2.2 The Futures market

In the E.U., four types of Futures contracts on German sovereign bonds are quoted on the Eurex marketplace:

- Euro-Schatz Future, delivering a German sovereign bond with a residual maturity between 1.75 and 2.25 years;
- Euro-Bobl Future, delivering a German sovereign bond with a residual maturity between 4.5 and 5.5 years;
- Euro-Bund Future, delivering a German sovereign bond with a residual maturity between 8.5 and 10.5 years;
- Euro-Buxl Future, delivering a German sovereign bond with a residual maturity between 24 and 35 years.

In the U.S., Futures contracts on Treasury bonds are quoted on the CME Group exchange. The following types of U.S. bond Futures contracts are available:

- 2-Year Treasury Note Futures, delivering U.S. Treasury notes with a residual maturity of at least 1 year and 9 months, and up to 5 years and 3 months;
- 5-Year Treasury Note Futures delivering U.S. Treasury notes with a residual maturity of at least 4 years and 2 months, and up to 5 years and 3 months;
- 10-Year Treasury Note Futures, delivering U.S. Treasury notes with a residual maturity of at least 6.5 years and up to 7 and three quarters years ;

- 20-Year Treasury Note Futures, delivering U.S. Treasury notes with a residual maturity between 19 years 2 months, and 19 years 11 months;
- U.S. Treasury Bond Futures, delivering U.S. Treasury bonds with a residual maturity of at least 15 years and less than 25 years.

Due to the higher liquidity and the wider range of products available in the U.S., our analysis in chapter 6 focuses on the U.S. cash and Futures sovereign bond markets. In particular, we establish new stylized facts regarding the direction of information propagation in these markets.

## 2.4 Conclusion

We have described the multiple market microstructures that shape the yield curve. The shortest maturity yields are defined on the interbank market thanks to secured transactions in the U.S. (the SOFR) or unsecured transactions in the E.U. (the ESTR). In order to hedge against the future moves of these short-term funding rates, banks cover their long-term loans thanks to interest rate derivatives. The most traded derivatives by volume are interest rate swaps, although they are difficult to observe. In fact, these products are custom made to client needs, so they are traded OTC without the oversight of an exchange. Therefore, price formation actually occurs within the Futures and bonds markets which are used by all swap dealers as a benchmark for setting their prices. Indeed, these products are traded within LOB so they are easily observable.

As a result, the rest of this thesis focuses on modeling two of these markets: (i) the interbank market, which uniquely defines the shortest maturity of the yield curve (see Part II: "Money Creation in the Repo Market") and (ii) the Futures and bonds markets, which are the most liquid markets defining long-term rates (see Part III: "Liquidity Flows on the Interest Rate Curve").

## Key takeaways

- The shortest maturity yields are defined on the interbank market thanks to secured transactions in the U.S. (the SOFR) or unsecured transactions in the E.U. (the ESTR).
- In order to hedge against future moves of the interbank rate, banks cover their long-term loans through interest rate derivatives.
- The most traded derivatives by volume are interest rate swaps, although they are difficult to observe.
- The Futures and bonds markets are the most liquid markets defining long-term rates.

# Part II

# Money creation in the repo market

# Chapter 3

# Stylized facts in money markets: an accounting and regulatory view

*In this chapter, we reproduce the contents of Le Coz et al. (2024a) and the stylized fact section of Le Coz et al. (2024b) written under the supervision of Michael Benzaquen and Damien Challet. The article Le Coz et al. (2024a) was written with the help of Nolwenn Allaire who allowed us accessing the data from the European Central Bank (ECB).*

Money markets are the place where banks conduct their refinancing operations. They serve as the engine of the money creation process which provides liquidity to the financial system, thus contributing to its stability. Following the surge in counterparty risk during the 2008's GFC, money markets in western countries have undergone significant transformations. In October 2008, the European Central Bank (ECB) introduced the so-called full allotment procedure, which allows banks to request unlimited central bank funding. Concurrently, the implementation of the Basel regulation regarding the Liquidity Coverage Ratio (Liquidity Coverage Ratio (LCR)) aims to enhance the short-term resilience of banks to a liquidity crisis. It requires banks to maintain an adequate level of high-quality liquid assets to fulfill their liquidity needs under a stress scenario. These measures have contributed to the emergence of excess reserves in the financial system (Renne, 2012; Luca Baldo et al., 2017; Piquard and Salakhova, 2019). Additionally, the refinancing of the banking system has shifted towards collateralized lending (using repos, see chapter 2 and section 3.2), and the practice of collateral re-use has become increasingly prevalent (Cheung et al., 2014; Keller et al., 2014; Fuhrer et al.,

2016; European Systemic Risk Board., 2017; Scaggs, 2018; Accornero, 2020).

In this chapter, we review the empirical literature of stylized facts observed recently in money markets and provide our own explanations for some of these phenomena. The network topology of money markets, where transactions among banks are identified as links between nodes, has evolved as a consequence of the recent evolution of these markets. Thus, we also complement these explanations by the presentation of our own measurements regarding the secured funding operations of the 50 largest banks in the eurozone. In particular, while the unsecured market experiences very low density (Boss et al., 2004; Bech and Monnet, 2016; Blasques et al., 2018; Vari, 2020), we observe that repo markets display higher density due to longer transaction maturities.

## 3.1 Excess liquidity and declining unsecured interbank markets

Following the GFC, the ECB implemented a so-called full allotment procedure, which accommodates any liquidity demand from banks in unlimited amounts, as documented by Renne (2017). Subsequently, the volumes of the overnight unsecured interbank market have decreased significantly (see Fig. 3.1). Indeed, the volumes in interbank secured markets drop when excess reserves (i.e. surplus from bank reserves requirements) increase (Piquard and Salakhova, 2019). As explained by a recent ECB survey (Luca Baldo et al., 2017), the increase in excess liquidity between 2012 and 2018 was mainly driven by (i) the greater demand of banks for central bank liquidity, (ii) the full allotment procedure, and (iii) the offer of longer-term refinancing operations. Since 2015, another ingredient has led to a new increase in excess liquidity: the ECB has injected central bank liquidity into the banking system through its asset purchase program (APP). This time, most banks cited increasing client inflows as the main reason for their excess liquidity (Luca Baldo et al., 2017). The resulting decline in unsecured lending was reinforced by the introduction of the LCR in January 2018, which hampered the redistribution of liquidity (Luca Baldo et al. (2017) and section 3.2).

Using individual bank balance sheets, one can show that the combination of the APP and LCR constraint leads to excess liquidity in the financial system. Indeed, for a bank $i$ at time $t$, let us denote, respectively, by $C_i(t)$ and $D_i(t)$, the cash owned by a bank and the deposits it received. We also denote by $S_i^u(t)$ its amount of securities usable as collateral and $S_i^c(t)$ the collateral it received as the lender of cash. The LCR is the ratio of unencumbered assets to net cash outflows over the next 30 days. These outflows are defined as a regulatory prescribed haircut of a bank's liabilities. Formally, within the simplified bank balance sheet

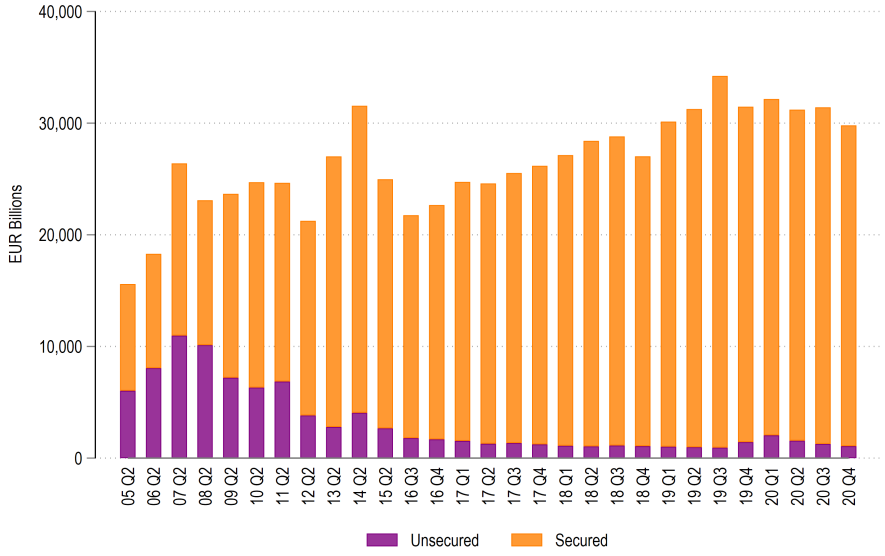


This figure shows cumulative quarterly turnover in the euro area unsecured and secured money market segments. Source: Euro Area Money Market Survey until Q2 2015, Money Market Statistical Repoting (MMSR) data thereafter. Only transactions with deposit-taking institutions and CCPs are considered. Both borrowing and lending transactions are included; all collateral types and maturities are considered.

**Figure 3.1:** Turnover in unsecured and secured euro area interbank money markets

we defined, the LCR is expressed as

$$LCR_i(t) = \frac{C_i(t) + S_i^u(t) + S_i^c(t)}{\beta D_i(t)} \geq 100\%, \tag{3.1}$$

where $\beta$ is the regulatory outflow rate for deposits. The excess liquidity $E(t)$ in the banking system at time $t$ is defined as the sum of the cash in excess of the minimum reserves of the individual banks:

$$E(t) := \sum_{i=1}^{N} C_i(t) - \alpha D_i(t), \tag{3.2}$$

where $\alpha$ is the share of minimum reserves required by the regulation. If we replace $C_i(t)$ by its expression in equation 3.1 and assume all banks cover the same outflow rate $\beta$, equation 3.2 can be written as:

$$E(t) \geq (\beta - \alpha)D(t) - S(t), \tag{3.3}$$

where $S(t)$ and $D(t)$ are respectively the total amount of collateral and deposits in the banking system. Eq. (3.3) shows that the larger the gap $\beta - \alpha$ between the regulatory outflow rate and the required minimum reserve, the higher the excess liquidity. In addition, a decrease in the amount of collateral available generates additional excess liquidity. However, this reasoning does not hold in the presence of interactions between banks. Our ABM actually shows that the asymmetric response of banks to payment shocks also generates excess liquidity even when there is no collateral scarcity (see Sec. 4.1.7).

## 3.2 Evergreen repos to answer LCR regulation

The GFC highlighted the existence of counterparty risk among banks. This led to a transition from unsecured to secured lending (Filippo et al., 2018). Within these markets, collateralized borrowings are performed thanks to repos, i.e., financial contracts exchanging collateral against cash for a given time period. In fact, the substitution effect towards secured markets was reinforced by the introduction of the LCR because of the ability of such contracts to circumvent this constraint. A repo contract continuously renewed by mutual agreement is called an evergreen repo. We show in the following that an evergreen repo with a one-month notice period has no effect on the LCR of the two involved parties. Empirical evidence shows that the introduction of the LCR regulation coincides with an increase in the volumes of traded evergreen repos with a notice period of more than a month (Allen, 2016). In fact, Fig. 3.2 shows that the volume of evergreen repos traded among the 50 largest banks in the eurozone increased from negligible amounts in

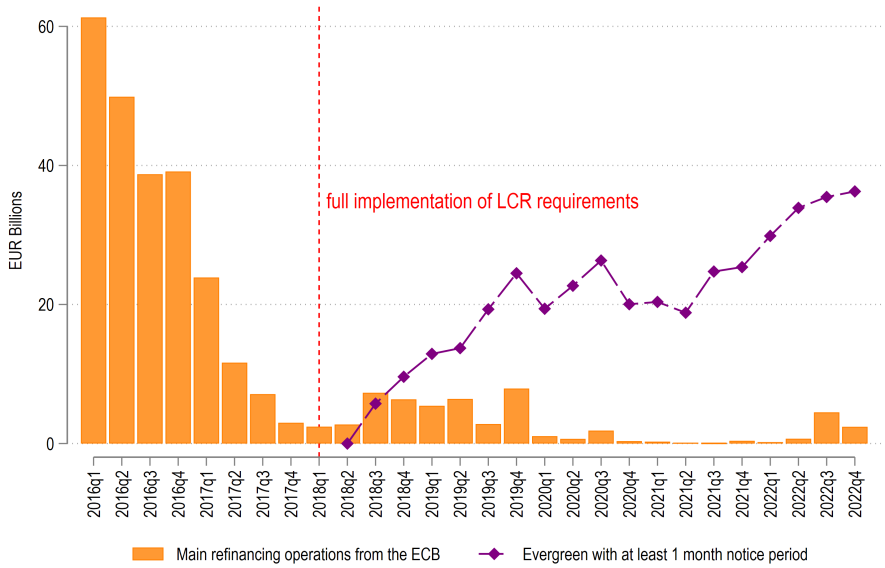


This figure shows aggregate quarterly volumes of main refinancing operations (MRO) implemented by the Eurosystem and aggregate volumes of traded evergreen repos with a notice period greater than 1 month. Source: Internal Liquidity Management for the MRO volumes and Money Market Statistical Reporting (MMSR) data for evergreen repos. Evergreen repos are identified by filtering on repo transactions with a notice period of at least 30 days, with repeating transactions for at least 1 day. Both borrowing and lending transactions are included; all collateral types are considered.

**Figure 3.2:** Evergreen repos

2017 to ten billions per day in 2019. All empirical results presented here were established for the 50 largest banks in the eurozone that are required to report their transactions to the Money Market Statistical Reporting Database (MMSR) as detailed in appendix A.

The use of evergreen repos to circumvent LCR regulation can be explained thanks to the simplified balance sheet of a bank. In the context of a repo agreement, the borrower of cash $i$ remains the owner of the collateral he provided for the transaction. This collateral remains on its balance sheet as *encumbered* securities denoted by $S_i^e(t)$. A new repo of notional $\Delta R$ leads to the increase of encumbered collateral to $S_i^e(t) + \Delta R$. This collateral cannot be used in any other transaction, thus it is excluded from the numerator of the LCR. In contrast, the lender $j$ of cash records this collateral as received collateral $S_i^c(t)$, which compensates for his loss of LCR due to its cash reduction. After the transaction, at $t + \Delta t$, the new

LCR of the borrower $i$ and the lender $j$ remain constant:

$$\begin{aligned} LCR_i(t+\Delta t) &= \frac{(C_i(t)+\Delta R)+(S_i^u(t)-\Delta R)+S_i^c(t)}{\beta D_i(t)} \\ &= LCR_i(t), \end{aligned} \tag{3.4}$$

$$\begin{aligned} LCR_j(t+\Delta t) &= \frac{(C_j(t)-\Delta R)+S_j^u(t)+(S_j^c(t)+\Delta R)}{\beta D_j(t)} \\ &= LCR_j(t). \end{aligned} \tag{3.5}$$

LCR' denominator is the total outflow, generated during a one-month stress test, by a bank's liabilities. In equation 3.4, one could be surprised not to see any outflow from the repo recorded as a liability for the cash borrower. This is possible only if we consider a repo with maturity (or notice period) greater than one month. In addition, to ensure the LCR conservation equation 3.4 for all time $t$, it is necessary to introduce *evergreen* contracts valid at all times. On the opposite, entering in a unsecured interbank loan $\Delta U$ would negatively impact the LCR of the lender and positively impact the LCR of the borrower:

$$LCR_{i,t+\Delta t} = \frac{C_i(t)+\Delta U+S_i^u(t)+S_i^c(t)}{\beta D_i(t)} \geq LCR_i(t), \tag{3.6}$$

$$LCR_{j,t+\Delta t} = \frac{C_{j,t}-\Delta U+S_{j,t}^u+S_{j,t}^c}{\beta D_{j,t}} \leq LCR_{j,t}. \tag{3.7}$$

The substitution effect between the unsecured and secured markets is also influenced by the asset purchase program, which (i) increases the spread between the secured and unsecured rates due to the lower availability of the collateral, and (ii) decreases the volumes on both the secured and unsecured markets as a consequence (Piquard and Salakhova, 2019).

## 3.3 Collateral re-use and bond scarcity

The one-month notice period of evergreen repo forbids the immediate unwinding of existing positions when a lender of cash experiences a liquidity need. Thus, these markets offer the possibility to "re-use" collateral: the lender of cash $j$ is allowed to re-use the collateral $S_{j,t}^c$ he received during a reverse repo in order to borrow cash within another repo transaction. Various definitions have been used to define the re-use rate of collateral within money markets (Accornero, 2020). Here we choose the following definition:

$$\text{re-use}(t) = \frac{\sum_{i=1}^N S_i^r(t)}{\sum_{i=1}^N S_i^c(t)}. \tag{3.8}$$

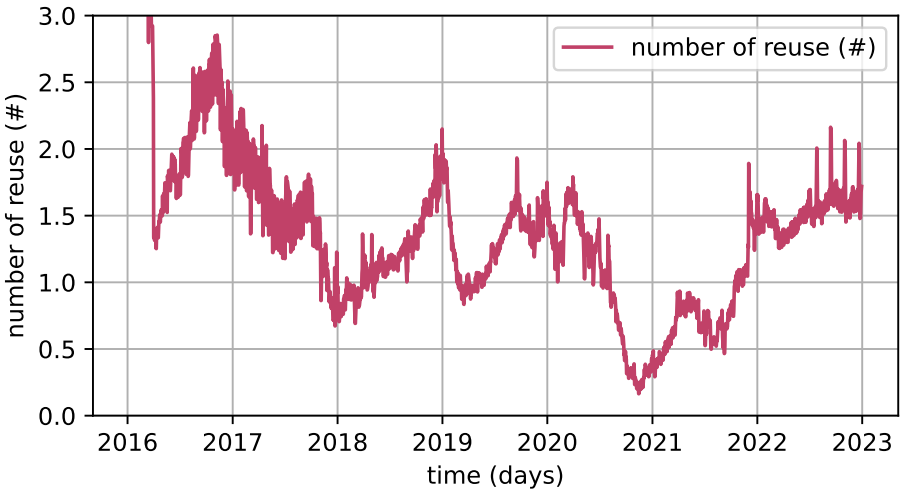


This figure shows aggregate daily number of collateral re-use for reporting banks in MMSR, measuring the length of collateral chains. Only transactions between deposit-taking corporations are considered, all types of collateral are included. Source: Money Market Statistical Reporting database (MMSR).

**Figure 3.3:** Length of the chain of collateral among the 50 largest banks of the eurozone

Various levels of collateral re-use, ranging from 0.1 to 3 have been measured across time and regions: notably a re-use rate around 1 was observed in European money markets (Keller et al., 2014; European Systemic Risk Board., 2017), 0.6 in Australia Cheung et al., 2014, 0.1 in Switzerland (Fuhrer et al., 2016), and 3 in the US (Scaggs, 2018). We confirm a re-use rate around 1 for the eurozone in Fig. 3.3 by measuring the weighted number of times the ISIN code of a given collateral appears in the banking system on a given day.

The high re-use rate observed on money markets is not a threat to the initial objective of the LCR regulation. In fact, the same collateral can appear only once in the numerator of the LCR of a given bank. The other appearances of this collateral are identified as encumbered securities, which are excluded from the LCR.

Re-use increases in response to the scarcity induced by the asset purchase program (Jank et al., 2021). Moreover, re-use contributes to the buildup of leverage (association, 2015; Brumm et al., 2018; Horen and Kotidis, 2018) by inflating balance sheet sizes. Using an infinite-horizon asset-pricing model with heterogeneous agents, Brumm et al. (2018) considers that this increased leverage then significantly increases volatility in financial markets, ultimately reducing welfare.

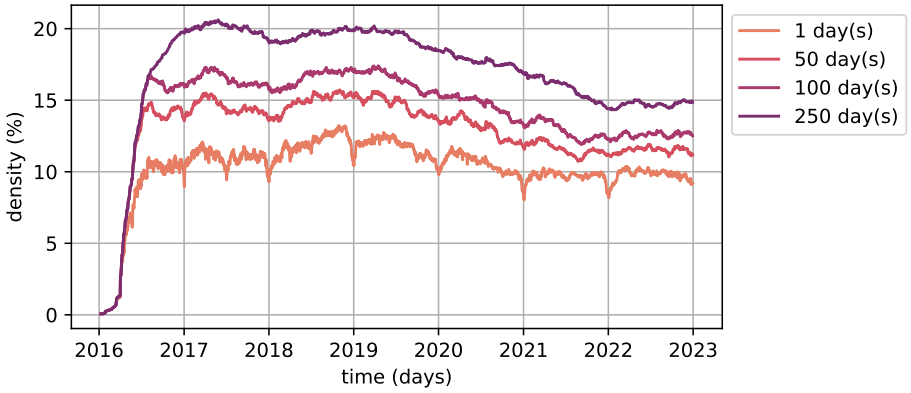


This figure shows the density of the secured segment of the interbank money markets in the euro zone. A link between two reporting banks is defined as the existence of at least one repo transaction over different aggregation periods, each corresponding to a different color: (1) over 1 day, (2) over 50 days, (3) over 100 days and (4) over 250 days. Only transactions between deposit-taking corporations are considered, all types of collateral are included. Source: Money Market Statistical Reporting database (MMSR).

**Figure 3.4:** Density of the repo interbank markets among the 50 largest banks of the eurozone

## 3.4 The interbank network topology

### 3.4.1 Sparse core periphery structure?

We define a link in the interbank network as the existence, over a given aggregation period (typically ranging from one day to one year), of at least one repo exposure between two banks. Historically, interbank market networks have been characterized by a low density and a core-periphery structure (Boss et al., 2004; Bech and Monnet, 2016; Blasques et al., 2018; Vari, 2020). In this network configuration, a central 'core' of highly interconnected nodes is surrounded by a 'periphery' of less connected nodes that primarily connect to the core rather than to each other.

The switch of these markets towards secured transactions led, according to the MMSR data, to an increased network density. Indeed, Fig. 3.4 shows a network density ranging from 10% to 20% depending on the link definition. We assume that this higher density is due to the longer transaction maturity. The limited number of banks in our sample (50) prevented us from studying the core-periphery structure of secured markets.

The limited number of banks in our sample (50) prevented us from studying the core-periphery structure of secured markets.

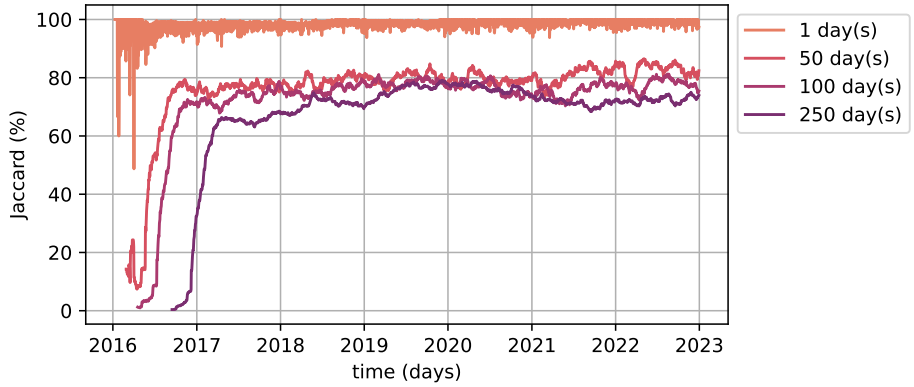


This figure shows the Jaccard similarity coefficient of the secured segment of the interbank money markets in the euro zone. A link between two reporting banks is defined as the existence of at least one repo transaction over different aggregation periods, each corresponding to a different color: (1) over 1 day, (2) over 50 days, (3) over 100 days and (4) over 250 days. Only transactions between deposit-taking corporations are considered, all types of collateral are included. Source: Money Market Statistical Reporting database (MMSR).

**Figure 3.5:** Stability of the repo interbank markets among the 50 largest banks of the eurozone

### 3.4.2 Stable bilateral relationships

The existence of stable interbank relationship lending has been documented, among others, by Furfine (1999), Afonso et al. (2013), and Blasques et al. (2018). We confirm this result in the case of secured markets by measuring the share of stable links from one period to another, namely the Jaccard network similarity index (Verma and Aggarwal, 2020). Fig. 3.5 shows a Jaccard network similarity index ranging from 80 to 100% depending on the aggregation period.

### 3.4.3 Asymmetric in and out degrees?

Several authors reported an asymmetry between in- and out-degrees within unsecured interbank lending networks (Craig and von Peter, 2014; Anand et al., 2015; Lux, 2015). In particular, Craig and von Peter (2014) and Anand et al. (2015) observe that banks in Germany generally have fewer lenders than borrowers.

We observe a more symmetrical pattern in the case of the repo exposures among the 50 largest banks of the eurozone. Figure 3.6 shows that in–degrees expressed as a function of out-degree are almost symmetrical.

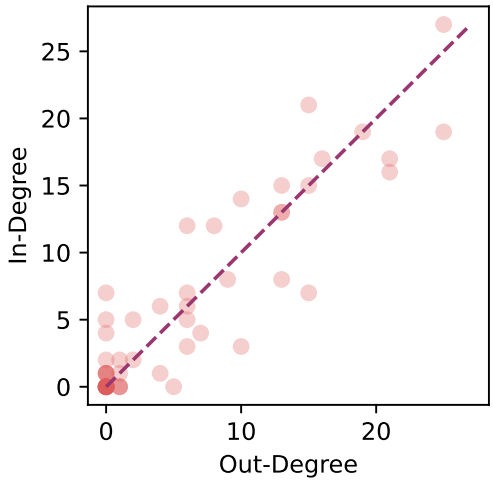


This figure presents the relationship between in and out-degree within the secured interbank money market segment in the eurozone, as of July 3rd 2022. Links are defined through the aggregation of transactions that occurred within the last 50 days. Only transactions between deposit-taking corporations are considered, all types of collateral are included. Source: Money Market Statistical Reporting database (MMSR).

**Figure 3.6:** In–degree as a function of out–degree on 3 July 2022

## 3.5 Conclusion

We have provided both accounting and regulatory explanations for the main recent stylized facts of money markets. One key finding is that excess liquidity can arise due to an insufficient supply of collateral to meet LCR requirements for all banks. The shift of interbank markets toward secured evergreen transactions can be attributed to the introduction of the LCR regulation. Collateral re-use, while widespread across countries, does not pose a threat to LCR compliance, as the same collateral can only appear once in the numerator of the LCR for any given bank. In fact, collateral re-use is essential to meet short-term liquidity needs, given the one-month notice period for evergreen repos.

We have also analyzed secured transactions reported in the MMSR database regarding the 50 largest banks in the eurozone. Our findings reveal a significant increase in the volume of evergreen repurchase agreements, which corresponds to the implementation of the LCR regulation. Furthermore, our assessment of collateral re-use rates is consistent with the existing literature. When examining the structure of the interbank network, our analysis confirms the high stability of trading relationships. However, we observe a higher network density and more balanced in-degree and out-degree connections in secured markets compared to

unsecured ones.

In the following chapter 4, we will present alternative explanations for these stylized facts and quantify them by modeling the interactions among banks.

## Key takeaways

- Excess liquidity can arise due to an insufficient supply of collateral to meet the LCR requirements for all banks.
- The shift of interbank markets toward secured evergreen transactions can be attributed to the introduction of the LCR regulation.

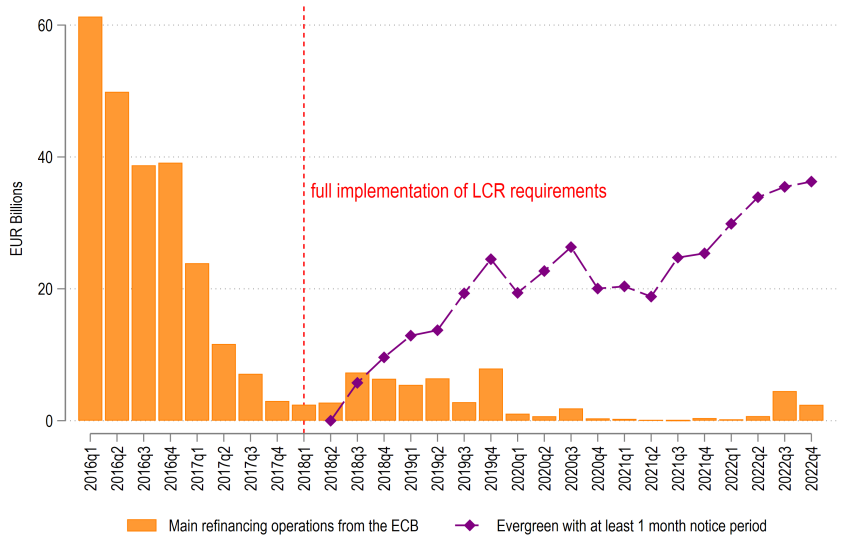


- Collateral re-use is essential to meet short-term liquidity needs, given the one-month notice period for evergreen repos.
- Our analysis of secured transactions reported in the MMSR database concerning the 50 largest banks in the eurozone confirms the high stability of trading relationships in these markets.
- However, we observe a higher network density and more balanced in-degree and out-degree connections in secured markets compared to unsecured ones.

# Chapter 4

# A minimal model of money creation under regulatory constraints

*In this chapter, we reproduce the content of Le Coz et al. (2024b), written under the supervision of Michael Benzaquen and Damien Challet, with the exception of the stylized fact section, which has been moved to the previous chapter.*

Several authors have proposed explanations for the recent changes in money markets presented in the previous chapter, notably excess liquidity or collateral re-use (Renne, 2012; Allen, 2016; Dubecq et al., 2016; Luca Baldo et al., 2017; Filippo et al., 2018; Piquard and Salakhova, 2019; Vari, 2020; Jank et al., 2021). However, these approaches generally refer to complex mechanisms that are difficult to quantify, for example, the high opportunity cost to not hold a non-risky coupon (Piquard and Salakhova, 2019), market fragmentation (Vari, 2020) or collateral scarcity (Jank et al., 2021). Moreover, as detailed in chapter 1, the literature on ABMs has focused so far on the absorption of payment shocks by the banking system through unsecured transactions under reserve constraints (Poole, 1968; Lux, 2015; Bech and Monnet, 2016; Blasques et al., 2018; Liu et al., 2020). In fact, banks endogenously produce money through lending (Jakab and Kumhof, 2015; 2018) and the use of secured transactions raises non-trivial stability questions.

Here we consider money creation and payment shocks within collateralized markets, subject to reserve, LCR, and leverage constraints. Our model shows that excess liquidity and re-use can be explained by regulatory constraints and repo contracts specificities. Our ABM also generates a trading network with high density, stable bilateral trading relationships, asymmetric in– and out– degree distributions as well as a core-periphery structure. Finally, this model is a useful

tool for simulating the systemic effects on financial stability of crisis scenarios or regulatory changes.

## 4.1 A minimal agent-based model

We consider a money market formed by $N$ bank agents, a representative economic agent, and a central bank. Banks can create money by lending to the economic agent. The latter then reallocates his deposits among bank agents, thus generating payment shocks. These shocks are absorbed by the banking system thanks to central bank funding and repos. We assume the existence of a single type of fungible security usable as collateral in the repo market, typically a government bond. Bank agents must respect at all times their reserves, LCR, and leverage regulatory requirements. None of the fixed income instruments in the system offers any coupon.

### 4.1.1 Balance sheet items

Each bank $i$ is characterized by the following accounting items, expressed in monetary units, at each time step $t$ (in units of day).

- Assets:

  - Cash: either deposits at the central bank or reserves, denoted by $C_i(t)$;
  - Securities usable as collateral, denoted by $S_i^u(t)$;
  - Securities encumbered in the context of a repo, denoted by $S_i^e(t)$;
  - Loans to the economic agent denoted by $L_i(t)$;
  - Reverse repos granted to other banks,

$$R_i^r(t) = \sum_{j \neq i} r_{i,j}^r(t),$$

    where $r_{j,i}(t)$ denotes the sum of the open repo exposures at time $t$ that were received by the bank $i$ from the bank $j$.

- Liabilities:

  - Own funds or equity, $O_i(t)$;
  - Deposits, $D_i(t)$;
  - Repo exposures received from other banks,

$$R_i(t) = \sum_{j \neq i} r_{i,j}(t);$$

– Central bank funding, denoted by $M_i(t)$;

• Off-balance sheet:

– Collateral received in the context of a reverse repo, denoted by $S_i^c(t)$;

– Collateral re-used in the context of a repo, denoted by $S_i^r(t)$.

### 4.1.2 Financial contracts

The financial contracts in the model can have either an infinite maturity or no maturity. Repos are evergreen (i.e. have unlimited maturity) with a one-month notice period for cancellation. Therefore, banks must create new repos to remediate immediate liquidity needs as the unwinding of existing reverse repos would provide liquidity too late. When a bank is in excess of cash, it would also have to wait 30 days to unwind its existing repo, while it could immediately earn the repo rate when entering a new reverse repo. Loans, central bank funding, and securities have unlimited maturity. Deposits and cash have no maturity.

As mentioned above, we assume that none of these financial instruments offers any coupon. Indeed, simulating yields dynamics is not necessary to reproduce excess liquidity, repo re-use, and network topology stylized facts. In fact, the yields of each financial contract are incorporated within banks' behavioral rules because they prefer holding the instrument delivering the highest coupon. This requires defining the relative static yields of each financial contract. Hence, in our model, securities used as collateral deliver a higher interest rate than the discount facility rate remunerating banks' cash balances. This assumption is consistent with empirical observations. For example, in the eurozone, 10-year German government bonds have almost systematically delivered higher coupons than the ECB discount facility rate. In addition, the rate of the central bank funding is higher than the repo rate, therefore banks have an incentive not to borrow from the central bank. The repo market rate is higher than the discount rate, so banks accept entering into reverse repo when they are in excess of cash. Finally, we assume that the loan rate to the real economy is the highest rate available to a bank agent.

### 4.1.3 Regulatory constraints

Banks are subject to three regulatory obligations.

1. The minimum reserves constraint: banks must keep a share of the deposits they receive in the form of central bank reserves, i.e.,

$$C_i(t) \geq \alpha D_i(t). \tag{4.1}$$

2. The LCR constraint, requiring banks to maintain the ratio of their unencumbered assets to cash outflows over the next 30 days above one; within our model's balance sheet for banks, the LCR constraint amounts to

$$C_i(t) + S_i^u(t) + S_i^c(t) \geq \beta D_i(t), \tag{4.2}$$

assuming a regulatory net deposit outflow $\beta$ and that the securities received in the context of a repo $S_i^c(t)$ will remain unencumbered during a one-month stress test. In the following sections, we will refer to the effective $\beta_i(t)$ defined by

$$\beta_i(t) = \frac{C_i(t) + S_i^u(t) + S_i^c(t)}{D_i(t)}, \tag{4.3}$$

as the liquidity ratio or the LCR ratio of the bank $i$. This means that the bank can face an outflow rate $\beta_i(t)$ of its deposits – which must be higher than the regulatory $\beta$.

3. The leverage ratio (or solvency ratio) constraint, requiring banks to keep their own funds above a certain share of their total assets:

$$O_i(t) \geq \gamma \left( C_i(t) + S_i^u(t) + S_i^e(t) + L_i(t) + R_i^r(t) \right). \tag{4.4}$$

It is worth mentioning that the leverage ratio plays the same role as the solvency ratio, as it requires banks to maintain a minimum level of own funds. The solvency ratio is more complex to account for as it involves risk measurement. It is also less binding than leverage constraints for low risk activities (Bourahla et al., 2018). Thus, we choose to ignore solvency ratio constraints in our model.

### 4.1.4 Initialization or money creation

All financial instruments in the model are created endogenously. Each bank $i$ can create an amount $\Delta X_i(t)$ of new money at step $t$ by lending cash to the representative economic agent. The latter must then store the same amount in the form of a deposit at the bank $i$. To ensure that the money creation process is compatible with the three regulatory constraints, the value of newly created securities and own funds must be proportional to that of new loans. Securities are typically government bonds issued by the representative economic agent and bought by the banking system. As the government also stores the borrowed cash in the form of a deposit to the banking system, this mechanism increases the usable deposits and securities in the banks' balance sheets. In addition, own funds are issued by banks and bought by the economic agent using some of the cash borrowed from banks.

In summary, the creation of $\Delta X_i(t)$ monetary units by the bank $i$ at step $t$ involves three steps: (i) lending, (ii) issuance of the government bonds, and (iii) capital increase of bank $i$ by issuing new shares. The combined effect of this three actions results in the increase of each of the balance sheet item $A$ by its corresponding variation $\Delta A$:

$$\begin{cases} \Delta D_i(t) := (1-\gamma_{\text{new}})\Delta X_i(t) \\ \Delta L_i(t) := \Delta X_i(t) - \beta_{\text{new}}(1-\gamma_{\text{new}})\Delta X_i(t) \\ \Delta S_i^u(t) := \beta_{\text{new}}(1-\gamma_{\text{new}})\Delta X_i(t) \\ \Delta O_i(t) := \gamma_{\text{new}}\Delta X_i(t), \end{cases} \tag{4.5}$$

where $\gamma_{\text{new}} \in [0,1]$ and $\beta_{\text{new}} \in [0,1]$ are the parameters governing respectively the issuance of shares and securities. In practice, unless otherwise specified, we assume $\beta_{\text{new}} = \beta$, such that enough collateral is created to meet regulatory obligations. The other accounting items are generated either by (i) repo transactions (encumbered securities, collateral received, and collateral re-used) or (ii) central bank funding (main refinancing operations and cash).

### 4.1.5 Money creation shocks

We simulate money creation thanks to a multiplicative random growth process in which shocks fluctuate around an average rate $g$ of new money. Let $(Z_i(t))$ be log-normal random variables of volatility $v$ independent across banks $i$ and steps $t$. The amount of created money $\Delta X_i(t) = X_i(t+1) - X_i(t)$ is given by

$$\begin{aligned} \Delta X_i(t) &= g Z_i(t) X_i(t), \\ X_i(0) &= x_0 Z_i(0), \end{aligned} \tag{4.6}$$

where $g$ is the growth rate of money.

Neither the process $X_i(t)$ nor its normalized version $\frac{X_i(t)}{\sum_{i=0}^{N} X_i(t)}$ converge towards a stationary distribution (Marsili et al., 1998; Gabaix, 1999; Bouchaud and Mézard, 2000; Mitzenmacher, 2004). However, we report in appendix B.1 that the normalized size of banks $\frac{X_i}{\sum_i X_i}$ behaves as a non-stationary log-normal distribution that evolves very slowly compared to the typical time scale of the model. Notably, the tail of this log-normal distribution remains stable within a given range, for a sufficiently long time (around 5000 steps) for the network to reach a state close to stationarity (see section 4.2.1). It is not feasible to design a random growth model that generates a stationary limit using the approaches proposed by Marsili et al. (1998), Gabaix (1999), and Bouchaud and Mézard (2000). Indeed, these models either require defining a negative drift (Marsili et al., 1998; Gabaix, 1999)

or facilitating cash exchanges between banks (Bouchaud and Mézard, 2000) (see appendix B.1).

In the empirical literature, there is no consensus regarding the size distribution of banks. Most authors (Janicki and Prescott, 2006; Lux, 2015; Cerqueti et al., 2022) suggest that this distribution follows a power law with a tail exponent between 1 (Zipf's law) and 3 across time and regions. However, Goddard et al. (2014) argue that bank sizes are better described by a truncated log-normal distribution. Differentiating between a power law and a log-normal distribution is challenging with small sample sizes. In the context of banks, there are only a few thousand financial institutions within a given monetary zone, which limits the ability to accurately assess their size distribution.

In our model, as long as bank sizes are sufficiently heterogeneous, we observe that the specific distribution of bank sizes (log-normal or power law) does not influence the stylized facts previously mentioned. Hence, in order to reach faster stationarity, we conduct our parameter space (see section 4.2.2) and stress tests analyses (see section 4.2.3) by initializing money creation $X_i(0)$ as a power law of tail exponent $\nu$. In such a case, the volatility $v$ of the random growth is set to zero to maintain the initial size distribution of banks over time.

### 4.1.6 Payment shocks

Once money is created, economic agents transact goods. Each transaction results in an increase in the deposits in the bank of the seller and a decrease in the deposits in the bank of the buyer. The total amount of deposits in the banking system remains constant during these transactions. Similarly to the approach of Lux (2015), we simulate payments thanks to normally distributed shocks defined to ensure that (i) the total sum of deposits is conserved and (ii) there is mean reversion toward the amount of deposits created by the bank. Formally, the deposits variation caused by payment shocks at step $t$ for the bank $i$ is defined by

$$\Delta' D_i(t) := \sigma \left[ \bar{D}_i(t) - D_i(t) + \epsilon_i(t) D_i(t) - \frac{1}{N} \sum_{j=1}^{N} \bar{D}_j(t) - D_j(t) + \epsilon_j(t) D_i(t) \right], \tag{4.7}$$

where $(\epsilon_i(t))$ are normalized centered and independent Gaussian shocks and $\bar{D}_i(t) = (1-\gamma_{\text{new}})X_i(t)$ is the target of the mean reversion, updated according to the money creation process $X_i(t)$.

For large values of $\sigma$, it is possible that the deposit shock $\Delta' D_i(t)$ increases in absolute value compared to current bank deposits $i$. To ensure that deposits after the shock (that is, $D_i(t) + \Delta' D_i(t)$) are positive, we choose $\sigma \leq 10\%$. This means that a shock must exceed $10 \times \sigma$ to generate negative deposits. Although

such events are very rare, we apply a floor to banks' deposits, preventing them from going below zero.

Stock flow consistency imposes to increase the cash balance of bank $i$ at each time step $t$ by the same amount, i.e.,

$$\Delta' C_i(t) := \Delta' D_i(t). \tag{4.8}$$

### 4.1.7 Banks' behavioral rules

Money creation and payment shocks modify the balance sheet of banks and can lead to a breach of their regulatory constraints. If that is the case, central bank funding and repo markets are used by bank agents to meet these obligations. To enhance readability in this section, we assume that all the inequalities characterizing regulatory constraints for bank agent $i$ are equalities before the money creation and payment shocks, i.e.

$$\begin{cases} C_i(t) = \alpha D_i(t), \\ C_i(t) + S_i^u(t) + S_i^c(t) = \beta D_i(t), \\ O_i(t) = \gamma^* \left( C_i(t) + S_i^u(t) + S_i^e(t) + L_i(t) + R_i^r(t) \right). \end{cases} \tag{4.9}$$

In fact, the model structurally generates excess liquidity (i.e. $C_t \geq \alpha D_t$) and excess LCR (i.e. $C_t + S_t^u + S_t^c \geq \beta D_t$), because of the asymmetric responses of banks to payment shocks, as further described below. At the beginning of step $t+1$, the bank $i$ receives a money creation shock and a payment shock. To meet its three regulatory constraints, the bank will act as follows.

1. *LCR management.* Secured lending keeps the LCR level unchanged (see section 3.2). Hence, in the absence of an unsecured market, banks optimize their LCR levels through central bank funding. We denote $\Delta M_i(t)$ the amount of central bank funding that the bank $i$ will request or end from to maintain its LCR at the level $\beta$. Bank $i$ must minimize their central bank funding $M_i(t)$ such that:

$$\Delta M_i(t) \geq \beta \left( \Delta D_i(t) + \Delta' D_i(t) \right) - \Delta S_i^u(t) - \Delta' D_i(t). \tag{4.10}$$

   We assume that the share of securities created during the money creation process is equal to the regulatory LCR level $\beta_{\text{new}} = \beta$. The optimal funding is given by

$$\Delta M_i(t) = \max \left\{ -(1-\beta)\Delta' D_i(t), -M_i(t) \right\}. \tag{4.11}$$

   Hence, a negative payment shock will lead the bank to request central funding. In contrast, a positive shock leads to a reduction in central bank funding or an excess of LCR. Overall, the net sum of central bank funding is positive, which introduces excess liquidity in the system.

2. *Reserve management.* Banks use repos to optimize their central bank reserves. The one-month notice period of these contracts requires banks to open new long or short positions to manage their short-term liquidity. Banks will close some of their existing repos only to meet their leverage ratio obligations (see next paragraph). We denote $\Delta R_i(t)$ the amount of repo requested by the bank $i$ (if $\Delta R_i(t) > 0$) or of reverse repo that the bank $i$ is willing to accept (if $\Delta R_i(t) < 0$) in order to maintain its LCR at a target level $\beta$. Bank $i$ must minimize its repo exposure $R_i(t)$ such that

$$C_i(t) + \Delta' D_i(t) + \Delta M_i(t) + \Delta R_i(t) \geq \alpha(D_i(t) + \Delta D_i(t) + \Delta' D_i(t)). \tag{4.12}$$

If $\beta = \beta_{\text{new}}$ and the bank was not in excess of reserve before the shocks, we have

$$\Delta R_i(t) = -\Delta M_i(t) - (1-\alpha)\Delta' D_i(t) + \alpha \Delta D_i(t). \tag{4.13}$$

If we also assume an absence of excess LCR, i.e. $\Delta M_i(t) = -(1-\beta)\Delta' D_i(t)$, the previous equation becomes

$$\Delta R_i(t) = -\left\{(1-\alpha) - (1-\beta)\right\} \Delta' D_i(t) + \alpha \Delta D_i(t). \tag{4.14}$$

Most banking regulations typically set $\alpha < \beta$, so the difference $(1-\alpha)-(1-\beta)$ is positive. If we neglect money creation shocks (i.e. $\Delta D_i(t) \ll \Delta' D_i(t)$), it is clear that receiving a negative payment shock implies requesting repos. In contrast, a positive shock leads the bank to be willing to enter into a reverse repo. Nevertheless, it is possible that this bank does not hold sufficient collateral to enter into a repo, in this case, it will request additional central bank funding.

3. *Leverage management.* The management of reserves through the opening of repos and reverse repos inflates banks' balance sheets (association, 2015; Brumm et al., 2018; Horen and Kotidis, 2018). If the current leverage ratio of a bank becomes lower than its targeted level $\gamma^*$, it will start ending its existing repos after each positive shock. Contrary to the LCR and reserves constraints, banks do not have immediate solutions available to reduce the size of their balance sheet. Hence they choose a target leverage ratio greater than the regulatory requirement, $\gamma^* > \gamma$. As a consequence, banks start closing their existing repos before risking a breach of their minimum leverage ratio.

### 4.1.8 Sequence of the interactions among agents

We assume that repos are initiated and ended by the borrowers of cash. Banks are ready to participate in the repo market after the individual management of their LCR. Market clearing is performed as follow:

1. All banks having to end existing repos do so one by one in a shuffled order. Bank $i$ starts by contacting its counterparts with the lowest trust level $\phi_{ij}$ (whose dynamics is described below). If the lender of cash $j$ has not sufficient collateral $S_j^c$ to end its reverse repo, bank $j$ must end some of its own repos. We assume that the lender of cash receives its cash back slightly before providing back the collateral to the cash borrower. This mechanism ensures that the lender of cash $j$ owns enough cash to close its existing repos and get back its re-used collateral. This situation can trigger a cascade of collateral call backs (further detailed below).

2. Then, banks having to enter into repos do so one by one in another reshuffled order. This time, the bank $i$ starts by contacting their counterparts with the highest trust factor $\phi_{ij}$. These latter accept entering into a reverse repo if they are in excess of cash, i.e. $\Delta R_{j,t} < 0$.

Naturally, banks can engage simultaneously into repos and reverse repos. However, this can lead to a collateral loop if a security is loaned to one bank and then re-loaned to the original lender. In such cases, in our model, the sequential call of collateral to unwind existing repos might not converge. Prohibiting all collateral loops would lead to a rapid collapse of money markets because of the high density of the repo network. Therefore, our model permits these loops, even though it means that some simulations may not run to completion. In actual markets, when two counterparties within a collateral loop want to unwind their positions, they compute directly their net exposures. It is possible that none of the two banks still owns the collateral. In this case, the counterparty who is short of collateral would usually borrow the security (using a reverse repo). In our model, as a simplification, only banks experiencing liquidity needs request funding through repos.

### 4.1.9 Trust coefficients

As proposed by Lux (2015), bilateral trading relationships rely on trust coefficients $\phi_{ij} \in [0, 1]$ indicating the strength of the ties established by repeated contact. The trust coefficient from the bank $i$ to $j$ is initialized randomly and updated each time $i$ requests a repo from bank $j$. $\phi_{ij}$ increases if $j$ agrees to lend to $i$ and decrease

otherwise: $\phi_{ij}(t+1) =$

$$\phi_{ij}(t) + \lambda \left( \frac{(\min(\Delta R_i(t), -\Delta R_{j,t}))^+}{\Delta R_i(t)} - \phi_{ij}(t) \right) \tag{4.15}$$

where $\lambda$ is a learning coefficient, governing the time scale at which banks update their trusts and $(x)^+$ is the maximum between $x$ and 0. Eq. (4.15) means the trust coefficients converge towards the share of the repo exposure accepted by the bank $j$.

### 4.1.10 Synthesis

We can sort the variables and parameters of the model into four categories:

1. Four exogenous variables are set by the economic agent through monetary and payment shocks: the amount of deposits $D$, loans $L$, securities $S^u$, and own funds $O$.

2. 7 parameters act as the control parameters of the model. They are constant across banks and time. $\beta_{\text{new}}$, the deposit outflow rate equivalent of new securities, tunes the creation of new securities in the system. $\gamma^*$, the target leverage ratio, and $\gamma_{\text{new}}$, the leverage ratio equivalent of new own funds, control the repo re-use rate. $g$ and $v$ are respectively the mean and volatility of monetary shocks. If specified, the exponent $\nu$ of the power law distribution of bank sizes governs the heterogeneity among banks. $\sigma$ is the volatility of payment shocks size and $\lambda$ controls the speed at which trust levels are updated.

3. The regulatory constraints are set by the regulator.

4. The other variables are endogenously updated.

Table 4.1 provides the list of variables defining and controlling the state of the bank agent $i$.

| | Definition | Type |
|---|---|---|
| $L_i$ | Loans | Exogenous |
| $D_i$ | Deposits | Exogenous |
| $\gamma^*$ | Target leverage ratio | Control |
| $\beta_{\text{new}}$ | Deposit outflow rate equivalent of new securities | Control |
| $\gamma_{\text{new}}$ | Leverage ratio equivalent of new own funds | Control |
| $v$ | Volatility of money creation shocks | Control |
| $g$ | Mean growth of money creation | Control |
| $\sigma$ | Volatility of payment shocks | Control |
| $\lambda$ | Learning coefficient to update trust | Control |
| $\phi_{ij}$ | Trust to the bank $j$ | Endogenous |
| $C_i$ | Cash account | Endogenous |
| $S_i^u$ | Securities usable | Endogenous |
| $S_i^e$ | Securities encumbered | Endogenous |
| $R_i^r$ | Reverse repos granted to other banks | Endogenous |
| $O_i$ | Own funds | Endogenous |
| $R_i$ | Repo exposures | Endogenous |
| $M_i$ | Central bank funding | Endogenous |
| $S_i^c$ | Collateral received | Endogenous |
| $S_i^r$ | Collateral re-used | Endogenous |
| $\alpha$ | Regulatory share of minimum reserves | Regulation |
| $\beta$ | Regulatory LCR outflow of deposits | Regulation |
| $\gamma$ | Regulatory leverage ratio | Regulation |

**Table 4.1:** List of parameters and variables.

## 4.2 Results

### 4.2.1 Dynamical behavior

A typical run of the model reproduces most of the money markets' stylized facts in its stationary state. Unless specified differently we fix $g = 0.04\%$, and $v = 5$. It means banks increase their balance sheet by 10% a year (1 year $\approx$ 250 steps) on average but some agents can grow on a given day at a 50% annualized rate. We also set $N = 300$ to obtain results comparable to those from MMSR database containing 50 banks (Le Coz et al., 2024a). Payment shocks are assumed to be quite volatile ($\sigma = 5\%$). All regulatory parameters are set according to their actual value in the euro zone $\alpha = 1\%$, $\beta_{\text{new}} = \beta = 50\%$ (that is, the average outflow rate for all types of client deposits), $\gamma^{=}3\%$. We choose $\gamma^* = 4.5\%$ to ensure that banks satisfy their leverage constraints and $\gamma_{\text{new}} = 9\%$ to generate sufficient collateral re-use. We also set the learning coefficient $\lambda$ to 0.5 and the average initial size of banks $x_0$, to 0.01 monetary units. Indeed, we assume that one monetary unit in the model corresponds to one billion euros. Thus, we initialize the average capital of all banks to 10 millions euros, which is close to the minimal own funds required for a banking license (5 millions in the eurozone, article 12 of CRD IV).

Excess liquidity naturally appears as the result of asymmetric responses to payment shocks (see Fig. 4.1). The amount of excess liquidity generated by the model is between 5 and 10% of total assets, in line with the levels observed in the eurozone (Hudepohl et al., 2024). This shows that the origin of excess liquidity can be traced back to the interactions between the reserves and LCR constraints, as banks cannot maintain both requirements to their minimum levels and absorb daily payment shocks. Note that the exponential growth of the banking system at a 10% rate requires measuring normalized values to observe a stationary state.

Figure 4.2 displays a phase in which securities are consumed faster by the banking system than they are issued by the government, leading to a decrease of usable securities. When no securities remain, banks start to re-use collateral. The average rate of re-use converges to approximately 0.9 (i.e., the typical length of a collateral chain is 2, in line with the observations of Le Coz et al. (2024a)), because of the leverage constraint, which limits the balance sheet size of banks.

The model generates a relatively high density network compared to an unsecured lending network (see the ABM of Lux (2015)). Figure 4.3a shows a slow convergence of network density towards a regime close to stationarity because of the slow evolution of bank size distribution. Indeed, the heterogeneity in bank sizes never reaches a stationary state, even though the typical time scale required to observe non-stationarity is longer than our simulation window (see appendix B.1). We also find that some other combinations of input parameters lead the model

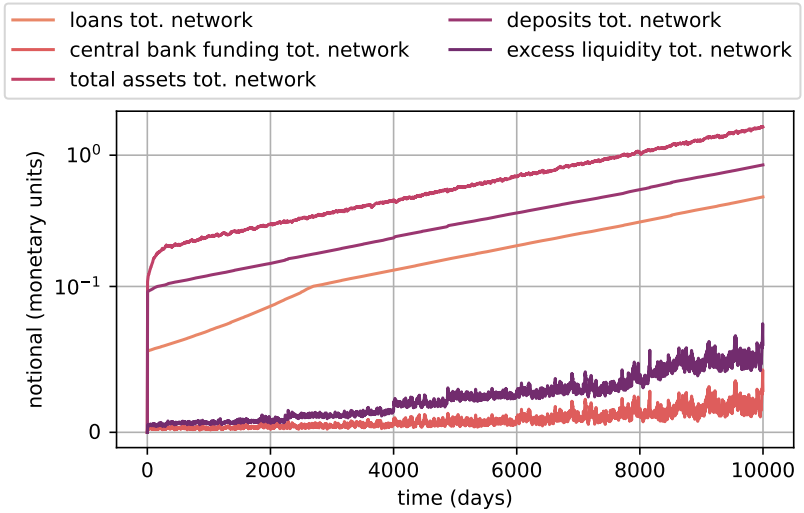


**Figure 4.1:** Time evolution of the main macroeconomic aggregates in the simulated banking system.

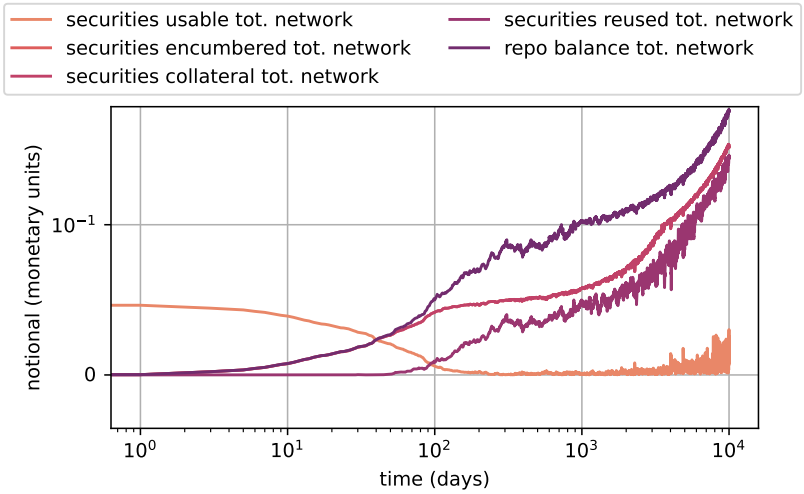


**Figure 4.2:** Time evolution of the collateral aggregates in the simulated banking system.

with random growth (i.e., when $v \neq 0$) to generate a slowly increasing or decreasing density.

However, the model with equal growth rate (i.e. $v = 0$) reaches a stationary state for a wider range of input parameters. In this case, the constantly increasing amount of new loans and deposits still slows down the convergence by increasing the average maturity of repos. However, a stationary regime is reached as long as the payment shocks are large enough to end these transactions (that is, $\sigma \geq 5\%$ according to our observations). Below this level, a stationary state can be reached by increasing the leverage constraint (i.e., a higher $\gamma^*$) or reducing the capital increase rate $\gamma_{\text{new}}$. This action would result in a reduction of collateral re-use (see section 4.2.2).

We use the Jaccard network similarity index to characterize the stability of bilateral trading relationships from one period to another. The level of network stability exhibited in Fig. 4.3b is consistent with observations on real financial networks (Furfine, 1999; Afonso et al., 2013; Blasques et al., 2018). As mentioned above, a stationary state cannot be reached because of the slow evolution of bank size heterogeneity. Once again, this instability vanishes in the model with uniform growth rate (i.e. $v = 0$).

Figures 4.4 and 4.5 show that a core-periphery structure emerges from the network, even if the density is much higher than the one reported in Lux (2015). Notably, Fig. 4.5 reports the time evolution of the p-values from the Lip core-periphery test (Lip, 2011): this kind of structure emerges after about 5000 steps and is then stationary. However, other methods for assessing the significance of core-periphery (Borgatti and Everett, 2000; Boyd et al., 2010; Rossa et al., 2013; Cucuringu et al., 2016; Rombach et al., 2017; Kojaku and Masuda, 2018a; b), based on different ways to characterize a core-periphery structure, do not lead to conclusive results.

Finally, the generated network exhibits a slightly asymmetric in– and out–degree distribution (see Fig. 4.6), in line with the literature (see section 3.4).

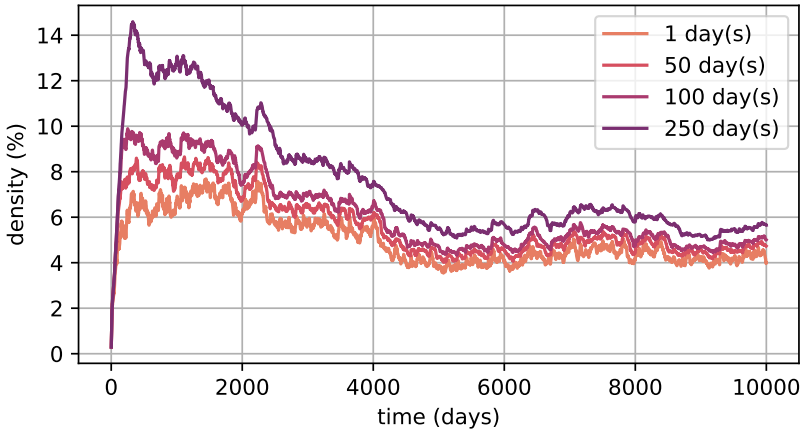


**(a)** Network density.

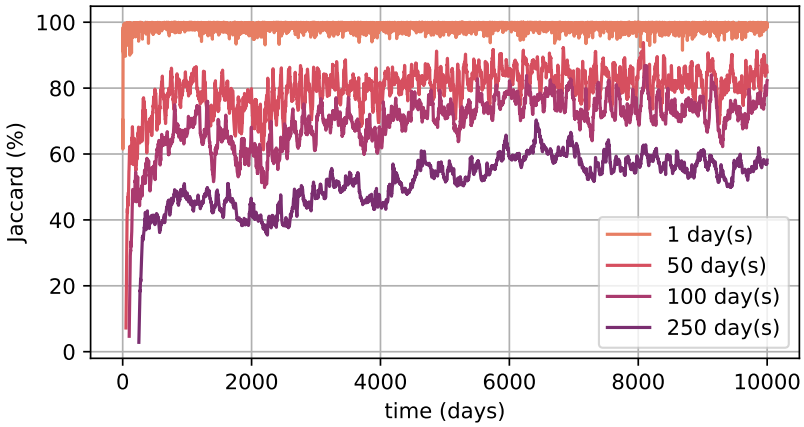


**(b)** Jaccard network similarity index.

**Figure 4.3:** Time evolution of the network density (4.3a) and the share of stable links from one period to another (4.3b) in the simulated money markets. A link is defined as the existence of at least one repo over different aggregation periods, each corresponding to a given color. Pseudo-stationarity is reached after 6000 steps due to the time of convergence toward a sufficiently unequal distribution of banks.

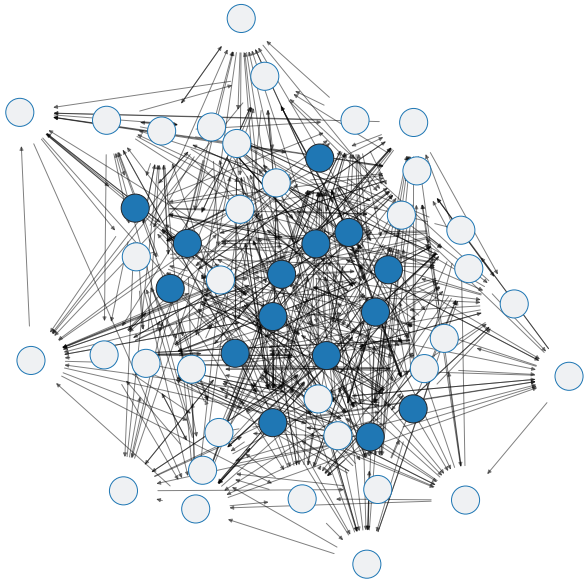

**Figure 4.4:** Core-periphery structure after 5000 steps for 50 banks. Links are defined through the aggregation of transactions that occurred within the last 50 days. The core banks are identified through the method proposed by Lip (2011), with a p-value of $10^{-10}$.

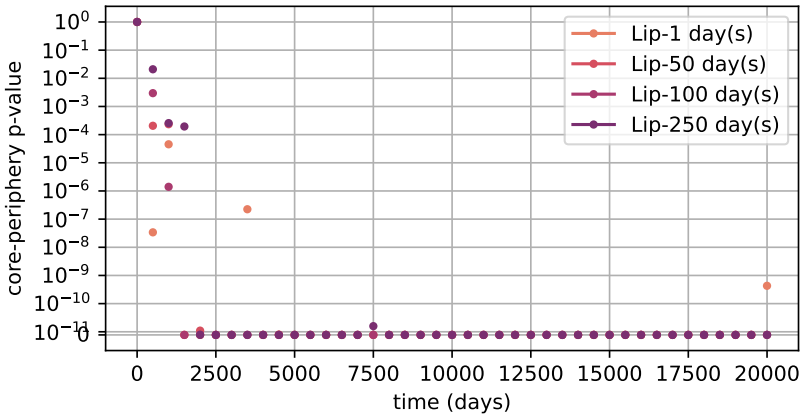


**Figure 4.5:** Time evolution of the p-values assessing the existence of a core-periphery structure according to the method proposed by Lip (2011) for 300 banks. A link is defined as the existence of at least a repo over different aggregation periods, corresponding to each color. The core-periphery structure emerges after 5000 steps for all aggregation periods.

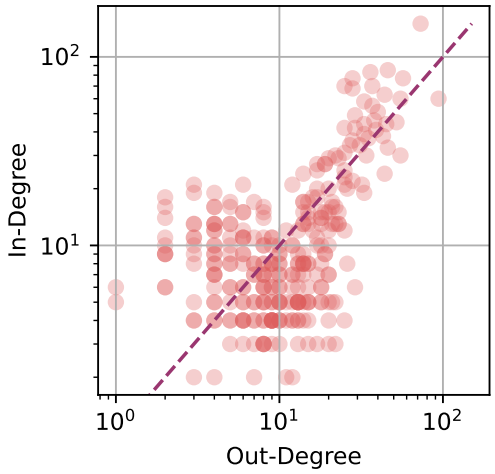


**Figure 4.6:** In–degree as a function of out–degree after 10000 steps. Links are defined through the aggregation of transactions that occurred within the last 50 days.

### 4.2.2 Parameter space

Here, unless specified differently, we fix $g = 0.04\%$, $v = 0$ and $\nu = 1.4$. It means that banks increase their balance sheet by 10% a year (1 year $\approx$ 250 steps) while keeping their size distribution (a power law with exponent 1.4) constant. We also set $N = 100$ and $\sigma = 8\%$ to reach the stationary state faster. All other parameters are set as in the section 4.2.1. Each simulation is conducted over 10000 steps. For a given simulation, we define the stationary value of a given observable metric (for example, the network density) as its average across the last 200 steps of the run. We simulate the same run (i.e. the same combination of input parameters) 100 times. We finally report the mean over 100 runs, excluding values outside of one standard deviation, of the stationary level of a given metric.

**4.2.2.0.1 The effect of deposit outflow rate** We assume $\beta = \beta_{\text{new}}$ in all simulations, ensuring that there is always enough collateral to meet the LCR needs of each bank.

For high values of $\beta$ (i.e. $\geq 90\%$) there is much collateral available to absorb the payments shocks. This results in shorter collateral chains or lower re-use rate (Fig. 4.7b). High values of $\beta$ are also associated to high network density (Fig 4.7c) because the amount of repo required by each bank is proportional to $(1 - \alpha) - (1 - \beta)$ (see section 4.1.7). In other worlds, banks do not use central bank funding to manage their LCR ($\Delta M = (1 - \beta) \ll 1$), therefore the excess liquidity is minimal (Fig. 4.7a) and even the smallest shocks must be absorbed on

the repo market.

When $\beta$ decreases ($\beta \in [40\%, 90\%]$), banks have to rely more on central banking funding to manage their LCR, thus generating higher excess liquidity (Fig. 4.7a) and lower network density (Fig 4.7c). One could have expected collateral re-use to decrease because excess liquidity reduces the effect of payment shocks. Yet, Fig. 4.7b shows the opposite. This is because the total collateral available in the system starts becoming insufficient to cover all shocks, a state that we define as collateral scarcity. It does not mean that there is not enough collateral for all banks to meet their LCR requirements, but that the total amount of repo required to absorb payment shocks is higher than the available collateral. Banks react to collateral scarcity by increasing the length of collateral chains (Fig. 4.7b) in line with empirical observations (Jank et al., 2021). We also observe a lower slope of the relationship between the density and the deposit outflow rate (Fig 4.7c) for $\beta \in [50\%, 75\%]$: this is because collateral scarcity reduces the chances of opening new repos, which allows existing repos to have a longer maturity.

However, for $\beta$ lower than $40\% \approx 5\sigma$, there is not enough collateral in the banking system to absorb the payment shocks, so banks start relying on central funding for reserves management, generating high excess liquidity (Fig. 4.7a), low network density (Fig 4.7b) and low collateral re-use (Fig. 4.7b).

Figure 4.8 shows that the core-periphery structure is significant for $\beta$ in the range of 40 to 80%. Outside of these limits, the density is either too high or too low to generate such a structure.

**4.2.2.0.2 The effect of payment shocks' volatility** The lower the volatility of payment shocks, the higher the repo maturity as shown in Fig. 4.9a (note the log-scale on the abscissa axis). In fact, a low volatility of deposits allows banks to hold their positions for longer periods. As a consequence, a low volatility of payment shocks is also associated with high network density (Fig. 4.9b), high Jaccard network similarity index (Fig. 4.9c), and high collateral re-use rate (Fig. 4.10). Conversely, the excess of liquidity in the banking system increases with the volatility of payment shocks (Fig. 4.11). Indeed, as explained in section 4.1.7 banks' LCR management generates excess liquidity to absorb payment shocks.

**4.2.2.0.3 Sensitivity analysis** Appendix B.2 shows the effect of three other control parameters: (i) the rate of capital increase, $\gamma_{\text{new}}$; the tail exponent, $\nu$, governing bank sizes heterogeneity; and the learning coefficient $\lambda$, controlling the speed at which trust levels are updated.

In particular, appendix B.2 shows that the rate of collateral re-use is related

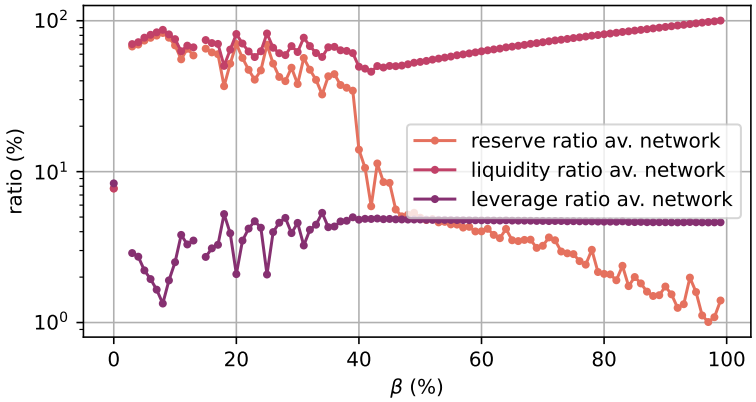


**(a)** Average regulatory ratios.

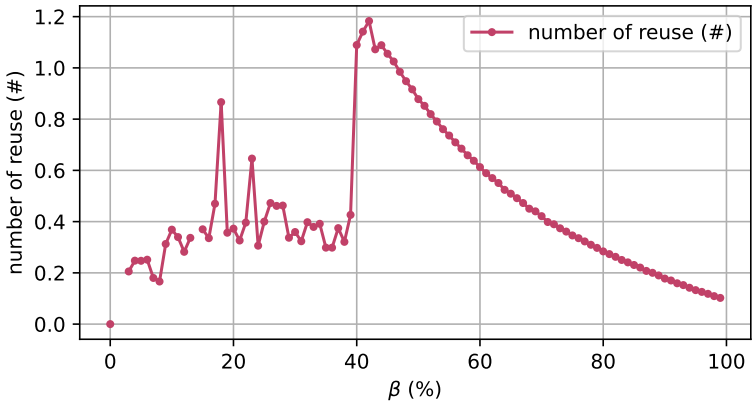


**(b)** Collateral re-use.

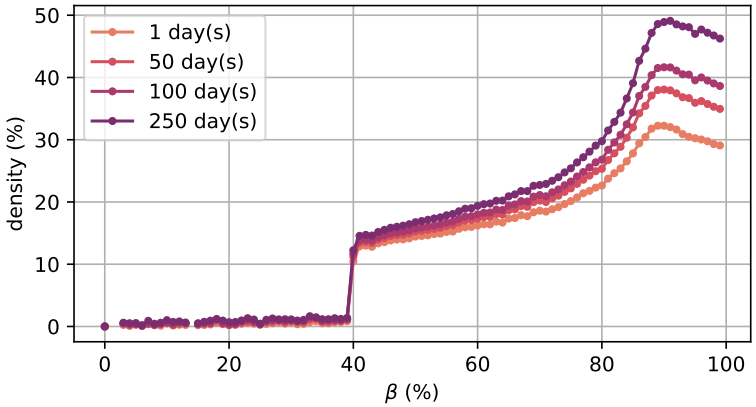


**(c)** Network density.

**Figure 4.7:** Regulatory ratios, collateral re-use, and network density as a function of the deposit outflow rate $\beta = \beta_{\text{new}}$.

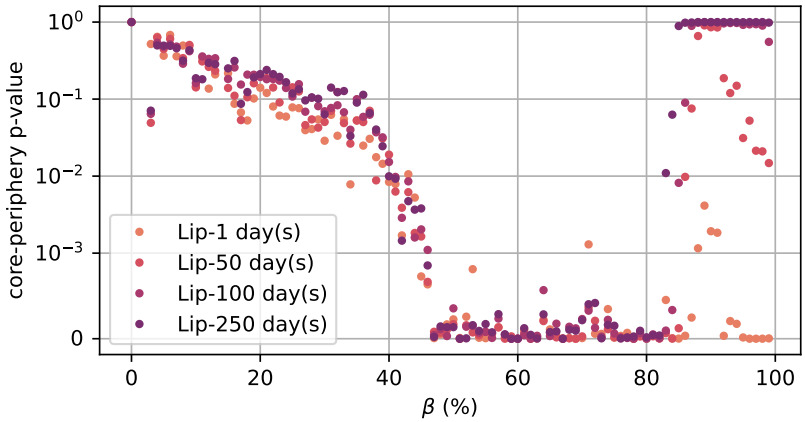


**Figure 4.8:** P-values assessing the existence of a core-periphery structure (Lip, 2011), as a function of the deposit outflow rate $\beta = \beta_{\text{new}}$.

to the ability of banks to increase their balance sheet size, which is tuned by $\gamma_{\text{new}}$.

### 4.2.3 Stress testing

This model can be used to study the response of money markets to various stress scenarios. We name these scenarios after the most relevant crises recently faced by the banking system. As in the previous section we fix $g = 0.04\%$, $v = 0$, $\nu = 1.4$ and $N = 100$. All the other parameters are fixed as in section 4.2.1.

**4.2.3.0.1 Asset Purchase Program (APP)** This scenario corresponds to the disappearance of new collateral in the system, as it is bought by the central bank at issuance. Accordingly the parameter $\beta_{\text{new}}$ is set to 0 between the steps 7000 and 14000.

Figures 4.12 and 4.13 show the impact of an APP on money markets. In essence, the APP provides money to the government that deposits this cash to the banking system, increasing excess liquidity (4.12a). This excess of deposits reduces the need to access the interbank market, reducing the density of the network (4.13a) and the number of transactions (4.13b). Concurrently, some banks receiving large negative payment shocks need funding on the repo markets, increasing the average size of repo transaction (4.13a). Yet, some of them do not find sufficient collateral available due to the APP, hence must resort to central bank funding (4.12a). Overall, the unwinding of existing repos for the bank receiving smaller shocks actually increases the amount of securities usable (4.12b). The fall of money markets is almost complete at the end of the APP, which ultimately leads to the collapse of the core-periphery structure (4.13c). Note the

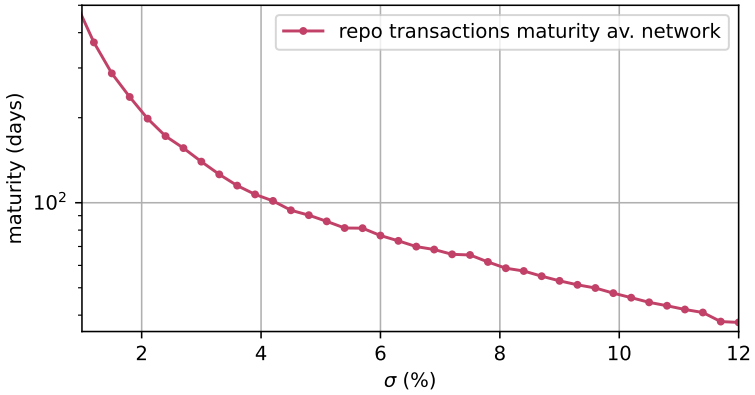


**(a)** Average maturity of repo transactions.

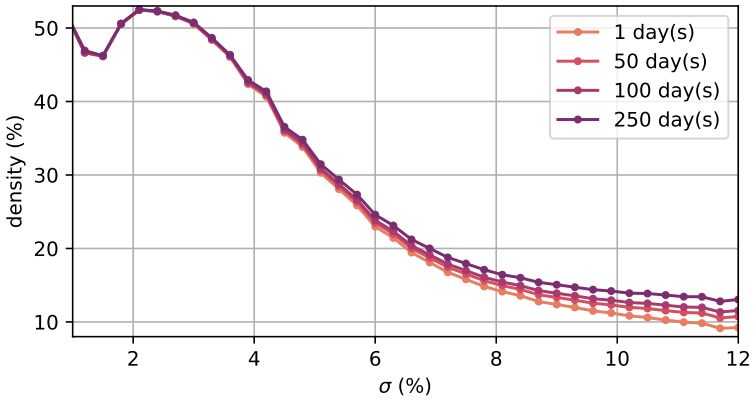


**(b)** Network density.

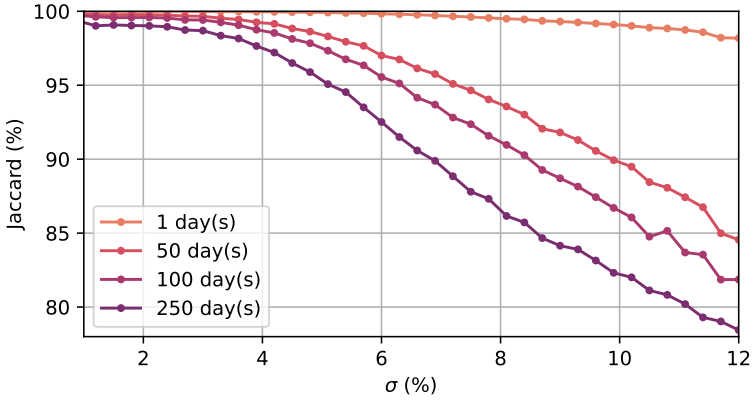


**(c)** Jaccard network similarity index.

**Figure 4.9:** Regulatory ratios, collateral re-use, and network density as a function of the volatility of payment shocks $\sigma$.

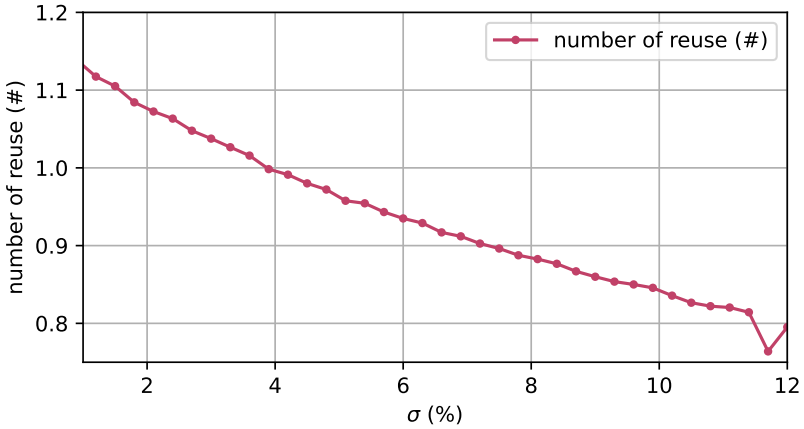


**Figure 4.10:** Collateral re-use as a function of the volatility of payment shocks $\sigma$.

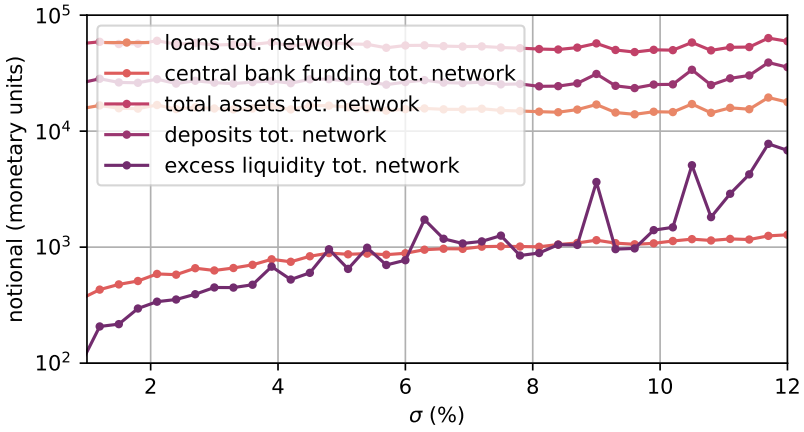


**Figure 4.11:** Macro-economic aggregates as a function of the volatility of payment shocks $\sigma$.

long recovery of the market after step 14000 (4.13a). Indeed, we did not simulate the maturing of existing collateral, which should mechanically decrease excess liquidity and reinforce the need for a repo market.

**4.2.3.0.2 Great financial crisis.** This scenario corresponds to the default of a large bank due to the failure of all its loans to an economic agent. In such a case, a chain of collateral callbacks can be triggered by the counterparts of the defaulted bank. As all transactions are secured, there should be no contagion to the rest of the network. However, the economic agent records a loss equal to the amount of the defaulted loan due to the loss of its deposits and shares in the defaulted bank. The only consequence in our model is a loss of trust among all bank agents, leading banks to contact their counterparties randomly between steps 7000 and 14000.

Fig. 4.14 and 4.15 show the impact of such a scenario on money markets. Banks contact randomly their counterparties which increases the network density (4.14a) and the number of transactions (4.14c) but reduces the average notional of repo transactions (4.14c). The network stability, measured by the Jaccard network similarity index, drops at the beginning of the crisis but quickly returns to almost its previous level (4.14b). The network is stable because banks are connected to almost all possible counterparties. As a consequence, the core-periphery structure vanishes (4.15). If we had added a minimum trust level for a transaction to occur, the market would have collapsed. There is no impact on macroeconomic and collateral aggregates.

**4.2.3.0.3 Greek crisis** This scenario translates into a haircut on the collateral value. Thus, all cash lenders simultaneously request the posting of additional collateral. As not enough new collateral can be produced, borrowers of cash reimburse their existing repos and request more central bank funding. We leave for future work the development of a mechanism to account for daily margin calls and collateral value fluctuations in order to assess the consequences of such a scenario.

**4.2.3.0.4 SVB bank run** This scenario materializes when a bank suddenly loses most of its deposits. In order to meet its regulatory constraint, such a bank would request large amounts of liquidity to the central bank and the other banks. In this model, this bank would survive the bank run because its liquidity need would be fulfilled by the access to infinite central bank funding. In practice, receiving central bank funding actually requires posting collateral, although it can be of lower quality than the one used in the repo markets. Hence, simulating such a crisis would require introducing a second type of collateral, which we leave for

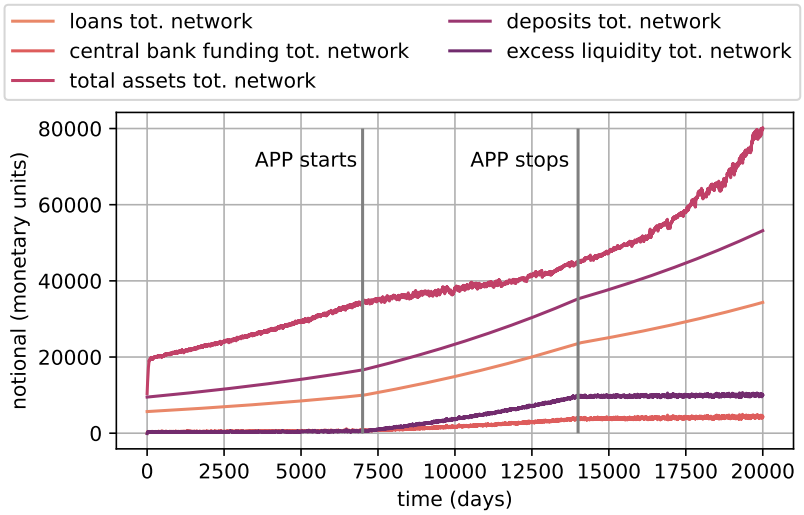


**(a)** Time evolution of the main macroeconomic aggregates in the simulated banking system.

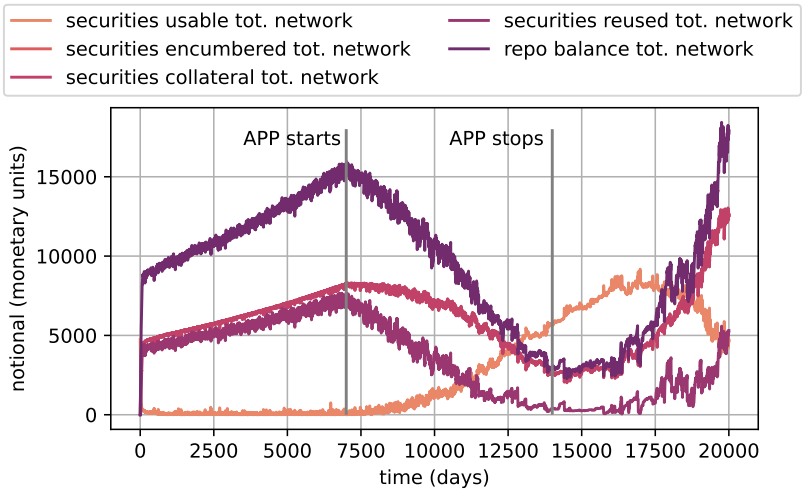


**(b)** Time evolution of the collateral aggregates in the simulated banking system.

**Figure 4.12:** Asset Purchase Program. We assume the central bank buys all the newly created securities from the step 7000 to 14000.

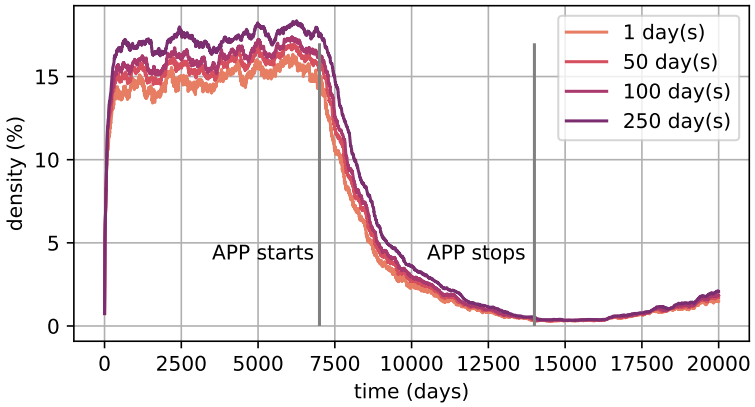


**(a)** Time evolution of the density in the simulated banking system.

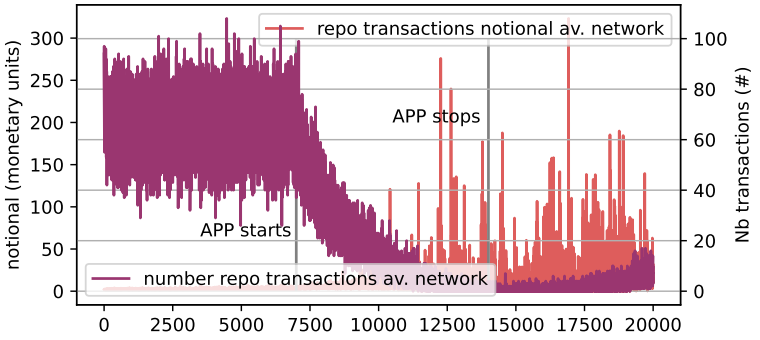


**(b)** Time evolution of the number and notional of new repo transactions in the simulated banking system.

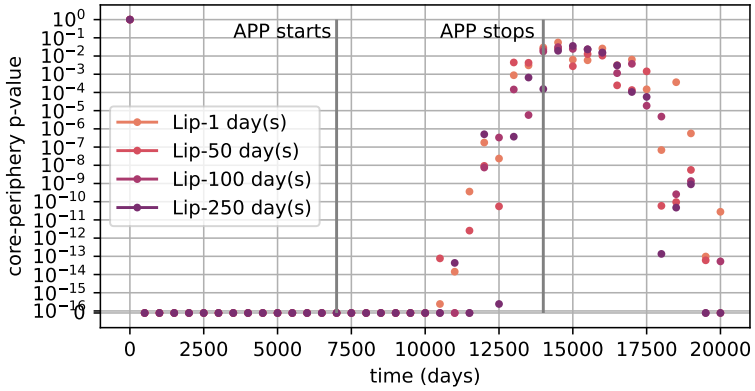


**(c)** Time evolution of the p-values assessing the existence of a core-periphery structure according to the method proposed by Lip (2011).

**Figure 4.13:** Asset Purchase Program. We assume the central bank buys all the newly created securities from the step 7000 to 14000. In Fig 4.13a and 4.13c, a link is defined as the existence of at least one repo over different aggregation periods, each corresponding to a given color.

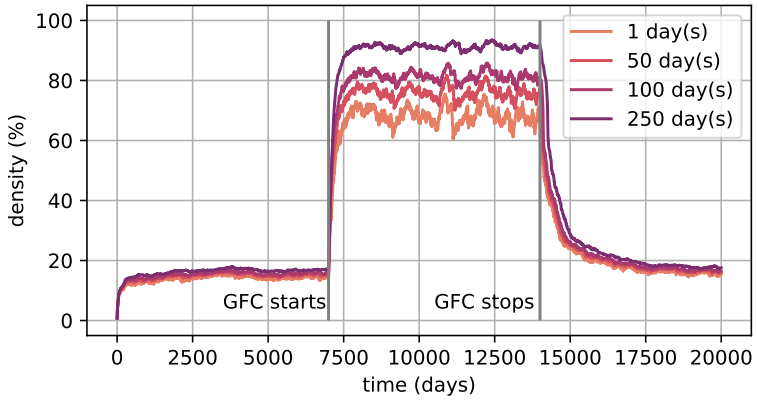


**(a)** Time evolution of the network density in the simulated banking system.

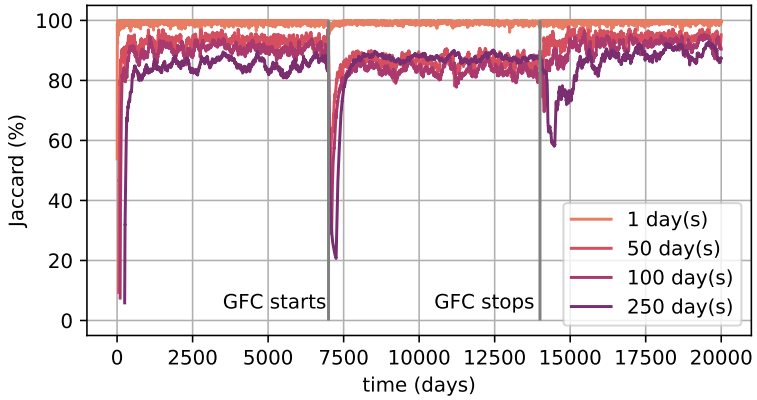


**(b)** Time evolution of the Jaccard network similarity index in the simulated banking system.

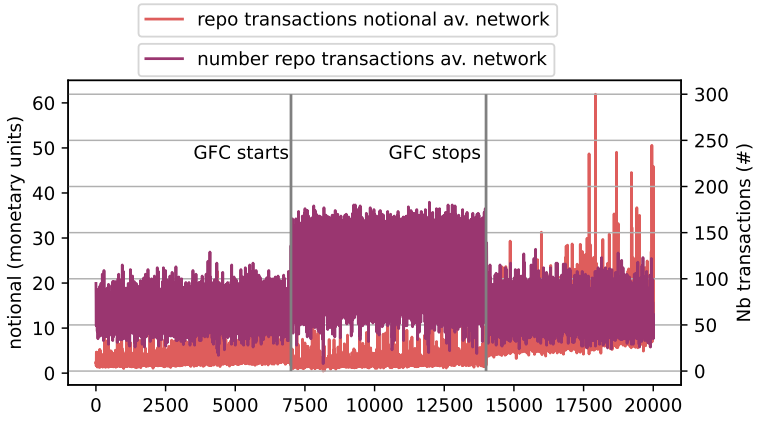


**(c)** Time evolution of the number and notional of new repo transactions in the simulated banking system.

**Figure 4.14:** Great financial crisis.We assume an absence of trust among banks from the step 7000 to 14000. In Fig 4.14a and 4.14b, a link is defined as the existence of at least one repo over different aggregation periods, each corresponding to a given color.

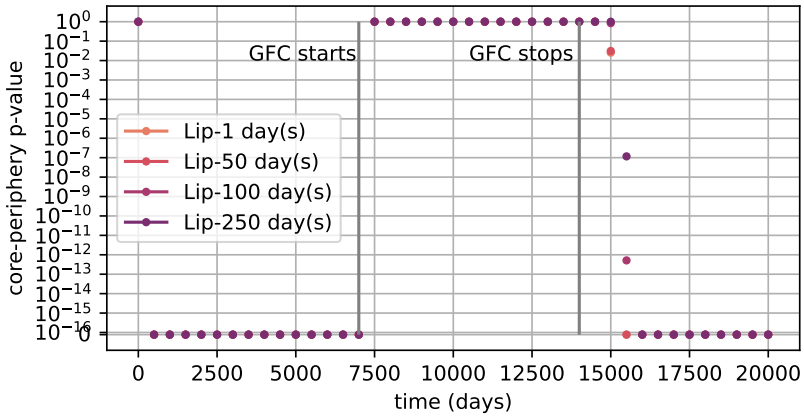


**Figure 4.15:** Great financial crisis. Time evolution of the p-values assessing the existence of a core-periphery structure according to the method proposed by Lip (2011). We assume an absence of trust among banks from the step 7000 to 14000. A link is defined as the existence of at least one repo over different aggregation periods, each corresponding to a given color.

future work.

## 4.3 Conclusion

We have designed a minimal model of money market cash flows. In this approach, banks create money endogenously while absorbing payment shocks thanks to repo transactions. They respect reserves, liquidity, and leverage constraints. This framework sheds light on recent puzzles. Excess liquidity arises from the asymmetric responses of banks to payment shocks when managing their LCR. Banks cannot maintain both their reserves and LCR at their minimum levels and absorb daily payment shocks. Hence, excess liquidity should not disappear after the end of the APP (the sale of all its bonds by the ECB). Moreover, we find from our model that collateral is re-used due to the long canceling notice period of repos. Hence, reducing this practice would limit the ability of banks to manage short term liquidity needs. Collateral scarcity increases collateral re-use because positive shocks must be absorbed by more borrowers. However, below a certain amount of securities in the banking system, the repo market collapses. Stable bilateral trading relationships, asymmetric in– and out–degree distributions, and a core-periphery structure emerge as the effect of trust among banks, similarly to the approach of Lux (2015) for unsecured markets.

We used this model to assess the impact of two stress scenarios: (i) the disappearance of new securities during an APP and (ii) the systematic loss of trust

during the GFC. Our findings confirm a positive impact of the full allotment procedure and LCR regulation on the stability of money markets. We notably observe that, even if the repo market collapses, loan production is maintained. In addition, secured transactions ensure the absence of contagion of a defaulted bank.

This model is also a policy tool to simulate any changes in the allotment procedure of central banks or regulatory constraints' modifications. It shows that changing individual regulation can affect the system in an unintended way. Notably, setting low levels (around $5\sigma$) of the deposit outflow rate significantly increases excess liquidity and collateral re-use but reduces network density. If we decrease the amount of securities held by banks below the size of the largest payment shocks, i.e. $\beta \leq 3\sigma$, the repo market collapses and excess liquidity explodes.

Interbank markets are more sensitive to liquidity risk than to interest rate risk because of the short maturity of exposures. However, introducing prices into this framework would allow one to model the transmission of central bank rates to money markets. Such a framework could explain another money market puzzle: the departure of the repo rates from the ECB's interest rate corridor (Piquard and Salakhova, 2019).

## Key takeaways

- We have assumed that banks create money endogenously while absorbing payment shocks thanks to repo transactions and respecting reserves, liquidity, and leverage constraints.
- In such a parsimonious framework, excess liquidity arises from the asymmetric responses of banks to payment shocks when managing their LCR.
- The observed level of collateral re-use can be generated by the long canceling notice period of repos.
- Collateral scarcity increases collateral re-use because positive shocks must be absorbed by more borrowers.
- Stable bilateral trading relationships, asymmetric in– and out–degree distributions, and a core-periphery structure emerge as the effect of trust among banks.
- The full allotment procedure and LCR regulation have increased the stability of money markets.
- Changing individual regulation can affect the system in an unintended way: if we decrease the amount of securities held by each bank below the size of the largest payment shocks, the repo market collapses and excess liquidity explodes.

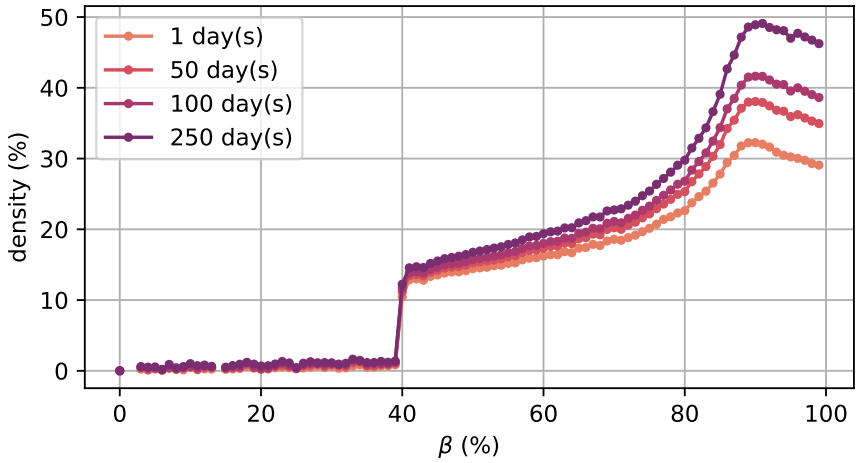

# Part III

# Liquidity flows on the interest rate curve

# Chapter 5

# Phenomenology of the yield curve

In this chapter, we define the interest rate curve as the set of rates derived from interbank Futures contracts quoted on LOBs. The time series of prices and order flows for each of these contracts individually exhibit all the stylized facts associated with organized markets (see section 5.1). However, examining the spatial structure across the entire set of these assets reveals several remarkable and specific patterns (see section 5.2). Additional relevant stylized facts regarding the impact of trading flows on prices are established in chapter 6. These empirical analyses will ultimately lead us to the development of a field theory of the yield curve in chapters 7 and 8.

To establish our empirical results, we interpret the instantaneous forward rate $f(t, \theta)$ as the mid-price at time $t$ of a 3-month SOFR Futures contract maturing at $t + \theta$. Our SOFR Futures data set comprises historical daily variations of the prices of these contracts from 1994 to 2023, covering tenors from 3 months to 117 months. 3-month SOFR Futures contracts were not available before March 2022; thus, Eurodollar contracts were used before that time, with an appropriate three-month shift accounting for the forward-looking nature of the Eurodollar Futures as opposed to the backward-accrued SOFR.

## 5.1 Temporal structure

### 5.1.1 Memory in the volatility process of prices

The price dynamics of any individual interest rate product exhibit all the stylized facts typical of financial time series. The first of these characteristics was established by Bachelier (1900), who observed that the diverse perspectives of

market participants on future price directions result in uncorrelated price fluctuations. However, subsequent research revealed that price variation time series display distinct patterns of temporal autocorrelation at small time scales (less than a few minutes) (Plerou et al., 2000; Cont, 2001; Bouchaud et al., 2004; 2018; Elomari-Kessab et al., 2024), challenging the traditional view of market efficiency. As shown in chapter 8, the field theory developed in chapter 7 successfully reproduces this scale-dependent decorrelation feature.

Research has also documented that the probability density functions of price increments vary with the time scale. At large time scales (over several days), these densities tend to be quasi-Gaussian, whereas at smaller time scales, they exhibit power-law tails (Gopikrishnan et al., 1999; Mantegna and Stanley, 1999; Plerou et al., 1999; Bouchaud and Potters, 2003). Another significant feature of financial time series is the so-called "volatility clustering", which refers to the persistence of volatility over time (Andersen, 2001; Cont, 2001; Cont, 2005b). Specifically, Sill (1996) found that the strong cyclicality of short- and long-term rate volatility is closely tied to the business cycle.

Significant advances were made with the identification of multifractality in financial returns (Fisher et al., 1997; Mandelbrot et al., 1997; Arnéodo et al., 1998; Schmitt et al., 1999; Brachet et al., 2000), leading to the development of the Multifractal Random Walk (MRW) model (Muzy et al., 2000; Bacry et al., 2001; 2011). This model, which effectively captures the long memory of volatility fluctuations, was succeeded by the Rough Volatility Model after Gatheral et al. (2018) demonstrated that the volatility process behaves like a fractional Brownian motion. In particular, Gatheral et al. (2018) analyzed the volatility dynamics of German Bond Futures prices, estimating a Hurst index $H = 0.082$ for these derivatives. The most recent advancement occurred when Zumbach (2010) identified a lack of time reversal symmetry in financial time series: future volatility can be predicted from past price trends, but not vice versa.

Finally, several studies have reported the presence of jumps in financial asset prices, particularly in the interest rate curve. Das (2002) and Piazzesi (2005) demonstrated that the incorporation of jump processes is essential for modeling central bank and interbank rates (see section 1.2.1.3). Furthermore, Johannes (2004) and Jiang and Yan (2009) detected jumps in the broader interest rate curve. Jumps in the volatility of long-term US sovereign bonds have also been observed (Andersen et al., 2007). Furthermore, Chen and Scott (2001) documented jumps in the implied volatility of interest rate options.

### 5.1.2 Long-range autocorrelation of trades

One of the most striking empirical facts in the market microstructure literature is the long-range persistence of order flows, as documented by Bouchaud et al.

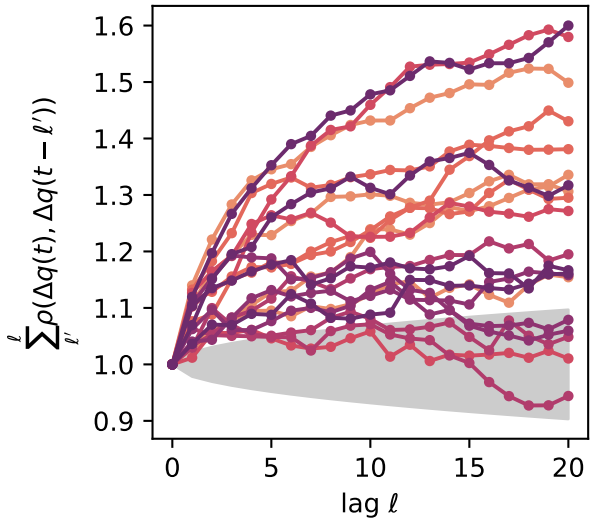


**Figure 5.1:** Accumulated temporal autocorrelation of 10-minutes bin trading flows $\Delta q(t)$ over $\ell$ days i.e., $\sum_{\ell'}^{\ell} \rho(\Delta q(t), \Delta q(t-\ell'))$, where $\rho(.,.)$ is the Pearson correlation operator. Each color corresponds to the tenor of a SOFR Future contract ranging from 3 to 60 months over the period $2016-2023$.

(2004), Lillo and Farmer (2004), Bouchaud et al. (2009a), Yamamoto and LeBaron (2010), Tóth et al. (2015), and Bouchaud et al. (2018). The surprising finding is that the autocorrelation of market-order signs decays extremely slowly with the lag and is well approximated by a power law (Bouchaud et al., 2018). Figure 5.1 illustrates that the signed order flow (i.e., the sum of the volumes of all trades during a time interval, with buy trades counted as positive and sell trades counted as negative; see chapter 6) is also highly autocorrelated. We show in chapter 8 that this effect is weaker at daily time scales and that Fourier analysis can help decorrelate the order flow to build an order-driven field theory.

## 5.2 Spatial structure

In a series of articles 20 years ago, Bouchaud et al. (1999), Matacz and Bouchaud (2000a), and b, and Bouchaud and Potters (2003) established several stylized facts regarding the spatial structure of the FRC. We reproduce these findings in this section using more recent data. We also complete these results with an analysis of the correlation structure of the signed order flows of the FRC.

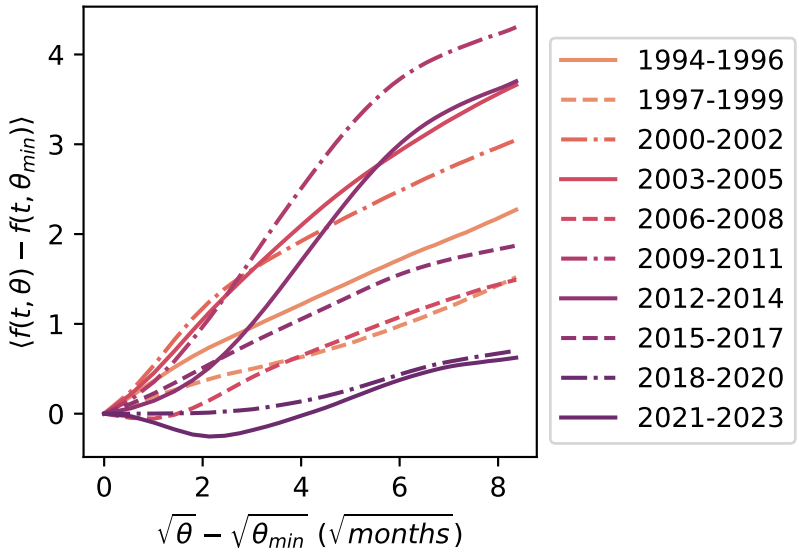


**Figure 5.2:** Unconditional mean of forward rates as a function of the square root of the tenor $\sqrt{\theta}$ across each of the three-year periods in our sample. The three periods where we observe a change of convexity ($2021-2023$, $2012-2014$, and $2009-2011$) correspond to the largest implementations of APPs in the U.S.

### 5.2.1 Square root law of forward rate means

We present in Fig. 5.2 the unconditional mean of forward rates as a function of the square root of tenor $\theta$ across each of the three-year periods in our sample. Except for the periods $2009-2011$, $2012-2014$, and $2021-2023$ which clearly demonstrate some change of convexity, we observe, as documented by Bouchaud et al. (1999) and Bouchaud and Potters (2003), that the mean of the FRC is a concave function of the tenor which is well approximated by a square root, i.e. $\langle f(t,\theta) - f(t,0)\rangle \propto \sigma_r\sqrt{\theta}$. The three periods where the "square root law" does not fit the data ($2021-2023$, $2012-2014$, and $2009-2011$) are precisely the ones corresponding to the largest implementations of APPs in the U.S. Our field theory of the yield also demonstrates its lowest fit quality for these periods (see section 7.5.5). This pattern suggests the forward rate $f(t,\theta)$ can be interpreted as the probable adverse move that lenders could be facing at time $t+\theta$, since the pre-factor $\sigma_r$ matches quite well with the volatility of the short term rate $f(t,0) = r(t)$ (Matacz and Bouchaud, 2000a; b; Bouchaud and Potters, 2003). In other words, the usual zero-coupon bond pricing formula (1.20) in chapter 1

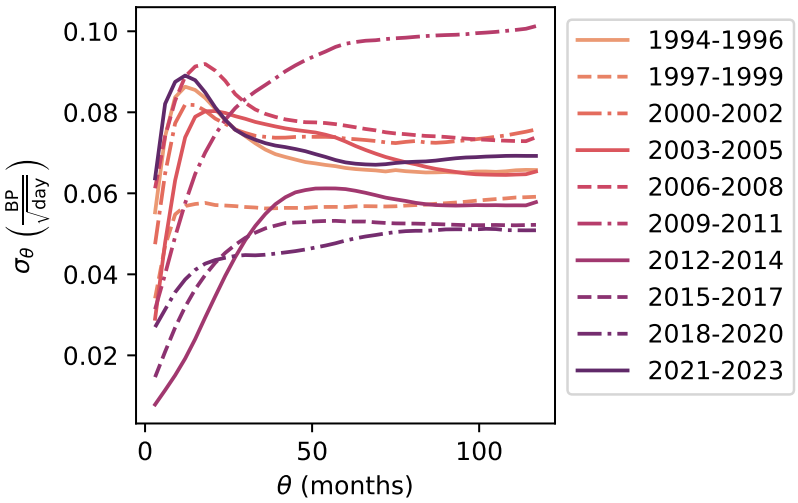


**Figure 5.3:** Unconditional volatility of daily forward rates increments per tenor $\theta$ across each of the three-year periods in our sample. We observe a peak of volatility around $\theta = 12$ months for several of the 3-year periods in our sample.

should be replaced by

$$\begin{cases} P(t,T) = \text{VaR}\left[\exp\left(-\int_t^T r(s)\mathrm{d}s\right)\right], \\ \mathrm{d}r(t) = \sigma_r(t)\mathrm{d}W^{\mathbb{P}}(t), \end{cases} \tag{5.1}$$

where VaR[.] designates the Value at Risk (or quantile) over the distribution of the future short rate. In this view, there is no need to define a risk-neutral measure to define the term premiums of the yield curve. These risk premiums correspond to the diffusion of the short-term rate over intervals of increasing length.

### 5.2.2 Humped volatility

Amin and Morton (1994), Hull and White (1994), Bouchaud et al. (1999), Bouchaud and Potters (2003), and Fabozzi and Mann (2005) have documented the humped shape of the volatility of the FRC. Let $\Delta t$ denote a time interval of one day and $\Delta f(t,\theta) = f(t+\Delta t,\theta) - f(t,\theta)$ the daily variations of the forward rate. We observe a peak in the volatility $\sigma_\theta := \sqrt{\langle \Delta f(t,\theta)^2 \rangle}$ of the forward rate variations around $\theta = 12$ months for several of the three-year periods in our sample (see Fig. 5.3). Matacz and Bouchaud (2000a), b interpreted this result, in the same adverse move spirit as above, as the recent trend of the short-term rate extrapolated into the future. Notably, as mentioned in chapter 1, fitting this humped volatility in the HJM framework requires defining a complex non-stationary volatility process. In

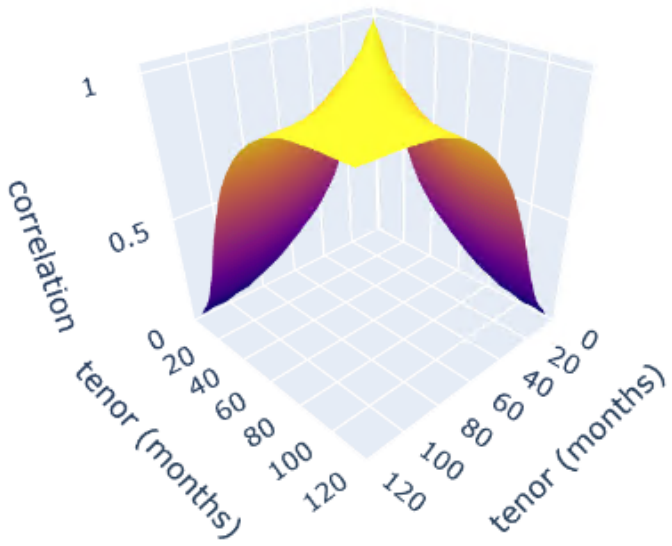


**Figure 5.4:** Empirical Pearson correlation surface between the daily forward rate increments of different tenors $\theta, \theta'$ for the period $2021 - 2023$. Notice that the surface is smooth across the diagonal $\theta = \theta'$, with a curvature that decreases with $\theta$.

contrast, the model proposed in chapters 7 and 8 faithfully reproduces the volatility structure of the FRC.

### 5.2.3 Correlation structure of an elastic string

A natural way to understand the interdependence of yields of different maturity is to study the empirical Pearson correlations $\rho(\Delta f(t,\theta), \Delta f(t,\theta'))$ among the daily forward rate increments of tenor $\theta$ and $\theta'$. Our data set includes tenors from 3 months to 117 months. Consequently, we observe up to $n = 39$ different tenors, resulting in 702 distinct points in the correlation matrix (excluding the trivial diagonal points) which is depicted in Fig. 5.4 for the specific period $2021-2023$. As noticed by Baaquie and Bouchaud, 2004 this correlation structure is particularly smooth, which is an important feature of the model we propose in chapter 7.

One of the first remark is that this correlation structure does not appear instantaneously but depends on the time scale $\Delta t$ chosen to observe price variations: this is the well-known "Epps effect"(Epps, 1979; Renò, 2003; Toth and Kertesz, 2009). Specifically, for SOFR Futures prices, Fig. 5.5 illustrates that the correlation between pairs of tenors ranging from 3 to 60 months emerges only after several minutes.

The eigenvalues of the decomposition of the FRC correlation matrix exhibit a

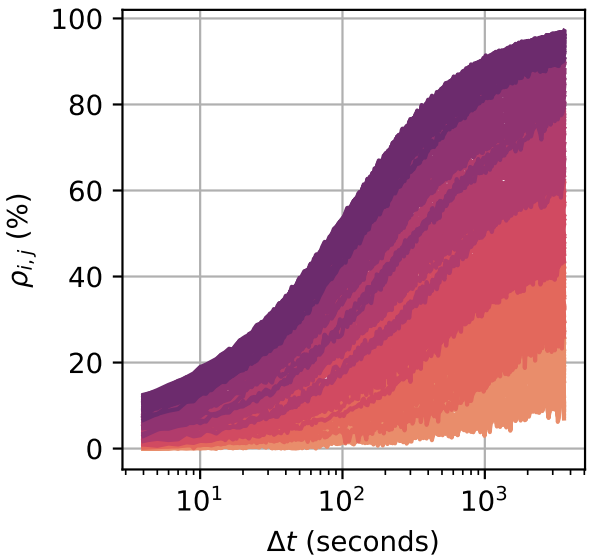


**Figure 5.5:** Pearson correlation coefficients $\rho(\theta, \theta')$ as a function of the time scale $\Delta t$ used to define returns, for each pair of SOFR Futures prices of time-to-maturity $\theta$ ranging from 3-month to 60-month for the year 2021. Each color corresponds to a pair ordered from the lowest (orange) to the highest (purple) correlation level at the 1-hour bin.

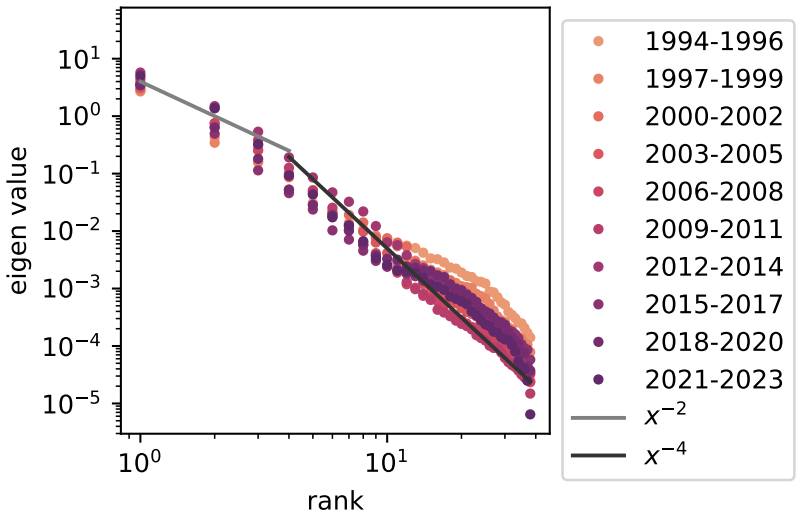


**Figure 5.6:** Eigenvalues of the empirical Pearson correlation matrix between the daily forward rate increments of different tenors, in logarithmic scale. We observe a decay that follows an inverse power law relative to the rank.

decay that follows an inverse power law relative to their rank, starting as $\xi^{-2}$ and transitioning to $\xi^{-4}$, as noted by Bouchaud et al. (1999). Figure 5.6 shows that this stylized fact has remained very stable in the last 30 years. As mentioned in chapter 1 this result cannot be generated by any model based on a lower number of diffusion factors than the number of observed forward rates, which would generate a singular correlation matrix.

Another interesting feature of the eigenvalue decomposition of the correlation matrix of the FRC is the peculiarity of its eigenvectors. Figure 5.7 shows that these eigenvectors resemble those of an elastic string. The first mode corresponds to a parallel shift, the second mode has one node (i.e. it crosses the abscissa axis once), the third mode exhibits two nodes, and so on. Bouchaud et al., 1999 proposed an heuristic explanation of these findings by interpreting the correlation matrix of the FRC as a linear operator relating the forward rate of a given maturity to all other forward rates. More precisely, they proposed to express the dynamic equation[8] of the forward rate variations $A = \frac{\partial f}{\partial t}$ as:

$$\frac{\partial A}{\partial t}(t,\theta) \propto \frac{1}{\mu^2}\frac{\partial^2 A(t,\theta)}{\partial \theta^2} - \frac{1}{\nu^4}\frac{\partial^4 A(t,\theta)}{\partial \theta^4} + \eta(t,T), \tag{5.2}$$

[8]Compared to the initial article form Bouchaud et al. (1999), we actually extend the argument of the authors up to the fourth order derivative, in line with the subsequent work of Baaquie and Bouchaud (2004).

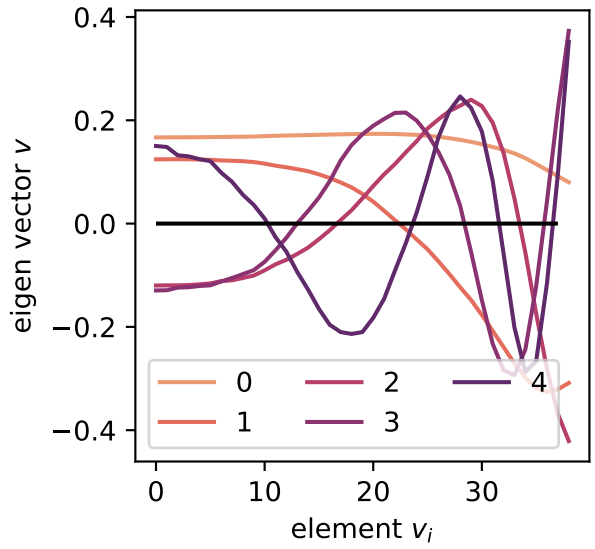


**Figure 5.7:** First five eigenvectors of the empirical Pearson correlation matrix between the daily forward rate increments of different tenors. We recognize the modes of an elastic string.

where $\mu$ and $\nu$ are two parameters governing respectively the line tension and "stiffness" of an elastic string (see also chapter 7), and $\eta$ is a two-dimensional uncorrelated Langevin noise such that $\mathbb{E}\left[\eta(t,\theta)\eta(t',\theta')\right] = \delta(t-t')\delta(\theta-\theta')$ with $\delta$ the Dirac function. The Fourier transform with respect to the tenor $\theta$ of this linear differential equation yields:

$$\frac{\partial \hat{A}}{\partial t}(t,\xi) \propto -\left[\left(\frac{\xi}{\mu}\right)^2 + \left(\frac{\xi}{\nu}\right)^4\right] \hat{A}(t,\xi) + \hat{\eta}(t,\xi), \tag{5.3}$$

where $\hat{A}$ and $\hat{\eta}$ are the Fourier transform of $A$ and $\eta$ with respect to the maturity. Hence, the Fourier transform of the forward rate variations reads

$$\hat{A}(t,\xi) \propto \int_{-\infty}^{t} \mathrm{d}t' e^{-(t-t')\left[\left(\frac{\xi}{\mu}\right)^2 + \left(\frac{\xi}{\nu}\right)^4\right]} \hat{\eta}(t',\xi). \tag{5.4}$$

It yields a covariance of the Fourier transform of the forward rate variations that decays as $\xi^{-2}$ and $\xi^{-4}$,

$$\mathbb{E}\left[\hat{A}(t,\xi)^2\right] \propto \frac{1}{\left(\frac{\xi}{\mu}\right)^2 + \left(\frac{\xi}{\nu}\right)^4}, \tag{5.5}$$

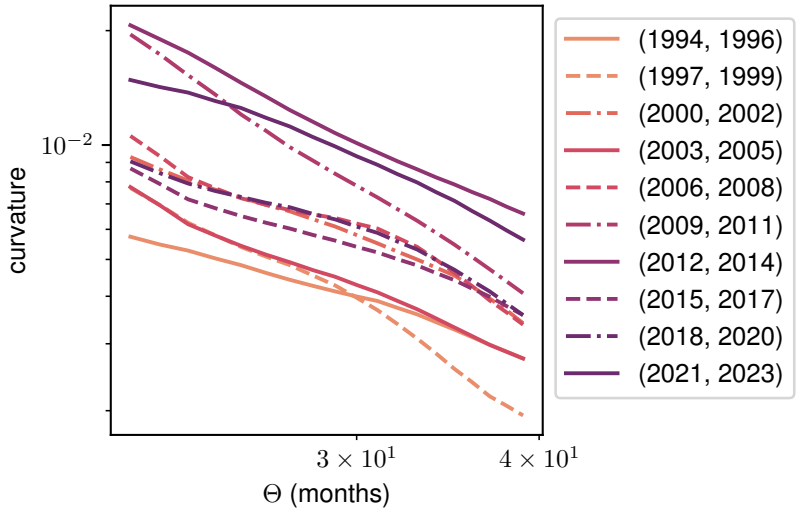


**Figure 5.8:** Curvature of the correlation surface along the stretches perpendicular to the diagonal, i.e. $\theta' = \Theta - \theta$ as a function of largest tenor $\Theta$ for each sub-period in our sample, in logarithmic scale.

consistently with the empirical observations in Fig. 5.6.

Finally, Baaquie and Bouchaud (2004) established that the curvature of the anti-diagonal of the correlation matrix of the FRC decays as a power law. Fig. 5.8 shows the empirically observed curvatures on the anti-diagonal for each of the 3-year periods in our sample. These estimations are produced through the fitting of parabolas using 20 points around the center of each anti-diagonal of the correlation surface of forward rate increments. We show in chapter 7 that this power law structure is faithfully reproduced by an elastic string model when accounting for the deformed perception of time by economic agents.

### 5.2.4 Uncorrelated order-flow

Another striking fact regarding the spatial structure of the yield curve is that the order flows by maturity are almost uncorrelated, as shown in Fig. 5.9. Indeed we observe peaks along the diagonal on this figure, while the other cross-sectional correlations are close to zero. This finding is at the origin of the proposal in chapter 8 to interpret the order flow as the uncorrelated noise that influences the formation of the FRC.

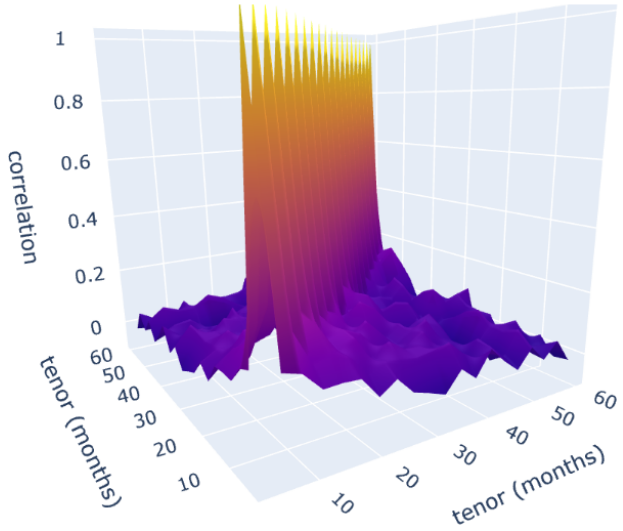


**Figure 5.9:** Spatial Pearson correlations among the signed daily order flows of SOFR Futures from 2016 to 2023.

## 5.3 Conclusion

The price dynamics of interest rate products exhibit typical characteristics of financial time series. Specifically, their increments are autocorrelated over short time scales, typically less than a few minutes, but become uncorrelated over longer time scales. In contrast, the autocorrelation of the signed order flow of these products decays very slowly with increasing lag, a behavior well modeled by a power law. Another significant feature of financial time series of prices is the so-called "volatility clustering", which refers to the persistence of volatility over time. The volatility process of bond Futures notably behaves like a fractional Brownian motion. The modeling of jumps in the price process is also particularly relevant in the case of interest rate products.

The mean of the FRC is a concave function of the tenor that is well approximated by a square root, suggesting that the forward rate $f(t, \theta)$ can be interpreted as the probable adverse move that lenders could face at time $t + \theta$ (Matacz and Bouchaud, 2000a). The humped shape of the volatility of the FRC can be interpreted as the recent trend of the extrapolated short-term rate into the future (Matacz and Bouchaud, 2000a).

The spatial correlation structure of the FRC does not manifest instantaneously but is dependent on the time scale used to observe price variations, an effect known as the Epps effect. The eigenvalues of the decomposition of the FRC correlation matrix exhibit a decay that follows an inverse power law relative to their rank,

starting as $\xi^{-2}$ and transitioning to $\xi^{-4}$, similarly to the behavior of an elastic string (Bouchaud et al., 1999). The curvature of the anti-diagonal of the FRC's correlation matrix also decays according to a power law (Baaquie and Bouchaud, 2004). In contrast, order flows by maturity are almost well uncorrelated.

Most stylized facts regarding the spatial structure of prices and order flows are reproduced by our field theory of the yield curve (see chapters 7 and 8). We also reproduce the effect of increasing time scales on the temporal decorrelation of prices and the emergence of their spatial correlation. However, in the rest of this thesis, we choose to ignore the existence of memory in the volatility process of prices.

## Key takeaways

- The price dynamics of interest rate products show typical financial time series characteristics. Notably, their increments are autocorrelated at small time scales (less than a few minutes) but are temporally uncorrelated at longer time scales.
- In contrast, the autocorrelation of the signed order flow of interest rate products decays extremely slowly with the lag and is well approximated by a power law.
- The spatial correlation structure of the FRC does not appear instantaneously but depends on the time scale chosen to observe price variations (Epps effect).
- The eigenvalues of the decomposition of the FRC correlation matrix exhibit a decay that follows an inverse power law relative to their rank, starting as $\xi^{-2}$ and transitioning to $\xi^{-4}$, similarly to the behavior of an elastic string (Bouchaud et al., 1999).

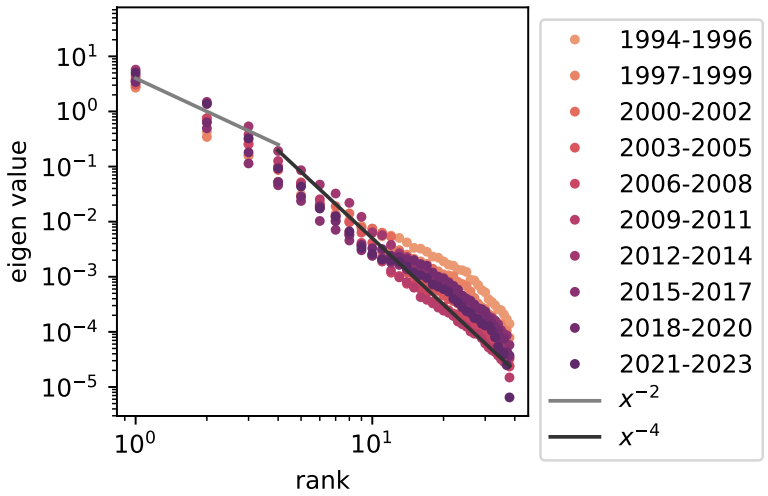


- The curvature of the anti-diagonal of the FRC's correlation matrix also decays according to a power law (Baaquie and Bouchaud, 2004).
- In contrast, order flows by maturity are almost uncorrelated.

# Chapter 6

# When is cross-impact relevant?

*In this chapter, we reproduce the contents of (Le Coz et al., 2024d), written under the supervision of Iacopo Mastromatteo, Damien Challet, and Michael Benzaquen, barring some changes in phrasing and notations.*

According to standard economic theory, the price of an asset should integrate all publicly available information regarding its fundamental value. In practice, price formation occurs through a trading system that mechanically forces information flow into prices via the order flow of market participants. This well-established phenomenon is known as *price impact*.

An early model of price impact was proposed by Kyle (1985), who assumed a linear dependence between absolute price differences and signed traded volumes. Further work established that the price impact of large (split) trades universally follows a square-root law of the traded volume (Loeb, 1983; Plerou et al., 2004; Almgren et al., 2005; Kissell and Malamut, 2005; Moro et al., 2009; Toth et al., 2011; Mastromatteo et al., 2014; Bacry et al., 2015; Donier and Bonart, 2015; Zarinelli et al., 2015; Tóth et al., 2017; Bouchaud et al., 2018; Kyle and Obizhaeva, 2023). Yet, the price impact of a single anonymous market order is a much weaker concave (almost constant) function of its volume when the latter is adequately normalized by the available liquidity in the order book (Hasbrouck, 1991; Chen et al., 2002; Lillo et al., 2003; Potters and Bouchaud, 2003; Zhou, 2012; Gomber et al., 2015; Bouchaud et al., 2018). This behavior is due to the *selective liquidity taking* effect (Taranto et al., 2014; Bouchaud et al., 2018): most of the large market order arrivals happen when there is a large volume available at the opposite-side best quote, specifically trying to avoid moving the mid-price. To overcome this effect, impact is often measured over a coarse-grained time scale $\tau$, by aggregating trades into a *signed order flow imbalance*. This method involves calculating the signed sum of the volumes of all trades within a time window of length $\tau$, while

observing price changes during the same interval. Within this framework, the magnitude of price impact crosses over from a linear to a concave behavior, as the signed order flow increases (Kempf and Korn, 1999; Evans and Lyons, 2002; Plerou et al., 2002; Chordia and Subrahmanyam, 2004; Gabaix et al., 2006; Hopman, 2007; Patzelt and Bouchaud, 2017; Bouchaud et al., 2018; Patzelt and Bouchaud, 2018). In addition, the aggregated price impact is a concave function of the time scale $\tau$ chosen for the aggregation (Bouchaud et al., 2018). Finally, in order to conciliate the long term positive auto-correlation of trades with the independence of price increments, Bouchaud et al. (2004) established that price impact must be *transient*. This assumption means that the magnitude of the price-impact of a trade decreases across time. This hypothesis was corroborated in the following years (Bouchaud et al., 2006; Hopman, 2007; Bouchaud et al., 2009b; Gatheral, 2010; Gatheral and Schied, 2013; Alfonsi et al., 2016; Gârleanu and Pedersen, 2016; Tóth et al., 2017; Taranto et al., 2018; Ekren and Muhle-Karbe, 2019).

A more subtle effect is that trading pressure from one asset can move the price of another. This effect, which is referred to as *cross-impact*, was studied initially by Hasbrouck and Seppi (2001) and later in Chordia et al. (2001), Evans and Lyons (2001), Harford and Kaul (2005), Pasquariello and Vega (2007), Andrade et al. (2008), Tookes (2008), Pasquariello and Vega (2015), Benzaquen et al. (2017), Wang and Guhr (2017), Schneider and Lillo (2019), Brigo et al. (2022), and Tomas et al. (2022a), b.

The simplest cross-impact models posit a linear relationship between signed trading volumes and prices variations in time windows of length $\tau$ (the binning frequency) (Hasbrouck and Seppi, 2001; Harford and Kaul, 2005; Pasquariello and Vega, 2007; 2015; Tomas et al., 2022a; b). While the time decay of the transient impact model was studied for bonds (Schneider and Lillo, 2019; Schneider, 2019) and stocks (Wang, 2017), the time scale maximizing the accuracy of linear cross-impact models has not yet been documented. Moreover, this optimal time scale is an indicator of the speed of information transmission among assets, which has not been studied extensively, although Zumbach and Lynch (2001), Lynch and Zumbach (2003), and Cordi et al. (2021) inferred typical time scales of market reactions of the volatility process. In addition, Rosenbaum and Tomas (2022), Tomas et al. (2022b), and Cordoni et al. (2023) link the magnitude of cross-impact to asset liquidity and to the correlation among assets.

Here, we quantitatively characterize the circumstances under which a model with cross-impact over-performs one that does not include impact across assets. Additionally, we identify the time scales that maximize the accuracy of linear cross-impact models. Our study includes an introduction to the linear cross-impact modeling framework and a methodology to evaluate the factors influencing cross-impact's relevance in explaining price return variance. The results are organized according to the studied features: the bin size, the trading frequency,

the correlation among assets, and the liquidity. In the final section, we provide applications of these findings to the interest rate curve.

## 6.1 Notations

The set of real-valued square matrices of dimension $n$ is denoted by $\mathcal{M}_n(\mathbb{R})$, the set of orthogonal matrices by $\mathcal{O}_n$, the set of real symmetric positive semi-definite matrices by $\mathcal{S}_n^+(\mathbb{R})$, and the set of real symmetric positive definite matrices by $\mathcal{S}_n^{++}(\mathbb{R})$. Given a matrix $A$ in $\mathcal{M}_n(\mathbb{R})$, $A^\top$ denotes its transpose. Given $A$ in $\mathcal{S}_n^+(\mathbb{R})$, we write $A^{1/2}$ for a matrix such that $A^{1/2}(A^{1/2})^\top = A$, and $\sqrt{A}$ for the matrix square root: the unique positive semi-definite symmetric matrix such that $(\sqrt{A})^2 = A$. We also write $\mathrm{diag}(A)$ for the vector in $\mathbb{R}^n$ formed by the diagonal items of $A$. Finally, given a vector $v$ in $\mathbb{R}^n$, we denote the components of $v$ by $(v_1, \cdots, v_n)$, and the diagonal matrix whose components are the components of $v$ by $\mathrm{diag}(v)$. Table 6.1 in section 6.7 provides the complete list of the notations used in this chapter.

## 6.2 Modeling framework

To relate trades to prices, we observe the mid-prices and market orders of $n$ different assets, both binned at a regular time interval of length $\tau$ seconds. We denote by $p_i(t)$ the opening price of asset $i$ in the time window $[t, t+\tau]$ and by $p(t) = (p_1(t), \cdots, p_n(t))$ the vector of asset prices at opening. We define $\Delta q_i(t)$ as the net market order flow traded during the time window $[t, t+\tau]$. This is calculated by taking the sum of the volumes of all trades during that time period, with buy trades counted as positive and sell trades counted as negative. Hence, $\Delta q(t) = (\Delta q_1(t), \cdots, \Delta q_n(t))$ is the vector of the net traded order flows.

Following the approach proposed by Tomas et al. (2022b), we study the relationship between the time series of net order flows $\{\Delta q_0, \Delta q_\tau, \cdots\}$ and the time series of prices $\{p_0, p_\tau, \cdots\}$, under the two following assumptions:

- prices variations $\Delta p(t) := p(t+\tau) - p(t)$ and order flow imbalances $\Delta q(t)$ are linearly related, i.e.,

$$\Delta p(t) = \Lambda(t)\Delta q(t) + \eta(t), \tag{6.1}$$

  where the $n \times n$ matrix $\Lambda(t)$ is the cross-impact matrix and $\eta(t) = (\eta_1(t), \cdots, \eta_n(t))$ is a vector of zero-mean random variables representing exogenous noise;

- the cross-impact matrix $\Lambda(t)$ is a function of the form:

$$\Lambda(t) = \Lambda(t)(\Sigma(t), \Omega(t), R(t)), \tag{6.2}$$

where $\Lambda(t) : \mathcal{S}_n^+(\mathbb{R}) \times \mathcal{S}_n^+(\mathbb{R}) \times \mathcal{M}_n(\mathbb{R}) \to \mathcal{M}_n(\mathbb{R})$ is called a cross-impact model, $\Sigma(t) := \mathrm{cov}(\Delta p(t))$ is the price variations covariance matrix, $\Omega(t) := \mathrm{cov}(\Delta q(t))$ is the order flows covariance matrix, and,

$$R(t) = \mathbb{E}\left[(\Delta p(t) - \mathbb{E}\left[\Delta p(t)\right])(\Delta q(t) - \mathbb{E}\left[\Delta q(t)\right])^\top\right] \tag{6.3}$$

is the response matrix.

We also define the price variations volatility by

$$\sigma(t) := (\sqrt{\Sigma_{11}(t)}, \cdots, \sqrt{\Sigma_{nn}(t)}), \tag{6.4}$$

and the signed order flows volatility by

$$\omega(t) := (\sqrt{\Omega_{11}(t)}, \cdots, \sqrt{\Omega_{nn}(t)}). \tag{6.5}$$

Finally, for a given asset $i$, we define the the average across time of its price variation volatility by

$$\bar{\sigma}_i := \langle \sigma_i(t) \rangle, \tag{6.6}$$

and the average across time of its signed order flow volatility by

$$\bar{\omega}_i := \langle \omega_i(t) \rangle. \tag{6.7}$$

### 6.2.1 Definition of the models

Let $Y$ denote a scalar called the *Y-ratio*. We study the following three cross-impact models:

- the diagonal model, defined by

$$\Lambda^{\mathrm{diag}}(\Sigma, \Omega, R) := Y \,\mathrm{diag}(R)\,\mathrm{diag}(\Omega^{-1}), \tag{6.8}$$

  which is the limit case where the cross-sectional impact is set to zero;

- the Maximum Likelihood model (*ML model* in the following sections), defined by

$$\Lambda_{\mathrm{ML}}(\Sigma, \Omega, R) := Y R \Omega^{-1}; \tag{6.9}$$

- and the Kyle model, defined by

$$\Lambda_{\mathrm{Kyle}}(\Sigma, \Omega, R) := Y (\Omega^{-1/2})^\top \sqrt{(\Omega^{1/2})^\top \Sigma \Omega^{1/2}}\; \Omega^{-1/2}. \tag{6.10}$$

The Y-ratio is a re-scaling adjustment parameter, estimated by minimizing, across all assets, the squared errors between the price variations predicted by the model and the realized prices. These models were investigated in several of the previously mentioned publications. Noteworthy, the diagonal model was studied in (Kempf and Korn, 1999; Evans and Lyons, 2002; Plerou et al., 2002; Chordia and Subrahmanyam, 2004; Gabaix et al., 2006; Hopman, 2007; Patzelt and Bouchaud, 2017; Bouchaud et al., 2018; Patzelt and Bouchaud, 2018). The Maximum Likelihood model was investigated in Hasbrouck and Seppi (2001), Harford and Kaul (2005), Pasquariello and Vega (2007), and 2015, and Tomas et al. (2022a), b. The multidimensional Kyle model was introduced by del Molino et al. (2020) and further Examined by Tomas et al. (2022b).

It is important to note that the diagonal model can be defined by

$$\Lambda^{\text{diag}} := \text{diag}(\lambda_{\text{diag}}), \tag{6.11}$$

where the vector $\lambda_{\text{diag}} = (\lambda_1, \cdots, \lambda_n)$ is defined by a set of linear equations:

$$\forall i \in [\![1, n]\!],\ \Delta p_i(t) = \lambda_i \Delta q_i(t) + \eta_i(t). \tag{6.12}$$

This means that the diagonal model assumes that each asset $i$ has its own unique relationship between price increments and order flows, as captured by the coefficient $\lambda_i$.

The comparison between the last two models and the first one will allow us to distinguish among the portion of cross-impact that is explained by order flow commonality (which the diagonal model can capture) and the contributions that cannot be explained by this effect, thus requiring models such as ML and Kyle.

### 6.2.2 Properties of the models

As demonstrated by Tomas et al. (2022b), the previously defined models satisfy a list of properties that characterize their behavior. These properties are recalled below.

1. *Symmetry* properties aim at ensuring that the cross-impact model behaves in a controlled manner under financially-grounded transformations of its variables $\Sigma(t),\ \Omega(t),\ R(t)$. The Kyle and ML models both adapt to (i) a re-ordering of the considered assets (*permutation invariance*), (ii) a change of currency (*cash invariance*) or (iii) volume units (*split invariance*) and, (iv) a change of basis in the asset space (*rotational invariance*). In contrast, the diagonal model crucially misses property (iv), as it regards the physical space of assets as a privileged basis for the description.

2. *Non-arbitrage* properties aim at ensuring the absence of arbitrage in the sense of Gatheral, 2010, i.e., round-trip trading strategies with positive average profit. Both the diagonal and Kyle model prevent (i) static arbitrage over a single-period (thanks to their *positive semi-definiteness*) and (ii) dynamic arbitrage over multi-period. Yet, the ML model does not satisfy any of these non-arbitrage properties.

3. *Fragmentation* properties aim at ensuring the equality of the price impacts generated from traded volumes of the same assets on fragmented markets (e.g. US stocks are traded on several venues). This property is satisfied by both the Kyle and ML models but is trivially violated by the diagonal model.

4. *Stability* properties aim at ensuring the impossibility to manipulate the price of liquid products using illiquid instruments. This property is satisfied by the Kyle model and the diagonal model, but not by the ML model.

## 6.3 Methodology

### 6.3.1 Estimation method

We use tick-by-tick trades and quotes for 500 assets quoted in LOB in the U.S.. Our sample includes stocks, bonds, Futures on bonds and Futures on stock indexes. Unless otherwise specified, our data set covers the $2017-2022$ period. For a given year, we consider the data from the preceding year as in-sample data, while the data from the current year is designated as out-of-sample data. We then aggregate in and out-of-sample results over all years.

A significant portion of our analysis involves the selection of pairs of assets from the pool of the 500 assets in our sample. For this purpose, we select $20,000$ pairs of assets per year. These pairs are chosen from the pool of ≈120,000 possible combinations among the 500 assets, aiming for a uniform coverage of existing correlations. Specifically, we categorize all potential pairs based on their correlation levels into 50,000 equally-sized correlation buckets. For instance, the first bucket encompasses pairs with correlations between 0% and 0.002%. Subsequently, we opt for the first pair within each of these buckets, resulting in the selection of 20,000 pairs. Our analysis is then aggregated over a five-year period, yielding a total of 100,000 year-pair combinations.

To overcome the conditional heteroskedasticity of price variations and signed order flows, we use a daily estimator of their volatility. Let $\{t_1, \cdots, t_k\} \in \mathbb{R}^N$ denote the $N$ business days of a year. For each day $t_k$, the estimators of the price

increments volatility and of the signed order flows volatility are defined by

$$\begin{aligned}\widehat{\sigma}(t_k) &:= \left(\sqrt{\langle \Delta p_1(t)^2\rangle(t_k)}, \cdots, \sqrt{\langle \Delta p_n(t)^2\rangle(t_k)}\right),\\ \widehat{\omega}(t_k) &:= \left(\sqrt{\langle \Delta q_1(t)^2\rangle(t_k)}, \cdots, \sqrt{\langle \Delta q_n(t)^2\rangle(t_k)}\right),\end{aligned} \tag{6.13}$$

respectively, where the average $\langle . \rangle(t_k)$ is computed using data on the day $t_k$. We assume that the correlation matrices $\rho(\Delta p, \Delta p) = \mathrm{diag}(\sigma(t))^{-1}\Sigma(t)\,\mathrm{diag}(\sigma_t)^{-1}$ and $\rho(\Delta q, \Delta q) = \mathrm{diag}(\omega(t))^{-1}\Omega(t)\,\mathrm{diag}(\omega_t)^{-1}$, as well as the normalized response matrix $\rho(\Delta p, \Delta q) = \mathrm{diag}(\sigma(t))^{-1}R(t)\,\mathrm{diag}(\omega_t)^{-1}$, are stationary. Let $\widehat{\rho}(\Delta p, \Delta p)$, $\widehat{\rho}(\Delta q, \Delta q)$ and $\widehat{\rho}(\Delta p, \Delta q)$ denote their respective long-period estimators using a year of data. The covariance of any variable $x$ and $y$ can be expressed as the product of their correlation and each of their respective volatilities. Thus, on the day $t_k$, the estimated covariance and response matrices $\widehat{\Sigma}(t_k)$, $\widehat{\Omega}(t_k)$ and $\widehat{R}(t_k)$ are obtained by

$$\begin{aligned}\widehat{\Sigma}(t_k) &= \mathrm{diag}(\widehat{\sigma}(t_k))\widehat{\rho}(\Delta p, \Delta p)\,\mathrm{diag}(\widehat{\sigma}(t_k)),\\ \widehat{\Omega}(t_k) &= \mathrm{diag}(\widehat{\omega}(t_k))\widehat{\rho}(\Delta q, \Delta q)\,\mathrm{diag}(\widehat{\omega}(t_k)),\\ \widehat{R}(t_k) &= \mathrm{diag}(\widehat{\sigma}(t_k))\widehat{\rho}(\Delta p, \Delta q)\,\mathrm{diag}(\widehat{\omega}(t_k)),\end{aligned} \tag{6.14}$$

respectively.

### 6.3.2 Metrics definition

#### 6.3.2.1 Goodness-of-fit

For a given cross-impact model $\Lambda(t)$, the predicted price change for the time window $[t, t+\tau]$ due to the order flow imbalance $\Delta q(t)$ is defined as

$$\widehat{\Delta p}(t) := \Lambda(t)(\widehat{\Sigma}(t), \widehat{\Omega}(t), \widehat{R}(t))\Delta q(t). \tag{6.15}$$

To evaluate the goodness-of-fit of the cross-impact model $\Lambda$, we compare the predicted price changes $\widehat{\Delta p}(t)$ to the realized price changes $\Delta p(t)$. For this purpose, we use a performance indicator parameterized by a symmetric, positive definite matrix $W \in \mathcal{S}_n^+(\mathbb{R})$, $W \neq 0$. Let $\{t_1, \cdots, t_N\} \in \mathbb{R}^N$ denote $N$ sample times, $\{\Delta p_{t_1}, \cdots, \Delta p_{t_N}\}$ be a realization of the price process, and $\{\widehat{\Delta p}_{t_1}, \cdots, \widehat{\Delta p}_{t_N}\}$ denote the corresponding series of predictions from the model. The $W$-weighted generalized $\mathcal{R}^2(W)$ is defined as

$$\mathcal{R}^2(W) := 1 - \frac{\Sigma_{k=1}^N \left(\Delta p(t_k) - \widehat{\Delta p}(t_k)\right)^\top W \left(\Delta p(t_k) - \widehat{\Delta p}(t_k)\right)}{\Sigma_{i=1}^N \Delta p(t_k)^\top W \Delta p(t_k)}. \tag{6.16}$$

The closer this score is to one, the better is the fit to the actual prices. To highlight different sources of error, different choices of $W$ can be considered:

- $W = W_\sigma := \mathrm{diag}(\langle \Sigma(t)^2 \rangle)^{-1}$, to account for errors relative to the typical deviation of the assets considered. This type of error is relevant for strategies predicting idiosyncratic moves of the constituents of the basket, rather than strategies betting on correlated market moves.
- $W = W_{\sigma_i} := \mathrm{diag}((0, \ldots, 0, \langle \sigma_i(t)^2 \rangle, 0, \ldots, 0))^{-1}$, to account for errors of a single asset $i$.
- $W = \langle \Sigma(t) \rangle^{-1}$, to consider how well the model predicts the individual modes of the return covariance matrix. This would be the relevant error measure for strategies that place a constant amount of risk on the modes of the correlation matrix, leveraging up combinations of products with low volatility and scaling down market direction that exhibit large fluctuations.

Within the following sections, we mainly study the cross-impact goodness-of-fit for pairs $(i, j)$ of assets. In these cases, unless stated otherwise, we calculate $\mathcal{R}^2(W_{\sigma_i})$ to measure solely the errors on the first asset $i$, the predicted asset, as a function of the characteristics of the second asset $j$, the explanatory asset.

Additionally, we define a second indicator to determine the extent to which the goodness-of-fit results from cross-sectional information. We define $\Delta\mathcal{R}^2(W)$, the accuracy increase from the cross sectional model as

$$\Delta\mathcal{R}^2(W) := \mathcal{R}^2(W) - \mathcal{R}^{2,\mathrm{diag}}(W), \tag{6.17}$$

where $\mathcal{R}^{2,\mathrm{diag}}(W)$ is the $W$-weighted generalized $\mathcal{R}^2(W)$ obtained from the degenerated model without cross-sectional impact $\Lambda^{\mathrm{diag}}$.

Tests that confirm the statistical significance of the $\mathcal{R}^2$ in the case of a single asset are reported in the appendix C.1. Nevertheless, appendix C.2 demonstrates that the auto-correlation of signed order flows invalidates the linear framework used in this chapter. Using of a more accurate *propagator model* (Bouchaud et al., 2006; Bouchaud, 2010; Alfonsi et al., 2016; Benzaquen et al., 2017; Bouchaud et al., 2018; Schneider and Lillo, 2019) would yield only marginal improvements in the goodness-of-fit (Tomas et al., 2022b) but it would impede conducting this study at the same scale across time and assets.

#### 6.3.2.2 Definition of the assets characteristics

Several assets characteristics are investigated in this chapter:

- the *bin size* $\tau$;
- the *trading frequency* $f$, defined by the number of trades per second;
- the *price increments correlation* $\rho_{ij}$ between the assets $i$ and $j$;

- the *liquidity*, defined by the risk of profit or loss in monetary units $\bar{\omega}_i \bar{\sigma}_i$ over a given time window.

These metrics are further described at the beginning of each corresponding subsections below.

## 6.4 Results

### 6.4.1 The effect of the bin size

Within the linear framework previously defined, the market price impact of a single asset is a non-trivial function of the bin size $\tau$ (Fig. 6.1). Specifically, the goodness-of-fit $\mathcal{R}^2(W_{\sigma_i})$ increases with the bin size up to a maximum ranging generally between 10 and 100 seconds before decreasing down to a negligible level at 1 hour. It is worth noting that, for a single asset, the performances of the three previously mentioned models actually coincide. Indeed, these models all express price increments as a linear function of the signed order flow.

At short time scales, effects similar to the Epps effect (Epps, 1979; Toth and Kertesz, 2009) may prevent the correlation between the order flow and the price impact to become fully apparent without further corrections. Indeed, the correlation between the signed order flows and the price variations $\frac{R_{ii}}{\sigma_i \bar{\omega}_i}$ decreases when the time scale shortens (Fig. 6.1). In fact, this correlation is simply the square-root of the model accuracy $\mathcal{R}^2(W_{\sigma_i})$. Yet, among the causes of the Epps effect (lead-lag effects, asynchronicity, and the minimal response time of traders) (Toth and Kertesz, 2009), only the third factor is deemed relevant. Indeed, for a given asset, its signed order flows and prices are updated synchronously with no lead-lag. More prosaically, when the bin size widens, the number of trades per bin increases and so does the accuracy of the model.

At larger time scales, the predictive power of the linear impact model decreases rapidly (Fig. 6.1). This decay cannot be attributed to the transient effect from the price impact. Indeed, the magnitude of the price impact follows a power law with a slow decline, typically remaining significant after a thousand trades (Bouchaud et al., 2018). In the above example, the number of trades accumulated within one hour (the largest bin) is around 1400. Consequently, it is reasonable to anticipate that the impact of the first trades within a bin would continue to be substantial at this time scale. However, we observe a decrease in the price impact model accuracy after a couple of minutes.

More generally, the impact from all the other trades, including the most recent ones, should be observable on the current price change in a bin, even at large time scales. However, as documented by Patzelt and Bouchaud (2017), 2018, the relationship between the signed order flows and the price changes is actually

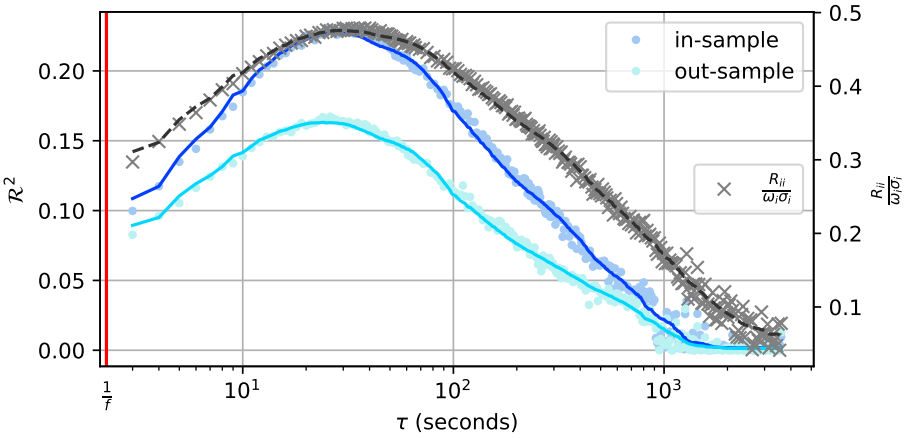


**Figure 6.1:** Single asset generalised R-squared $\mathcal{R}^2(W_{\sigma_i})$ as a function of the bin size $\tau$ for the asset $TRMB$ (*Trimble Navigation*). In-sample results were calibrated on the year 2021, while out-of-sample outcomes cover 2022. The vertical red line indicates the average time interval between two trades $1/f$.

reasonably fitted by a sigmoid function. This latter is indeed linear for reasonably small sizes of signed order flows. Yet, the non-linear relationship between price impacts and larger sizes of signed order flows, which is frequently observed in large-scale bins, explains the lower precision of linear models at these scales.

The relationship between the bin size $\tau$ and the model accuracy $\mathcal{R}^2(W)$ provides an avenue to determine the maximum goodness-of-fit $\mathcal{R}^{2*}(W)$ and its corresponding optimal time scale $\tau^*(W)$. The ensuing sections investigate how these latter are influenced by the trading frequency of the assets, correlation among assets, and liquidity of the assets.

### 6.4.2 The effect of the trading frequency

#### 6.4.2.1 Time scales

For a given asset, we define its trading frequency $f$ as its average number of trades per second during open market hours. Intuitively, one could expect higher trading frequencies to be associated with shorter optimal time scales $\tau^*$, due to the quickest accumulation of trades in a bin. Empirically, higher trading frequencies do decrease the minimum optimal time scales achievable, yet other factors cause the considered assets to deviate from this limit. Specifically, the envelope of the normalized density plot associating optimal time scales to trading frequencies does not contain the lower left section of Fig. 6.2. Thus, a minimum number of trades is required to reach the optimal bin size. Specifically, the blue straight line on this

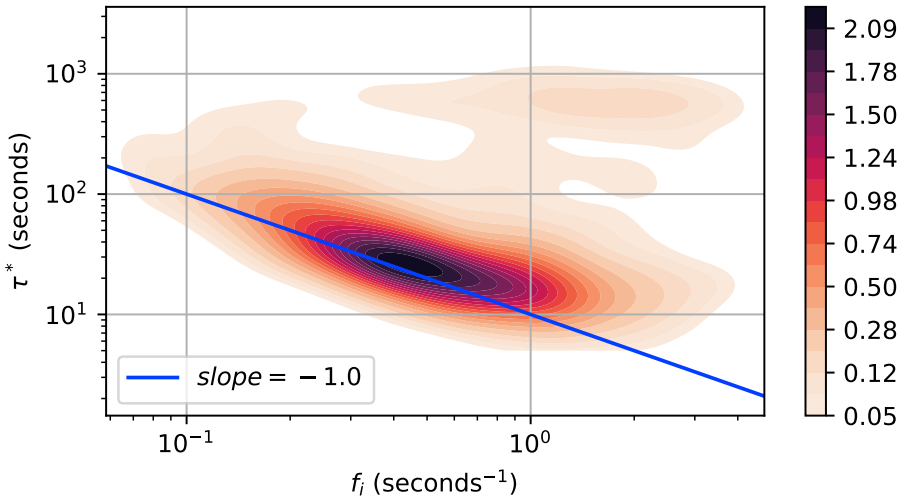


**Figure 6.2:** Empirical distribution of the optimal time scale out-of-sample $\tau^*(W_{\sigma_i})$ as a function of the trading frequency $f$ for single assets.

figure represents the function $f \to 1/f$. Hence, one can estimate this minimum number of trades as the intercept ensuring that the majority of the data points are above this line. We find that a minimum of 10 to 20 trades is required to reach the optimal time scale of a linear cross-impact model.

The light brown area at the top right of Fig. 6.2 reveals a smaller group of assets with maximum cross-impact accuracy $\mathcal{R}^{2*}(W_{\sigma_i})$ for extended time scales. This group includes mainly large capitalization stocks (e.g. AMZN, AAPL, TSLA) and highly traded Futures (E-mini S&P Future, 10-year bond Future). For these assets, the causes decreasing the accuracy of the model seems to become effective for a larger number of trades (500 to 5000 trades).

Figure 6.3b shows the impact of the trading frequency of the explanatory asset $j$ regarding the goodness-of-fit on asset $i$, when calibrating the model on pairs of assets. Specifically, $\tau^*_\Delta(W_{\sigma_i})$ corresponds to the time scale maximizing the added accuracy, $\Delta\mathcal{R}^{2*}(W_{\sigma_i})$, when predicting asset $i$'s price increments. This indicator is driven by the trading frequency of the explanatory asset, as shown by the triangle form of Fig. 6.3b. As expected, this behavior cannot be observed when one increases the trading frequency of the predicted asset (Fig. 6.3a).

On one hand, the optimal time scale for the cross-sectional effect is influenced by the trading frequency of the explanatory asset. On the other hand, the optimal time scale in the diagonal model is influenced by the frequency of the predicted asset. Consequently, significant deviations between the optimal time scales of the diagonal and cross section models are expected. As depicted in Fig. 6.4, these

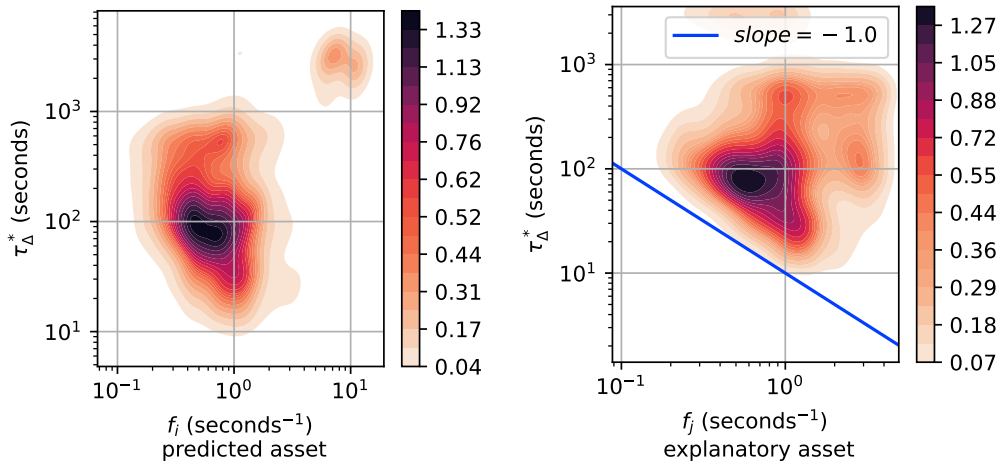


**(a)** As a function of $f_i$, the trading frequency of the predicted asset.

**(b)** As a function of $f_j$, the trading frequency of the explanatory asset.

**Figure 6.3:** Empirical distribution of the optimal time scale out-of-sample $\tau^*_\Delta(W_{\sigma_i})$ as a function of the trading frequency of the predicted asset $f_i$ (Fig. 6.3a) or the explanatory asset $f_j$ (Fig. 6.3b). The asset pairs are filtered on the 7% of the sample exhibiting a correlation higher than 50% (see section 6.4.3).

deviations increase when the trading frequencies of the two assets diverge. This may decrease the relevance of linear cross-impact models. Indeed, the optimal time scale of the cross sectional impact may be reached when the loss of accuracy from the direct price impact is higher than the marginal gain. However, this effect remains limited as demonstrated in section 6.5.2.

Finally, Fig. 6.5b demonstrates that the time scale $\tau^*_\Delta(W_{\sigma_i})$ maximizing the added accuracy, is affected by the minimum of the trading frequencies of the assets pair. In contrast, the maximum of these two frequencies has little effect on this time scale (Fig. 6.5a). We observe the same behavior with respect to the optimal time scale $\tau^*(W_{\sigma_i})$ (Fig. 6.6). Consistently with the single asset case, we find that a minimum of 10 to 20 trades in both assets is required to reach the optimal time scale of a two-dimensional cross-impact model.

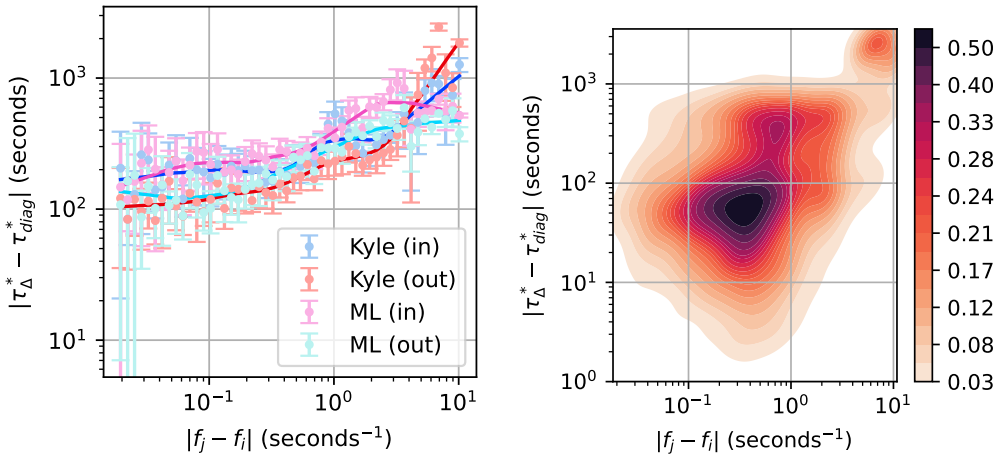


**(a)** Mean deviation $\left|\tau^*_\Delta(W_{\sigma_i}) - \tau^*_{\text{diag}}(W_{\sigma_i})\right|$ by buckets of trading frequency gaps $|f_j - f_i|$.

**(b)** Empirical distribution of the deviation $\left|\tau^*_\Delta(W_{\sigma_i}) - \tau^*_{\text{diag}}(W_{\sigma_i})\right|$ in the Kyle model.

**Figure 6.4:** Asynchronicity of the diagonal and cross sectional models $\left|\tau^*_\Delta(W_{\sigma_i}) - \tau^*_{\text{diag}}(W_{\sigma_i})\right|$, aggregated by buckets of trading frequency gaps (Fig. 6.4a) or unaggregated (Fig. 6.4b). The asset pairs are filtered on the 7% of the sample exhibiting a correlation higher than 50% (see section 6.4.3).

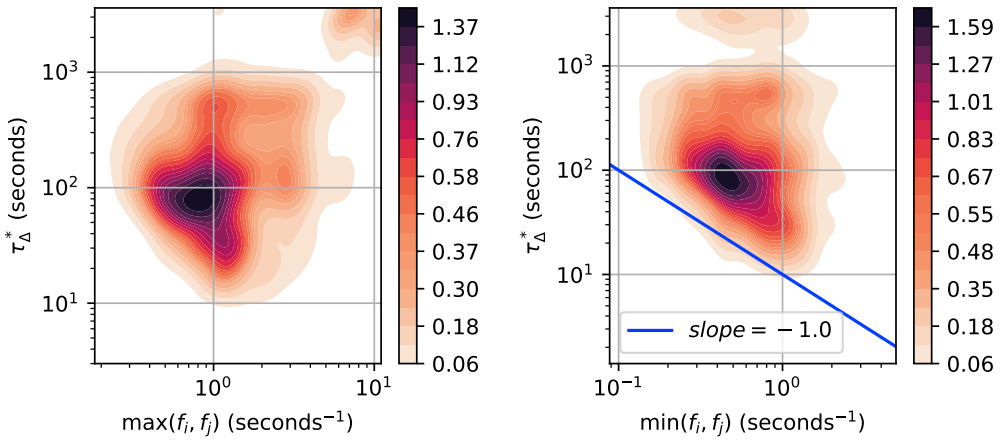


**(a)** As a function of the maximum of the trading frequencies.

**(b)** As a function of the minimum of the trading frequencies.

**Figure 6.5:** Empirical distribution of the added accuracy optimal time scale out-of-sample $\tau^*_\Delta(W_{\sigma_i})$ as a function of the maximum (Fig. 6.5a) or the minimum (Fig. 6.5b) of the trading frequencies of the assets pairs. The asset pairs are filtered on the 7% of the sample exhibiting a correlation higher than 50% (see section 6.4.3).

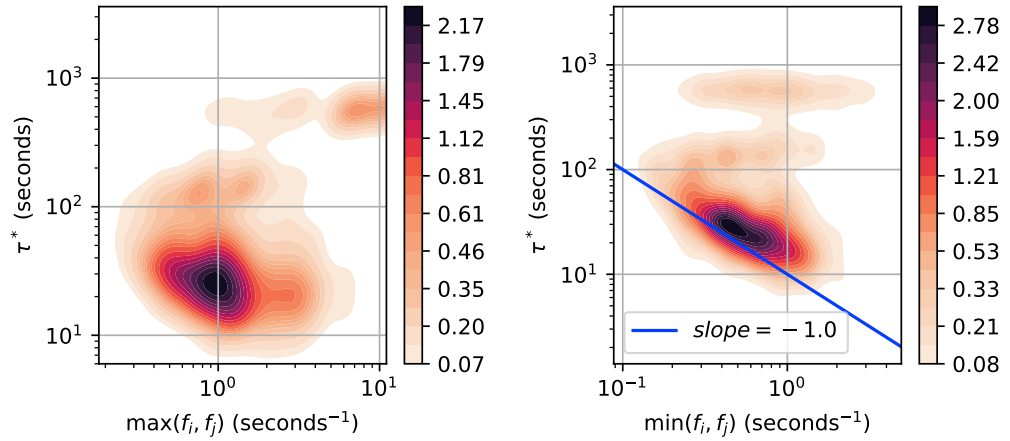


**(a)** As a function of the maximum of the trading frequencies.

**(b)** As a function of the minimum of the trading frequencies.

**Figure 6.6:** Empirical distribution of the optimal time scale out-of-sample $\tau^*(W_{\sigma_i})$ as a function of the maximum (Fig. 6.6a) or the minimum (Fig. 6.6b) of the trading frequencies of the assets pairs. The asset pairs are filtered on the 7% of the sample exhibiting a correlation higher than 50% (see section 6.4.3).

#### 6.4.2.2 Goodness-of-fit

The trading frequency has a positive effect on the maximal accuracy $\mathcal{R}^{2*}(W_{\sigma_i})$ observed across the tested bin sizes. Indeed, Fig. 6.7 shows that an increase in the trading frequency improves the mean $\mathcal{R}^{2*}(W_{\sigma_i})$ per bucket. Here, the bars shaded in light pastel colors denote the range of two standard deviations surrounding the mean $\mathcal{R}^{2*}(W_{\sigma_i})$ of the assets bucketed by trading frequency. The continuous lines in bright colors are the *Locally Weighted Scatterplot Smoothing* (Cleveland, 1979) of these mean values. The following figures portraying bucketed data conform to the same convention.

The higher accuracy of the cross-impact model on highly traded assets can be attributed to the stronger correlation between prices and order flows when a sufficiently large number of market participants ensure the consistency of the two. However, it must be underlined that the impact of trading frequency is partially offset by observing the optimal accuracy $\mathcal{R}^{2*}(W_{\sigma_i})$ across bin sizes, resulting in a relatively stable number of trades across trading frequencies. This effect probably explains the low slope in Fig. 6.7 when excluding data points with large error bars.

Notice also the ML model out-of-sample performance in Fig. 6.7b is significantly larger than that of the Kyle model, as previously reported in Tomas et al. (2022b). The ML model can be easily over-fitted if one uses too little data, as

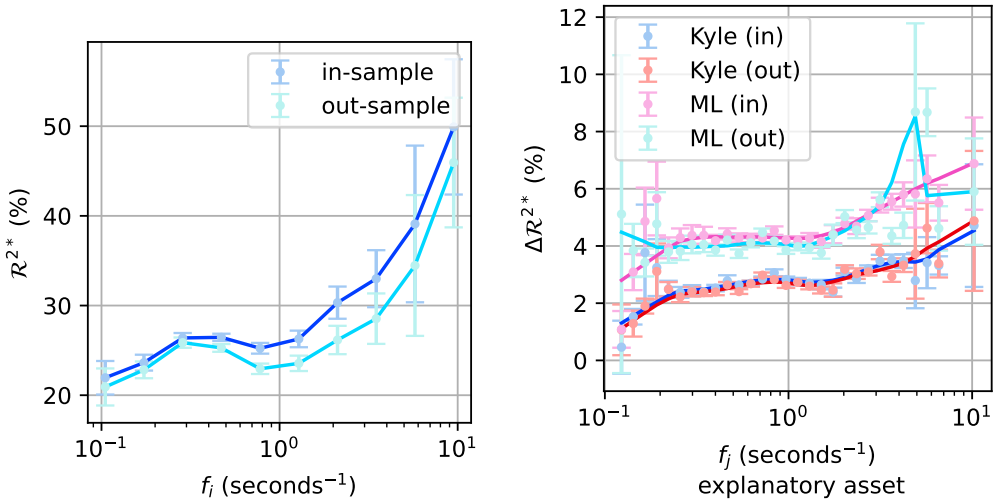


**(a)** Single assets in the diagonal model.

**(b)** Pairs of assets. The asset pairs are filtered on the 7% of the sample exhibiting a correlation higher than 50%.

**Figure 6.7:** Mean per trading frequency bucket of the optimal goodness-of-fit $\mathcal{R}^{2*}(W_{\sigma_i})$ for single assets (Fig. 6.7a) and pairs of assets (Fig. 6.7b).

it is more flexible than the Kyle model that imposes a no arbitrage condition. The fact that the out-of-sample performance of ML is better than Kyle shows that: (i) frictions in the market (bid-ask spread, fees) at least partially spoil the no-arbitrage assumption, as documented in Schneider (2019); (ii) this effect is significant enough to generalize well to yet unseen data.

To provide a broader view of the distribution of $\mathcal{R}^{2*}(W_{\sigma_i})$ across trading frequencies in our sample, we also present this data by density in Fig. 6.8. The figure shows that most assets exhibit a trading frequency around 0.5 trades per second, with an $\mathcal{R}^{2*}(W_{\sigma_i})$ of 25%.

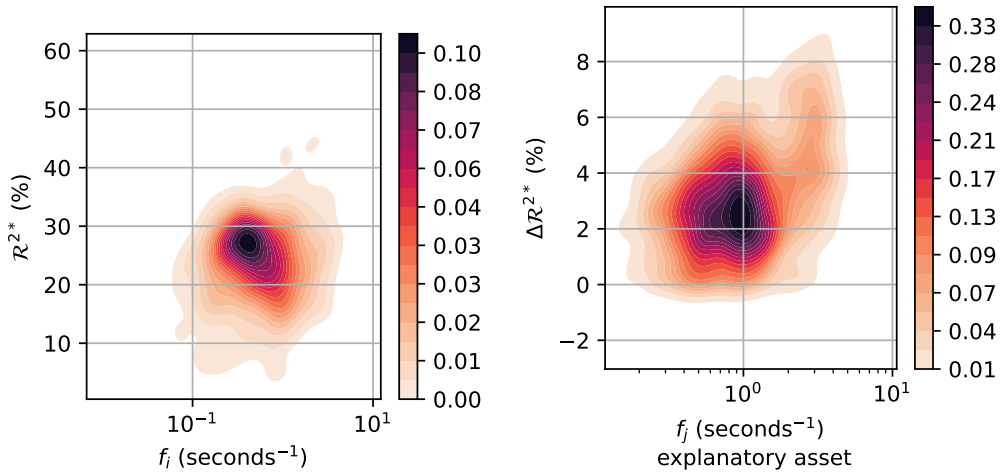


**(a)** Single assets in the diagonal model.

**(b)** Pairs of assets in the Kyle model. The asset pairs are filtered on the 7% of the sample exhibiting a correlation higher than 50%.

**Figure 6.8:** Empirical distribution of the optimal out-of-sample $\mathcal{R}^{2*}(W_{\sigma_i})$ as a function of the trading frequency $f$ for single assets (Fig. 6.7a) and pairs of assets (Fig. 6.8b).

### 6.4.3 The effect of the correlation among assets

In this section, we examine the influence of asset correlations on cross-impact, emphasizing a clear distinction between these two concepts. This differentiation is pivotal since cross-impact effects reveal intricate relationships between correlation and liquidity. For example, when trading a diversified portfolio, execution costs are magnified on low liquidity factors regardless of correlation.

As detailed in chapter 5 correlations among assets are influenced by the time scale at which prices are sampled (Epps, 1979; Renò, 2003; Toth and Kertesz, 2009). Therefore, we use a bin size sufficiently large for the Epps effect to be negligible. Relying on the analysis presented on Fig. 6.9, we choose a 5-minute bin. This time scale is a good compromise between Epps effect and noise.

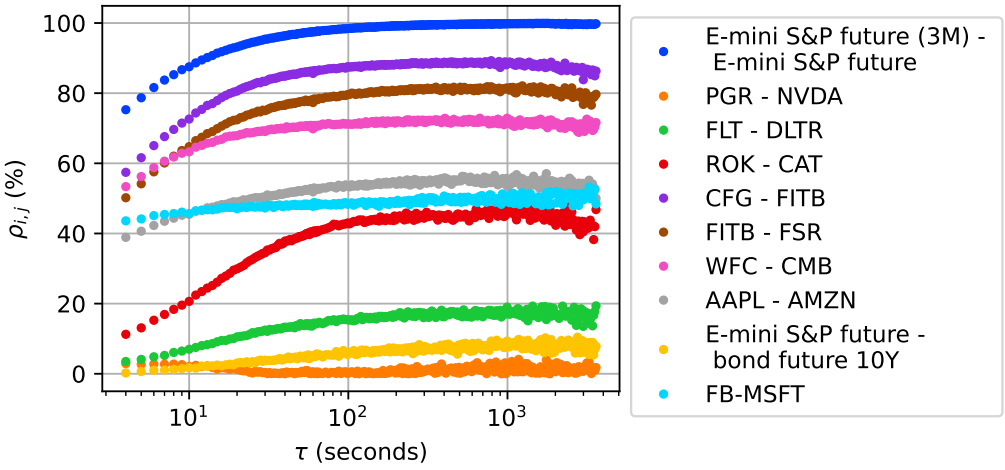


**Figure 6.9:** Pearson correlation coefficients $\rho_{i,j}$ as a function of the bin size $\tau$, for a selection of assets couples. Bin size can chosen arbitrarily small when utilizing tick-by-tick data.

#### 6.4.3.1 Goodness-of-fit

As expected, we observe a positive and monotonous relationship between the added accuracy from the cross sectional information $\Delta\mathcal{R}^{2*}(W_\sigma)$ and the correlation $\rho_{ij}$ among pairs of assets. For both the Kyle and ML models, $\Delta\mathcal{R}^{2*}(W_\sigma)$ increases from 0 to above 5% over the range of correlation levels in our sample (Fig. 6.10). Regarding Fig. 6.10a and the following density plots, the continuous line slope represents the Theil-Sen estimator (Sen, 1968; Siegel, 1982; Theil, 1992), while the dotted lines indicate the 95% confidence interval around this estimate.

#### 6.4.3.2 Time scales

The optimal time scale $\tau^*(W_\sigma)$ seems unaffected by the correlation level $\rho_{ij}$ among pairs of assets. Indeed, Fig. 6.11b shows that the mean value of $\tau^*_\Delta(W_\sigma)$ is almost independent from the correlation level.

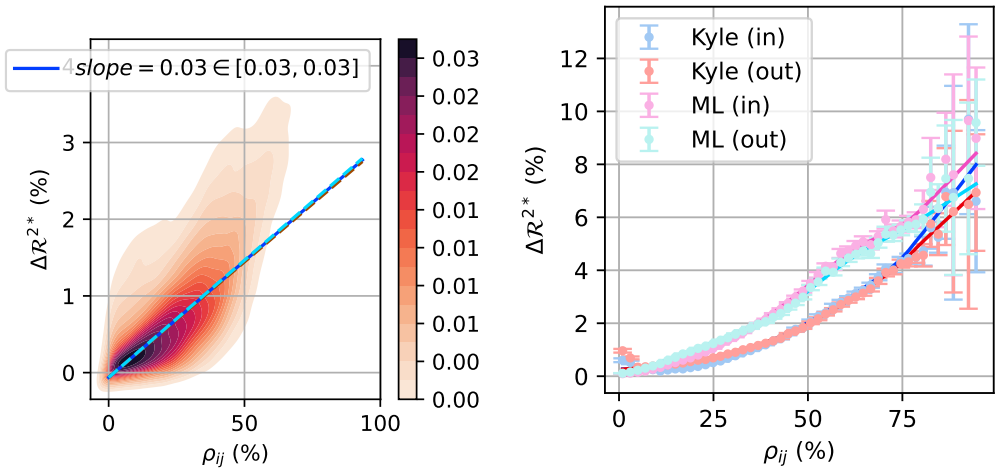


**(a)** Empirical distribution of the out-of-sample $\Delta\mathcal{R}^{2*}(W_\sigma)$ in the Kyle model.

**(b)** Mean per correlation bucket of the optimal $\Delta\mathcal{R}^{2*}(W_\sigma)$.

**Figure 6.10:** Optimal $\Delta\mathcal{R}^{2*}(W_\sigma)$, accounting for errors relative to both assets, as a function of the correlation $\rho_{ij}$ for pairs of assets.

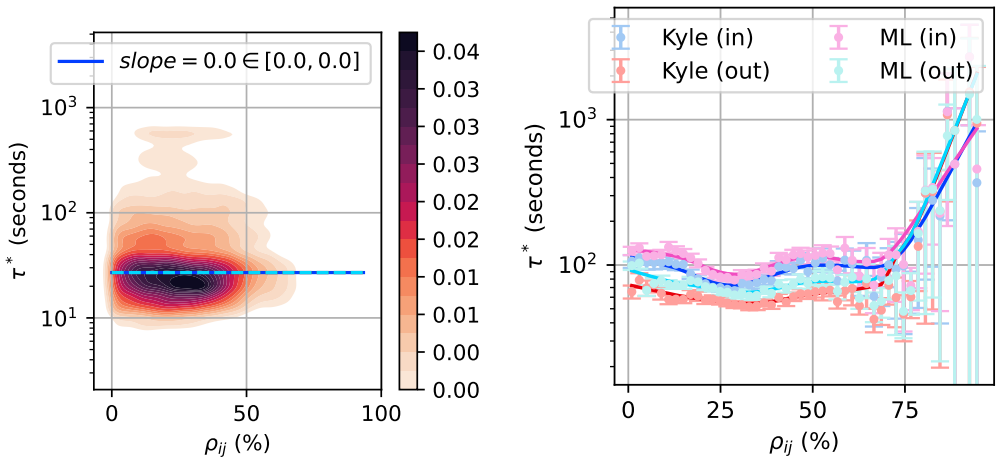


**(a)** Out-of-sample empirical distribution in the Kyle model.

**(b)** Mean per correlation bucket.

**Figure 6.11:** Optimal time scale $\tau^*(W_\sigma)$ as a function of the correlation level $\rho_{ij}$ for pairs of assets.

### 6.4.4 The effect of the liquidity

#### 6.4.4.1 Goodness-of-fit

The liquidity of each individual asset is measured using a risk indicator that represents the typical size of gains or losses during a given time interval. Specifically, the liquidity of the asset $i$ is defined by $\bar{\omega}_i \bar{\sigma}_i$, estimated at a given bin size. We set the bin size to 5 minutes, consistently with the binning frequency for the correlation estimation (see section 6.4.3).

Liquidity has a positive effect on the accuracy of the cross-impact models tested, both for single assets and pairs of assets. Indeed, we observe that the out-of-sample goodness-of-fit increases from below 20% to around 30% across the liquidity levels in our sample for the diagonal model (Fig. 6.12a). Like the interpretation proposed in section 6.4.2, the higher score on liquid assets can be explained by the stronger correlation between prices and order flows when market liquidity is sufficient to ensure their consistency. As previously, we also present these results through density plots in Fig. 6.13. These plots illustrate that most assets exhibit a liquidity level of 500 USD per 5 minutes and an $\mathcal{R}^{2*}(W_{\sigma_i})$ of around 25%.

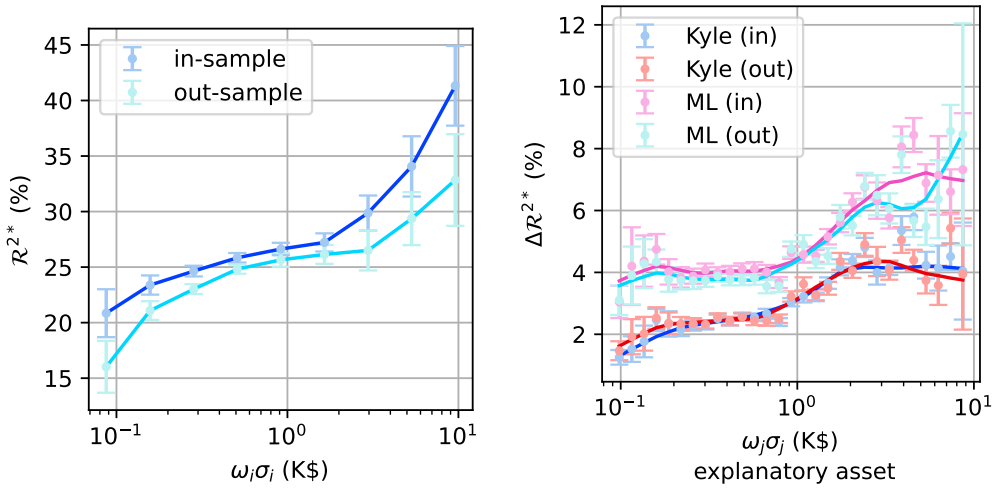


**(a)** Single assets.

**(b)** Pairs of assets filtered on the 7% of the sample exhibiting a correlation higher than 50%.

**Figure 6.12:** Mean $\mathcal{R}^{2*}(W_{\sigma_i})$ by liquidity bucket for single assets (Fig. 6.12a) and pairs of assets (Fig. 6.12b).

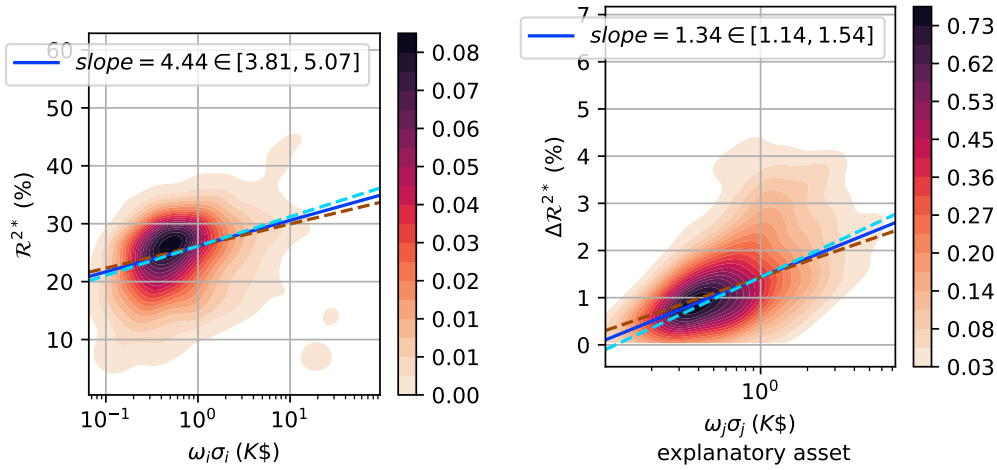


**(a)** Single assets in the diagonal model.

**(b)** Pairs of assets filtered on the 7% of the sample exhibiting a correlation higher than 50%.

**Figure 6.13:** Empirical distribution of the out-of-sample $\mathcal{R}^{2*}(W_{\sigma_i})$ as a function of the liquidity, for single assets (6.13a) and pairs of assets (6.13b).

#### 6.4.4.2 Time scales

In contrast, liquidity has an ambiguous effect on the optimal time scale $\tau^*(W_{\sigma_i})$. Notably, Fig. 6.14b exhibits two groups of assets: (i) a large group with medium liquidity and time scales around 90 seconds, (ii) a smaller group with higher liquidity and time scales around 10 minutes. Within both groups, the liquidity seems to have a limited effect on the optimal time scale. These results suggest that other underlying properties of the considered assets influence the optimal time scale.

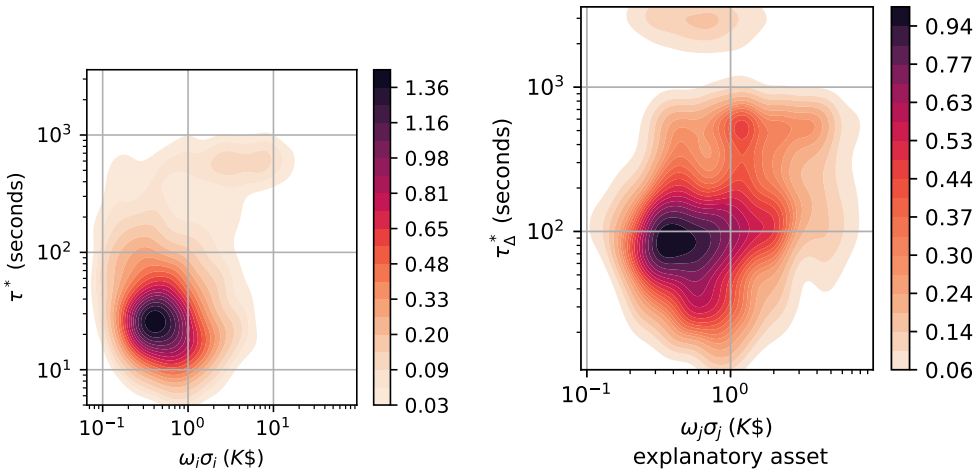


**(a)** Single assets.

**(b)** Pairs of assets in the Kyle model, filtered on the 7% of the sample exhibiting a correlation higher than 50%.

**Figure 6.14:** Empirical distribution of the optimal bin size $\tau^*(W_{\sigma_i})$ as a function of the liquidity, for single assets (Fig. 6.14a) and pairs of assets (Fig. 6.14b).

#### 6.4.4.3 Cross effects of individual assets' liquidity

Our objective is to evaluate whether the added accuracy in the Kyle model is consistent with the stability properties outlined in section 6.2.2. Specifically, we seek to determine whether $\Delta\mathcal{R}^2(W_{\sigma_i})$ decreases as stock $i$'s liquidity increases, but increases as stock $j$'s liquidity increases, for a given pair $(i, j)$ of assets. Notably, we expect that incorporating trades information from a high-liquidity asset to predict the prices of a low-liquidity asset will significantly enhance accuracy. However, this effect is not evident in Fig. 6.15 due to the cross-effect of the correlation among assets. In fact, the greatest increase in accuracy for predicting asset $i$'s prices is observed for relatively high levels of liquidity of asset $i$. Empty cells in Fig. 6.15 and the following heatmaps correspond to either an absence of assets in the associated buckets or to filtered-out results due to measurement errors being greater than than 50% of the mean value. As previously, these errors are defined by two standard deviations.

Thus, we neutralize the effect of the correlation in Fig. 6.16 by grouping the asset pairs of our sample into correlation buckets. While at low correlations levels (from 0% to 20%) the lowest liquid asset remains poorly predicted by the highest liquid asset, the effect of the cross sectional information becomes significant when looking at pairs of well correlated assets (above 50%). In a nutshell, cross-impact is significant if the predicted asset has a lower liquidity than the explanatory asset.

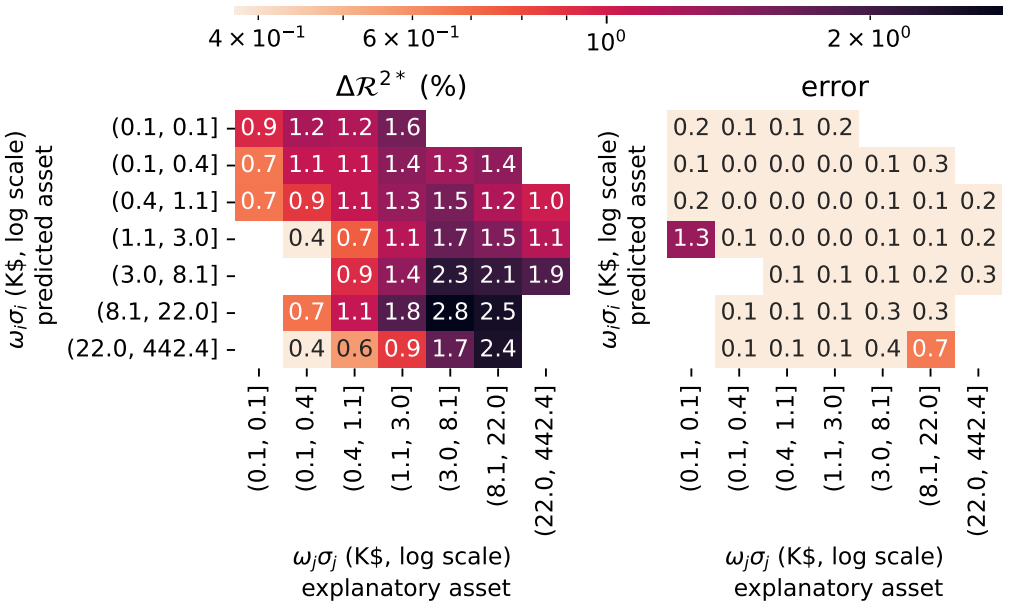


**Figure 6.15:** Mean out-of-sample added accuracy on asset $i$ $\Delta\mathcal{R}^2(W_{\sigma_i})$, as a function of the individual risk levels of each asset in the Kyle model.

### 6.4.5 Discussion

Cross-impact is not relevant under all circumstances. Following this analysis, one can establish three requirements to accurately predict prices from cross sectional trades. Firstly, cross-impact does not occur at every time scale. A minimum number of trades in both assets, between 10 to 20, is required to observe a significant added accuracy on the prediction of asset prices. Secondly, trades only significantly explain the prices of highly correlated assets (correlations higher than 50%), regardless of the time scale. Thirdly, cross-impact explains a larger share of price variances if the predicted asset has a lower liquidity than the explanatory asset.

The previous section also establishes that on a pairwise basis, cross-impact is not a dominant effect among instruments with small correlations and comparable liquidity. This is in line with the results of Cont et al. (2023), showing that on US stock markets, where correlations are on average quite low (i.e. 25 % in our sample for the $2017 - 2022$ period), pairwise cross-impact does not explain a large part of the price variance. However, cross-impact being small on a pairwise basis does not imply it remains a subdominant effect along factors or portfolio, as reported in Tomas et al. (2022b) and Benzaquen et al. (2017). Indeed, the aggregation of flow from a large number of weakly correlated instruments can still lead to a

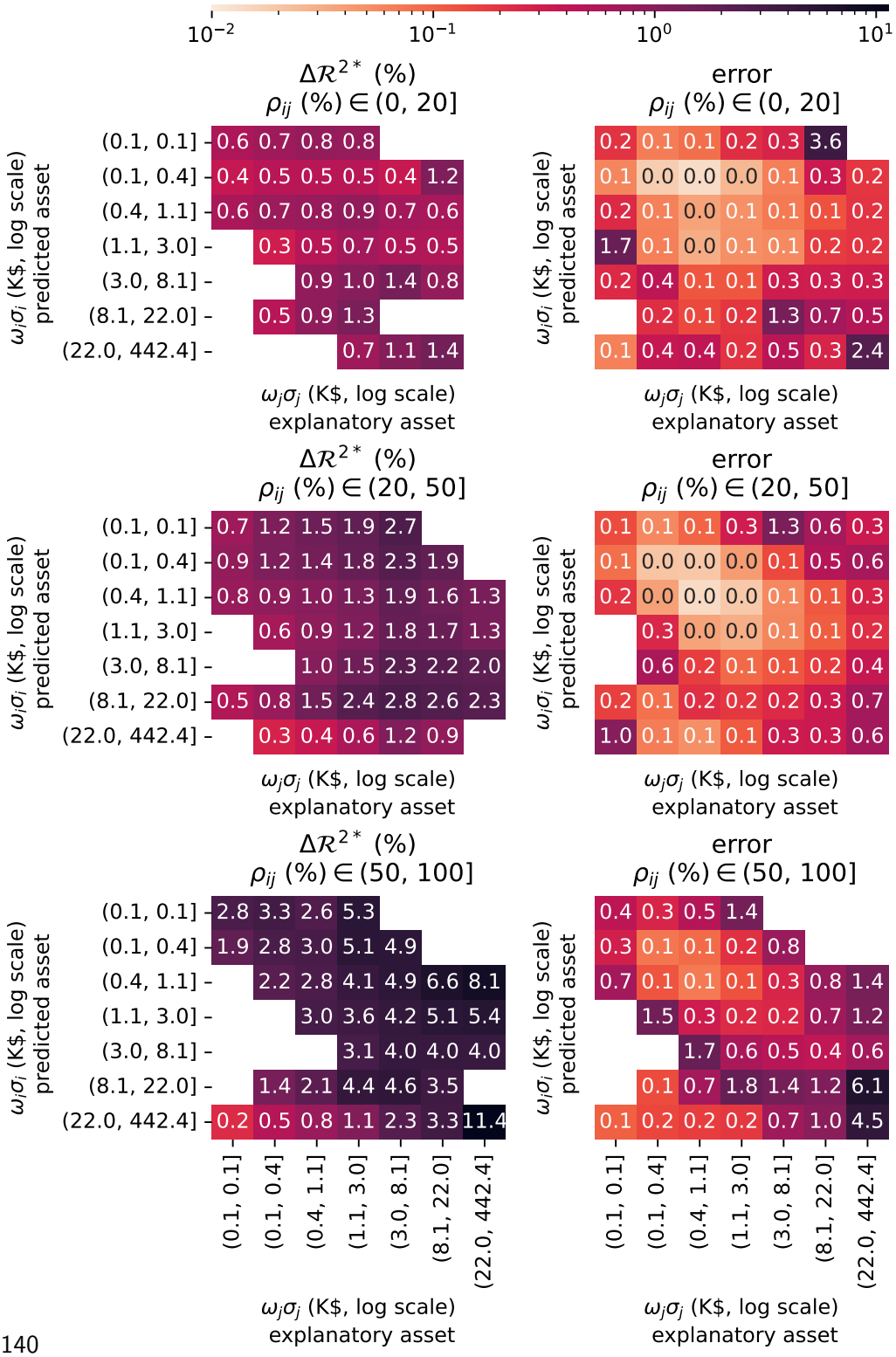




**Figure 6.16:** Mean out-of-sample added accuracy on asset $i$ $\Delta\mathcal{R}^2(W_{\sigma_i})$, as a function of the individual risk levels of each asset in the Kyle model.

significant increase of explanatory power for the price of a factor or a complex portfolio (Cont et al., 2023). The next section will illustrate this effect in the case of bonds.

To conclude, we can draw the following narrative. Price formation occurs endogenously within highly liquid assets. Then, trades in these assets influence the prices of their less liquid correlated products, with an impact speed constrained by their minimum trading frequency.

## 6.5 Application to the interest rate curve

### 6.5.1 Assets pairs

According to the previously established narrative, the interest rate curve should be a good candidate to apply a cross-impact model. Indeed, bonds of different tenors are highly correlated and display a wide range of liquidity levels. In this context, we run our previous analysis on a restriction of our initial sample to sovereign cash bonds and bonds Futures in the United States for the $2021 - 2022$ period. Figure 6.17 shows that including the trades of the most liquid assets (the 10-year Future and cash bond) significantly increases the prediction accuracy concerning most of the other less liquid tenors.

Of particular significance, Fig. 6.17 reveals that the trading information transmission flows from the most liquid tenors to that of lower liquid. This behavior challenges the validity of the theory in Financial Economics that regards long-term rates as agents anticipations of future short term rates. In practice, the prices of the low-liquidity tenors are more strongly impacted by the trades of the high-liquidity tenors than vice-versa (e.g. the 2-year cash bond in Fig. 6.18). Future work could be devoted to the extension of this analysis to repurchase agreements of shorter tenors (such as 1-day, 1-week and 1-month tenors).

Because of the correlation among assets, the total added accuracy from using all asset trades information is not the summation of a given row of the matrix displayed in Fig. 6.17. Therefore, we display the multidimensional case in the next section.

### 6.5.2 Multidimensional case

To measure the contribution of each explanatory asset in the multidimensional case, we run the Kyle model using an increasing number of instruments. The results are presented in Fig. 6.18. Each matrix item $\mathcal{R}^2_{ij}$ corresponds to the out-of-sample goodness-of-fit $\mathcal{R}^2(W_{\sigma_i})$ regarding the prediction of asset $i$ from the set $\{1, \ldots, j\}$ of explanatory assets. In the case of diagonal items, each $\mathcal{R}^2_{ii}$ represents the effect of the diagonal model using the explanatory asset $i$. For example, the

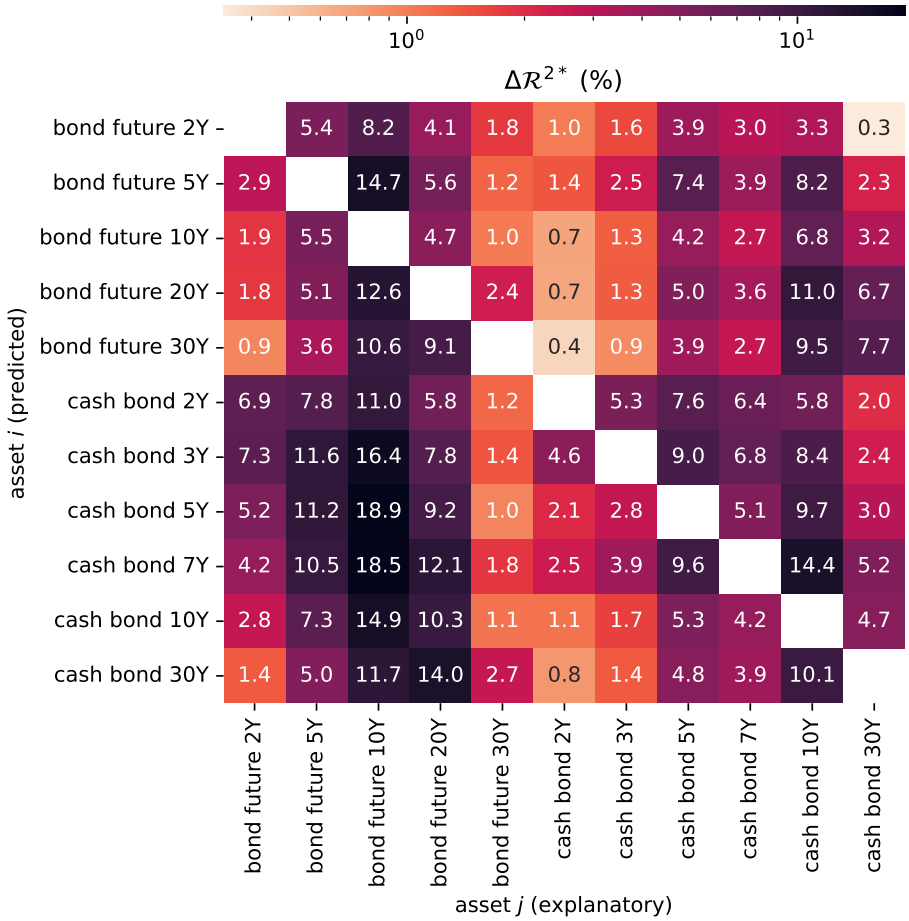


**Figure 6.17:** Out-of-sample added accuracy $\Delta\mathcal{R}^2(W_{\sigma_i})$ in the Kyle model for each pair of assets of the interest rate curve.

row *cash bond 5Y* can be understood as follow: its own trades explain 11.8% of its price increments variance, but the contribution of the other assets increase this score from 14.1% (using the 2-year cash bond) to 45.2% (using all assets).

Thus, Fig. 6.18 shows that we can significantly increase the explanatory power of even the most liquid asset when using a sufficiently large number of instruments of lower liquidity. More generally, this example demonstrates that a minor cross-impact effect between a pair of assets may not necessarily translate to a minor cross-impact effect at the portfolio level.

### 6.5.3 Kyle matrix analysis

Figures 6.19 and 6.20 display the Kyle matrix on 9 November 2021 under two different normalization conventions.

First, Fig. 6.19 exhibits the Kyle matrix normalized by assets' mean prices $\frac{\Lambda_{i,j}}{\bar{p}_i \bar{p}_j}$, where $\bar{p}_j = \langle p_j \rangle(t)$. Thus, it defines the relative estimated price impact $\frac{\widehat{\Delta p_i}(t)}{\bar{p}_i}$ on asset $i$ from the traded volumes in dollars $\bar{p}_j \Delta q_j(t)$ on asset $j$. Indeed, one can rewrite equation 6.2 as

$$(\operatorname{diag} \bar{p})^{-1} \widehat{\Delta p}(t) = (\operatorname{diag} \bar{p})^{-1} \Lambda(t) (\operatorname{diag} \bar{p})^{-1} \operatorname{diag} \bar{p} \Delta q(t). \tag{6.18}$$

However, this re-scaling result in over-weighting the longest tenors. Indeed, for a given interest rate $r$, the price of a zero-coupon bond contract of tenor $T$ and notional $N$ can be written as $p = \frac{N}{(1+r)^T} \approx \frac{N}{rT}$ for $r \ll 1$ and $rT \gg 1$. Consequently, the bond or Future contract value decreases linearly with the tenor, so the normalized cross-impact matrix coefficients $\frac{\lambda_{i,j}}{\bar{p}_i \bar{p}_j}$ are proportional to the squared tenor $T^2$. This effect explains the regularities observed in Fig. 6.19.

To neutralize the effect of the maturity, we propose a second normalization approach. Fig. 6.20 presents the Kyle matrix items normalized by the opposite of the tenor on the left and by the product of the price and tenor on the right: $-10 \frac{\lambda_{i,j}}{T_i \bar{p}_j T_j}$, where $T_i$ is the tenor of the bond $i$. These values define the absolute change in the interest rate $-\frac{\widehat{\Delta p_i}(t)}{T_i}$ of the bond $i$ from the traded volumes (in USD) in equivalent 10-year contract in the bond $j$: $\frac{T_j}{10} \bar{p}_j \Delta q_j(t)$. Formally, it is the reformulation of equation 6.2 as

$$-(\operatorname{diag}(T))^{-1} \widehat{\Delta p}(t) = -(\operatorname{diag}(T))^{-1} \Lambda(t) (\operatorname{diag}(T) \operatorname{diag}(\bar{p}))^{-1} \operatorname{diag}(T) \operatorname{diag}(\bar{p}) \Delta q(t). \tag{6.19}$$

This second approach neutralizes the effect of the tenor on both input volumes and observed prices. Thus, the remaining differences among assets are notably due to correlation and liquidity levels.

In this context, we are able to make four observations from Fig. 6.20.

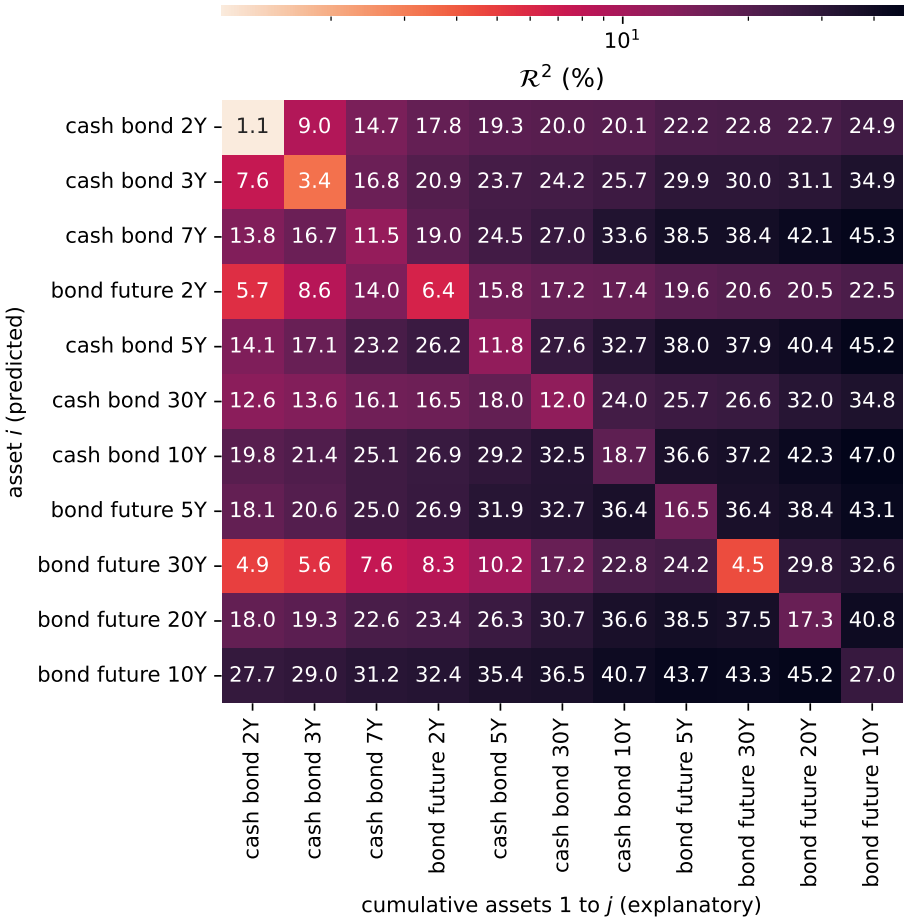


**Figure 6.18:** Out-of-sample goodness-of-fit $\mathcal{R}^2(W_{\sigma_i})$ for an increasing number of explanatory assets. The bin size was set to 30 minutes, which is close to the optimal time scale for these assets.

1. Overall impacts are of similar sign and magnitude across all assets, which highlights the first factor of the interest rate curve, the *parallel shift* (Brigo and Mercurio, 2006), due to high correlations.

2. Volumes traded on the Future of a given tenor affect more significantly the interest rates of the closest tenors, which shows that correlations are higher among assets of close maturity. Equivalently, it exhibits the structure of other factor(s) beyond the parallel shift.

3. We observe a similar behavior for cash and Futures contracts, because of the high correlations between an underlying and its derivative.

4. As a last observation, notice that models relying on no-arbitrage in order to propagate liquidity shocks through a small number of factors (parallel shift, slope, convexity) usually predict that trading a low-liquidity asset is not expensive, as long as it is exposed to a liquid factor. In our framework, trading a low-liquidity asset is still expensive, which limits the ability to close arbitrage opportunities. This is because the empirical correlation matrices are never exactly low rank, as assumed in an idealized factor model, and heterogeneity in liquidity amplifies impact on directions of low volatility (for e.g. spread between tenor-matched cash bonds and Futures).

## 6.6 Conclusion

Prices at a given time are actually influenced by the history of all previous trades through a complex process that can be formalized within the *propagator model*. As its calibration is computationally intensive, our study of multidimensional price formation focuses on linear models. While the auto-correlation of signed order flows invalidates these models, they remain significant to predict prices. Notably, we have demonstrated that accurate predictions of price variations can be achieved by appropriately considering the time scale, the correlation among assets, and the liquidity, while increasing the number of explanatory assets. More importantly, we have shown that highly liquid assets determine their prices internally and that their trades influence the prices of correlated, less liquid assets. In other worlds, price-volume correlations depend on the liquidity of the considered assets. In the case of interest rate markets, the 10-year bond Future serves as the main liquidity reservoir influencing the prices of the other tenors, contrary to prevailing Financial Economics theories.

However, our analysis has revealed certain gaps. Certain asset prices are best explained by their trades at significantly longer time scales than suggested by their trading frequency. More generally, our investigation into the sensitivity of optimal

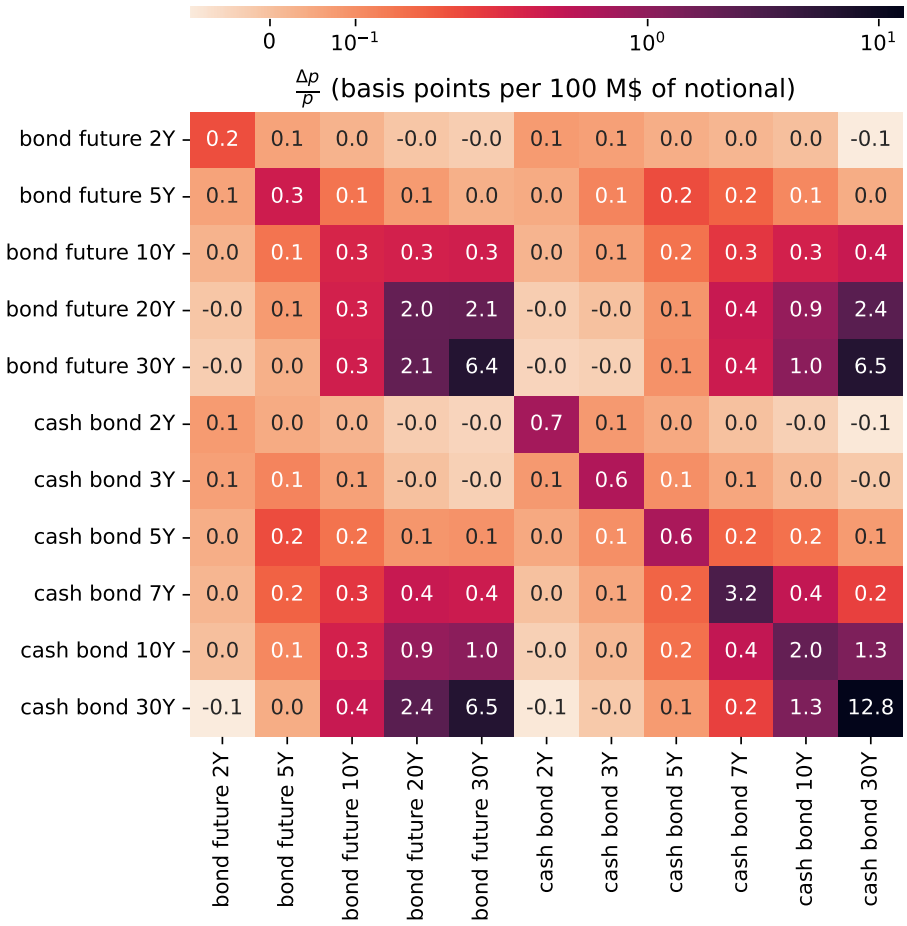


**Figure 6.19:** Kyle matrix $\Lambda_{\text{Kyle}}$ on 9 November 2021 for a bin size of 30 minutes. Units are chosen to represent relative price changes in basis point ($10^{-4}$ of the asset price) by 100 millions USD worth of contract traded.

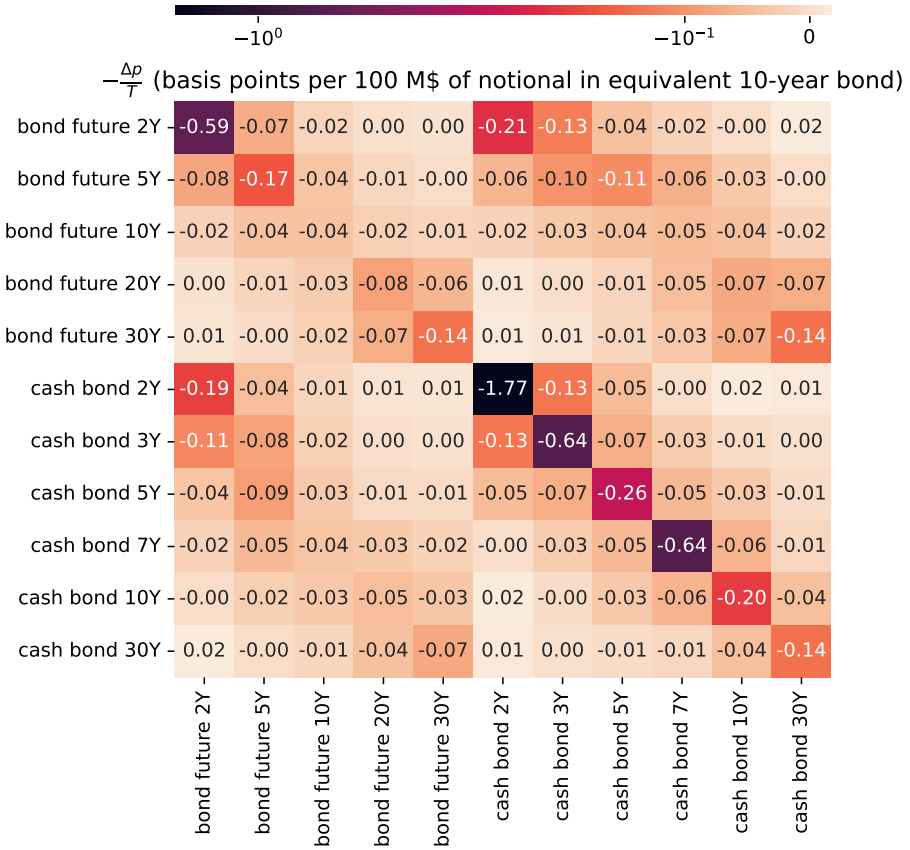


**Figure 6.20:** Kyle matrix $\Lambda_{\text{Kyle}}$ on 9 November 2021 for a bin size of 30 minutes. Units are chosen to represent absolute variations of annual yield in basis point ($10^{-4}$ of the asset price) by 100 millions USD worth in equivalent 10-year bond.

cross-impact time scales to asset characteristics has identified two distinct groups of asset pairs in multiple cases. Further research could explore the factors that differentiate these groups.

## 6.7 Table of notations

Table 6.1 summarizes the notations used in this chapter.

**Table 6.1:** Notations

| Expression | Definition |
|---|---|
| $n$ | The number of assets. |
| $\mathcal{M}_n(\mathbb{R})$ | The set of real-valued square matrices of dimension $n$. |
| $\mathcal{O}_n$ | The set of orthogonal matrices. |
| $\mathcal{S}_n^+(\mathbb{R})$ | The set of real symmetric positive semi-definite matrices. |
| $\mathcal{S}_n^{++}(\mathbb{R})$ | The set of real symmetric positive definite matrices. |
| $A$ | A matrix. |
| $A^\top$ | The transpose of matrix $A$. |
| $A^{1/2}$ | A matrix such that $A^{1/2}(A^{1/2})^\top = A$. |
| $\sqrt{A}$ | The unique positive semi-definite symmetric matrix such that $(\sqrt{A})^2 = A$. |
| $\mathrm{diag}(A)$ | The vector in $\mathbb{R}^n$ formed by the diagonal items of $A$. |
| $\mathrm{diag}(v)$ | The diagonal matrix whose components are the components $(v_1, \cdots, v_n)$ of $v \in \mathbb{R}^n$. |
| $\tau$ | The bin size. |
| $p_i(t)$ | The opening price of asset $i$ in the time window $[t, t+\tau]$. |
| $p(t)$ | The vector of asset prices at opening in the time window $[t, t+\tau]$. |
| $\Delta q_i(t)$ | The net market order flow traded during the time window $[t, t+\tau]$. |
| $\Delta q(t)$ | The vector of the net traded order flows during the time window $[t, t+\tau]$. |
| $\Delta p(t)$ | the prices changes $p(t+\tau) - p(t)$ during the time window $[t, t+\tau]$. |
| $\Lambda(t)$ | The cross-impact matrix at time $t$. |
| $\eta(t)$ | The vector of zero-mean random variables representing exogenous noise at time $t$. |
| $\Sigma(t)$ | The price change covariance matrix at time $t$. |
| $\Omega(t)$ | The order flow covariance matrix at time $t$. |
| $R(t)$ | The response matrix between price variations and order flows at time $t$. |
| $\Sigma(t)$ | The vector of price variation volatility at time $t$. |
| $\Omega(t)$ | The vector of the signed order flow volatility at time $t$. |

Continued on next page

| Expression | Definition |
|---|---|
| $\mathcal{R}^2(W)$ | The $W$-weighted generalized R-squared. |
| $\Delta\mathcal{R}^2(W)$ | The accuracy increase from the cross sectional model. |
| $\mathcal{R}^{2*}(W)$ | The maximum goodness-of-fit observed empirically across the tested bin size $\tau$. |
| $\tau^*(W)$ | The optimal time scale corresponding to the maximum goodness-of-fit $\mathcal{R}^{2*}(W)$. |
| $\Delta\mathcal{R}^{2*}(W)$ | The maximum accuracy increase $\Delta\mathcal{R}^2(W)$ observed empirically across the tested bin size $\tau$. |
| $\tau^*_\Delta(W)$ | The optimal time scale corresponding to the maximum accuracy increase $\Delta\mathcal{R}^{2*}(W)$. |
| $f_i$ | The trading frequency of the predicted asset $i$. |
| $f_j$ | The trading frequency of the explanatory asset $j$. |
| $\rho_{ij}$ | Price increments correlation between the assets $i$ and $j$. |
| $\bar{\sigma}_i$ | The average across time of the price variation volatility of asset $i$. |
| $\bar{\omega}_i$ | The average across time of the signed order flow volatility of asset $i$. |
| $\bar{\omega}_i\bar{\sigma}_i$ | The liquidity of the predicted asset $i$. |
| $\bar{\omega}_j\bar{\sigma}_j$ | The liquidity of the explanatory asset $j$. |

## Key takeaways

- The accumulation of a minimum number of trades in both assets, between 10 to 20, is required to observe a significant added accuracy of trading pressure on the prediction of asset prices.
- Trades only significantly explain the prices of highly correlated assets (correlations higher than 50%), regardless of the time scale.
- Price-volume correlations depend on the liquidity of the considered assets. In particular, cross-impact explains a larger share of price variances if the predicted asset has a lower liquidity than the explanatory asset.
- The aggregation of flow from a large number of weakly correlated instruments can still lead to a significant increase of explanatory power.
- Contrary to economic theories considering long-term rates as agents anticipations of short-term rates (see chapter 1), prices of low-liquidity tenors are impacted by the trades of high-liquidity tenors.

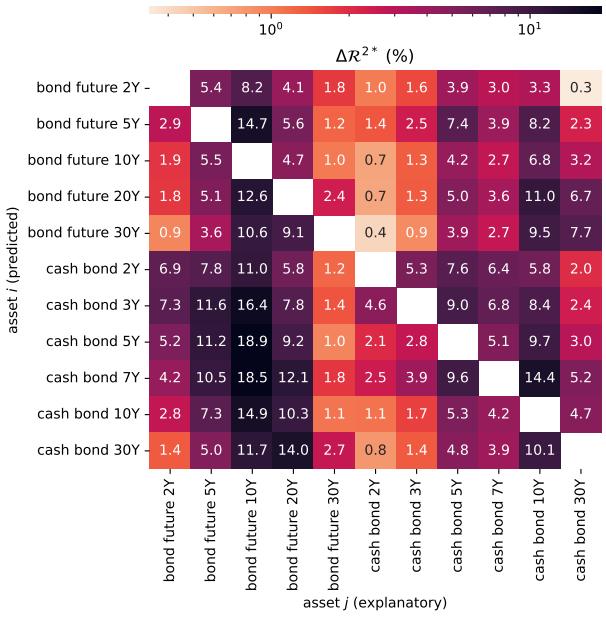


- Although arbitrage-free models predict that trading a low-liquidity asset is not expensive as long as it is exposed to a liquid factor (see chapter 1), here, trading a low-liquidity asset is still expensive, which limits the ability to close arbitrage opportunities.

# Chapter 7

# Revisiting Elastic String Models of Forward Interest Rates

*In this chapter, we reproduce the contents of (Le Coz and Bouchaud, 2024), co-written with Jean-Philippe Bouchaud, barring a slight reorganization and some minor changes in phrasing.*

The collection of forward interest rate $f(t, T)$ defines a kind of "string" that moves and deforms with time, the FRC. As explained extensively in chapter 1, understanding the dynamics of the FRC is crucial in a wide spectrum of financial applications, ranging from the valuation of interest rate derivatives to risk management (Brigo and Mercurio, 2006; Hull, 2018). This problem is also fascinating from a theoretical point of view: whereas the stochastic process governing the dynamics of single assets (point-like objects) has been thoroughly investigated (see e.g. (Bachelier, 1900; Osborne, 1959; Black and Scholes, 1973; Heston, 1993; Bacry et al., 2001; Zumbach, 2010; Gatheral et al., 2018; Dandapani et al., 2021; Wu et al., 2022; Morel et al., 2023)), the stochastic process of higher dimensional objects like lines or graphs is much more involved (Filipović, 2001; Aihara and Bagchi, 2005; Ekeland and Taflin, 2005; Carmona and Tehranchi, 2006). There is a long tradition in the physics literature of modeling string-like (or surface-like) objects which has not yet pervaded into the financial mathematics literature, despite early attempts Bouchaud et al., 1999; Santa-Clara and Sornette, 2001; Baaquie and Bouchaud, 2004.

The aim of this chapter is to revisit the 2004 proposal of Belal Baaquie and one of the author (JPB), to describe the returns of different tenors of the FRC in terms of the fluctuations of a "stiff" elastic string – called henceforth the BB04 model

Baaquie and Bouchaud, 2004. We will see that up to a redefinition of their model that accounts for the discrete set of maturities defining the FRC (instead of the continuum limit of BB04), the proposed framework allows one to account quite remarkably for the full cross-maturity correlation structure of the FRC, across the whole period 1994-2023 and a single adjustable parameter – when the BB04 model was only tested for the period 1994-1996 and had three parameters.

## 7.1 Random-field models

Beyond the fact that the HJM model has no ambition to capture the "physical", one-dimensional nature of the FRC, we have seen in chapter 1 that this framework generates singular correlations matrix as soon as the number of considered maturities is larger than the number of diffusion factors. Addressing these limitations, various researchers have ventured beyond the conventional boundary of a finite number of driving Brownian motions. Notably, Kennedy (1994), 1997 proposed to simulate each forward rate by a Gaussian random field while Cont (2005a), Goldstein (2000) and Santa-Clara and Sornette (2001) developed stochastic string approaches, partly based on the empirical work of Bouchaud et al., 1999 where the idea of the FRC as an elastic string was first put forth.

Among these advancements, Baaquie (2001), 2002, 2004 has pioneered a field theory approach, which will be discussed further in the following section. In the following years, these random field theories have been applied to solve interest rate derivative pricing problems (Baaquie, 2007; Baaquie and Liang, 2007; Baaquie, 2009; 2010; Baaquie and Tang, 2012; Wu and Xu, 2014; Bueno-Guerrero et al., 2015; 2016; Baaquie, 2018; Bueno-Guerrero et al., 2020; 2022).

## 7.2 A field theory for the FRC

Baaquie (2001), 2002, 2004 introduced a two-dimensional field theory to describe the forward interest rate curve. This approach was generalized in BB04 Baaquie and Bouchaud (2004) to account for the pronounced smoothness observed in the correlation matrix of forward rate increments. More precisely, it was observed that the eigenvectors of the covariance matrix of the FRC returns had the same structure as those of a elastic string and can be indexed by the number $k$ of zeroes in the $\theta$ direction. The corresponding eigenvalues were found to behave as $k^{-2}$ for small $k$, crossing over to a faster decay $\approx k^{-4}$ for larger $k$ (see section 5.2.3).

A way to encode this empirical finding is to posit that the dynamics of the FRC $f(t,\theta)$ is specified by a drift velocity $\gamma(t,\theta)$ and a volatility $\sigma(t,\theta)$, such that

(Baaquie and Bouchaud, 2004):

$$\frac{\partial f}{\partial t}(t,\theta) = \gamma(t,\theta) + \sigma(t,\theta)A(t,\theta), \tag{7.1}$$

where $A(t,\theta)$ represents a driftless (Langevin) noise field.

The "field theory" formulation assumes that $\theta$ is a continuous variable $\in \mathbb{R}_+$ and the joint probability distribution across time and tenor for the set of noises $\{A(t,\theta)\}_{(t,\theta)\in\mathbb{R}_+^2}$ is determined by the exponential of an action $S[A]$. This action is a functional defined over the semi-infinite domain $\mathbb{R}_+^2$, and is given by (Baaquie and Bouchaud, 2004):[9]

$$S[A] := -\frac{1}{2}\iint_0^\infty \mathrm{d}t\mathrm{d}\theta \left( A^2(t,\theta) + \left(\frac{1}{\mu}\frac{\partial A}{\partial \theta}(t,\theta)\right)^2 + \left(\frac{1}{\nu^2}\frac{\partial^2 A}{\partial \theta^2}(t,\theta)\right)^2 \right), \tag{7.2}$$

with $\mu^{-2}$ and $\nu^{-4}$ denoting respectively the "line tension" and "stiffness" (also called bending rigidity) parameters, which have the physical dimensions of frequencies. More precisely, small values of $\mu$ disfavor large local slopes of $A(t,\theta)$ whereas small values of $\nu$ disfavor large local curvatures. A boundary condition is needed for the theory to be complete, and was postulated in Baaquie and Bouchaud, 2004 to be of the Neumann type, i.e.

$$\left.\frac{\partial A(t,\theta)}{\partial \theta}\right|_{\theta=0} = 0, \tag{7.3}$$

thereby enforcing a uniform motion of the forward interest rates at very short maturities. This assumption is justified considering the spot rate $f(t,0)$ is typically set by the Central Bank, and very short-term maturities carry minimal additional risk.

Note that the absence in Eq. (7.2) of any coupling between different infinitesimal *time* slices (i.e. along the $t$ direction) means that $A(t,\theta)$ has no temporal correlations and behaves as a white noise. More precisely, $\mathrm{d}W(t,\theta) := A(t,\theta)\mathrm{d}t$ is a standard Wiener noise, with non trivial covariance along the $\theta$-direction

$$\mathbb{E}\left[\mathrm{d}W(t,\theta)\mathrm{d}W(t',\theta')\right] = \mathcal{D}_{BB}(\theta,\theta')\mathrm{d}t, \tag{7.4}$$

where $\mathbb{E}[.]$ denote an expectation over the functional weight $e^{S[A]}$ and where $\mathcal{D}_{BB}(\theta,\theta')$ is found to be (Baaquie and Bouchaud, 2004)

$$\mathcal{D}_{BB}(\theta,\theta') = \frac{\nu^4}{\alpha_+ - \alpha_-}\left[\frac{F(\theta,\theta',\sqrt{\alpha_-})}{\alpha_-} - \frac{F(\theta,\theta',\sqrt{\alpha_+})}{\alpha_+}\right], \tag{7.5}$$

[9] Note that throughout this chapter, we only speak of *classical* (i.e. non quantum) field theories, describing the statistical physics of extended objects.

with

$$\alpha_{\pm} = \frac{\nu^4}{2\mu^2}\left[1 \pm \sqrt{1 - 4\left(\frac{\mu}{\nu}\right)^4}\right]$$

and

$$F(\theta, \theta', p) := \frac{p}{2}\left(e^{-p(\theta+\theta')} + e^{-p|\theta-\theta'|}\right). \tag{7.6}$$

Formally, absence of arbitrage among zero-coupon bond prices imposes the following condition on the drift $\gamma(t, \theta)$ (Baaquie, 2004):

$$\gamma(t, \theta) = \sigma(t, \theta) \int_0^{\theta} \mathrm{d}\theta' \mathcal{D}_{BB}(\theta')\sigma(t, \theta'), \tag{7.7}$$

but this term is usually completely negligible numerically (Bouchaud et al., 1999), and we will drop it henceforth.

Baaquie and Bouchaud further introduced the concept of *psychological* time which explains how the perceived time $\theta' - \theta$ between tenors varies with their distance $\theta$ from the observer standing at time $t$, introducing one more parameter called $\psi$ below (see section 7.3.2 below). This framework allows one to fit the *whole* empirical correlation matrix $\rho_{\theta\theta'}$ with only three meaningful parameters $\mu, \nu$ and $\psi$. Within this model, and in line with observations, the *curvature* of the forward rate correlation perpendicular to the diagonal, decays as power-law with respect to maturity (see appendix D.9). This was perhaps the most salient success of the BB04 model, which however fell into almost complete oblivion (only 12 citations to date!).

In spite of its phenomenological success, the BB04 model has two main limitations.

1. First, the theory assumes a continuous spectrum of futures contracts across different tenors $\theta$, whereas in reality, futures contracts are available only at discrete tenors, usually every three calendar months. In other words, continuous derivatives like $\partial_\theta A$ have no physical existence.

2. Second, it predicts a constant correlation structure across all time scales used to define returns. This contradicts the well known "Epps effect", i.e. the influence of the temporal granularity used to analyze prices (Epps (1979), Renò (2003), and Toth and Kertesz (2009), see also section 5.1).

The aim of this chapter is to revisit the BB04 model with the two above deficiencies in mind. We reformulate the model in a way that makes its micro-foundations more apparent. We show in particular that market participants enforce a self-referential dynamic to the FRC, where each tenor is directly influenced

by the motion of its neighbors. Furthermore, our dynamical formulation encapsulates market microstructure phenomena, including the Epps effect, non-martingale prices at short scales and price-impact and cross-impact effects. The latter will be detailed in the next chapter 8.

## 7.3 A Dynamical Reformulation

### 7.3.1 The continuous limit

We now want to interpret the above driftless noise field $A(t,\theta)$, as the solution to a stochastic Langevin equation that will generate temporal correlations over a time scale $\tau \ll 1$ day, instead of instantaneous correlations as in Eq. (7.4).

We then define $\eta(t,\theta)$ to be a two-dimensional Gaussian (Langevin) noise, characterized by the covariance function

$$\mathbb{E}\left[\eta(t,\theta)\eta(t',\theta')\right] = 2D\delta(t-t')\delta(\theta-\theta'),$$

where $\delta(\cdot)$ represents the Dirac delta function and $2D$ is the variance of the noise. [In order to give a precise meaning to the following expressions, we adopt the physicists' convention and consider $\mathrm{d}t$ and $\mathrm{d}\theta$ to be very small compared to all relevant time scales of the problem, but not infinitesimal, so that time and maturities can be thought as discrete but very densely probed.]

We now postulate the following stochastic evolution for $A(t,\theta)$:

$$\frac{\partial A}{\partial t}(t,\theta) = \frac{1}{\tau}\left(\frac{\delta S[A]}{\delta A(t,\theta)} + \eta(t,\theta)\right), \tag{7.8}$$

where $\tau$ is the characteristic time scale for the emergence of correlations (see below). We will not attempt to define the "functional derivative" $\delta S[A]/\delta A(t,\theta)$ in a mathematically rigorous manner, but note that it boils down to the usual derivative if we think of time and maturities as discrete.

Eq. (7.8), alongside the Neumann boundary condition specified in Eq. (7.3), can be expressed through the following linear differential equation:

$$\begin{cases} \dfrac{\partial A}{\partial t}(t,\theta) = \dfrac{1}{\tau}\left[-\mathcal{L}[A](t,\theta) + \eta(t,\theta)\right], \\ \dfrac{\partial A}{\partial \theta}(t,0) = 0, \quad \forall t \end{cases} \tag{7.9}$$

where

$$\mathcal{L}[A](t,\theta) := A(t,\theta) - \frac{1}{\mu^2}\frac{\partial^2 A}{\partial \theta^2}(t,\theta) + \frac{1}{\nu^4}\frac{\partial^4 A}{\partial \theta^4}(t,\theta).$$

Eq. (7.9) describes how the correlated noise field $A(t,\theta)$ responds to the uncorrelated shocks $\eta(t,\theta)$, for example the order flow at the microstructure level. An

important property of the dynamics described by Eq. (7.9) is that it leads, for a fixed single time $t \to \infty$, to a stationary measure $P[\{A\}]$ for $A(t,\theta)$ given by

$$P[\{A(t,\theta)\}] = \exp\left[-\frac{1}{4D}\int_0^\infty \mathrm{d}\theta \left( A^2(t,\theta) + \left(\frac{1}{\mu}\frac{\partial A}{\partial \theta}(t,\theta)\right)^2 + \left(\frac{1}{\nu^2}\frac{\partial^2 A}{\partial \theta^2}(t,\theta)\right)^2 \right)\right], \tag{7.10}$$

(see e.g. Kampen (2007) for a detailed discussion). In other words, for $2D = 1$, the marginal of $e^{S[A]}$ for a given time $t$ with $S[A]$ defined in Eq. (7.10) coincides with $P[\{A\}]$. Therefore, all equal-time correlations of the field $A(t,\theta)$ coincide with the BB04 model. However, as we will discuss in section 7.3.4, non-trivial temporal correlations develop when $\tau > 0$, and only disappear in the limit $\tau \to 0$ , which is the limit where BB04 is recovered.

### 7.3.2 Psychological time

(Baaquie and Bouchaud, 2004) observed that the curvature of the forward rate correlations along the diagonal decays as a power law of the maturity (see appendix D.9). To capture this behavior, BB04 proposed the change of variable $\bar{z}(\theta) = \theta^{\bar{\psi}}$ with $\bar{\psi} < 1$ (see also Baaquie and Srikant (2004)). This new variable, referred to as the *psychological time*, ensures that the perceived time between events is a decreasing function of the maturity since $\mathrm{d}\bar{z} = \bar{\psi}\theta^{\bar{\psi}-1}\mathrm{d}\theta$. In other words, a month in a year appears longer than a month in ten years.

In spite of its phenomenological success, this formulation violates the constraint that for very small maturities, psychological time and real time should become equivalent, i.e. tomorrow and a day after tomorrow are perceived (nearly) exactly the same way, whereas the above specification leads to a diverging value of $\mathrm{d}\bar{z}$ in that limit. Moreover, several studies in Neuroscience, Behavioral Economics or Finance (see chapter I) suggest economic agents use hyperbolic discounting, which is tantamount to a *logarithmic* increase of the perceived time:[10]

$$z(\theta) = \psi \log\left(1 + \frac{\theta}{\psi}\right), \tag{7.11}$$

which is such that $z(\theta) \approx \theta$ for $\theta \ll \psi$ and $\mathrm{d}z \approx \psi \mathrm{d}\theta/\theta$ for $\theta \gg \psi$. Indeed, an exponential discount with rate $r$ in psychological time reads

$$e^{-rz(\theta)} = \left(1 + \frac{\theta}{\psi}\right)^{-r\psi}, \tag{7.12}$$

[10] Such logarithmic form was also recently discussed by C. Tebaldi (unpublished). Note that if we insist on a regularized power-law dependence, $\bar{z}(\theta) = \bar{\psi}/\zeta\left(1 + \theta/\bar{\psi}\right)^\zeta - 1$, such that $\bar{z} \approx \theta$ when $\theta \to 0$, empirical calibration always returns a small value of $\zeta$, i.e. a logarithmic behaviour.

which coincides with hyperbolic discounting in real time.

Applying the change of variable $z \to \theta(z) = \psi(e^{z/\psi} - 1)$ to the linear operator $\mathcal{L}[A](z,t)$ in Eq.(7.9) yields a non-linear differential equation,

$$\begin{cases} \dfrac{\partial A}{\partial t}(t,\theta) = \dfrac{1}{\tau}\left[-\mathcal{O}[A](t,\theta) + \eta(t,\theta)\right], \\ \dfrac{\partial A}{\partial \theta}(t,0) = 0, \quad \forall t, \end{cases} \tag{7.13}$$

where $\mathcal{O}$ is the operator defined by

$$\begin{aligned} \mathcal{O}[A](t,\theta) := A(t,\theta) &+ \left(\frac{1}{\psi^3\nu^4} - \frac{1}{\psi\mu^2}\right)\left(1+\frac{\theta}{\psi}\right)\frac{\partial A}{\partial \theta}(t,\theta) \\ &+ \left(\frac{7}{\psi^2\nu^4} - \frac{1}{\mu^2}\right)\left(1+\frac{\theta}{\psi}\right)^2\frac{\partial^2 A}{\partial \theta^2}(t,\theta) \\ &+ \frac{6}{\psi\nu^4}\left(1+\frac{\theta}{\psi}\right)^3\frac{\partial^3 A}{\partial \theta^3}(t,\theta) \\ &+ \frac{1}{\nu^4}\left(1+\frac{\theta}{\psi}\right)^4\frac{\partial^4 A}{\partial \theta^4}(t,\theta). \end{aligned} \tag{7.14}$$

The above formulation presumes a continuous (or at least very dense) spectrum of tenors $\theta$, whereas, in practice, forward rates are observed at discrete maturities only. As will be shown below, this is not a trivial difference. In order to enhance the realism of our model, we now explicitly discretize the above equation with respect to $\theta$.

### 7.3.3 A discrete counterpart

In the following sections, we denote by $x_\theta$ any variable defined on the discrete space of tenors. $x(t)$ denotes the vector of components $x_\theta(t)$. Notably, $f(t,\theta)$ becomes $f_\theta(t)$ and $A(t,\theta)$ becomes $A_\theta(t)$. $f(t)$ and $A(t)$ are respectively the vectors of the forward rate and the noise field at time $t$. We also define $I_k$ with $k \in \mathbb{Z}$ as a matrix of infinite size with ones ones only on the $k$-th diagonal above the main diagonal, i.e.,

$$(I_k)_{ij} = \begin{cases} 1 & \text{if} \quad j - i = k, \\ 0 & \text{otherwise.} \end{cases} \tag{7.15}$$

Note that $I_0$ is the identity matrix denoted simply $I$. Using a centered scheme, the discretization of Eq. (7.13) reads:

$$\begin{cases} \dfrac{\mathrm{d}A}{\mathrm{d}t}(t) = \dfrac{1}{\tau}\left[-\mathcal{M}A(t) + \eta(t)\right] \\ A_1(t) - A_{-1}(t) = 0, \end{cases} \tag{7.16}$$

where $\mathcal{M}$ is a matrix of infinite size defined by

$$\begin{aligned}\mathcal{M}_{\theta\theta'} := I_{\theta\theta'} \\ &+ \left(\frac{1}{\psi^3\nu^4} - \frac{1}{\psi\mu^2}\right)\left(1+\frac{\theta}{\psi}\right)\left(\frac{1}{2}I_1 - \frac{1}{2}I_{-1}\right)_{\theta\theta'} \\ &+ \left(\frac{7}{\psi^2\nu^4} - \frac{1}{\mu^2}\right)\left(1+\frac{\theta}{\psi}\right)^2\left(I_1 - 2I + I_{-1}\right)_{\theta\theta'} \\ &+ \frac{6}{\psi\nu^4}\left(1+\frac{\theta}{\psi}\right)^3\left(\frac{1}{2}I_2 - I_1 + I_{-1} - \frac{1}{2}I_{-2}\right)_{\theta\theta'} \\ &+ \frac{1}{\nu^4}\left(1+\frac{\theta}{\psi}\right)^4\left(I_2 - 4I_1 + 6I - 4I_{-1} + I_{-2}\right)_{\theta\theta'}. \end{aligned} \tag{7.17}$$

In the above equation, $\theta \in \mathbb{N}$ is counted in multiple of 3 months and $\mu$ and $\nu$ are now dimension-less. The discretization of Eq. (7.13) also requires to replace the continuous noise $\eta(t,\theta)$ by a discrete Langevin noise $\eta_\theta(t)$, such that:

$$\mathbb{E}\left[\eta_\theta(t)\eta_{\theta'}(t')\right] = 2D\delta(t-t')\delta_{\theta\theta'}, \tag{7.18}$$

where $\delta_{\theta\theta'}$ is the Kronecker delta. Note that the boundary condition in Eq. (7.16) exhibits a term $A_{-1}$ generated by the use of an Euler scheme centered in 0 to ensure the validity of the method of images (see appendices D.1 and D.4).

Unfortunately, Eq. (7.16) cannot be solved in closed form for arbitrary values of $\psi$, but simplifies in the two limits $\psi \to \infty$ (i.e. $z = \theta$, see section 7.3.4) and $\psi \to 0$ (see section 7.3.5). It will turn out that the latter limit allows us to calibrate the model with a single parameter, with the best goodness-of-fit over all other formulations.

### 7.3.4 Building a correlated discrete random field when $\psi \gg 1$

In the limit $\psi \gg 1$, the change of variable accounting for psychological time vanishes (i.e. $z = \theta$). Eq. 7.16 becomes

$$\begin{cases} \dfrac{\mathrm{d}A_\theta}{\mathrm{d}t}(t) = \dfrac{1}{\tau}\left[-\mathcal{L}_d[A]_\theta(t) + \eta_\theta(t)\right], \\ A_1(t) - A_0(t) = 0, \end{cases} \tag{7.19}$$

where the linear operator $\mathcal{L}$ have been substituted by its naive discrete counterpart $\mathcal{L}_d$:

$$\mathcal{L}_d[A]_\theta(t) := A_\theta(t) - \frac{1}{\mu^2}\sum_{i=0}^{2}(-1)^i\binom{2}{i}A_{\theta+(1-i)}(t) + \frac{1}{\nu^4}\sum_{i=0}^{4}(-1)^i\binom{4}{i}A_{\theta+(2-i)}(t).$$

This discrete operator $\mathcal{L}_d$ mimics the impact of economic agents who compare the change of rate of a given tenor to the interpolation of the rates of its closest tenors. In fact, it seems intuitively plausible that agents primarily look at the two nearest tenors $\theta \pm 1$, corresponding to $1/\nu \to 0$. We will see below that the calibration of the model suggests that this is indeed the case.

The solution to Eq. (7.19) is given by

$$A_\theta(t) = \frac{1}{\tau}\int_{-\infty}^{t} \mathrm{d}t' \sum_{\theta'=0}^{+\infty} G_{\theta\theta'}(t-t')\eta_{\theta'}(t'), \tag{7.20}$$

where $G_{\theta\theta'}(t-t')$ is the *propagator* of the noise $\eta_{\theta'}$ defined by

$$\begin{aligned} &G_{\theta\theta'}(t-t') := \\ &\frac{1}{2\pi}\int_{-\pi}^{\pi} \mathrm{d}\xi \left(e^{i\xi(\theta-\theta')} + e^{i\xi(\theta+\theta')}\right) e^{-\frac{L_d(\xi)}{\tau}(t-t')}, \end{aligned} \tag{7.21}$$

with $L_d(\xi) = 1 + 2\frac{(1-\cos\xi)}{\mu^2} + 4\frac{(1-\cos\xi)^2}{\nu^4}$ denoting the Fourier transform of $\mathcal{L}_d$. The derivation of this result is detailed in appendix D.1.

A crucial characteristic of the noise field $A(t,\theta)$ is its auto-covariance across time and space. For $\tau$ approaching 0, the auto-covariance of $A$ is found to be given by

$$\mathbb{E}\left[A_\theta(t)A_{\theta'}(t')\right] = \begin{cases} 0, \text{ if } |t-t'| \gg \tau, \\ \dfrac{D}{\tau}\mathcal{D}_1(\theta,\theta'), \text{ if } t = t', \end{cases} \tag{7.22}$$

where the quantity $\mathcal{D}_k(\theta,\theta')$ is defined by

$$\mathcal{D}_k(\theta,\theta') = \frac{1}{\pi}\int_0^{\pi} \mathrm{d}\xi \frac{2\cos\xi\theta\cos\xi\theta'}{[L_d(\xi)]^k}. \tag{7.23}$$

The coarse-grained cumulative sum of $A$ over a time interval $\Delta t \gg \tau$, defined as

$$\Delta A(t) := \int_{t-\Delta t/2}^{t+\Delta t/2} A_\theta(u)\mathrm{d}u,$$

exhibits a behavior similar to its infinitesimal counterpart. For $\tau \to 0$, the auto-covariance of $\Delta A$ is given by

$$\mathbb{E}\left[\Delta A_\theta(t)\Delta A_{\theta'}(t')\right] = \begin{cases} 0, \text{ if } |t-t'| > \Delta t, \\ 2D\Delta t\,\mathcal{D}_2(\theta,\theta'), \text{ if } t = t'. \end{cases} \tag{7.24}$$

Therefore, for $\tau \ll 1$, both the infinitesimal and cumulative sum of $A$ demonstrate martingale properties along the time axis while manifesting structured correlations

across the spatial dimension $\theta$. The proofs of these properties are provided in appendix D.2.

Following Baaquie and Bouchaud, 2004, it is tempting to still account for psychological time by replacing $\theta$ by $z(\theta)$ in Eq.(7.24), i.e.

$$\mathbb{E}\left[\Delta A_\theta(t)\Delta A_{\theta'}(t)\right] = 2D\Delta t\mathcal{D}_2(z(\theta), z(\theta')). \tag{7.25}$$

Section 7.4 shows that the equal-time Pearson correlation between the forward rates variations $\Delta f_\theta(t)$ and $\Delta f_{\theta'}(t)$ can be expressed thanks to the equal-time auto-covariance of $\Delta A$. We will refer to the forward rate correlation model using Eq. 7.25 as BBD3, for Baaquie-Bouchaud Discrete, three parameters.

Interestingly, one can derive closed-form formulas for $\mathcal{D}_2(\theta, \theta')$ and $\mathcal{D}_1(\theta, \theta')$ when $(\theta, \theta') \in \mathbb{N}^2$, (see appendix D.3). However, we find that the numerical evaluation of integral (7.23) yields more stable results when extending the correlator $(k, k') \mapsto \mathcal{D}_2(k, k')$ to $\mathbb{R}^2$ as required by equation (7.25).

### 7.3.5 Building a correlated discrete random field when $\psi \ll 1$

If $\psi \ll 1$, the model can be written as a function of the products $\mu\psi$ and $\nu\psi$ only (see appendix D.4). Hence, one can choose the parameter $\psi$ to be arbitrarily small to ensure that $\psi \ll 1 \leq \theta$. If we further consider that $\nu\psi \gg 1$ – which will turn out to be a reasonable assumption, as explained in section 7.5.3 – the matrix $\mathcal{M}$ becomes:

$$\mathcal{M}_{\theta\theta'} = I_{\theta\theta'} - \frac{\theta}{2\kappa^2}\left(I_1 - I_{-1}\right)_{\theta\theta'} - \frac{\theta^2}{\kappa^2}\left(I_1 - 2I + I_{-1}\right)_{\theta\theta'} \tag{7.26}$$

where $\kappa := \mu\psi$. Let $\mathcal{J}$ denote a matrix defined by

$$\mathcal{J}_{\theta\theta'} = \begin{cases} 2, \text{ if } \theta = \theta' = 0, \\ 1, \text{ if } \theta = \theta' > 0, \\ 0, \text{ if } \theta \neq \theta'. \end{cases} \tag{7.27}$$

In the limit $\psi \ll 1$ and $\nu \gg 1$, the solution to Eq. (7.16) is given by

$$A(t) = \frac{1}{\tau}\int_{-\infty}^{t} \mathrm{d}t' e^{-\frac{t-t'}{\tau}\mathcal{M}}\mathcal{J}\eta(t'). \tag{7.28}$$

The derivation of this result is detailed in appendix D.4 in the general case of a finite $\nu$. Note that in the continuous time limit one recovers the BB model with a logarithmic psychological time.

We are interested in the auto-covariance across time and space of the noise field $A(t, \theta)$. For $\tau$ near 0, appendix D.5 shows that the autocovariance of $\Delta A$,

the coarse-grain cumulative sum of $A(t)$ over the time interval $\Delta t \gg \tau$, is given by

$$\mathbb{E}\left[\Delta A(t)\Delta A(t')^\top\right] = \begin{cases} 0, \text{ if } |t-t'| > \Delta t, \\ 2D\Delta t \mathcal{M}^{-1}\mathcal{J}^2(\mathcal{M}^{-1})^\top, \text{ if } t = t'. \end{cases} \tag{7.29}$$

We will refer to the forward rate correlation model using Eq. (7.29) as BBDL, for Baaquie-Bouchaud Discrete Logarithmic time, with only one parameter. Note that we have to invert numerically the matrix $\mathcal{M}$ in Eq 7.29 to compute forward rate correlations. To limit artificial deformations due to boundary effects for large $\theta$, we choose the dimension of the matrix $\mathcal{M}$ to be large ($\approx 500$) compared to the number of quoted forward rate contracts ($\approx 40$). This however has a minor impact on the final results.

## 7.4 Modeling forward rates

### 7.4.1 Forward rate diffusion

The noise field previously defined is now employed to describe the dynamics of the forward rates. The diffusion equation for the variations of the forward rate, denoted as $\mathrm{d}f_\theta(t)$, is expressed as

$$\frac{\mathrm{d}f_\theta}{\mathrm{d}t}(t) = \gamma_\theta(t) + \sigma_\theta \widetilde{A}_\theta(t), \tag{7.30}$$

where the drift term $\gamma_\theta$ is set to zero, as discussed above, and

$$\widetilde{A}_\theta(t) = \frac{A_\theta(t)}{\sigma_A}$$

is the correlated noise field normalized by $\sigma_A$ where $\sigma_A^2 := \frac{1}{\Delta t}\mathbb{E}\left[\Delta A_\theta(t)\Delta A_\theta(t)\right]$. This normalization ensures that $\sigma_\theta^2$ is the variance of the noise term driving the forward rate $f_\theta$. Note that because of this normalization, the value of $D$ is immaterial and can be set arbitrarily. We however keep it explicitly in the following for clarity.

Consequently, at the mesoscopic scale $\Delta t \gg \tau$, the variance of the forward rate increments

$$\Delta f_\theta(t) := \int_{t-\Delta t/2}^{t+\Delta t/2} \mathrm{d}f_\theta(t')$$

is given by

$$\mathbb{E}\left[\Delta f_\theta(t)^2\right] = \sigma_\theta^2 \Delta t. \tag{7.31}$$

Here we have assumed that the volatility of the infinitesimal forward rate variation is constant across time. The same formulas can be derived when considering constant per piece volatility on each day of length $\Delta t$.

Finally, the equal-time Pearson correlation between the forward rates variations $\Delta f_\theta(t)$ and $\Delta f_{\theta'}(t)$ reads

$$\rho_{\theta\theta'} = \frac{\mathbb{E}\left[\Delta A_\theta(t)\Delta A_{\theta'}(t)\right]}{\sqrt{\mathbb{E}\left[\Delta A_\theta(t)\Delta A_\theta(t)\right]\mathbb{E}\left[\Delta A_{\theta'}(t)\Delta A_{\theta'}(t)\right]}}. \tag{7.32}$$

It is clear from Eq. (7.32) that forward rate correlations can be expressed as a function of the noise field correlations $\mathbb{E}\left[\Delta A_\theta(t)\Delta A_{\theta'}(t)\right]$. The calibration of our models in the following section is performed using Eq. (7.32) for different definitions of the noise field correlator (Eq. (7.25) or Eq. (7.29)).

## 7.5 Calibration on correlation surfaces

### 7.5.1 Data

As in chapter 5, we interpret the instantaneous forward rate $f(t,\theta)$ as the mid-price at time $t$ of a 3-month SOFR future contract maturing at $t+\theta$. Our SOFR dataset comprises historical daily variations of these contracts' prices from 1994 to 2023, covering tenors from 3 months to 117 months. As mentioned in section 5.2.3, the empirical Pearson correlations $\hat{\rho}_{\theta\theta'}$ among the daily forward rate increments of tenor $\theta$ and $\theta'$ form a very smooth surface – necessitating the introduction, within a continuous $\theta$ model, of a stiffness term in Eq. (7.2), without which this surface would exhibit a cusp singularity along the diagonal. Note furthermore that the curvature along the diagonal decreases as the tenor $\theta$ increases which, as already alluded to, did motivate the introduction of a perceived, "psychological time".

### 7.5.2 Calibration over the whole sample

We fit our micro-founded three parameter discrete model BBD3 (using Eq. (7.25)) to the observed correlation matrix over the period $1994-2023$, defining our whole sample. For this purpose, we define the error variance $\Sigma^2$ by

$$\Sigma^2 := \frac{1}{n^2}\sum_{\theta,\theta'}\left(\mathcal{E}_{\theta\theta'} - \frac{1}{n^2}\sum_{\theta,\theta'}\mathcal{E}_{\theta\theta'}\right)^2, \tag{7.33}$$

where $\mathcal{E}_{\theta\theta'} = \rho_{\theta\theta'} - \hat{\rho}_{\theta\theta'}$ is the difference between theoretical and empirical correlations for the forward rates of tenor $\theta$ and $\theta'$. We will refer to $\Sigma$ as the typical error of fit. We will use this indicator to assess the accuracy of our model.

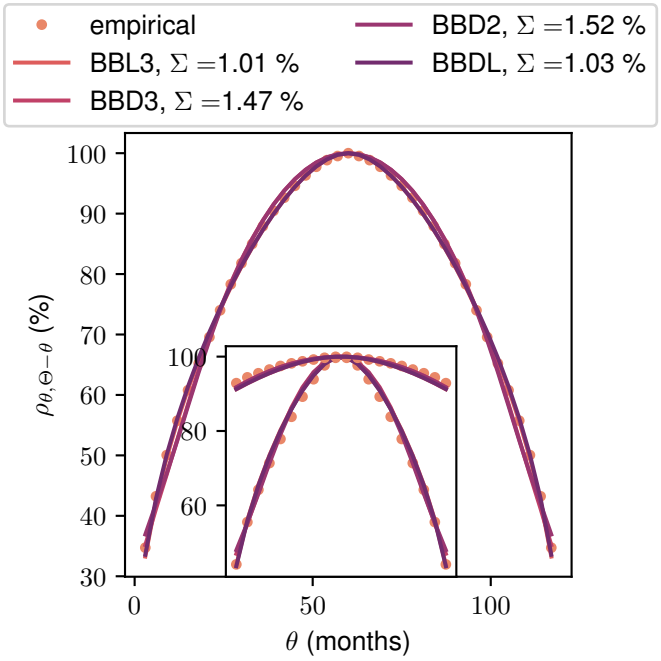


**Figure 7.1:** Dots represent the empirical correlation $\rho_{\theta\theta'}$ along the longest stretch perpendicular to the diagonal, i.e. $\theta' = \Theta - \theta$ , where $\Theta$ is the maximum available maturity. The plain lines are the best fit for the period $1994 - 2023$ in the continuous regularized model BBL3 (Eq. (D.51)) and our micro-founded discrete models: BBD3 (Eq. (7.25)), BBD2 (Eq. (7.25) with $\nu \to \infty$), and BBDL (Eq. (7.29)). The inset represent empirical and fitted correlations along two other anti-diagonals, defined by $\theta' = \frac{1}{2}\Theta - \theta$ and $\theta' = \frac{3}{2}\Theta - \theta$ respectively.

The minimization of the error variance $\Sigma^2$ yields an optimal set of parameters $\mathbf{p}^* = (\psi^*, \mu^*, \nu^*)$ for the period $1994 - 2023$. The results in Fig. 7.1 represent such a fit along the largest anti-diagonal direction and gives the typical error over the whole surface, showing the high accuracy of the BBD3 model. We find the optimal parameters $\psi^* = 2.06$ months, $\mu^* = 1.06$, and $\nu^* = 2.21$, for which $\Sigma = 1.47\%$.

### 7.5.3 A two-parameter version

The interpretation of the discrete model in terms of a mean reverting force driving back tenor $\theta$ to the average of its two nearby tenors $\theta \pm 1$ suggests that the discrete fourth order derivative may in fact not be needed, since the discrete second order derivative effectively leads to a fourth order term in the continuous limit. In other

words, one can set $\nu = \infty$ without creating a "kink" in $\rho_{\theta\theta'}$. This reduces the number of parameters to just two, $\psi$ and $\mu$, a version of the model that we will call BBD2.

The calibration of BBD2 fully vindicates the above intuition: we find that the optimal values of the parameters over the full sample are given by $\psi^* = 2.00$ months and $\mu^* = 1.01$, corresponding to a typical error $\Sigma$ of 1.52 %, only 5 basis points larger than to the one found for BBD3 with one less parameter (see Fig. 7.1).

To analyze the structure of our two-parameter model, we study the sensitivity of the calibration error to each parameter. For this purpose, we define the Hessian matrix $\mathcal{H}$ as the second-order derivative of the typical error $\Sigma$, computed at the optimal set of parameters $\mathbf{p}^*$, i.e.

$$\mathcal{H}_{ij} := p_i^* p_j^* \left. \frac{\partial^2 \Sigma}{\partial p_i \partial p_j} \right|_{p_i = p_i^*, p_j = p_j^*} \tag{7.34}$$

The eigenvalues $\lambda = (\lambda_1, \lambda_2)$ and eigenvectors $(\mathbf{e_1}, \mathbf{e_2})$ of the Hessian matrix $\mathcal{H}$ are presented in Fig. 7.2 for the BBD2 model. It appears that $\lambda_1 \gg \lambda_2$, which means that only the combination of parameters along the $\mathbf{e}_1$ direction is relevant, the other direction being "sloppy" (see for example Brown and Sethna (2003), Waterfall et al. (2006), and Gutenkunst et al. (2007)). Fig. 7.2 reveals that the main sensitivity mode of the BBD2 model is the a-dimensional product of parameters $\kappa := \psi \times \mu$. This suggests that we can further reduce the number of parameters to just one, as shown by the calculations of section 7.3.5 and successfully explored in the next section.

### 7.5.4 A one-parameter version

The formulation of the model as a non-linear differential equation shows the line tension $\mu$ and psychological time parameter $\psi$ play similar roles. The line tension sets the weight on the second derivative while the psychological time defines the distance $\mathrm{d}\theta$ between two consecutive tenors (see Eq. 7.13). Section 7.3.5 shows that these two parameters actually collapse as soon as $\psi$ is sufficiently small. This reduces the number of parameters to just $\kappa$, a version of the model previously mentioned as BBDL.

The calibration of BBDL outperforms all other tested models. We find that the optimal value for $\kappa$ is 0.92, corresponding to a typical error $\Sigma$ of 1.03%. This time, the error is 44 basis points lower than to the one found for BBD3 which has two more parameters, but is unable to explore the regime probed by BBDL (see Fig. 7.1). In view of this, we focus on the more parsimonious version BBDL in the following, where we calibrate the model independently on each three-year sub-period.

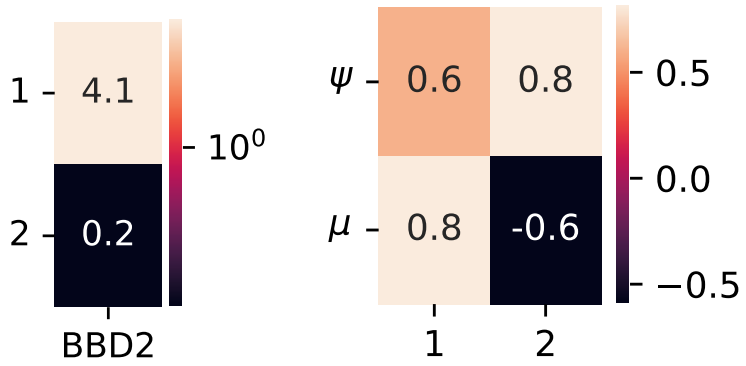


**(a)** Eigenvalues $\lambda_{1,2}$ **(b)** Eigenvectors $\mathbf{e}_{1,2}$

**Figure 7.2:** Eigenvalues $\lambda$ and eigenvectors $\mathbf{e}$ of the Hessian matrix at $\mathbf{p}^*$ in the BBD2 model.

### 7.5.5 BBDL calibration on separate three-year periods

Fig. 7.3 represents the largest anti-diagonal of the fit of the BBDL model over the whole correlation surface, for each three-year sub-period. The typical error and calibrated parameters for these intervals, detailed in Figure 7.4, demonstrate the stability of the parameter $\kappa$ throughout the assessed periods. However, periods characterized by significant monetary policy shifts exhibit a decrease in line tension (reflected in a higher value of $\kappa$) and goodness-of-fit (higher typical error $\Sigma$). Specifically, three periods present line tension lower than its long-term value: (i) the $2009-2011$ span, during the first and second rounds of Quantitative Easing, with the Federal Reserve purchasing 900 billion dollars in US treasury bonds; (ii) the $2012-2014$ phase, with an additional 800 billion in bond purchases (third Quantitative Easing); and (iii) the $2021-2023$ period, notable for the fourth Quantitative Easing amid the COVID-19 pandemic. This suggests that asset purchase programs induce periods of heightened curvature on the forward rate curve, i.e. more decoupling between nearby tenors.

### 7.5.6 Comparison with Baaquie and Bouchaud (2004)

In this section we perform a comparison of the accuracy and stability of all the tested models with the approach initially proposed by Baaquie and Bouchaud (2004). For the ease of convenience, table 7.2 in section 7.8 summarizes the definition of these models.

We show in Fig. 7.1 that the continuous Baaquie-Bouchaud model with logarithmic psychological time (BBL3), see Eq. (D.51) achieves the same global ac-

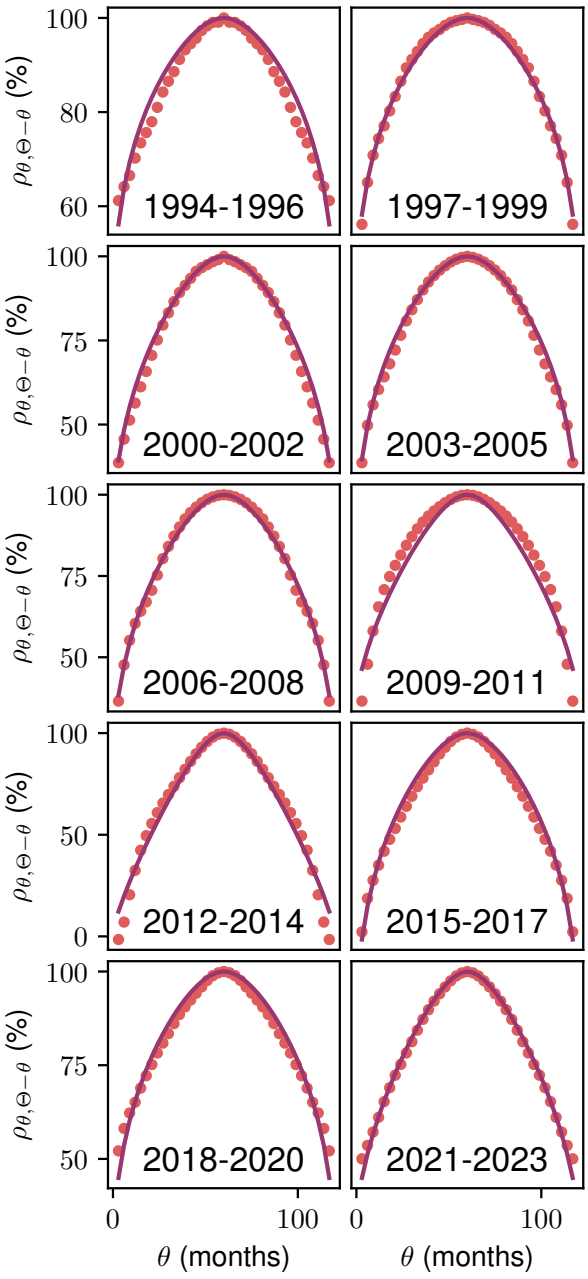


**Figure 7.3:** Dots represent the empirical correlation $\rho_{\theta\theta'}$ along the longest stretch perpendicular to the diagonal, i.e. $\theta' = \Theta - \theta$ , where $\Theta$ is the maximum available maturity. The plain lines are the best fit for our micro-founded discrete model BBDL (using Eq. (7.29)). It is clear from these plots that BBDL provides very accurate fits for all sub-periods, except 2009-2014.

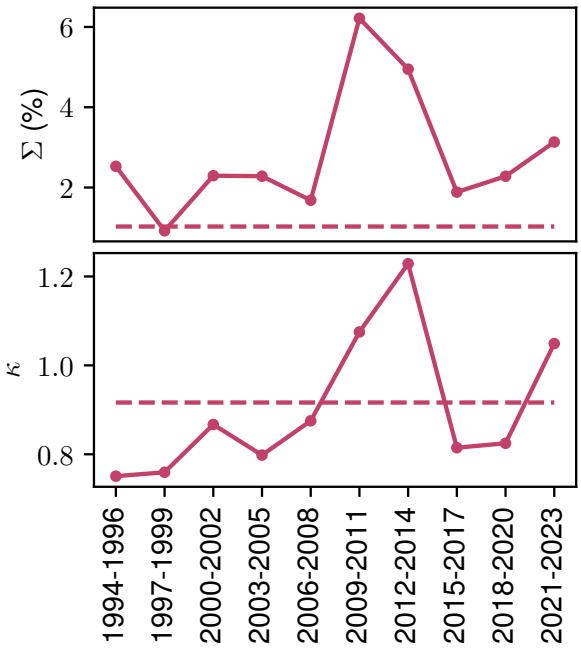


**Figure 7.4:** Optimal typical error and fitted parameter $\kappa$ obtained with our one-parameter micro-founded discrete model BBDL, Eq. (7.29). The dotted lines corresponds to the calibration results on the $1994-2023$ period. Note that the typical error $\Sigma$ yielded by the fit on the whole sample is not equal to the average error across sub-periods.

curacy with $\Sigma = 1.01\%$, compared to 1.03% for BBDL. However, removing only one of its three parameters now considerably degrades the goodness-of-fit. For example, removing the stiffness term increases the typical error $\Sigma$ from 1.01% to 4.06%. As obvious from appendix D.7, Fig. D.1, this is chiefly because the correlation surface develops a cusp around the diagonal $\theta = \theta'$, which was actually the very reason why Baaquie and Bouchaud (2004) introduced such a stiffness term!

The discrete BBDL model therefore appears superior not only because it is micro-founded and intuitively compelling, but also because it is more parsimonious: it naturally gets rid of the diagonal cusp without having to introduce any additional parameter. The discrete second derivative $f_{\theta+1} + f_{\theta-1} - 2f_\theta$ indeed formally contains continuous derivatives $\partial_\theta^{2k} f(\theta)$ of all even orders, and is therefore sufficient to regularize the correlation function across the diagonal. Furthermore, the psychological time parameter $\psi$ merges, in the limit $\psi \to 0$, with the line tension parameter $\mu$, if the change of variable is encoded in the dynamical master equation (7.13). Indeed, intuitively, changing the distance between tenors ($\psi$) or the line tension ($\mu$) is equivalent.

Lastly, we compare the stability of all the tested models over successive three-year intervals within our dataset. Fig. 7.5 displays the typical error and calibrated parameters across all periods, illustrating a consistent fit quality except during significant monetary policy shifts (refer to section 7.5.5). However the continuous and discrete three-parameter models (BBL3 and BBD3) demonstrate a high parameter instability across periods (note the log scale for $\mu$ and $\nu$). The more parsimonious approaches (BBD2 and BBDL), with only a slightly higher level of error on some periods, exhibit significantly more stable parameters. Notably, BBDL emerges as the most stable model, with its single parameter $\kappa$ ranging from 0.8 to 1.2 across all periods.

## 7.6 The Epps effect

An important vindication of our framework, in particular the *dynamical* construction of the field $A_\theta$ using Eq. (7.8), is our ability to account for the so-called Epps effect Epps, 1979 in a very natural way. Indeed, the auto-covariance of $\Delta A/\sqrt{\Delta t}$ is predicted by the theory to increase from 0 for $\Delta t \to 0$ at fixed $\tau$, to $2D\,\mathcal{D}_2(\theta, \theta')$ when $\Delta t \gg \tau$ (see Eq. (D.16) in appendix D.2 for the case $\psi \gg 1$ and Eq. (D.45) in appendix D.5 for the case $\psi \ll 1$).

Without modifying our model at the daily time scale, we may postulate that an additional, small white noise contributes to $A_\theta$, originating for example from the idiosyncratic dynamics of the order flow, or from the bid-ask bounce. We shall assume that the variance of such a noise is $2D\varepsilon\Delta t$, with $\varepsilon$ an extra $\theta$-independent

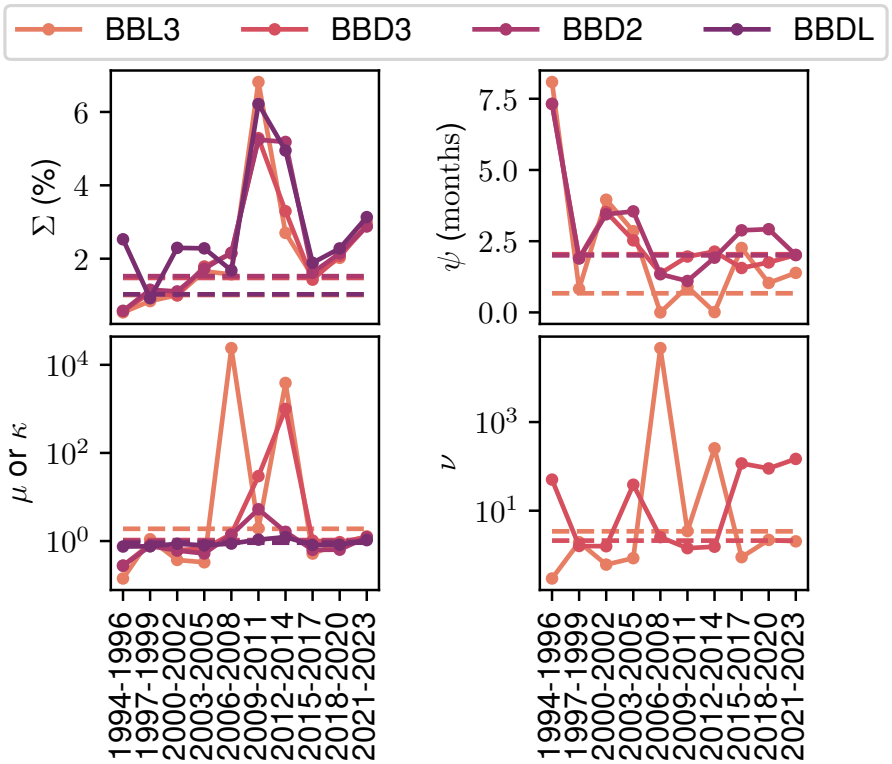


**Figure 7.5:** Typical error and fitted parameters within the continuous regularized model BBL3 (Eq. (D.51)) and our micro-founded discrete models: BBD3 (Eq. (7.25)), BBD2 (Eq. (7.25) with $\nu \to \infty$), and BBDL (Eq. (7.29)). The dotted lines correspond to the calibration results for each model over the $1994 - 2023$ period. The bottom left figure shows the parameter $\kappa$ for the BBDL model or the parameter $\mu$ for all the others. While $\mu$ (or $\kappa$) and $\nu$ are dimensionless in the discrete models, these parameters are expressed in 3 months$^{-1}$ in the case of the BBL3 model. Table 7.2 in section 7.8 summaries the definition of the tested models.

parameter such that

$$\varepsilon \ll \mathcal{C}(\theta, \theta), \tag{7.35}$$

where $\mathcal{C}(\theta, \theta')$ is the auto-covariance the noise field $\Delta A/\sqrt{2D\Delta t}$ without idiosyncratic noise for $\Delta t \gg \tau$ [11]. We then obtain the following scale-dependent covariance structure for $\Delta A$:

$$\mathbb{E}\left[\Delta A_\theta(t)\Delta A_{\theta'}(t)\right] = \begin{cases} 2D\varepsilon\,\delta_{\theta\theta'}\,\Delta t + O(\Delta t^2) & \text{for } \Delta t \ll \tau, \\ 2D\mathcal{C}(\theta,\theta')\,\Delta t & \text{for } \Delta t \gg \tau, \end{cases} \tag{7.36}$$

that we can compare with empirical data. Each plain line in Fig. 7.6 represents the correlation $\rho_{\theta\theta'}$ across different time scales $\Delta t$ among pairs of forward rate variations $(\Delta f_\theta, \Delta f_{\theta'})$, as given by our model in the case $\psi \gg 1$ (see Eq. (D.45)) calibrated on daily correlations (cf. section 7.5.2) with an additional fitting parameter $\varepsilon$.[12] Fig. 7.6 clearly demonstrates that our model is able to reproduce the whole dependence of the empirical correlations of pairs of SOFR Futures binned at different time scales (dots in Fig.7.6, see also Fig. 5.5). In fact, one can back out from this exercice the correlation time scale $\tau$ through a minimization of the differences between empirical and theoretical correlations across time scales. For the pair 30-33 months, this leads to a very reasonable value $\tau \approx 36$ minutes that can be interpreted as the information propagation time along the FRC. This calibration also yields an optimal value for the size of the idiosyncratic noise $\varepsilon \approx 1.6 \times 10^{-3}$, which is an order of magnitude smaller than $\mathcal{C}(\theta, \theta')$ (ranging from 0.02 to 4 when $\psi \ll 1$). In addition, Fig. 7.6 shows the theoretical correlations yielded by $\tau = 36$ minutes and $C = 1.6 \times 10^{-3}$ for two other pairs (15-48 and 3-60 months). It indicates that a similar set of calibrated parameters would be obtained if we had used a different pair.

One could have used Eq. D.16 in the case $\psi \gg 1$ to generate the Epps effect. It yields a similar shape of the correlation $\rho_{\theta\theta'}$ across different time scales $\Delta t$ among pairs of forward rate variations (see Fig D.2 in appendix D.8). Using this approach, we find a larger $\varepsilon \approx 0.026$, consistently with higher value of $\mathcal{C}(\theta, \theta')$ when $\psi \gg 1$ (in the range of 0.14 to 0.48) and a very similar value for $\tau \approx 21$ minutes.

[11] More precisely, in the case $\psi \gg 1$, $\mathcal{C}(\theta, \theta') = \mathcal{D}(z(\theta), z(\theta'))$, and when $\psi \ll 1$, $\mathcal{C}(\theta, \theta') = (\mathcal{M}^{-1}\mathcal{J}^2(\mathcal{M}^{-1})^\top)_{\theta\theta'}$.

[12] A natural extension would be to let $\varepsilon$ depend on $\theta$. A rank one specification, for example, would read $\varepsilon_{\theta\theta'} = (C_1 + C_2 \log\theta)(C_1 + C_2 \log\theta')$. We have not tried to calibrate such a model, since the simplest version $C_2 = 0$ is satisfactory for our purpose.

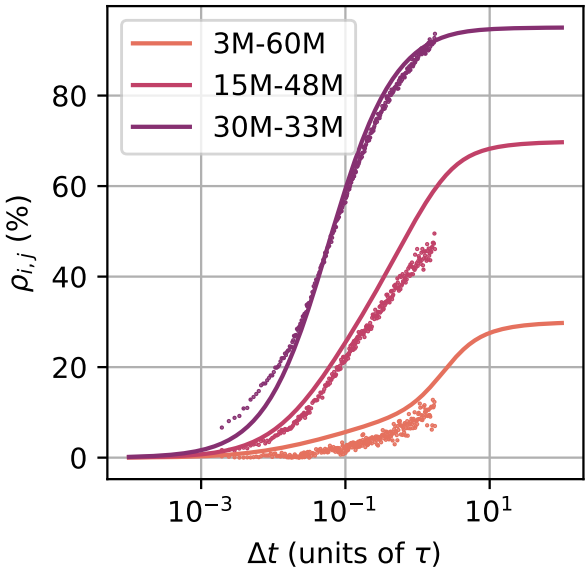


**Figure 7.6:** Plain lines: theoretical Pearson correlation coefficients among three pairs of forward rate variations $(\Delta f_\theta, \Delta f_{\theta'})$ as a function of the time scale $\Delta t$ (see (D.45)). Using the empirical correlations of the pair 30-33 months, the parameter $\varepsilon$ of the idiosyncratic white noise was calibrated to $1.6 \times 10^{-3}$, and the characteristic time of the Epps effect $\tau$ to 36 minutes. This figure also shows the theoretical correlations yielded by this set of parameters for two other pairs (15-48 and 3-60 months). Dots: empirical Pearson correlation coefficients for three pairs of SOFR Futures prices for the year 2021 at time scales ranging from 4 seconds to one hour.

## 7.7 Conclusion

In this chapter, we have reformulated the forward interest rate field theory of Baaquie and Bouchaud (2004) to account in a unified manner for two important features: (a) the discrete set of traded maturities and (b) the scale dependent structure of the correlation matrix across maturities (the Epps effect). Both points are related to market mechanisms underlying our modeling assumptions.

Indeed, we believe that the emergent correlation structure is a result of market participants reacting to high frequency shocks affecting the different tenors along the forward rate curve, which get corrected in time and transmitted along maturities through a self-referential mechanism. Intuitively, the dynamics of rates maturing at $t+\theta$ in the future cannot be decoupled from rates maturing at $t+\theta'$ when $|\theta-\theta'|$ is small. This is encoded, within our framework, via relative mean-reverting forces proportional to the discrete Laplacian and discrete fourth derivative of the returns along the maturity axis. As it turns out, the discrete fourth derivative plays a minor role and can be neglected – whereas this term was crucial in the continuous time version of Baaquie and Bouchaud (2004).

We have shown that such a parsimonious specification, further equipped with the notion of "psychological time" that shrinks the perceived distance between far away maturities, allows one to reproduce remarkably well (with an error around 1%) the full correlation structure of the forward rate curve, in particular the maturity dependent curvature of the correlation perpendicular to the diagonal $\theta=\theta'$. The single parameter of the model is found to be particularly stable across all the tested periods. Quite remarkably, we find that the data is compatible with the assumption of a logarithmic dependence of the perceived time as a function of real time, which translates into the hyperbolic discounting factor advocated in the behavioral economics literature (Farmer and Geanakoplos, 2009). From our calibration to the data, we find that the cross-over time between normal time flow and logarithmic time flow occurs around 2 months in the future. This also means that a year ten years from now is perceived by the bond markets as one week in real time. This is quite an extreme distortion of future time that reflects the extremely myopic nature of financial markets.

Finally, our approach also quantitatively reproduces the empirical finding of negligible correlations at high frequencies (Epps, 1979), which slowly build up at lower frequencies, see Fig. 7.6, with a characteristic time scale of the order of 30 minutes. The modeling framework we advocate also captures several phenomena consistent with the market microstructure literature, including (i) non-martingality of prices at short time scales and (ii) price-impact and cross-impact effects. These phenomena that will be detailed in the next chapter 8.

## 7.8 Table of notations

Table 7.1 summarizes the notations used in this chapter.

**Table 7.1:** Notations

| Expression | Definition |
|---|---|
| $n$ | The number of available SOFR Futures. |
| $t$ | The current time. |
| $T$ | The maturity. |
| $P(t,T)$ | The price at time t of a zero-coupon bond maturing at $T$. |
| $\theta$ | The time-to-maturity or tenor, in units of 3 months. |
| $f(t,\theta)$ | The value at time t of the instantaneous forward rate of tenor $\theta$ (continuous notation). |
| $f_\theta(t)$ | The value at time t of the instantaneous forward rate of tenor $\theta$ (discrete notation). |
| $A(t,\theta)$ | The driftless correlated noise field (continuous notation). |
| $A_\theta(t)$ | The driftless correlated noise field (discrete notation). |
| $\eta(t,\theta)$ | The two-dimensional white noise on continuous space. |
| $\eta_\theta(t)$ | The discrete white noise of tenor $\theta$. |
| $\sigma(t,\theta)$ | The volatility at time $t$ of the infinitesimal variation of the instantaneous forward rate of time-to-maturity $\theta$ (continuous notation). |
| $\sigma_\theta(t)$ | The volatility at time $t$ of the infinitesimal variation of the instantaneous forward rate of time-to-maturity $\theta$ (discrete notation). |
| $\gamma(t,\theta)$ | The drift at time $t$ of the infinitesimal variation of the instantaneous forward rate of time-to-maturity $\theta$ (continuous notation). |
| $z(\theta)$ | The psychological time. |
| $\psi$ | The psychological time parameter in the change of variable $z(\theta) = \psi \log\left(1+\frac{\theta}{\psi}\right)$. |
| $\bar{\psi}$ | The psychological time parameter in the change of variable $\bar{z}(\theta) = \theta^{\bar{\psi}}$ (Baaquie and Bouchaud, 2004). |
| $\mu$ | The line tension parameter. |
| $\nu$ | The stiffness (or bending rigidity) parameter. |
| $\kappa$ | Unique a-dimensional parameter in the BBDL model defined by $\kappa := \mu\psi$. |
| $\mathcal{D}_{BB}(\theta,\theta')$ | The Baaquie-Bouchaud correlator (Baaquie and Bouchaud, 2004). |
| $\tau$ | The time scale for the emergence of correlations. |
| $\Delta t$ | The time scale at which forward variations are observed, corresponding to one day unless specified otherwise. |

Continued on next page

| Expression | Definition |
|---|---|
| $\Delta\eta_\theta$ | The coarse-grained cumulative sum over the time scale $\Delta t$ of the two-dimensional white noise $\eta_\theta$. |
| $\Delta A_\theta$ | The coarse-grained cumulative sum over the time scale $\Delta t$ of the correlated noise field $A_\theta$. |
| $\Delta f_\theta$ | The forward rate increments over the time scale $\Delta t$. |
| $\mathbb{E}[.]$ | The expectation operator over the functional weight $e^{S[A]}$. |
| $\delta(.)$ | The Dirac delta function. |
| $\delta_{\theta\theta'}$ | The Kronecker delta. |
| $\mathcal{L}[.]$ | The continuous linear differential operator on space. |
| $\mathcal{O}[.]$ | The continuous non-linear differential operator on space. |
| $\mathcal{L}_d[.]$ | The discrete linear differential operator on space. |
| $\mathcal{M}$ | The discrete non-linear differential operator on space, using matrix notations. |
| $L_d[.]$ | The Fourier transform of the discrete linear differential operator on space. |
| $G_{\theta\theta'}(.)$ | Green function or *propagator* of the discretized Eq. (7.19) |
| $\mathcal{D}_2(\theta,\theta')$ | The spatial correlator in the discrete BBD model. |
| $\mathcal{D}_1(\theta,\theta')$ | The spatial correlator of the noise field. |
| $I_k$ | A matrix with ones only on the $k$-th diagonal above the main diagonal. |
| $I$ | The identity matrix. |
| $\mathcal{J}$ | A diagonal matrix whose first entry is 2 while all the other entries are ones. |
| $2D\Delta t$ | The variance of $\Delta\eta$. |
| $2D\epsilon\Delta t$ | The variance of the cumulative sum of the idiosyncratic two-dimensional white noise. |
| $\mathcal{F}[f]$ | The Fourier transform of the function of the maturity $\theta \mapsto f_\theta$. |
| $\Sigma$ | The typical error between the empirical and the theoretical correlations. |

Table 7.2 summarizes the definition of the models used in this chapter.

| Model | Noise correlator $\mathbb{E}\left[\Delta A_\theta(t)\Delta A_{\theta'}(t)\right]$ |
|---|---|
| BB04 | $\mathcal{D}_{BB}(\theta^{\bar{\psi}}, (\theta')^{\bar{\psi}})$ (see Eq. (7.5)) |
| BBL3 | $\mathcal{D}_{BB}(z(\theta), z(\theta'))$ (see Eq. (7.5)) |
| BBL2 | $\mathcal{D}_{BB}(z(\theta), z(\theta'))$ with $\nu \to \infty$ (see Eq. (7.5)) |
| BBD3 | $2D\Delta t\mathcal{D}_2(z(\theta), z(\theta'))$. (see Eq. (7.23)) |
| BBD2 | $2D\Delta t\mathcal{D}_2(z(\theta), z(\theta'))$ with $\nu \to \infty$ (see Eq. (7.23)) |
| BBDL | $2D\Delta t\mathcal{M}^{-1}\mathcal{J}^2(\mathcal{M}^{-1})^\top$ with $\nu\psi \to \infty$ and $\psi \to 0$ (see Eq. (7.26)). |

**Table 7.2:** Models' definition

## Key takeaways

- The correlation structure of the FRC is described as the result of market participants reacting to high frequency shocks transmitted along maturities through a self-referential mechanism.
- This parsimonious specification is then further equipped with the notion of "psychological time" which translates into the hyperbolic discounting factor advocated in the behavioral economics literature (Farmer and Geanakoplos, 2009).
- The single parameter of the model is found to be particularly stable across all the tested periods, which allows us to reproduce remarkably well (with an error around 1%) the full correlation structure of the FRC.
- From our calibration to the data, we find a strong distortion of future time that reflects the extremely myopic nature of financial markets.
- This approach also quantitatively reproduces the empirical finding of negligible correlations at high frequencies (Epps, 1979), which slowly build up at lower frequencies, with a characteristic time scale of the order of 30 minutes.

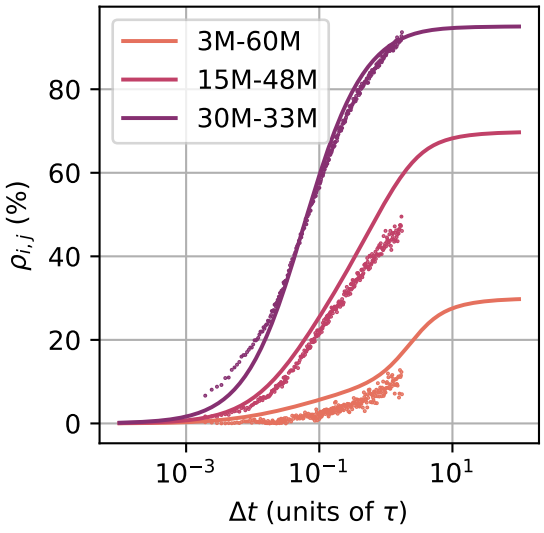

# Chapter 8

# How does liquidity shape the yield curve?

*In this chapter, we reproduce the contents of (Le Coz et al., 2024c), written under the supervision of Iacopo Mastromatteo and Michael Benzaquen, barring a slight reorganization and some minor changes in phrasing.*

In the previous chapter we have revisited a model of the FRC based on the fluctuations of a stiff elastic string (henceforth called the BBDL model for *Baaquie-Bouchaud Discrete Logarithm*. The objective of this chapter is to demonstrate that this model can be given a microstructural interpretation, which allows for new predictions. Specifically, we establish a connection between a non-measurable auxiliary noise field that appears in the construction of the original model and the physically measurable volumes traded across the interest rates curve, thus promoting the string model of chapter 7 to a microstructural model capable of predicting the price reaction to traded volumes along the curve. The resulting model is more parsimonious than other cross-impact models while maintaining comparable, if not superior, performance. We will show that it faithfully accounts for the effect of liquidity on the price-volume correlations between the forward rates of different maturities and the order flow (identified in chapter 6). Additionally, within this framework, prices appear to exhibit short-term temporal autocorrelations, consistent with established findings in the literature (see chapter 5).

## 8.1 Definitions and notations

As in the previous chapter, the instantaneous forward rate $f_\theta(t)$ is interpreted as the mid-price at time $t$ of a 3-month SOFR Future contract maturing at $t + \theta$. More precisely, in this chapter, $f_\theta(t)$ denotes the closing forward rate of tenor $\theta$

in the time window $[t - \Delta t, t]$ with a length of $\Delta t = 1$ day. As previously, we also denote any variable $x$ defined in the discrete space of the existing tenors as a vector $(x_\theta)$.

We define $\Delta q_\theta(t)$ as the net market order flow traded during the time window $[t - \Delta t, t]$ for the Future contract maturing in $t + \theta$. This is calculated by taking the sum of the volumes of all trades during that time period, with buy trades counted as positive and sell trades counted as negative. Thus, $\Delta q(t) = (\Delta q_1(t), \cdots, \Delta q_n(t))$ is the column vector of net traded order flows.

The set of real-valued square matrices of dimension $n$ is denoted by $\mathbf{M}_n(\mathbb{R})$. Given $A$ a positive symmetric matrix, we write $A^{1/2}$ for a matrix such that $A^{1/2}(A^{1/2})^\top = A$, and $\sqrt{A}$ for the matrix square root: the unique positive semi-definite symmetric matrix such that $(\sqrt{A})^2 = A$. We also write $\mathrm{diag}(A)$ for the vector in $\mathbb{R}^n$ formed by the diagonal elements of $A$. Given a vector $v$ in $\mathbb{R}^n$, we denote the components of $v$ by $(v_1, \cdots, v_n)$, and the diagonal matrix whose components are the components of $v$ by $\mathrm{diag}(v)$. Table 8.2 in appendix 8.8 provides a complete list of notations used in this chapter.

## 8.2 A field theory of the FRC

In this section, we summarize the technical results related to the correlated noise field developed in the previous chapter. We also introduce an additional property of such a noise field and simplified notations.

In contrast to the previous chapter, here we set $D = 1/2$, so the auto-covariance of the independent Gaussian noise $\eta(t)$ becomes:

$$\mathbb{E}\left[\eta_\theta(t)\eta_{\theta'}(t')\right] = \delta(t - t')\delta_{\theta\theta'}. \tag{8.1}$$

This choice has no impact on the results. Moreover, we consider $\nu \to \infty$ and a finite number $n$ of diffusion factors, one for each tenor of the FRC, although the model could be written with an infinite-dimensional white noise $\eta$. In any case, only the first $n$ component of the vector $Y$ (see section 8.3.2) would be non-zero. Thus, the vector of the driftless discrete noise field $A(t)$ is defined for $\theta \in [\![1, n]\!]$ as the solution to a differential equation which operates on a temporal scale $\tau \ll 1$ day:

$$\begin{cases} \dfrac{\mathrm{d}A}{\mathrm{d}t}(t) = \dfrac{1}{\tau}\left[-\mathcal{M}A(t) + \eta(t)\right], \\ A_1(t) - A_{-1}(t) = 0, \end{cases} \tag{8.2}$$

where $\mathcal{M}$ is a matrix of $\mathbf{M}_n(\mathbb{R})$ defined by

$$\mathcal{M}_{\theta\theta'} = 1 - \frac{1}{2\psi\mu^2}\left(1 + \frac{\theta}{\psi}\right)(I_1 - I_{-1})_{\theta\theta'} - \frac{1}{\mu^2}\left(1 + \frac{\theta}{\psi}\right)^2 (I_1 - 2I + I_{-1})_{\theta\theta'}. \tag{8.3}$$

We recall that the general solution to Eq. (8.2) is expressed as

$$A(t) = \frac{1}{\tau}\int_{-\infty}^{t} \mathrm{d}t' G(t-t')\eta(t'), \tag{8.4}$$

where the matrix $G(t-t')$ is the *propagator* of the noise $\eta(t')$. When $\psi \gg 1$, for $(\theta, \theta') \in [\![1, n]\!]^2$, $G_{\theta\theta'}$ is given by:

$$G_{\theta\theta'}(t) := \frac{1}{2\pi}\int_{-\pi}^{\pi} \mathrm{d}\xi \left(e^{i\xi(\theta-\theta')} + e^{i\xi(\theta+\theta')}\right) e^{-\frac{L_d(\xi)}{\tau}t}, \tag{8.5}$$

where $L_d(\xi) = 1 + 2\frac{(1-\cos\xi)}{\mu^2}$. When $\psi \ll 1$, $G$ becomes:

$$G(t) := e^{-\frac{t}{\tau}\mathcal{M}}\mathcal{J}. \tag{8.6}$$

In this limit, the matrix $\mathcal{M}$ can be written as a function of a single parameter $\kappa = \mu\psi$:

$$\mathcal{M}_{\theta\theta'} = I_{\theta\theta'} - \frac{\theta}{2\kappa^2}\left(I_1 - I_{-1}\right) - \frac{\theta^2}{\kappa^2}\left(I_1 - 2I + I_{-1}\right). \tag{8.7}$$

We also define the matrix $C$, the *correlator* of $\Delta A$ by

$$C := \begin{cases} \mathcal{D}_2 & \text{if } \psi \gg 1, \\ \mathcal{M}^{-1}\mathcal{J}^2(\mathcal{M}^{-1})^\top & \text{if } \psi \ll 1, \end{cases} \tag{8.8}$$

where we recall that the matrix $\mathcal{D}_k$ is given by

$$(\mathcal{D}_k)_{\theta\theta'} := \frac{1}{\pi}\int_0^{\pi} \mathrm{d}\xi \frac{2\cos\xi\theta\cos\xi\theta'}{L_d(\xi)^k}. \tag{8.9}$$

Thus, for $\tau$ near 0, the auto-covariance of the cumulative noise field $\Delta A$ is given by:

$$\mathbb{E}\left[\Delta A(t)\Delta A^\top(t')\right] = \begin{cases} 0, \text{ if } |t-t'| > \Delta t, \\ \Delta t\, C, \text{ if } t = t'. \end{cases} \tag{8.10}$$

An other important property of the cumulative sum of $A$, not presented in the preivous chapter, is its response to the generating white noise. For $\tau$ near 0, the covariance between $\Delta A(t)$ and $\Delta\eta(t)$ reads

$$\mathbb{E}\left[\Delta A(t)\Delta\eta^\top(t)\right] = \Delta t\, R, \tag{8.11}$$

where the matrix $R$ is the response of $\Delta A$ to $\Delta\eta$ given by:

$$R := \begin{cases} \mathcal{D}_1 & \text{if } \psi \gg 1, \\ \mathcal{M}^{-1}\mathcal{J} & \text{if } \psi \ll 1. \end{cases} \tag{8.12}$$

Hence, the correlation matrix $\rho(\Delta A(t), \Delta\eta(t))$ between $\Delta A(t)$ and $\Delta\eta(t)$ reads

$$\rho(\Delta A(t), \Delta\eta(t)) = \mathrm{diag}(\sigma_A)^{-1} R, \tag{8.13}$$

where we recall that $\sigma_A$ is the volatility vector of $\Delta A$ defined by

$$(\sigma_A)_\theta = \sqrt{\mathrm{diag}(C)_\theta}. \tag{8.14}$$

The proofs of these properties are provided in appendices E.1 and E.2.

The noise field $A$ is now employed to model forward rates, as in the previous chapter:

$$\frac{\mathrm{d}f}{\mathrm{d}t}(t) = \mathrm{diag}(\sigma)\,\mathrm{diag}(\sigma_A)^{-1} A(t), \tag{8.15}$$

where the component $\sigma_\theta$ of the vector $\sigma$ is the volatility of the noise term driving the forward rate $f_\theta$. Thus, using the notation introduced here, the equal-time Pearson correlation coefficient among coarse-grained forward rate variations $\Delta f := \int_{t-\Delta t}^{t} \mathrm{d}f(u)$ is given by:

$$\rho(\Delta f, \Delta f) = \mathrm{diag}(\sigma_A)^{-1} C\,\mathrm{diag}(\sigma_A)^{-1}. \tag{8.16}$$

## 8.3 Towards a cross-impact model

Even though this field theory provides an accurate account of the correlation structure of the FRC, it does not clarify the nature of the exogenous noise $\eta$ driving the dynamics of the curve. In this section we want to provide a microstructural foundation for the $\eta$ noise by linking it to the surprise in the order flow, thus promoting the model (that only describes price variations) to a microstructural model accounting for the joint dynamics of prices and volumes.

### 8.3.1 Order flow decomposition

Trading flows exhibit significantly lower spatial correlation compared to prices, however, they display long-range temporal autocorrelation (see chapter 5). Therefore, we provide a natural physical interpretation of the white noise $\eta$ by assuming that this noise corresponds to the surprise (i.e. the martingale component) in the signed order flow. However, only a fraction of the volatility of price increments is expected to be explained by trades (see section 8.6), so the white noise column vector $\eta(t)$ is decomposed into an idiosyncratic component $\eta^\perp$, and a component related to order flow $\eta^q$:

$$\eta(t) = \mathrm{diag}(Y)\eta^q(t) + \mathrm{diag}(Y^\perp)\eta^\perp(t), \tag{8.17}$$

where $\eta^\perp$ is a normalized white noise independent from $\eta^q$ and $Y$ is the vector of the parameters $Y_\theta \in [0,1]$ governing, for each tenor $\theta$, the share of forward rates variance explained by the order flow imbalance. The components of the vector $Y^\perp$ are $Y_\theta^\perp = \sqrt{1-Y_\theta^2}$. Formally, the surprise $\eta^q(t)$ is defined as

$$\eta^q(t) := O \int_{-\infty}^{t} \mathrm{d}t' J(t-t') \frac{\mathrm{d}q}{\mathrm{d}t}(t'), \tag{8.18}$$

where $\frac{\mathrm{d}q}{\mathrm{d}t}(t')$ is the infinitesimal order flow imbalance, and $J(t-t')$ is a matrix-valued function that ensures the diffusivity of the process $\eta^q(t)$, i.e., $\mathbb{E}\left[\eta_\theta^q(t)\eta_{\theta'}^q(t')\right] = \delta_{\theta\theta'}\delta(t-t')$. Such an operator is defined up to an arbitrary rotation matrix $O$ which leaves the price process invariant.

In appendix E.3 we justify the existence of the kernel $J$ in Eq. (8.18), assuming the lagged variance-covariance matrix of the infinitesimal order flows $\Omega(t,t') := \mathbb{E}\left[\frac{\mathrm{d}q}{\mathrm{d}t}(t)\frac{\mathrm{d}q}{\mathrm{d}t}^\top(t')\right]$ is stationary: $\Omega(t,t') = \Omega(t-t')$. We further assume that the order flow has a factorized structure[13]

$$\Omega(t-t') = \mathrm{diag}(\phi(t-t'))\Omega, \tag{8.19}$$

where the function $\ell \mapsto \phi(\ell)$ is valued in vector space, and $\Omega$ is the equal-time variance-covariance matrix of the infinitesimal order flows. Then, it is quite simple to obtain an explicit expression for $J(t-t')$ (see appendix E.3):

$$J(t-t') = \Omega^{-1/2}\,\mathrm{diag}\left(\Phi(t-t')\right), \tag{8.20}$$

where $\Phi(\ell)$ is an operator, valued in vector space, denoting the element-wise convolutional inverse of $\phi(\ell)$.

Note that this construction leaves the rotation matrix $O$ undefined. In section 8.3.4, we propose several methods to determine this matrix to satisfy the consistency requirements of a cross-impact model.

Finally, one can define $\tilde{q}(t)$, the martingale component of $q(t)$, through:

$$\frac{\mathrm{d}\tilde{q}}{\mathrm{d}t}(t) := \int_{-\infty}^{t} \mathrm{d}t'\,\mathrm{diag}\left(\Phi(t-t')\right)\frac{\mathrm{d}q}{\mathrm{d}t}(t'), \tag{8.21}$$

such that the surprise $\eta^q$ is given by

$$\eta^q(t) = O\Omega^{-1/2}\frac{\mathrm{d}\tilde{q}}{\mathrm{d}t}(t). \tag{8.22}$$

[13] Even though this assumption is not strictly required in our construction, we prefer to stick to this simpler case, which is an acceptable first order approximation of the empirical order flow structure, see (Benzaquen et al., 2016).

### 8.3.2 Noise field decomposition

The decomposition of the white noise $\eta$ enables us to write the noise field $A$ as the sum of two independent components:

$$A(t) = A^q(t) + A^\perp(t), \tag{8.23}$$

where the correlated noise $A^q$ is the solution of

$$\begin{cases} \dfrac{\mathrm{d}A^q}{\mathrm{d}t}(t) = \dfrac{1}{\tau}\left[-\mathcal{M}A^q(t) + \mathrm{diag}(Y)\eta^q(t)\right], \\ A^q_1(t) - A^q_{-1}(t) = 0. \end{cases} \tag{8.24}$$

The correlated noise $A^\perp$ solves a similar equation with the generating white noise $\mathrm{diag}(Y^\perp)\eta^\perp(t)$.

### 8.3.3 Large-bin approximation

Even though Eq. (8.4) shows that $\Delta A(t)$ depends upon the whole history of $\eta(t')$ for $t' \leq t$, we are interested in approximating $\Delta A_\theta(t)$ as a function of coarse-grained variables $\Delta\eta$ defined over intervals of finite width $\Delta t$, as in practice we will have empirical access to order flows sampled on a discrete time grid. The proofs of the results presented in this section are detailed in appendix E.4.

We decompose the white noise column vector $\eta(t')$ into the sum of its observed empirical averages over the time intervals $[t - \Delta t, t]$ (i.e. its moving average) and its fluctuations around this mean. Formally, we write

$$\eta(t') = \bar{\eta}_{\Delta t}(t) + \eta(t') - \bar{\eta}_{\Delta t}(t), \tag{8.25}$$

where $\bar{\eta}_{\Delta t}(t)$ is the empirical mean of $\eta(t)$ over the time window $[t - \Delta t, t]$ i.e.,

$$\bar{\eta}_{\Delta t}(t) := \frac{1}{\Delta t}\int_{t-\Delta t}^{t} \mathrm{d}t'\eta(t'). \tag{8.26}$$

If we further consider that $\tau \ll \Delta t$ one can express $\Delta A_\theta(t)$ as a function of $\bar{\eta}_{\Delta t}(t)$:

$$\Delta A(t) = R\ \Delta t\ \bar{\eta}_{\Delta t}(t) + \int_{t-\Delta t}^{t} \mathrm{d}t'\epsilon^\tau(t'), \tag{8.27}$$

where $\epsilon^\tau(t) = \frac{1}{\tau}\int_{t-\Delta t}^{t} \mathrm{d}t' G(t-t')\left(\eta(t') - \bar{\eta}_{\Delta t}(t)\right)$ is a noise independent of $\bar{\eta}_{\Delta t}(t)$ (see appendix E.4). One can substitute $\eta$ with $\eta^q$ or $\eta^\top$ and $A$ with $A^q$ or $A^\top$ in Eq. (8.27). It yields a relationship between forward rate daily increments and the martingale component of the daily order flow $\Delta\tilde{q}(t) := \int_{t-\Delta t}^{t} \mathrm{d}t'\tilde{q}(t')$:

$$\widehat{\Delta f}(t) = \mathrm{diag}(\sigma)\,\mathrm{diag}(\sigma_A)^{-1} R\,\mathrm{diag}(Y) O \Omega^{-1/2} \Delta\tilde{q}(t), \tag{8.28}$$

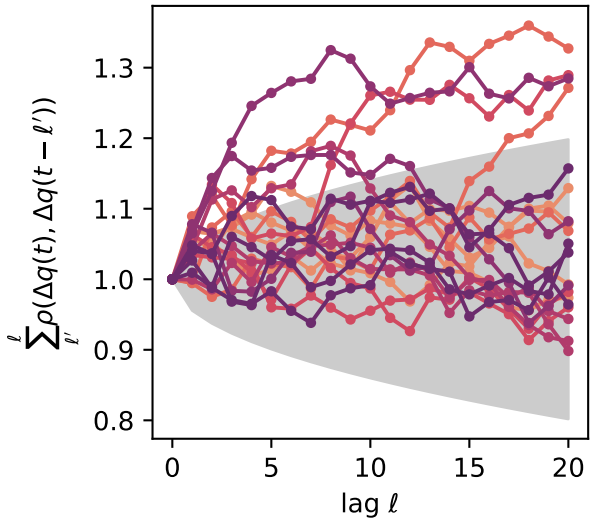


**Figure 8.1:** Accumulated temporal autocorrelation of daily trading flows over $\ell$ days i.e., $\sum_{\ell'}^{\ell} \rho(\Delta q(t), \Delta q(t-\ell'))$. Each color corresponds to the tenor of a SOFR Future contract ranging from 3 to 60 months over the period $2016-2023$. Only 4 maturities (15, 21, 27 and 45 months) out-of 20 are outside the confidence interval after 20 days. Only 4 maturities $(15, 21, 27$ and 45 months) out-of 20 are outside the confidence interval after 20 days.

where $\widehat{\Delta f}$ denotes the conditional expectancy of the forward rates increments $\Delta f$ with respect to these flows:

$$\widehat{\Delta f}(t) := \mathbb{E}\left[\Delta f(t) |\, \Delta \tilde{q}(t)\right]. \tag{8.29}$$

As in chapter 6, we neglect the autocorrelation of the order flows, such that $\Delta\tilde{q}(t) \approx \Delta q(t)$. This approximation is adequate on the daily time scale for 80% of the maturities considered in our sample (see Fig. 8.1). Hence, one can write the conditional expectancy of the forward rates daily increments with respect to the order flow as

$$\widehat{\Delta f}(t) = \mathrm{diag}(\sigma)\,\mathrm{diag}(\sigma_A)^{-1} R\,\mathrm{diag}(Y) O \Omega^{-1/2} \Delta q(t). \tag{8.30}$$

### 8.3.4 Cross-impact matrix

Equation (8.30) can be used to define a cross-impact model. Let $\Lambda \in \mathbf{M}_n(\mathbb{R})$ be the matrix such that the equal-bin linear relationship between forward rates increments and order flows reads

$$\Delta f(t) = \Lambda \Delta q(t) + \mathcal{E}(t), \tag{8.31}$$

where $\mathcal{E}$ is a temporally uncorrelated noise independent from $\Delta q$. Identifying $\Lambda$ in Eq. (8.30) yields

$$\Lambda = \mathrm{diag}(\sigma)\,\mathrm{diag}(\sigma_A)^{-1} R\,\mathrm{diag}(Y) O \Omega^{-1/2}. \tag{8.32}$$

This formula can also be derived by computing $\Lambda$ as the linear response of the forward rates to the equal-time order-flow:

$$\Lambda := \mathbb{E}\left[\Delta f(t) \Delta q(t)^\top\right] \mathbb{E}\left[\Delta q(t) \Delta q(t)^\top\right]^{-1}. \tag{8.33}$$

The proof of this alternative approach is provided in appendix E.5. In addition, appendix E.6 shows that the correlation between the forward rate and the order flow is well defined.

The cross-impact model in Eq. (8.32) is fully determined up to an arbitrary rotation matrix $O$. This free parameter can be used to ensure that our model has the required (i) rotational invariance, (ii) non-arbitrage, (iii) fragmentation invariance, and (iv) stability properties (Tomas et al., 2022b). In fact, it was shown that the cross-impact matrix $\Lambda$ that satisfies these properties must be symmetric positive definite (Tomas et al., 2022b). The rotation $O_{\mathrm{sym}}$ ensuring that $\Lambda$ fulfills these properties is given by (del Molino et al., 2020):

$$O_{\mathrm{sym}}(M, \Omega^{1/2}) := M^{-1} (\Omega^{-1/2})^\top \sqrt{(\Omega^{1/2})^\top M M^\top \Omega^{1/2}}, \tag{8.34}$$

where $M = \mathrm{diag}(\sigma)\,\mathrm{diag}(\sigma_A)^{-1} R\,\mathrm{diag}(Y)$.

As an alternative model that does not meet these constraints, one can also simply choose $O = I$ the identity matrix. We will refer to the cross-impact model using Eq. (8.32) as BBDLW for Baaquie-Bouchaud Discrete Logarithm Whitening when $O = I$ and BBDLS for Baaquie-Bouchaud Discrete Logarithm Symmetric when $O = O_{\mathrm{sym}}$.

## 8.4 Calibration

The best empirical fits of the BB model are obtained in the limit $\psi \to 0$ (see chapter 7), which is therefore chosen for calibration.

In contrast to the previous chapter, our dataset consists of historical daily price variations and net market order flows of SOFR Futures contracts from July 2015 to 2023. In fact, before July 2015, only price variations were available, without corresponding trading volumes. Due to the limited number of trades for longer tenors, we restrict our dataset to $n = 20$ different tenors, ranging from 3 to 60 months. Furthermore, to ensure precise alignment between traded volumes and prices, we set the daily binning cut-off point at noon each day, whereas in chapter 7, the daily price variation cut-off was at the end of the trading day.

### 8.4.1 Methodology

In line with the approach of chapter 7, we fit the parameter $\kappa$ in formula (8.16) to the observed forward rate correlation matrix within our dataset segmented into 3 periods: $2015-2017$, $2018-2020$ and $2021-2023$. In addition, we fit the vector $Y$ by minimizing the square differences between the daily increments of modeled forward rates, $\widehat{\Delta f}$, and the empirical ones, $\Delta f$, using Eq. (8.30).

As in chapter 6, in order to overcome the conditional heteroskedasticity of forward rate variations, we use a daily estimator of their volatility. Let $\{t_1, \cdots, t_N\}$ denote the $N$ business days of a period of 3 years. For each day $t_k$, the estimators of the forward rates increments and order flow's volatility are defined by

$$\begin{aligned}\widehat{\sigma}^2(t_k) &:= (\langle \Delta f_1(t)^2 \rangle(t_k), \cdots, \langle \Delta f_n(t)^2 \rangle(t_k)),\\ \widehat{\omega}^2(t_k) &:= (\langle \Delta q_1(t)^2 \rangle(t_k), \cdots, \langle \Delta q_n(t)^2 \rangle(t_k)),\end{aligned} \tag{8.35}$$

where the operator $\langle . \rangle(t_k)$ denotes the moving-average computed using the last 20 daily data points before the day $t_k$. On day $t_k$, the estimated variance-covariance matrices of the flows, rates variations and the response matrix are respectively given by

$$\begin{aligned}\widehat{\Omega}(t_k) &:= \operatorname{diag}(\widehat{\omega}(t_k))\widehat{\rho}(\Delta q, \Delta q)\operatorname{diag}(\widehat{\omega}(t_k)),\\ \widehat{\Sigma}(t_k) &:= \operatorname{diag}(\widehat{\sigma}(t_k))\widehat{\rho}(\Delta f, \Delta f)\operatorname{diag}(\widehat{\sigma}(t_k)),\\ \widehat{R}(t_k) &:= \operatorname{diag}(\widehat{\sigma}(t_k))\widehat{\rho}(\Delta f, \Delta q)\operatorname{diag}(\widehat{\omega}(t_k)).\end{aligned} \tag{8.36}$$

where $\widehat{\rho}(x, y)$ is the empirical Pearson correlation matrix between the multidimensional random process $x$ and $y$ estimated using 3 years of data, assumed to be stationary.

The predicted forward rate change on day $t_k$ is defined as

$$\widehat{\Delta f}(t_k) = \widehat{\Lambda}^{\text{model}}(t_k)\Delta q(t_k), \tag{8.37}$$

where $\widehat{\Lambda}^{\text{model}}(t_k)$ is the cross-impact matrix estimated on day $t_k$ in the tested model.

In the case of our noise field approach, the cross-impact matrix is given by

$$\widehat{\Lambda}^{\text{BB}}(t_k) = \operatorname{diag}(\widehat{\sigma}(t_k))\operatorname{diag}(\sigma_A)^{-1} R \operatorname{diag}(Y) O \widehat{\Omega}(t_k)^{-1/2}, \tag{8.38}$$

where $O = O_{\text{sym}}$ or $O = I$ depending on the tested model.

In order to compare the results of our model with other cross-impact models, we recall the definition of the three other cross-impact matrices studied in chapter 6. Denoting the Y-ratio by $y$, we consider:

- the diagonal model, defined by

$$\widehat{\Lambda}^{\mathrm{diag}}(t_k) := y\,\mathrm{diag}(\widehat{R}(t_k))\,\mathrm{diag}(\widehat{\Omega}(t_k)^{-1}); \tag{8.39}$$

- the ML model, defined by

$$\widehat{\Lambda}^{\mathrm{ML}}(t_k) := y\widehat{R}(t_k)\widehat{\Omega}(t_k)^{-1}; \tag{8.40}$$

- and the Kyle model, defined by

$$\widehat{\Lambda}^{\mathrm{Kyle}}(t_k) := \quad y\widehat{\Sigma}(t_k)^{1/2}O_{\mathrm{sym}}\Big(\widehat{\Sigma}(t_k)^{1/2},\widehat{\Omega}(t_k)^{1/2}\Big)\widehat{\Omega}(t_k)^{-1/2}. \tag{8.41}$$

As explained in chapter 6, the ML model does not impose any constraints on the cross-impact model, so it generates the best possible in-sample fit. The Kyle model ensures (i) rotational invariance, (ii) non-arbitrage, (iii) fragmentation invariance, and (iv) stability properties. However, none of these models prescribes the form of the price variance-covariance matrix. Such a matrix is fully determined within the BBDL model thanks to a single parameter $\kappa$ in the case $\psi \ll 1$ (see section 8.2).

### 8.4.2 Goodness-of-fit

To assess the model goodness-of-fit, we compare the predicted price changes $\widehat{\Delta f}(t)$ with the realized price changes $\Delta f(t)$. For this evaluation, we employ the $W$-weighted generalized R-squared defined in section 6.3.2.1, replacing $\Delta p$ by $\Delta f$ in Eq. (6.16). As in chapter 6, to highlight different sources of error, different choices of $W$ can be considered:

- $W_\sigma(t) := \mathrm{diag}(\widehat{\sigma}^2(t))^{-1}$, to account for errors relative to the typical deviation of the assets considered.
- $W_{\sigma_\theta}(t) := \mathrm{diag}((0,\dots,0,\widehat{\sigma}^2_\theta(t),0,\dots,0))^{-1}$, to account for the errors of a single asset $\theta$.

The weights $W_\sigma$ are used in section 8.4.3 to compare the overall performance of cross-impact models, while the weights $W_{\sigma_\theta}(t)$ are used in section 8.6 to measure their properties in a pairwise setting.

### 8.4.3 Results

The results of the calibration of the BBDL model on empirical correlations of the forward rate are presented in table 8.1. This confirms the high accuracy and good parameter stability of the BBDL model.

| Period | $\kappa$ | $\mathcal{R}^2$ |
|---|---|---|
| 2015–2017 | 0.84 | 99.9% |
| 2018–2020 | 0.82 | 99.4% |
| 2021–2023 | 1.3 | 97.1% |

**Table 8.1:** Calibrated line tension parameter $\kappa$ in the BBDL model for each 3-year period in our sample. Here, $\mathcal{R}^2$ denotes the share of the explained variance of the empirical correlations among forward rates of time-to-maturity ranging from 3 to 60 months.

Using the calibrated line tension parameter $\kappa$ reported in table 8.1, we fit the share of explained volatility $Y$ to the time series of rates and order flows of SOFR Futures. The calibrated share $Y$ of the explained forward rate volatility is reported for each period in Fig. 8.2.[14] It shows that the most liquid products (the shortest time-to-maturity $\theta$) are associated with the highest values of $Y_\theta$. We also observe that building the symmetric cross-impact model BBDLS requires setting the less liquid maturities of $Y$ to zero (see Fig. 8.2) in order to avoid instabilities. One could improve the R-squared by putting more weight on the non-liquid products, but this would compromise the model's no-arbitrage property.

The in-sample R-squared values reported in Fig. 8.3 show that, as expected, the BBDLW model performs worse than the unconstrained ML model, whereas on the other hand the out-of-sample results show that the two models have similar performances. It is noteworthy because the BBDLW model uses only $n+1$ parameters (excluding the parameters used for the whitening of the correlation matrix), while the ML model requires calibrating $n^2$ parameters. Furthermore, the BBDLS model is actually at least as accurate as the Kyle model in predicting forward rate moves. Once again, this is remarkable because the BBDLS model is more parsimonious than the Kyle model, which uses $\frac{n(n+1)}{2}$ parameters. In fact, the Kyle model, which features a unique Y-ratio for all assets, cannot explore the regime probed by BBDLS.

As expected, compared to the less constrained approaches (ML and BBDLW), the symmetrical models (Kyle and BBDLS) perform poorly in-sample (see Fig. 8.3). However, the out-of-sample results favor these symmetrical models, demonstrating that the market does not feature arbitrage opportunities large enough to rule out those models.

Using this set of calibrated parameters, one can draw the response of the

[14] More precisely, this calibration is performed by assuming $Y \in [0,1]$ and calibrating the *prices* of SOFR Futures $p(t,\theta) = 100 - f(t,\theta)$ to the signed order flow. If we relax this constraint, the search for values $Y \in [-1,1]$ also yields (almost) systematically positive coefficients because of the well-documented positive correlation between order flow and prices (Le Coz et al., 2024d). Indeed, across all periods and maturities (60 calibrated coefficients), we observe only 2 parameters $Y_\theta$ with slightly negative values (around $-0.1$).

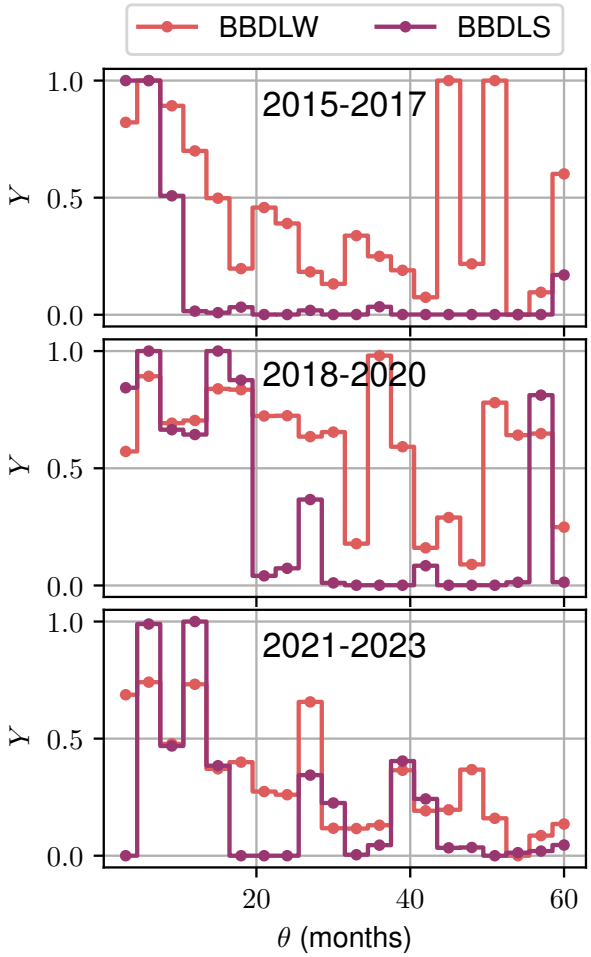


**Figure 8.2:** Optimal parameters $Y_\theta$ governing the share of forward rates variances explained by order flows for each maturity $\theta$.

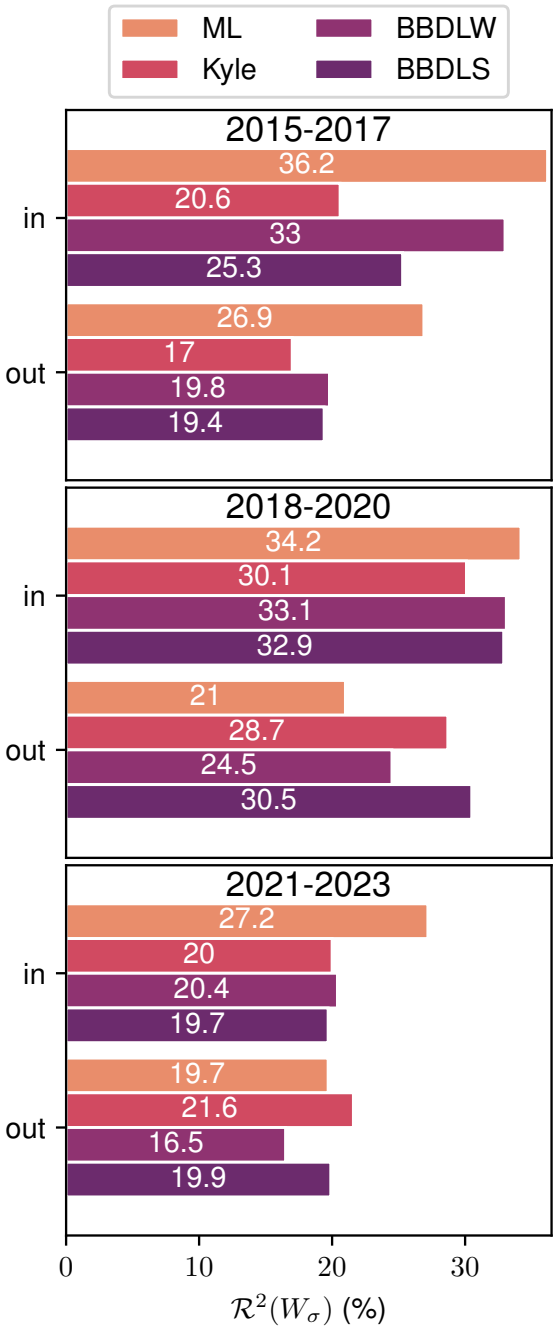


**Figure 8.3:** Generalized R-squared $\mathcal{R}^2(W_\sigma)$ values both in- and out-sample for each period and model. The out–sample values are derived using the parameters calibrated from the preceding period. For the first period $2015 - 2017$, the out–sample R-squared values are calculated using the parameters calibrated from the $2021 - 2023$ period.

forward rate curve to a trade with a notional value of one billion dollars in a single maturity over the course of one day. As our cross-impact models are re-scaled everyday by the daily volatility of prices and order flows (see section 8.4.1), Fig. 8.4 presents one column of the matrix $\Lambda$ on a randomly chosen day within each three-year period. It shows that all models except the ML model predict a high price impact for the tenor being bought (in this case, 21 months).

## 8.5 Non-martingality at small time scales

Several authors have shown that price variations exhibit autocorrelation patterns over short time intervals (see the literature cited in chapter 5). Our model is compatible with these results because, for time scales $\mathrm{d}t \leq \tau$ the forward rate process is not yet a martingale.

To illustrate this phenomenon, we assume that a volume $V$ of the SOFR Future of time-to-maturity $\theta_0$ is purchased during the time interval $\mathrm{d}t$. Our goal is to calculate the progressive deformation of the FRC in response to this single trade. Formally, we define $\mathrm{d}\tilde{q}(0) = V_{\theta_0}$, where $V_{\theta_0} = (0, \ldots, 0, V, 0, \ldots, 0)$ is a vector with a single non-zero component $V$ in the position $\theta_0$ and $\mathrm{d}\tilde{q}(t) = 0$ for $t > 0$. We now discretize time in Eqs (8.2), (8.15), (8.22), and (8.24). This yields an expression for the forward rate variations $\mathrm{d}f$ at discrete times $k\mathrm{d}t$ in response to this single transaction:

$$\mathrm{d}f(k\mathrm{d}t) = \mathrm{d}\widehat{f}(k\mathrm{d}t) + \epsilon'(k\mathrm{d}t). \tag{8.42}$$

Here, $\epsilon'(k\mathrm{d}t)$ is a noise independent from the forward rate variations caused by trading activity $\mathrm{d}\widehat{f}(k\mathrm{d}t)$, which is defined as $\mathrm{d}\widehat{f}(k\mathrm{d}t) :=$

$$\frac{1}{\tau}\,\mathrm{diag}(\sigma)\,\mathrm{diag}(\sigma_A)^{-1}\left(I - \frac{\mathrm{d}t}{\tau}\mathcal{M}\right)^{k}\mathrm{diag}(Y)\Omega^{-1/2}V_{\theta_0}. \tag{8.43}$$

Fig. 8.5 shows the predicted FRC responses to a transaction of volume $V = 1$ billion dollar in the 24-month Futures occurring between $t = 0$ and $t = 0.25\% \times \tau$. Immediately following the trade, cross-impact peaks at the traded maturity. The effect of this trade on the other tenors progressively spreads up to $3\tau$, where it becomes negligible. According to the calibration in chapter 7, $\tau \approx 30$ minutes. Thus, Fig. 8.5 represents the resulting deformation of the FRC between 5 seconds and 1.5 hours after the trade.

## 8.6 Influence of liquidity on price-volume correlations

We now focus on the pair of assets with tenors $\theta$ and $\theta'$. Our aim is to measure the degree to which the goodness-of-fit on the forward rate $\theta$ in a linear cross-impact

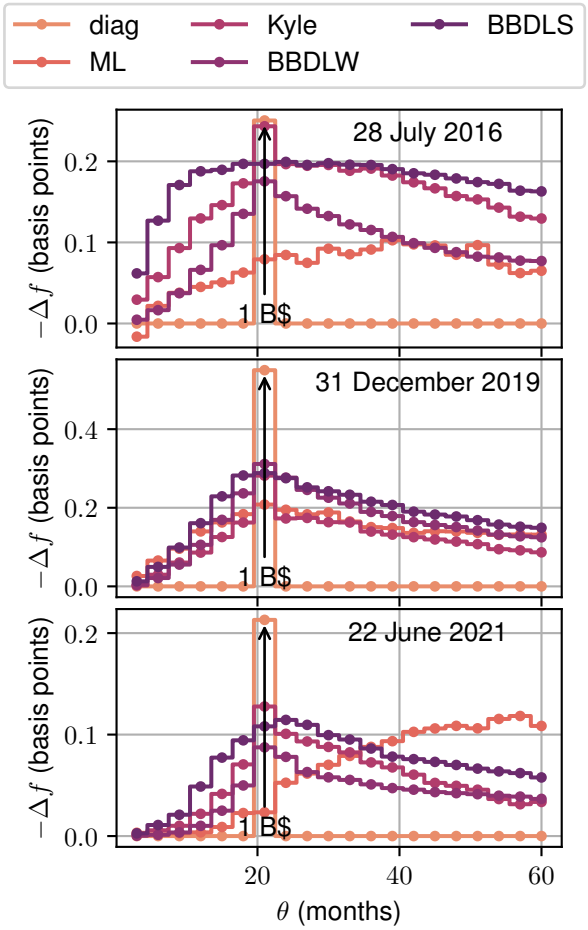


**Figure 8.4:** Modeled FRC moves in response to a trade in the SOFR Future of maturity 21 months with a notional value of one billion dollars over the course of one randomly chosen day for each of the three calibration periods.

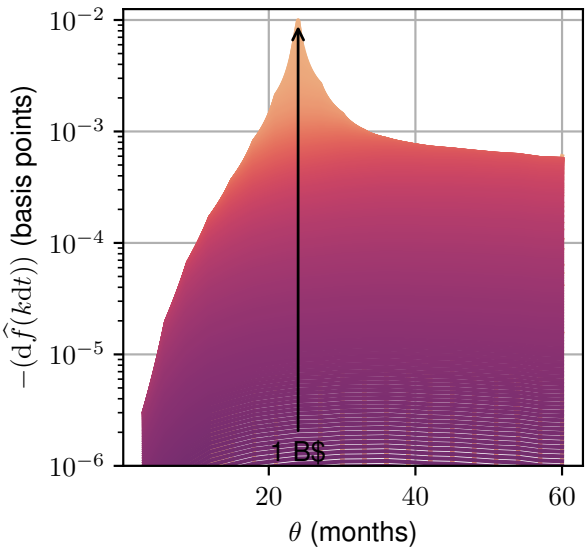


**Figure 8.5:** FRC moves in the BBDLW model in response to a trade in the SOFR Future of maturity 24 months with a notional value of one billion dollars executed at time $t = 0$. Each color corresponds to a time step ordered from $t = 0.25\% \times \tau$ (orange) to $3\tau$ (purple). The total response $\Delta\widehat{f}$ over the time interval $\Delta t = 3\tau$ is the sum of all the infinitesimal responses $\mathrm{d}f(k\mathrm{d}t)$.

model results from the order flow at $\theta'$. For this purpose, we define the accuracy increase of cross-sectional information as

$$\Delta\mathcal{R}^{2,\text{model}}_{\theta'\to\theta} := \mathcal{R}^{2,\text{model}}(W_{\sigma_\theta}) - \mathcal{R}^{2,\text{diag}}(W_{\sigma_\theta}), \tag{8.44}$$

where the R-squared values are computed in a two-asset model. Le Coz et al. (2024d) established that the price-volume correlation between different US sovereign bonds depends on the respective liquidity of the considered assets. Formally Le Coz et al. (2024d) derive these results by observing that the pairwise additional R squared $\Delta\mathcal{R}^2_{\theta'\to\theta}$ obtained by the regression of a bond price on the order flow of another bond is highly asymmetrical. We reproduce these results for SOFR Futures contracts in Fig. 8.6. The vertical stripes show the effect of the liquidity of each asset on the price-volume correlation. In fact, in a 2-asset framework, the additional R-squared $\Delta\mathcal{R}^2_{\theta'\to\theta}$ is roughly equivalent to the squared price-volume correlation $\rho^2(\Delta f_\theta, \Delta q_{\theta'})$, due to the low spatial correlation of the order flow (see section 8.6.1).

In this section, we demonstrate that the BBDLW and BBDLS models capture this stylized fact, primarily due to the vector $Y$, which represents the share of price volatility attributable to trades. These liquidity-dependent responses are neither replicated by the Kyle model (see section 8.6.2) nor by the noise fields $A$ and $\eta$ (see section 8.6.3), highlighting the significance of the parameter vector $Y$.

### 8.6.1 Theoretical ML model

In a two-asset ML model, the R-squared obtained from regressing the prices of the first asset to the order flow imbalance of the both assets is given by

$$\begin{aligned}\mathcal{R}^{2,\text{ML}}(W_{\sigma_1}) = \\ \frac{1}{1-\rho^2(\Delta q_1,\Delta q_2)}\left[\rho^2(\Delta f_1,\Delta q_1)+\rho^2(\Delta f_1,\Delta q_2)\right. \\ \left.-2\rho(\Delta q_1,\Delta q_2)\rho(\Delta f_1,\Delta q_1)\rho(\Delta f_1,\Delta q_2)\right],\end{aligned} \tag{8.45}$$

where $\Delta p_i$ and $\Delta q_i$ are respectively the price increments and the order flow of assets $i \in [\![1,2]\!]$. If one subtracts from the previous quantity the R-squared obtained when regressing the first asset prices on its own trading flow, one gets the theoretical added accuracy $\Delta\mathcal{R}^{2,\text{ML}}_{2\to1}$ in the ML model when regressing asset 1's prices on the order flow imbalance of assets 1 and 2 instead of solely asset 2:

$$\begin{aligned}\Delta\mathcal{R}^{2,\text{ML}}_{2\to1} &= \mathcal{R}^{2,\text{ML}}(W_{\sigma_1}) - \rho^2(\Delta f_1,\Delta q_1) \\ &= \frac{(\rho(\Delta f_1,\Delta q_2)-\rho(\Delta q_1,\Delta q_2)\rho(\Delta f_1,\Delta q_1))^2}{1-\rho^2(\Delta q_1,\Delta q_2)}.\end{aligned} \tag{8.46}$$

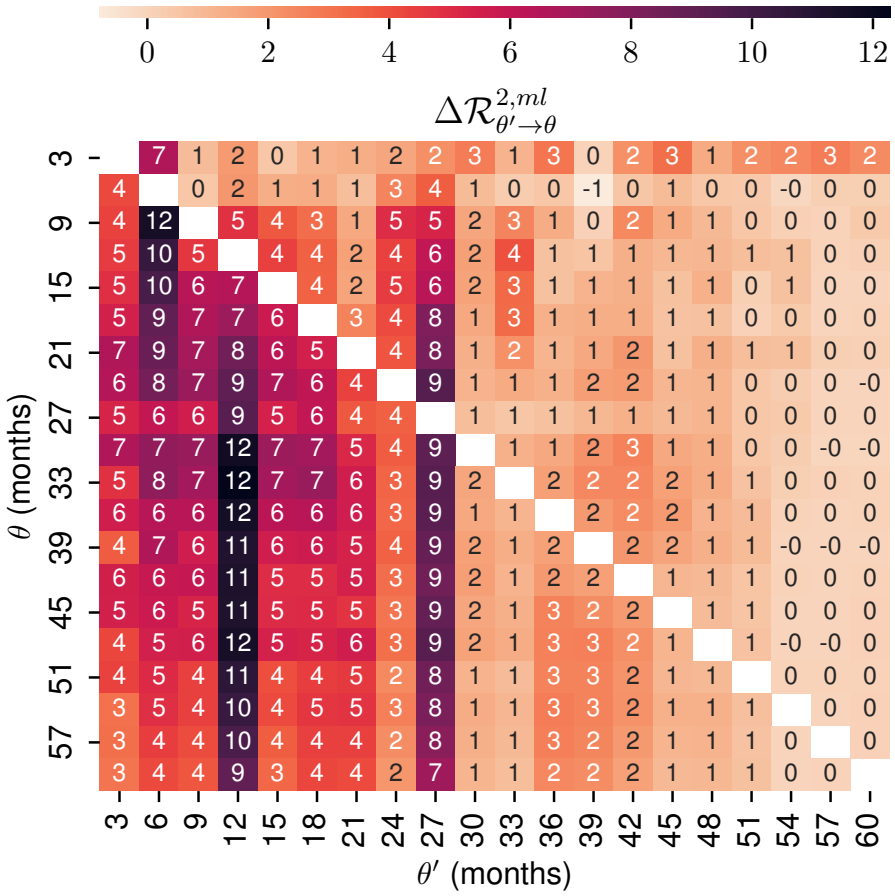


**Figure 8.6:** Empirical added accuracy $\Delta\mathcal{R}^2_{\theta'\to\theta}$ when regressing daily forward rate increments of tenor $\theta$ on the order flows of tenor $\theta$ and $\theta'$ instead of solely on its own order flow, for the period $2021 - 2023$. The calibration methodology is described in section 8.4.1.

Equation (8.46) indicates that $\Delta\mathcal{R}^{2,\mathrm{ML}}_{2\to1}$ depends solely on price and order flow correlations. A priori $\Delta\mathcal{R}^{2,\mathrm{ML}}_{2\to1}$ should be independent of the respective liquidity (i.e., the product $\sigma_i \times \omega_i$, where $\sigma_i$ is the volatility of prices and $\omega_i$ the volatility of the order flow imbalance) of each asset. In fact, Fig. 8.6 illustrates that these R-squared values vary significantly across assets, suggesting that price-volume correlations are influenced by the liquidity of the assets in question (see Le Coz et al. (2024d) for a detailed analysis of liquidity's effect on cross-impact).

### 8.6.2 Theoretical Kyle model

A numerical simulation clearly demonstrates the effect of liquidity in the Kyle model. Figure 8.7 shows the added precision $\Delta\mathcal{R}^{2,\mathrm{Kyle}}_{2\to1}$ in the Kyle model, when regressing the prices of the asset 1 on the order flow imbalance of the assets 1 and 2 instead of solely on the asset 2. Each pair of assets is identified by the liquidity $\sigma_i\omega_i$ of its individual assets. We assume that the $Y$-ratio remains constant for all pairs considered and $y = \rho(\Delta f_1, \Delta q_1)$. In other words, the $Y$-ratio is precisely equal to the correlation between price and volume for the explained asset. Figure 8.7 shows that, in this scenario, $\Delta\mathcal{R}^{2,\mathrm{Kyle}}_{2\to1}$ is close to zero for all the liquidity levels tested. This means that the Kyle model consistently generates an R-squared $\mathcal{R}^{2,\mathrm{Kyle}}(W_\sigma)$ close to $y^2$. It yields another interpretation of the Y-ratio in the Kyle model as the average effective correlation between prices and volumes.

### 8.6.3 Theoretical BBDL models

**8.6.3.0.1 Responses of $A$ to $\eta$.** We first study the response of the correlated field $A$ to its generating white noise $\eta$ given by Eq. (8.13). Figure 8.8 shows the squared correlation between $\Delta A_\theta(t)$ and $\Delta\eta_{\theta'}(t)$ for a typical value of the calibrated parameter $\kappa$. This quantity represents the additional R squared from the regression of $\Delta A_\theta(t)$ to $\Delta\eta_{\theta'}(t)$ and $\Delta\eta_\theta(t)$ instead of only $\Delta\eta_\theta(t)$. Indeed, as $\Delta\eta_\theta(t)$ in independent from $\Delta\eta_{\theta'}(t)$ we have

$$\Delta\mathcal{R}^2_{\theta'\to\theta} = \frac{\mathbb{E}\left[\Delta A_\theta(t)\Delta\eta_{\theta'}(t)\right]^2}{\mathbb{E}\left[\Delta A_\theta(t)^2\right]\mathbb{E}\left[\Delta\eta_{\theta'}(t)^2\right]} = \frac{R^2_{\theta\theta'}}{(\sigma_A)_\theta}. \tag{8.47}$$

Figure 8.8 shows that the correlation between noise $A$ and its generating white noise $\eta$ is asymmetrical and decreases with distance $|\theta-\theta'|$. This asymmetry arises from the rescaling by the norm $\sigma_A$ of the noise field $A$, which decreases when $\theta$ increases. This decreasing volatility is an effect of psychological time: the higher the maturity, the shorter the distance between the nearby tenors; thus, the lower the volatility of each noise $A_{\theta'}$ generated from the normalized white noise $\eta_\theta$.

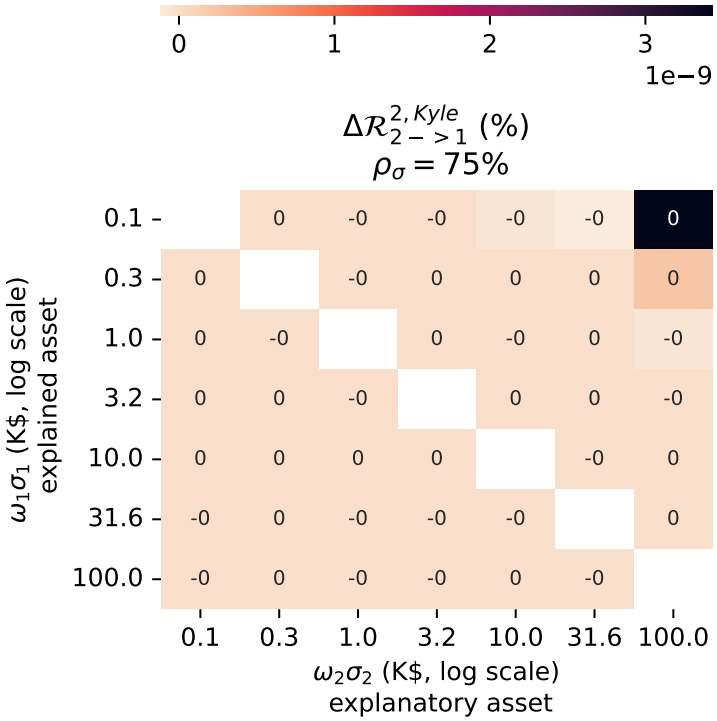


**Figure 8.7:** Theoretical added accuracy $\Delta\mathcal{R}^2_{2\to1}$ in the Kyle model, when regressing the price of asset 1 on the order flow imbalance of assets 1 and 2 instead of solely asset 2. $\Delta\mathcal{R}^{2,\text{Kyle}}_{2\to1}$ is represented as a function of the individual risk levels of each asset. The correlation between the order flows of assets 1 and 2 is $\rho_\omega = 50\%$. The correlation between the prices of assets 1 and 2 is $\rho_\omega = 75\%$. The volatility of prices and volumes is defined as the square root of the risk level: $\sigma_1 = \omega_1 = \sqrt{\sigma_1\omega_1}$.

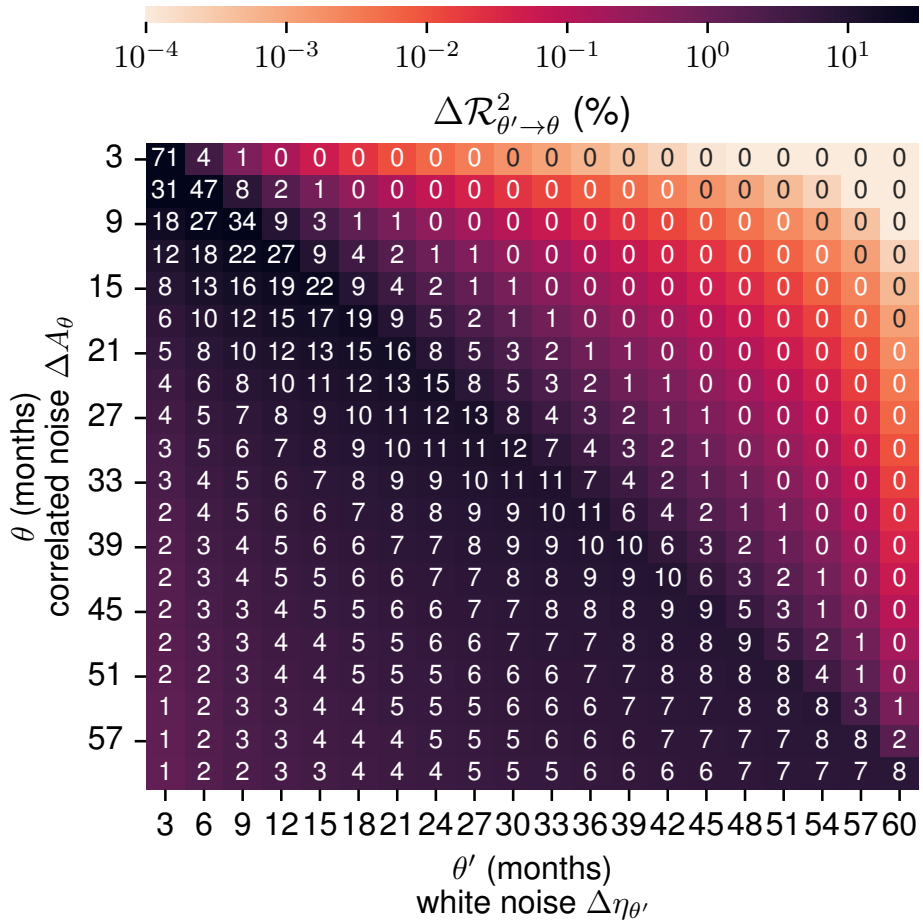


**Figure 8.8:** Theoretical additional R-squared from regressing $\Delta A_\theta(t)$ on $\Delta\eta_{\theta'}(t)$ and $\Delta\eta_\theta(t)$ instead of solely $\Delta\eta_\theta(t)$, according to Eq. (8.13). The parameter $\kappa$ is calibrated on forward rate correlations for the period $2021 - 2023$ (i.e., $\kappa = 1.3$).

**8.6.3.0.2 Responses of the forward rate to $\eta$.** In the BBDLW model, the additional R-squared from regressing $\Delta f_\theta(t)$ on $\Delta\eta^q_{\theta'}(t)$ and $\Delta\eta^q_\theta(t)$ instead of solely $\Delta\eta^q_\theta(t)$ is given by

$$\Delta\mathcal{R}^2_{\theta'\to\theta} = \frac{\mathbb{E}\left[\Delta f_\theta(t)\Delta\eta_{\theta'}(t)\right]^2}{\mathbb{E}\left[\Delta f_\theta(t)^2\right]\mathbb{E}\left[\Delta\eta_{\theta'}(t)^2\right]} = (\mathrm{diag}(\sigma_A)^{-1}R)^2_{\theta\theta'}Y^2_{\theta'}. \tag{8.48}$$

Figure 8.9 shows that the correlation between the forward rate and its generating white noise $\eta^q$ exhibits vertical stripes related to the liquidity of the products considered. This is an effect of differences in the share $Y_\theta$ of the volatility explained by each white noise $\eta_\theta$. However, the model cannot correct for the decreasing volatility of the noise field $A$, as shown by the lower R-squared in the top right of the matrix in Fig. 8.9. We would have obtained similar results in the BBDLS model, although it would require inserting a rotation factor $O^2_{\mathrm{sym}}(\mathrm{diag}(\sigma_A)^{-1}R\,\mathrm{diag}(Y), I)$ into Eq. (8.48). As shown in the following section, this rotation also creates horizontal stripes that correspond to the symmetrization of the cross-impact matrix.

**8.6.3.0.3 Responses of the forward rate to the order flow.** In the BBDLS model, the additional R-squared from regressing $\Delta f_\theta(t)$ on $\Delta q_{\theta'}(t)$ and $\Delta q_\theta(t)$ instead of solely $\Delta q_\theta(t)$ is given by

$$\Delta\mathcal{R}^{2,\mathrm{BBDLS}}_{\theta'\to\theta} = \lambda^2_{\theta\theta'}\omega^2_{\theta'} + 2\rho^q_{\theta\theta'}\lambda_{\theta\theta}\lambda_{\theta\theta'}\omega_\theta\omega_{\theta'}, \tag{8.49}$$

where $\lambda = \mathrm{diag}(\sigma_A)^{-1}R\,\mathrm{diag}(Y)O_{\mathrm{sym}}\Omega^{-1/2}$ is $2\times2$ normalized cross-impact matrix in the BBDLS model. More precisely, the matrix $\mathrm{diag}(\sigma_A)^{-1}R\,\mathrm{diag}(Y)$ is given by the model of dimension $n$ restricted to Futures contracts of tenor $\theta$ and $\theta'$. The matrix $\Omega^{-1/2}$ is defined from a matrix $\Omega$ restricted to two Futures contracts of tenor $\theta$ and $\theta'$.

Figure 8.10 shows that these additional R-squares exhibit vertical stripes related to the liquidity of the products considered. Although we reproduce the order of magnitude of the empirical measures (see Fig. 8.6), we do not precisely match the observed R-squared. In fact, we only have one parameter $Y_{\theta'}$ per column to correct the asymmetric shape of the correlation between $\Delta A$ and $\Delta\eta$ in Fig. 8.8. Thus, while the price-volume correlation depends on the respective liquidity of the considered asset pair (Le Coz et al., 2024d), in our model, it depends only on the explanatory asset. For a given order flow $\theta$, we optimize the average $Y_\theta$ that best matches the liquidity of all assets.

Furthermore, in contrast with the empirical results, we observe that the BBDLS model generates horizontal stripes in the additional pairwise R-squared values (see Fig. 8.10). This occurs because of the symmetry of the cross-impact

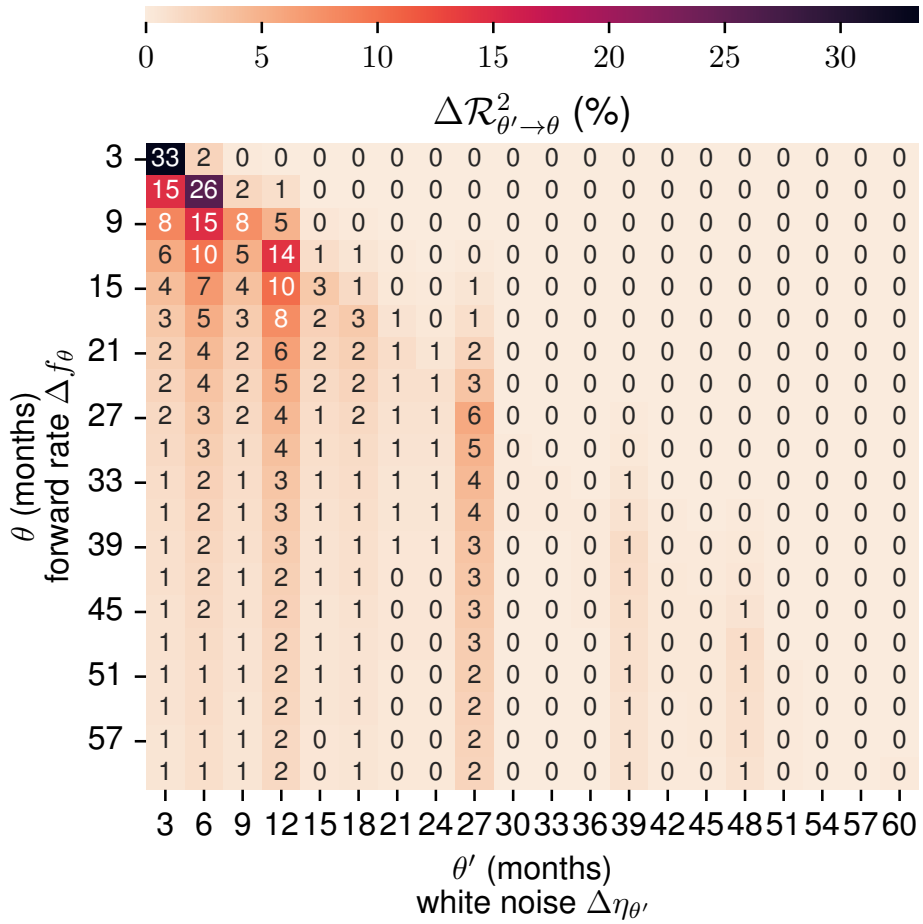


**Figure 8.9:** Theoretical additional R-squared from regressing $\Delta f_\theta(t)$ on $\Delta\eta^q_{\theta'}(t)$ and $\Delta\eta^q_\theta(t)$ instead of solely $\Delta\eta^q_\theta(t)$. The parameter $\kappa$ is calibrated on forward rate correlations for the period $2021-2023$ (i.e., $\kappa = 1.3$) and $Y$ is calibrated on the same period using the BBDLW model.

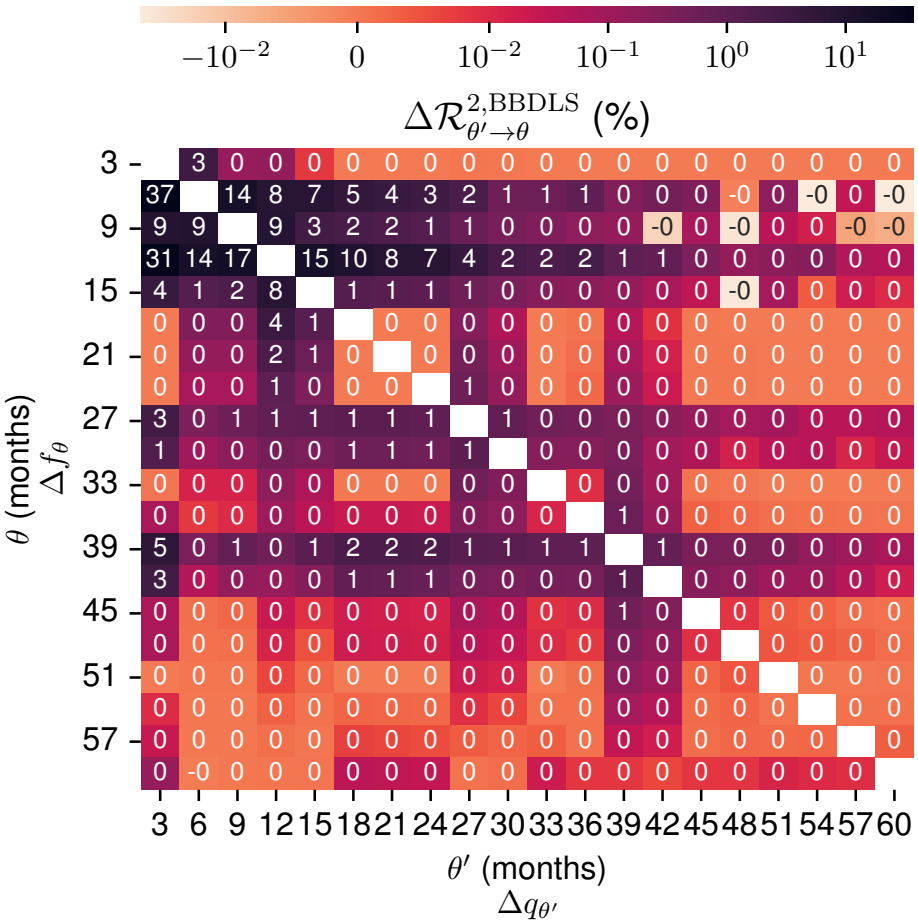


**Figure 8.10:** Theoretical additional R-squared from regressing $\Delta f_\theta(t)$ on $\Delta q_{\theta'}(t)$ and $\Delta q_\theta(t)$ instead of solely $\Delta q_\theta(t)$. The parameter $\kappa$ is calibrated on forward rate correlations for the period $2021-2023$ (i.e., $\kappa = 1.3$) and $Y$ is calibrated on the same period using the BBDLS model.

matrix imposed by the absence of arbitrage. As mentioned previously, the spatial correlation of the order flow is low, rendering the second term in Eq. (8.49) negligible. Consequently, pairwise R-squared values are primarily influenced by the term $\lambda^2_{\theta\theta'}\omega^2_{\theta'}$. We have seen that in the Kyle model, the liquidity $\omega^2_{\theta'}$ does not alter the price-volume correlation, so the R-squared values in Fig. 8.10 can be approximated by the product $YY^\top$, which is symmetric.

## 8.7 Conclusion

Let us start by summarizing what we have achieved. First, we have shown that the BBDL model defined in chapter 7 is consistent with the well-documented temporal autocorrelation of forward rates at short time scales. It appears that the time scale $\tau$ at which spatial correlations among asset prices emerge (Epps, 1979) is also the point where temporal correlations begin to dissipate. Therefore, this framework describes how the spatial and temporal correlation structure of prices evolves across time scales.

Most importantly, we have proposed a new interpretation of the BBDL model of chapter 7 in which high-frequency shocks are identified to trades. The latter, which exhibit low spatial correlations, affect each point of the interest rate curve independently on the smallest time scale. The spatial correlation structure of prices emerges from market participants reacting to these independent trades and external shocks, such as news events, that simultaneously affect multiple points along the yield curve. These participants then propagate the impact of these shocks across other maturities through a self-referential mechanism, as described in chapter 7.

Consequently, this model can be interpreted as a cross-impact model, linking order flows to price movements. A key feature is that only the surprise component of trades influences prices, similarly to a propagator model. To address the challenge of temporal independence, we calibrate the model at a daily time scale, where trades show low autocorrelation. Using this approach, we can match or exceed the precision of the multivariate Kyle model in fitting price moves to order flows, but with far fewer parameters ($n+1$ compared to $\frac{n(n-1)}{2}$). Furthermore, unlike the Kyle model, this framework accounts for liquidity-dependent correlations between the forward rate of one maturity and the order flow of another.

A promising direction for future research is to explore the micro-level mechanisms that connect liquidity with price-volume correlations. This would likely involve the development of a multidimensional model of the limit order book, shedding light on liquidity dynamics across different assets and maturities.

## 8.8 Table of notations

Table 8.2 summaries the notations used in this chapter.

**Table 8.2:** Notations

| Expression | Definition |
|---|---|
| $n$ | The number of available SOFR Futures. |
| $\mathbf{M}_n(\mathbb{R})$ | The set of real-valued square matrices of dimension $n$. |
| $M^\top$ | The transpose of matrix $M$. |
| $\text{diag}(M)$ | The vector in $\mathbb{R}^n$ formed by the diagonal items of the matrix $M$. |
| $\text{diag}(v)$ | The diagonal matrix whose components are the components $(v_1, \cdots, v_n)$ of the vector $v \in \mathbb{R}^n$. |
| $M^{1/2}$ | A matrix such that $M^{1/2}(M^{1/2})^\top = M$. |
| $\sqrt{M}$ | The unique positive semi-definite symmetric matrix such that $(\sqrt{M})^2 = M$. |
| $\Lambda(t)$ | The cross-impact matrix at time $t$. |
| $\sigma(t)$ | The vector of price variation volatility at time $t$. |
| $\omega(t)$ | The vector of the signed order flow volatility at time $t$. |
| $\mathcal{R}^2(W)$ | The $W$-weighted generalized R-squared. |
| $\Delta\mathcal{R}^2(W)$ | The accuracy increase from the cross sectional model. |
| $t$ | The current time. |
| $T$ | The maturity. |
| $P(t,T)$ | The price at time t of a zero-coupon bond maturing at $T$. |
| $\theta$ | The time-to-maturity or tenor. |
| $f_\theta(t)$ | The value at time t of the instantaneous forward rate of tenor $\theta$ (discrete notation). |
| $f(t)$ | The vector of forward rates at time $t$. |
| $\Delta q_\theta(t)$ | The net market order flow traded during the time window $[t, t+\Delta t]$. |
| $\Delta q(t)$ | The vector of the net traded order flows during the time window $[t, t+\Delta t]$. |
| $A_\theta(t)$ | The driftless correlated noise field. |
| $\eta_\theta(.)$ | The discrete white noise of tenor $\theta$. |
| $\sigma_\theta(t)$ | The volatility at time $t$ of the infinitesimal variation of the instantaneous forward rate of time-to-maturity $\theta$. |
| $\mu$ | The line tension parameter. |
| $\psi$ | The psychological time parameter. |
| $\kappa$ | Unique a-dimensional parameter in the BBDL model, defined as the product $\mu \times \psi$. |
| $\tau$ | The time scale for the emergence of correlations. |

Continued on next page

| Expression | Definition |
|---|---|
| $\Delta t$ | The temporal duration of a day. |
| $\mathbb{E}[.]$ | The unconditional expectancy. |
| $\langle . \rangle(t)$ | The empirical average operator over the interval $[t - \Delta t, t]$. |
| $\hat{x}(t)$ | The estimator of $x$ at time $t$. |
| $\eta_\theta(.)$ | The discrete white noise of tenor $\theta$. |
| $\delta(.)$ | The Dirac delta function. |
| $\rho(x, y)$ | The linear Pearson correlation matrix between the random vector $x$ and $y$. |
| $\delta_{\theta\theta'}$ | The Kronecker delta. |
| $I_k$ | A matrix with ones only on the $k$-th diagonal above the main diagonal. |
| $I$ | The identity matrix. |
| $\mathcal{J}$ | A diagonal matrix whose first entry is 2 while all the other entries are ones. |
| $\mathcal{L}_d[.]$ | The discrete linear differential operator on space. |
| $\mathcal{M}$ | The discrete non-linear differential operator on space, using matrix notations. |
| $L_d[.]$ | The Fourier transform of the discrete linear differential operator on space. |
| $G_{\theta\theta'}(.)$ | Green function or *propagator* of Eq. (8.2) |
| $N$ | The number of days in a 3-year period of our sample. |
| $H(.)$ | The Heaviside function. |
| $\mathcal{F}[f]$ | The Fourier transform of the function of time $f$. |

## Key takeaways

- The field theory introduced in the previous chapter is consistent with the temporal autocorrelation of forward rates at short time scales.
- The time scale $\tau$ at which spatial correlations emerge is also the point at which these temporal correlations begin to dissipate.

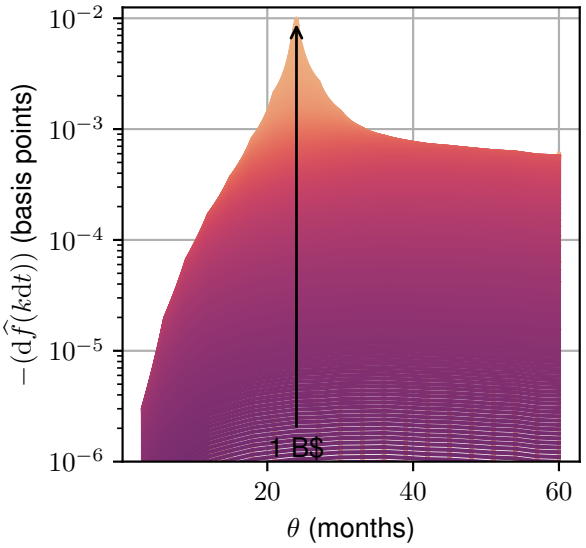


- We have proposed a new interpretation of this field theory in which high-frequency shocks are identified to trades.
- The spatial correlation structure of prices emerges from the responses of market participants to these trades and external shocks.
- Using this approach, we can match or exceed the precision of the multivariate Kyle model in fitting price moves to order flows, but with far fewer parameters ($n+1$ compared to $\frac{n(n-1)}{2}$).
- Unlike the Kyle model, this framework accounts for liquidity-dependent correlations between the forward rate of one maturity and the order flow of another.

# Part IV

# Conclusion and future works

# Conclusion

## Overview of the results

In line with standard economic theory, we have seen that most yield curve models in the literature assume the existence of a rational agent that optimizes its utility between present and future consumption. These models, which are often misspecified, are incompatible with the observed volatility of long-term rates (the excess volatility puzzle).

To address these limitations, we have examined the microstructure of the markets that compose the yield curve. Short-term yields are primarily defined by the interbank market, where secured transactions take place in a highly regulated environment. Banks hedge their long-term loans using interest rate derivatives, whose prices are based on the value of Futures and bonds quoted on limit order books.

To faithfully model the interbank market, we have assumed that banks create money endogenously while absorbing payment shocks through repo transactions, subject to reserves, liquidity, and leverage constraints. Our agent-based model sheds light on recent puzzles in money markets. While excess liquidity might initially be attributed to insufficient collateral to meet LCR requirements, our model shows that even with sufficient collateral supply, excess liquidity can emerge from banks' asymmetric responses to payment shocks. The observed level of collateral re-use is driven by the long cancelation notice period of repos. Collateral scarcity increases re-use as positive shocks must be absorbed by more borrowers. Furthermore, we observe that the full allotment procedure and LCR regulation have increased market stability. This modeling framework also illustrates how regulatory changes can have unintended systemic consequences: reducing securities held by each bank below the size of the payment shocks collapses the repo market, leading to a surge in excess liquidity.

The rest of the yield curve presents stylized facts related to its multidimensional nature, not commonly seen in other financial assets. On the one hand, the price dynamics of interest rate products show typical financial time series characteristics, with increments being autocorrelated at small time scales (less than a

few minutes) but decorrelated at longer ones. On the other hand, the spatial correlation structure of the forward rate curve resembles that of an elastic string. In contrast, order flows on the yield curve are temporally decorrelated but spatially correlated.

Furthermore, our analysis of the relationship between prices and signed order flows led to the identification of new stylized facts. We find that price formation occurs endogenously within highly liquid assets. Then, trades in these assets influence the prices of their less liquid correlated products, with an impact speed constrained by their minimum trading frequency. In particular, price-volume correlations depend on the liquidity of the assets considered. In fact, contrary to traditional economic theory, which considers long-term rates as expectations of short-term rates, low-liquidity tenors are mainly influenced by the trades in high-liquidity tenors.

All these stylized facts can be captured within a single model. The correlation structure of the forward rate curve is the result of market participants reacting to high-frequency shocks, which are transmitted along maturities through a self-referential mechanism. This model is further enhanced by incorporating the concept of "psychological time", which translates into the hyperbolic discounting factor from behavioral economics literature (Farmer and Geanakoplos, 2009). The single parameter of the model remains stable throughout the last 30 years, allowing it to reproduce the correlation structure of the forward rate curve with remarkable precision (approximately 1% error), including the power-law decay of its eigenvalues and curvature perpendicular to the diagonal. Our calibration reveals a strong distortion of future time, reflecting the myopic nature of financial markets. This model also quantitatively reproduces the empirical observation of negligible correlations at high frequencies (Epps, 1979), which build up slowly at lower frequencies with a characteristic timescale of around 30 minutes. Additionally, the model captures the temporal autocorrelation of forward rates at short time scales. In this framework, spatial correlations emerge precisely when temporal correlations dissipate.

Finally, interpreting high-frequency shocks as trades and news allows us to develop a cross-impact model that matches or exceeds the precision of the multivariate Kyle model when fitting price moves to order flows, while using far fewer parameters. Unlike the Kyle model, this framework accounts for liquidity-dependent correlations between the forward rate of one maturity and the order flow of another.

In summary, the key message of this thesis can be summarized as follows. Economic theory has traditionally micro-founded interest rates as a trade-off between present and future consumption. This view is incompatible with the data. In fact, because of banks' significant market power, long-term rates are largely determined by financial markets that are almost indifferent to fundamental values

but very sensitive to supply and demand. The most significant implication of this model for economic theory, explored in more detail in the following section, is the absence of a binding link between inflation and nominal rates.

## Extensions and closing remarks

Throughout the manuscript, we have highlighted some unresolved questions and potential extensions that could enhance the understanding of the formation of the yield curve. In particular, introducing prices into our agent-based model could help understanding the transmission of central bank rates to money markets, potentially shedding light on the departure of repo rates from the ECB's interest rate corridor (Piquard and Salakhova, 2019). Additionally, the identified gaps in describing the multidimensional price formation mechanism should be addressed. Certain asset prices are best explained by trades occurring over significantly longer time scales than their trading frequency suggests, which requires exploring other factors influencing cross-impact. Another promising direction for future research would be investigating the micro-level mechanisms linking liquidity and price-volume correlations, likely involving the development of a multidimensional model of the limit order book.

However, these extensions would not fully address the broader question of defining the level of the yield curve if fundamental factors such as demographic growth and inflation have little influence. On the one hand, we have a model that explains rates fluctuations across different maturities thanks to trading flows, which are known to be influenced by the hedging activity of banks. On the other hand, we developed a model of monetary flows in the interbank market. Thus, it is tempting to merge these frameworks into a single, micro-founded model of the yield curve. Achieving this would likely require modeling the behavior of additional actors such as investment funds, insurance corporations, and other financial intermediaries, who play a role in shaping the supply and demand for money across maturities. As shown in appendix A, data on the interactions between these actors and the banking system exists, providing the potential for the development of an agent-based model that would connect money creation and investors' behavior to the shape of the yield curve.

The interest rate on a risk-free investment is one of the most fundamental variables in Economics. It serves as a key indicator of the time value of money, representing the required return for deferring a guaranteed payoff from the present to a future date. However, the main conclusion of this thesis is that, like any other financial asset, safe assets experience price fluctuations driven by market forces. These assets offer a "convenience yield" that reflects their liquidity, suitability as collateral, ability to meet regulatory capital requirements, and other functions that

resemble the role of money (see also van Binsbergen et al. (2021) for a detailed discussion of convenience yields). In other words, interest rates are effectively determined by financial markets which are more influenced by the forces of supply and demand than by fundamental values.

The main implication of these findings for monetary policy transmission is that the nominal rate may never converge to an equilibrium rate, breaking the relationship between inflation and nominal rates. This leads to an alternative interpretation of the Fisher equation (1.9): the nominal rate is determined by the supply and demand for money in financial markets, the inflation rate is set by the supply and demand for goods, and the real rate reflects the imbalance between the two. This raises questions about the adequacy of current monetary policy tools for handling inflation. Policies that bypass the bank lending channel of money creation could be considered, such as "helicopter money" programs (Reis and Tenreyro, 2022). Alternatively, we could view consumer goods inflation as a matter of industrial and labor market policies, suggesting that central banks should focus on other quantifiable objectives where nominal rates have a direct impact.

Since the GFC, a large amount of money has been created in western economies. For years, central banks were disappointed that this money did not generate inflation. It took a real-life test of a helicopter money policy during the COVID-19 crisis to finally see inflation emerge[15]. These events highlight a significant shift in the use of money created by modern financial systems. This money is no longer primarily used to purchase consumption goods, but still serves as a powerful allocation tool for influencing development. The apparent disconnect between consumer goods inflation and long-term rates may actually present an opportunity to develop innovative central bank policies. In this view, one could envision setting differentiated rates depending on the social benefits of specific investments, which could be a means of financing the ecological transition without significantly increasing taxes or public debt.

As a final remark, I would like to emphasize that the money creation process is not neutral in the production of inequalities. By relying on private firms and risk metrics to grant loans, the current system inherently favors wealthier households. This approach has the significant advantage of decentralization, while alternative methods would require central banks to determine how much money should be allocated or loaned to each consumer or firm –a task that was unfeasible in previous centuries. However, with the advent of digitalization, implementing a fairer money creation process may now be within reach. This idea is not as radical as it may seem when we consider that welfare states in advanced economies have already

[15]For a review of the multiple causes of post-COVID-19 inflation, including demand-pull, cost-push, and profit-driven factors, see Knicker et al. (2024).

generated substantial amounts of money through public debt to support social systems. One way to make this process more sustainable would be to monetize this debt, thereby creating money in a manner that benefits those with fewer resources.

# Acronyms

**ABM** Agent Based Model . . . . . 36–38, 40, 62, 71, 82

**APP** Asset Purchase Program . . . . . 90, 97

**COVID-19** COronaVIrus Disease of 2019 . . . . . v, 167, 212

**DSGE** Dynamic Stochastic General Equilibrium . . . . . 12, 14, 15, 25, 29–32

**E.U.** European Union . . . . . 16, 40, 42, 50, 53–56

**ECB** European Central Bank . . . . . 59, 60

**EONIA** Euro OverNight Index Average . . . . . 42, 252

**ESTR** Euro Short-Term Rate . . . . . 4, 40, 42, 44, 51–53, 55, 56, 252

**EURIBOR** Euro Interbank Offered Rate . . . . . 51–53

**FRC** Forward Rate Curve . 9, 13, 26, 28, 29, 105–108, 110, 112–115, 153, 154, 156, 172, 178–180, 182, 192

**GFC** Great Financial Crisis . . . . . 8, 11, 15, 31, 40, 59, 60, 62, 98, 212

**LCR** Liquidity Coverage Ratio . . . . . 59, 60, 62–65, 68, 70

**LOB** Limit Order Book . . . . . 51, 52, 54, 55, 103, 122

**NK** New Keynesian . . . . . 29, 30

**SOFR** Secured Overnight Funding Rate 4, 40, 42, 44, 47, 53, 55, 103, 108, 164, 172, 175, 275, 279

**U.S.** United States of America8, 11–13, 16, 23, 24, 30, 32, 33, 40, 44, 47, 50, 51, 53–56, 106, 122

# Bibliography


Accornero, Matteo (2020). *Repo Markets, Collateral Re-use and Systemic Fragility. A Literature Review*. Sapienza Universita di Roma.

Afonso, Gara, Anna Kovner, and Antoinette Schoar (2013). "Trading Partners in the Interbank Lending Market". In: *SSRN Electronic Journal*. DOI: 10.2139/ssrn.2266527.

Afonso, Gara and Ricardo Lagos (2015). "Trade Dynamics in the Market for Federal Funds". In: *Econometrica* 83.1, pp. 263–313. DOI: 10.3982/ECTA10586.

Aihara, Shin Ichi and Arunabha Bagchi (2005). "Stochastic Hyperbolic Dynamics For Infinite-Dimensional Forward Rates And Option Pricing". In: *Mathematical Finance* 15.1 (Jan. 2005), pp. 27–47. DOI: 10.1111/j.0960-1627.2005.00209.x.

Alfonsi, Aurélien, Florian Klöck, and Alexander Schied (2016). "Multivariate Transient Price Impact and Matrix-Valued Positive Definite Functions". In: *Mathematics of Operations Research* 41.3 (Aug. 2016), pp. 914–934. DOI: 10.1287/moor.2015.0761.

Allen, Franklin (2016). *Liquidity Regulation, Extended Repo and the Real Economy*.

Almgren, Robert, Chee Thum, Emmanuel Hauptmann, and Hong Li (2005). "Direct Estimation of Equity Market Impact". In: *Risk* 18.7, pp. 58–62.

Altunbas, Yener, Leonardo Gambacorta, and David Marques-Ibanez (2010). "Bank Risk and Monetary Policy". In: *Journal of Financial Stability* 6.3, pp. 121–129.

*Amended MMSR Regulation (EU) 2019/ 113* (2019).

Amin, Kaushik I. and Andrew J. Morton (1994). "Implied Volatility Functions in Arbitrage-Free Term Structure Models". In: *Journal of Financial Economics* 35.2 (Apr. 1994), pp. 141–180. DOI: 10.1016/0304-405X(94)90002-7.

Anand, Kartik, Ben Craig, and Goetz Von Peter (2015). "Filling in the Blanks: Network Structure and Interbank Contagion". In: *Quantitative Finance* 15.4 (Apr. 3, 2015), pp. 625–636. DOI: 10.1080/14697688.2014.968195.

Andersen, T (2001). "The Distribution of Realized Stock Return Volatility". In: *Journal of Financial Economics* 61.1 (July 2001), pp. 43–76. DOI: 10.1016/S0304-405X(01)00055-1.

Andersen, Torben G., Tim Bollerslev, and Francis X. Diebold (2007). "Roughing It Up: Including Jump Components in the Measurement, Modeling, and Forecasting of Return Volatility". In: *The Review of Economics and Statistics* 89.4 (Nov. 1, 2007), pp. 701–720. DOI: 10.1162/rest.89.4.701.

Andrade, Sandro C., Charles Chang, and Mark S. Seasholes (2008). "Trading Imbalances, Predictable Reversals, and Cross-Stock Price Pressure". In: *Journal of Financial Economics* 88.2 (May 2008), pp. 406–423. DOI: 10.1016/j.jfineco.2007.04.005.

Andrés, Javier, David Lopez-Salido, and Edward Nelson (2009). "Money and the Natural Rate of Interest: Structural Estimates for the United States and the Euro Area". In: *Journal of Economic Dynamics and Control* 33.3, pp. 758–776.

Arnéodo, A., J.-F. Muzy, and D. Sornette (1998). ""Direct" Causal Cascade in the Stock Market". In: *The European Physical Journal B - Condensed Matter and ComplexSystems* 2.2 (Mar. 1, 1998), pp. 277–282. DOI: 10.1007/s100510050250.

association, The international capital market (2015). *The Current State and Future Evolution of the European-repo Market.* ICMA.

Auerbach, Alan and Laurence Kotlikoff (1987). "Evaluating Fiscal Policy with a Dynamic Simulation Model". In: *American Economic Review* 77.2, pp. 49–55.

Ayuso, Juan, Andrew G. Haldane, and Fernando Restoy (1997). "Volatility Transmission along the Money Market Yield Curve". In: *Weltwirtschaftliches Archiv* 133.1 (Mar. 1, 1997), pp. 56–75. DOI: 10.1007/BF02707676.

Baaquie, B. E. (2018). *Quantum Field Theory for Economics and Finance.* Cambridge, United Kingdom: Cambridge University Press.

Baaquie, Belal and Jean-Philippe Bouchaud (2004). ""Stiff" Field Theory of Interest Rates and Psychological Future Time". In: *Wilmott Magazine*, pp. 2–6.

Baaquie, Belal E. (2001). "Quantum Field Theory of Treasury Bonds". In: *Physical Review E* 64.1 (June 22, 2001), p. 016121. DOI: 10.1103/PhysRevE.64.016121.

— (2002). "Quantum Field Theory of Forward Rates with Stochastic Volatility". In: *Physical Review E* 65.5 (May 20, 2002), p. 056122. DOI: 10.1103/PhysRevE.65.056122.

— (2004). *Quantum Finance: Path Integrals and Hamiltonians for Options and Interest Rates.* 1st ed. Cambridge: Cambridge University Press, Nov. 15, 2004. DOI: 10.1017/CBO9780511617577.

— (2007). "Feynman Perturbation Expansion for the Price of Coupon Bond Options and Swaptions in Quantum Finance. I. Theory". In: *Physical Review E* 75.1 (Jan. 11, 2007), p. 016703. DOI: 10.1103/PhysRevE.75.016703.
— (2009). "Interest Rates in Quantum Finance: The Wilson Expansion and Hamiltonian". In: *Physical Review E* 80.4 (Oct. 26, 2009), p. 046119. DOI: 10.1103/PhysRevE.80.046119.
— (2010). "Interest Rates in Quantum Finance: Caps, Swaptions and Bond Options". In: *Physica A: Statistical Mechanics and its Applications* 389.2 (Jan. 2010), pp. 296–314. DOI: 10.1016/j.physa.2009.09.031.
Baaquie, Belal E. and Cui Liang (2007). "Feynman Perturbation Expansion for the Price of Coupon Bond Options and Swaptions in Quantum Finance. II. Empirical". In: *Physical Review E* 75.1 (Jan. 11, 2007), p. 016704. DOI: 10.1103/PhysRevE.75.016704.
Baaquie, Belal E. and Marakani Srikant (2004). "Comparison of Field Theory Models of Interest Rates with Market Data". In: *Physical Review E* 69.3 (Mar. 31, 2004), p. 036129. DOI: 10.1103/PhysRevE.69.036129.
Baaquie, Belal E. and Pan Tang (2012). "Simulation of Nonlinear Interest Rates in Quantum Finance: Libor Market Model". In: *Physica A: Statistical Mechanics and its Applications* 391.4 (Feb. 2012), pp. 1287–1308. DOI: 10.1016/j.physa.2011.08.021.
Bachelier, L. (1900). "Théorie de La Spéculation". In: *Annales scientifiques de l'École normale supérieure* 17, pp. 21–86. DOI: 10.24033/asens.476.
Bacry, E., J. Delour, and J. F. Muzy (2001). "Multifractal Random Walk". In: *Physical Review E* 64.2 (July 17, 2001), p. 026103. DOI: 10.1103/PhysRevE.64.026103.
Bacry, E., A. Kozhemyak, and J. F. Muzy (2011). "Log-Normal Continuous Cascade Model of Asset Returns: Aggregation Properties and Estimation". In: *Quantitative Finance* 13.5, pp. 795–818.
Bacry, Emmanuel, Adrian Iuga, Matthieu Lasnier, and Charles-Albert Lehalle (2015). "Market Impacts and the Life Cycle of Investors Orders". In: *Market Microstructure and Liquidity* 01.02 (Dec. 2015), p. 1550009. DOI: 10.1142/S2382626615500094.
Barberis, Nicholas, Robin Greenwood, Lawrence Jin, and Andrei Shleifer (2015). "X-CAPM: An Extrapolative Capital Asset Pricing Model". In: *Journal of Financial Economics* 115.1 (Jan. 2015), pp. 1–24. DOI: 10.1016/j.jfineco.2014.08.007.
Baumol, William J (1959). *Business Behavior, Value and Growth.* New York: Macmillan.
Bech, Morten and Cyril Monnet (2016). "A Search-Based Model of the Interbank Money Market and Monetary Policy Implementation". In: *Journal of Economic Theory* 164 (July 2016), pp. 32–67. DOI: 10.1016/j.jet.2015.08.007.

Beechey, Meredith J. (2006). *Excess Sensitivity and Volatility of Long Interest Rates: The Role of Limited Information in Bond Markets*. SSRN Scholarly Paper ID 938510. Rochester, NY: Social Science Research Network, Oct. 1, 2006. DOI: 10.2139/ssrn.938510.

*Benchmarks Regulation (EU) 2016/1011* (2016). DOI: 10.5040/9781782258674.

Benjamini, Yoav and Yosef Hochberg (1995). "Controlling the False Discovery Rate: A Practical and Powerful Approach to Multiple Testing". In: *Journal of the Royal Statistical Society: Series B (Methodological)* 57.1 (Jan. 1995), pp. 289–300. DOI: 10.1111/j.2517-6161.1995.tb02031.x.

Benner, Mats, ed. (2013). *Before and Beyond the Global Economic Crisis: Economics, Politics and Settlement*. Cheltenham: Edward Elgar Publishing, May 29, 2013. 272 pp.

Benzaquen, Michael, Jonathan Donier, and Jean-Philippe Bouchaud (2016). "Unravelling the Trading Invariance Hypothesis". In: *Market Microstructure and Liquidity* 02 (03n04 Dec. 2016), p. 1650009. DOI: 10.1142/S238262661650009X.

Benzaquen, Michael, Iacopo Mastromatteo, Zoltan Eisler, and Jean-Philippe Bouchaud (2017). "Dissecting Cross-Impact on Stock Markets: An Empirical Analysis". In: *Journal of Statistical Mechanics: Theory and Experiment* 2017.2 (Feb. 13, 2017), p. 023406. DOI: 10.1088/1742-5468/aa53f7.

Bernanke, Ben Shalom and Alan Blinder (1988). *Credit, Money, and Aggregate Demand*. Working Paper 2534. National Bureau of Economic Research, Mar. 1988. DOI: 10.3386/w2534.

Bhar, Ramaprasad and Carl Chiarella (2011). "A Maximum Likelihood Approach to Estimation of a Class of the Heath-Jarrow-Morton Models". In: (Oct. 29, 2011).

Bielecki, Marcin, Marcin Kolasa, and Michał Brzoza-Brzezina (2018). *Demographics, Monetary Policy and the Zero Lower Bound*. 810. Society for Economic Dynamics.

Björk, Tomas (1998). *Arbitrage Theory in Continuous Time*. Oxford ; New York: Oxford University Press. 312 pp.

— (2019). *Arbitrage Theory in Continuous Time*. 4th ed. Oxford University Press, Dec. 5, 2019. DOI: 10.1093/oso/9780198851615.001.0001.

Black, Fischer (1986). "Noise". In: *The Journal of Finance* 41.3, pp. 528–543. DOI: 10.1111/j.1540-6261.1986.tb04513.x.

Black, Fischer and Myron Scholes (1973). "The Pricing of Options and Corporate Liabilities". In: *Journal of Political Economy* 81.3, pp. 637–654. JSTOR: 1831029.

Blanchard, Olivier J. (1985). "Debt, Deficits, and Finite Horizons". In: *Journal of Political Economy* 93.2, pp. 223–247. JSTOR: 1832175.

Blasques, Francisco, Falk Bräuning, and Iman van Lelyveld (2018). "A Dynamic Network Model of the Unsecured Interbank Lending Market". In: *Journal of*

*Economic Dynamics and Control* 90 (May 2018), pp. 310–342. DOI: 10.1016/j.jedc.2018.03.015.

Boissay, Frédéric, Fabrice Collard, and Frank Smets (2016). "Booms and Banking Crises". In: *Journal of Political Economy* 124.2 (Apr. 2016), pp. 489–538. DOI: 10.1086/685475.

Bomfim, Antulio N. (1997). "The Equilibrium Fed Funds Rate and the Indicator Properties of Term-Structure Spreads". In: *Economic Inquiry* 35.4, pp. 830–846.

Bordalo, Pedro, Nicola Gennaioli, Yueran Ma, and Andrei Shleifer (2020). "Overreaction in Macroeconomic Expectations". In: *American Economic Review* 110.9 (Sept. 2020), pp. 2748–2782. DOI: 10.1257/aer.20181219.

Borgatti, Stephen P and Martin G Everett (2000). "Models of Core/Periphery Structures". In: *Social Networks* 21.4 (Oct. 1, 2000), pp. 375–395. DOI: 10.1016/S0378-8733(99)00019-2.

Borio, Claudio and Haibin Zhu (2012). "Capital Regulation, Risk-Taking and Monetary Policy: A Missing Link in the Transmission Mechanism?" In: *Journal of Financial Stability* 8.4, pp. 236–251. DOI: 10.1016/j.jfs.2011.12.003.

Borio, Claudio E. V. (1995). "The Structure of Credit to the Non-Government Sector and the Transmission Mechanism of Monetary Policy: A Cross-Country Comparison". In: *SSRN Electronic Journal*. DOI: 10.2139/ssrn.868430.

Boss, Michael, Helmut Elsinger, Martin Summer, and Stefan Thurner (2004). "Network Topology of the Interbank Market". In: *Quantitative Finance* 4.6 (Dec. 1, 2004), pp. 677–684. DOI: 10.1080/14697680400020325.

Bouchaud, J. P. (2009). *Price Impact*. Mar. 13, 2009. arXiv: 0903.2428 [q-fin].

Bouchaud, Jean-Philippe (2010). "Price Impact". In: *Encyclopedia of Quantitative Finance*. John Wiley & Sons, Ltd. DOI: 10.1002/9780470061602.eqf18006.

Bouchaud, Jean-Philippe, Julius Bonart, Jonathan Donier, and Martin Gould (2018). *Trades, Quotes and Prices: Financial Markets Under the Microscope*. Cambridge, UK ; New York: Cambridge University Press, Mar. 22, 2018. 460 pp.

Bouchaud, Jean-Philippe, Stefano Ciliberti, Yves Lemperiere, Adam Aleksander Majewski, Philip Andrew Seager, and Kevin Sin Ronia (2017). "Black Was Right: Price Is Within a Factor 2 of Value". In: *SSRN Electronic Journal*. DOI: 10.2139/ssrn.3070850.

Bouchaud, Jean-Philippe, J. Doyne Farmer, and Fabrizio Lillo (2009a). "Chapter 2 - How Markets Slowly Digest Changes in Supply and Demand". In: *Handbook of Financial Markets: Dynamics and Evolution*. Ed. by Thorsten Hens and Klaus Reiner Schenk-Hoppé. Handbooks in Finance. San Diego: North-Holland, Jan. 1, 2009, pp. 57–160. DOI: 10.1016/B978-012374258-2.50006-3.

Bouchaud, Jean-Philippe, J. Doyne Farmer, and Fabrizio Lillo (2009b). "How Markets Slowly Digest Changes in Supply and Demand". In: *Handbook of Financial Markets: Dynamics and Evolution*. arXiv.

Bouchaud, Jean-Philippe, Yuval Gefen, Marc Potters, and Matthieu Wyart (2004). "Fluctuations and Response in Financial Markets: The Subtle Nature of 'Random' Price Changes". In: *Quantitative Finance* 4.2 (Apr. 2004), pp. 176–190. DOI: 10.1080/14697680400000022.

Bouchaud, Jean-Philippe, Julien Kockelkoren, and Marc Potters (2006). "Random Walks, Liquidity Molasses and Critical Response in Financial Markets". In: *Quantitative Finance* 6.2 (Apr. 2006), pp. 115–123. DOI: 10.1080/14697680500397623.

Bouchaud, Jean-Philippe and Marc Mézard (2000). "Wealth Condensation in a Simple Model of Economy". In: *Physica A: Statistical Mechanics and its Applications* 282.3-4 (July 2000), pp. 536–545. DOI: 10.1016/S0378-4371(00)00205-3.

Bouchaud, Jean-Philippe and Marc Potters (2003). *Theory of Financial Risk and Derivative Pricing: From Statistical Physics to Risk Management*. 2nd ed. Cambridge: Cambridge University Press, Dec. 11, 2003. DOI: 10.1017/CBO9780511753893.

Bouchaud, Jean-Philippe, Nicolas Sagna, Rama Cont, Nicole El-Karoui, and Marc Potters (1999). "Phenomenology of the Interest Rate Curve". In: *Applied Mathematical Finance* 6.3 (Sept. 1999), pp. 209–232. DOI: 10.1080/135048699334546.

Bourahla, Samira, Émilie Fialon, Alexandre Garcia, and Aurélien Violon (2018). *Leverage Ratio and Client Clearing*. Banque de France.

Box, G. E. P. and G. S. Watson (1962). "Robustness to Non-Normality of Regression Tests". In: *Biometrika* 49.1-2, pp. 93–106. DOI: 10.1093/biomet/49.1-2.93.

Boyd, John P., William J. Fitzgerald, Matthew C. Mahutga, and David A. Smith (2010). "Computing Continuous Core/Periphery Structures for Social Relations Data with MINRES/SVD". In: *Social Networks* 32.2 (May 2010), pp. 125–137. DOI: 10.1016/j.socnet.2009.09.003.

Brachet, Marc-Etienne, Erik Taflin, and Jean Marcel Tcheou (2000). "Scaling Transformation and Probability Distributions for Financial Time Series". In: *Chaos, Solitons & Fractals* 11.14 (Nov. 2000), pp. 2343–2348. DOI: 10.1016/S0960-0779(99)00159-9. arXiv: cond-mat/9905169.

Brand, Claus, Marcin Bielecki, and Adrian Penalver (2018). "The Natural Rate of Interest: Estimates, Drivers, and Challenges to Monetary Policy". In: *SSRN Electronic Journal*. DOI: 10.2139/ssrn.3328536.

Brei, Michael, Claudio Borio, and Leonardo Gambacorta (2020). "Bank Intermediation Activity in a Low-interest-rate Environment". In: *Economic Notes* 49.2 (July 2020). DOI: 10.1111/ecno.12164.

Brennan, Michael J. and Eduardo S. Schwartz (1977). "Savings Bonds, Retractable Bonds and Callable Bonds". In: *Journal of Financial Economics* 5.1 (Aug. 1, 1977), pp. 67–88. DOI: 10.1016/0304-405X(77)90030-7.

Brigo, Damiano, Federico Graceffa, and Eyal Neuman (2022). "Price Impact on Term Structure". In: *Quantitative Finance* 22.1 (Jan. 2, 2022), pp. 171–195. DOI: 10.1080/14697688.2021.1983201.

Brigo, Damiano and Fabio Mercurio (2006). *Interest Rate Models, Theory and Practice: With Smile, Inflation and Credit*. 2nd ed. Springer Finance. Berlin: Springer.

Brooks, Jordan, Michael Katz, and Hanno Lustig (2018). "Post-FOMC Announcement Drift in U.S. Bond Markets". In: *NBER Working Papers*. NBER Working Papers 25127 (Oct. 2018).

Brown, Kevin S. and James P. Sethna (2003). "Statistical Mechanical Approaches to Models with Many Poorly Known Parameters". In: *Physical Review E* 68.2 (Aug. 12, 2003), p. 021904. DOI: 10.1103/PhysRevE.68.021904.

Brumm, Johannes, Michael Grill, Felix Kübler, and Karl Schmedders (2018). *Re-Use of Collateral: Leverage, Volatility, and Welfare*. LU: European Central Bank.

Brunnermeier, Markus K (2009). "Deciphering the Liquidity and Credit Crunch 2007–2008". In: *Journal of Economic Perspectives* 23.1 (Jan. 1, 2009), pp. 77–100. DOI: 10.1257/jep.23.1.77.

Bueno-Guerrero, Alberto, Manuel Moreno, and Javier F. Navas (2015). "Stochastic String Models with Continuous Semimartingales". In: *Physica A: Statistical Mechanics and its Applications* 433 (Sept. 2015), pp. 229–246. DOI: 10.1016/j.physa.2015.03.070.

— (2016). "The Stochastic String Model as a Unifying Theory of the Term Structure of Interest Rates". In: *Physica A: Statistical Mechanics and its Applications* 461 (Nov. 2016), pp. 217–237. DOI: 10.1016/j.physa.2016.05.044.

— (2020). "Valuation of Caps and Swaptions under a Stochastic String Model". In: *Physica A: Statistical Mechanics and its Applications* 559 (Dec. 2020), p. 125103. DOI: 10.1016/j.physa.2020.125103.

— (2022). "Bond Market Completeness under Stochastic Strings with Distribution-Valued Strategies". In: *Quantitative Finance* 22.2 (Feb. 1, 2022), pp. 197–211. DOI: 10.1080/14697688.2021.2018483.

Calvo, Guillermo A. (1983). "Staggered Prices in a Utility-Maximizing Framework". In: *Journal of Monetary Economics* 12.3 (Sept. 1, 1983), pp. 383–398. DOI: 10.1016/0304-3932(83)90060-0.

Campbell, John Y. and John H. Cochrane (1999). "By Force of Habit: A Consumption-Based Explanation of Aggregate Stock Market Behavior". In: *Journal of Political Economy* 107.2 (Apr. 1999), pp. 205–251. DOI: 10.1086/250059.

Cantero-Saiz, María, Sergio Sanfilippo-Azofra, Begoña Torre-Olmo, and Carlos López-Gutiérrez (2014). "Sovereign Risk and the Bank Lending Channel in Europe". In: *Journal of International Money and Finance* 47.C, pp. 1–20. DOI: 10.1016/j.jimonfin.2014.0.

Cantero-Saiz, María, Sergio Sanfilippo-Azofra, and Begoña Torre-Olmo (2021). "Sovereign Risk and the Bank Lending Channel: Differences across Countries and the Effects of the Financial Crisis". In: *Journal of Money, Credit and Banking*, jmcb.12794. DOI: 10.1111/jmcb.12794.

Carmona, René A. and Michael Tehranchi (2006). *Interest Rate Models: An Infinite Dimensional Stochastic Analysis Perspective*. Springer Finance. Berlin, Heidelberg: Springer Berlin Heidelberg. DOI: 10.1007/b138563.

Cass, David (1965). "Optimum Growth in an Aggregative Model of Capital Accumulation1". In: *The Review of Economic Studies* 32.3 (July 1, 1965), pp. 233–240. DOI: 10.2307/2295827.

Cerqueti, Roy, Claudio Lupi, Filomena Pietrovito, and Alberto Franco Pozzolo (2022). "Rank–Size Distributions for Banks: A Cross-Country Analysis". In: *Physica A: Statistical Mechanics and its Applications* 585 (Jan. 2022), p. 126336. DOI: 10.1016/j.physa.2021.126336.

Chaboud, Alain, Ellen Correia-Golay, Caren Cox, Michael J. Fleming, Yesol Huh, Frank M. Keane, Kyle Lee, Krista Schwarz, Clara Vega, and Carolyn Windover (2022). "All-to-All Trading in the U.S. Treasury Market". In: *SSRN Electronic Journal*. DOI: 10.2139/ssrn.4256637.

Chen, Ren-Raw and Louis Scott (2001). *Stochastic Volatility and Jumps in Interest Rates: An Empirical Analysis*. Rutgers University, p. 35.

Chen, Zhiwu, Werner Stanzl, and Masahiro Watanabe (2002). *Price Impact Costs and the Limit of Arbitrage*. Yale School of Management Working Papers ysm251. Yale School of Management.

Cheung, Belinda, Mark Manning, and Angus Moore (2014). *The Effective Supply of Collateral in Australia*. Reserve Bank of Australia.

Chordia, Tarun and Avanidhar Subrahmanyam (2004). "Order Imbalance and Individual Stock Returns: Theory and Evidence". In: *Journal of Financial Economics* 72.3 (June 2004), pp. 485–518. DOI: 10.1016/S0304-405X(03)00175-2.

Chordia, Tarun, Avanidhar Subrahmanyam, and V.Ravi Anshuman (2001). "Trading Activity and Expected Stock Returns". In: *Journal of Financial Economics* 59.1 (Jan. 2001), pp. 3–32. DOI: 10.1016/S0304-405X(00)00080-5.

Christensen, Jens H. E., Francis X. Diebold, and Glenn D. Rudebusch (2011). "The Affine Arbitrage-Free Class of Nelson–Siegel Term Structure Models". In: *Journal of Econometrics*. Annals Issue on Forecasting 164.1 (Sept. 1, 2011), pp. 4–20. DOI: 10.1016/j.jeconom.2011.02.011.

Cincotti, Silvano, Marco Raberto, and Andrea Teglio (2012). "The EURACE Macroeconomic Model and Simulator". In: *Complexity and institutions : markets, norms and corporations*. Complexity and Institutions : Markets, Norms and Corporations. - Basingstoke, Hampshire [u.a.] : Palgrave Macmillan, ISBN 1-137-03420-3. - 2012, p. 81-104.

Clarida, Richard, Jordi Galí, and Mark Gertler (2000). "Monetary Policy Rules and Macroeconomic Stability: Evidence and Some Theory". In: *The Quarterly Journal of Economics* 115.1, pp. 147–180.

Cleveland, William S. (1979). "Robust Locally Weighted Regression and Smoothing Scatterplots". In: *Journal of the American Statistical Association* 74.368 (Dec. 1979), pp. 829–836. DOI: 10.1080/01621459.1979.10481038.

Cochrane, John H (2017). "Macro-Finance*". In: *Review of Finance* 21.3 (May 1, 2017), pp. 945–985. DOI: 10.1093/rof/rfx010.

Cochrane, John H. and Monika Piazzesi (2002). "The Fed and Interest Rates - A High-Frequency Identification". In: *American Economic Review* 92.2 (May 2002), pp. 90–95. DOI: 10.1257/000282802320189069.

— (2009). *Decomposing the Yield Curve*. SSRN Scholarly Paper ID 1333274. Rochester, NY: Social Science Research Network, Jan. 26, 2009. DOI: 10.2139/ssrn.1333274.

Coibion, Olivier and Yuriy Gorodnichenko (2015). "Information Rigidity and the Expectations Formation Process: A Simple Framework and New Facts". In: *American Economic Review* 105.8 (Aug. 2015), pp. 2644–2678. DOI: 10.1257/aer.20110306.

Coimbra, Nuno and Hélène Rey (2024). "Financial Cycles with Heterogeneous Intermediaries". In: *The Review of Economic Studies* 91.2 (Mar. 1, 2024), pp. 817–857. DOI: 10.1093/restud/rdad039.

Cont, R. (2001). "Empirical Properties of Asset Returns: Stylized Facts and Statistical Issues". In: *Quantitative Finance* 1.2 (Feb. 2001), pp. 223–236. DOI: 10.1080/713665670.

Cont, Rama (2005a). "Modeling Term Structure Dynamics: An Infinite Dimensional Approach". In: *International Journal of Theoretical and Applied Finance* 08.03 (May 2005), pp. 357–380. DOI: 10.1142/S0219024905003049.

— (2005b). *Volatility Clustering in Financial Markets: Empirical Facts and Agent–Based Models*.

Cont, Rama, Mihai Cucuringu, and Chao Zhang (2023). "Cross-Impact of Order Flow Imbalance in Equity Markets". In: *Quantitative Finance* 23.10 (Oct. 3, 2023), pp. 1373–1393. DOI: 10.1080/14697688.2023.2236159.

Cordi, Marcus, Damien Challet, and Serge Kassibrakis (2021). "The Market Nanostructure Origin of Asset Price Time Reversal Asymmetry". In: *Quantitative Finance* 21.2 (Feb. 1, 2021), pp. 295–304. DOI: 10.1080/14697688.2020.1753883.

Cordoni, Francesco, Caterina Giannetti, Fabrizio Lillo, and Giulio Bottazzi (2023). "Simulation-Driven Experimental Hypotheses and Design: A Study of Price Impact and Bubbles". In: *SIMULATION* 99.6 (June 2023), pp. 599–620. DOI: 10.1177/00375497221138923.

Cox, John C., Jonathan E. Ingersoll, and Stephen A. Ross (1981). "A Re-Examination of Traditional Hypotheses about the Term Structure of Interest Rates". In: *The Journal of Finance* 36.4, pp. 769–799. DOI: 10.2307/2327547. JSTOR: 2327547.

— (1985a). "A Theory of the Term Structure of Interest Rates". In: *Econometrica* 53.2, pp. 385–407. DOI: 10.2307/1911242. JSTOR: 1911242.

— (1985b). "An Intertemporal General Equilibrium Model of Asset Prices". In: *Econometrica* 53.2, pp. 363–384. DOI: 10.2307/1911241. JSTOR: 1911241.

Craig, Ben and Goetz von Peter (2014). "Interbank Tiering and Money Center Banks". In: *Journal of Financial Intermediation* 23.3 (July 1, 2014), pp. 322–347. DOI: 10.1016/j.jfi.2014.02.003.

Cucuringu, Mihai, Puck Rombach, Sang Hoon Lee, and Mason A. Porter (2016). "Detection of Core–Periphery Structure in Networks Using Spectral Methods and Geodesic Paths". In: *European Journal of Applied Mathematics* 27.6 (Dec. 2016), pp. 846–887. DOI: 10.1017/S095679251600022X.

Cui, Xu (2011). "Hyperbolic Discounting Emerges from the Scalar Property of Interval Timing". In: *Frontiers in Integrative Neurosci* 5. DOI: 10.3389/fnint.2011.00024.

Culbertson, J. M. (1957). "The Term Structure of Interest Rates". In: *The Quarterly Journal of Economics* 71.4 (Aug. 1, 1957), pp. 485–517. DOI: 10.2307/1885708.

Cúrdia, Vasco, Andrea Ferrero, Ging Cee Ng, and Andrea Tambalotti (2015). "Has U.S. Monetary Policy Tracked the Efficient Interest Rate?" In: *Journal of Monetary Economics* 70.C, pp. 72–83.

D'Arienzo, Daniele (2020). *Maturity Increasing Overreaction and Bond Market Puzzles*. SSRN Scholarly Paper ID 3733056. Rochester, NY: Social Science Research Network, Nov. 18, 2020. DOI: 10.2139/ssrn.3733056.

Dai, Qiang and Kenneth J Singleton (2000). "Specification Analysis of Affine Term Structure Models". In: *The Journal of Finance*, p. 36.

Dandapani, Aditi, Paul Jusselin, and Mathieu Rosenbaum (2021). "From Quadratic Hawkes Processes to Super-Heston Rough Volatility Models with Zumbach Effect". In: *Quantitative Finance* 21.8 (Aug. 3, 2021), pp. 1235–1247. DOI: 10.1080/14697688.2020.1841906.

Das, Sanjiv R. (2002). "The Surprise Element: Jumps in Interest Rates". In: *Journal of Econometrics* 106.1 (Jan. 1, 2002), pp. 27–65. DOI: 10.1016/S0304-4076(01)00085-9.

Dasgupta, Partha and Eric Maskin (2005). "Uncertainty and Hyperbolic Discounting". In: *American Economic Review* 95.4 (Aug. 1, 2005), pp. 1290–1299. DOI: 10.1257/0002828054825637.

Dawid, Herbert and Simon Gemkow (2014). "How Do Social Networks Contribute to Wage Inequality? Insights from an Agent-Based Analysis". In: *Industrial and Corporate Change* 23.5 (Oct. 1, 2014), pp. 1171–1200. DOI: 10.1093/icc/dtt049.

Dawid, Herbert, Simon Gemkow, Philipp Harting, Sander van der Hoog, and Michael Neugart (2012). "The Eurace@Unibi Model: An Agent-Based Macroeconomic Model for Economic Policy Analysis". In: *SSRN Electronic Journal*. DOI: 10.2139/ssrn.2408969.

— (2018). *Agent-Based Macroeconomic Modeling and Policy Analyses: The Eurace@Unibi Model*. 110863. Darmstadt Technical University, Department of Business Administration, Economics and Law, Institute for Business Studies (BWL).

Dawid, Herbert, Philipp Harting, Sander van der Hoog, and Michael Neugart (2016). *A Heterogeneous Agent Macroeconomic Model for Policy Evaluation: Improving Transparency and Reproducibility*. SSRN Scholarly Paper ID 2773539. Rochester, NY: Social Science Research Network, Apr. 29, 2016. DOI: 10.2139/ssrn.2773539.

De Fiore, Fiorella, Marie Hoerova, and Harald Uhlig (2021). *Money Markets, Collateral and Monetary Policy*. SSRN Scholarly Paper. Rochester, NY, Dec. 14, 2021. DOI: 10.2139/ssrn.3288767.

De Jong, Frank and Pedro Santa-Clara (1999). "The Dynamics of the Forward Interest Rate Curve: A Formulation with State Variables". In: *The Journal of Financial and Quantitative Analysis* 34.1 (Mar. 1999), p. 131. DOI: 10.2307/2676249. JSTOR: 2676249.

Del Molino, Luis Carlos García, Iacopo Mastromatteo, Michael Benzaquen, and Jean-Philippe Bouchaud (2020). "The Multivariate Kyle Model: More Is Different". In: *SIAM Journal on Financial Mathematics* 11.2 (Jan. 2020), pp. 327–357. DOI: 10.1137/18M1231997.

Diamond, Peter A. (1965). "National Debt in a Neoclassical Growth Model". In: *The American Economic Review* 55 (5, 1965), pp. 1126–1150. JSTOR: 1809231.

Diebold, Francis X. and Canlin Li (2006). "Forecasting the Term Structure of Government Bond Yields". In: *Journal of Econometrics* 130.2 (Feb. 1, 2006), pp. 337–364. DOI: 10.1016/j.jeconom.2005.03.005.

Diebold, Francis X., Glenn D. Rudebusch, and S. Borag˘an Aruoba (2006). "The Macroeconomy and the Yield Curve: A Dynamic Latent Factor Approach". In: *Journal of Econometrics* 131.1 (Mar. 1, 2006), pp. 309–338. DOI: 10.1016/j.jeconom.2005.01.011.

Donier, J. and J. Bonart (2015). "A Million Metaorder Analysis of Market Impact on the Bitcoin". In: *Market Microstructure and Liquidity* 01.02 (Dec. 2015), p. 1550008. DOI: 10.1142/S2382626615500082.

Dosi, Giovanni, Giorgio Fagiolo, Mauro Napoletano, and Andrea Roventini (2013). "Income Distribution, Credit and Fiscal Policies in an Agent-Based Keynesian Model". In: *Journal of Economic Dynamics and Control* 37.8, pp. 1598–1625.

Dosi, Giovanni, Giorgio Fagiolo, Mauro Napoletano, Andrea Roventini, and Tania Treibich (2015). "Fiscal and Monetary Policies in Complex Evolving Economies". In: *Journal of Economic Dynamics and Control* 52.C, pp. 166–189.

Dosi, Giovanni, Giorgio Fagiolo, and Andrea Roventini (2010). "Schumpeter Meeting Keynes: A Policy-Friendly Model of Endogenous Growth and Business Cycles". In: *Journal of Economic Dynamics and Control*. Computational Perspectives in Economics and Finance: Methods,Dynamic Analysis and Policy Modeling 34.9 (Sept. 1, 2010), pp. 1748–1767. DOI: 10.1016/j.jedc.2010.06.018.

Dosi, Giovanni, Marcelo Pereira, Andrea Roventini, and Maria Enrica Virgillito (2017). "When More Flexibility Yields More Fragility: The Microfoundations of Keynesian Aggregate Unemployment". In: *Journal of Economic Dynamics and Control* 81.C, pp. 162–186.

Dubecq, Simon, Alain Monfort, Jean-Paul Renne, and Guillaume Roussellet (2016). "Credit and Liquidity in Interbank Rates: A Quadratic Approach". In: *Journal of Banking & Finance* 68 (July 1, 2016), pp. 29–46. DOI: 10.1016/j.jbankfin.2016.03.014.

Duffie, Darrell (2001). *Dynamic Asset Pricing Theory – Third edition*. 3e édition. Princeton, N.J: Princeton University Press, Oct. 29, 2001. 488 pp.

Duffie, Darrell and Kenneth J. Singleton (1997). "An Econometric Model of the Term Structure of Interest-Rate Swap Yields". In: *The Journal of Finance* 52.4, pp. 1287–1321. DOI: 10.2307/2329437. JSTOR: 2329437.

Ekeland, Ivar and Erik Taflin (2005). "A Theory of Bond Portfolios". In: *The Annals of Applied Probability* 15.2 (May 1, 2005), pp. 1260–1305. DOI: 10.1214/105051605000000160.

Ekren, Ibrahim and Johannes Muhle-Karbe (2019). "Portfolio Choice with Small Temporary and Transient Price Impact". In: *Mathematical Finance* 29.4 (Oct. 2019), pp. 1066–1115. DOI: 10.1111/mafi.12204.

Elomari-Kessab, Salma, Guillaume Maitrier, Julius Bonart, and Jean-Philippe Bouchaud (2024). *Disentangling the Joint Dynamics of Prices & Order Flow*. Version 1. DOI: 10.48550/ARXIV.2405.10654.

Epps, Thomas W. (1979). "Comovements in Stock Prices in the Very Short Run". In: *Journal of the American Statistical Association* 74 (366a June 1979), pp. 291–298. DOI: 10.1080/01621459.1979.10482508.

European Systemic Risk Board. (2017). *Collateral Scarcity Premia in Euro Area Repo Markets*. LU: Publications Office.

Evans, Martin D D and Richard K Lyons (2001). *Why Order Flow Explains Exchange Rates*. University of California.

— (2002). "Order Flow and Exchange Rate Dynamics". In: *Journal of Political Economy* 110.1 (Feb. 2002), pp. 170–180. DOI: 10.1086/324391.

Fabozzi, Frank J. and Steven V. Mann, eds. (2005). *The Handbook of Fixed Income Securities*. 7th ed. New York: McGraw-Hill. 1495 pp.

Fagiolo, Giorgio and Andrea Roventini (2016). *Macroeconomic Policy in DGSE and Agent-Based Models Redux*. Apr. 1, 2016.

Fama, Eugene F. and Robert R. Bliss (1987). "The Information in Long-Maturity Forward Rates". In: *The American Economic Review* 77.4, pp. 680–692. JSTOR: 1814539.

Farmer, J. Doyne and John Geanakoplos (2009). *Hyperbolic Discounting Is Rational: Valuing the Far Future with Uncertain Discount Rates*. Cowles Foundation Discussion Papers. Cowles Foundation for Research in Economics, Yale University.

Filipovic, Damir (2009). *Term-Structure Models*. Berlin, Heidelberg: Springer International Publishing. DOI: 10.1007/978-3-540-68015-4.

Filipović, Damir (2001). *Consistency Problems for Heath-Jarrow-Morton Interest Rate Models*. Vol. 1760. Lecture Notes in Mathematics. Berlin, Heidelberg: Springer Berlin Heidelberg. DOI: 10.1007/b76888.

Filippo, Mario di, Angelo Ranaldo, and Jan Wrampelmeyer (2018). *Unsecured and Secured Funding*. Tinbergen Institute Discussion Paper 18-038/IV. Tinbergen Institute, Apr. 14, 2018.

Fisher, Adlai J., Laurent E. Calvet, and Benoit B. Mandelbrot (1997). *Multifractality of Deutschemark / Us Dollar Exchange Rates*. SSRN Scholarly Paper. Rochester, NY, Sept. 15, 1997.

Fisher, Irving (1907). *The Rate of Interest*. History of Economic Thought Books. McMaster University Archive for the History of Economic Thought.

— (1930). *The Theory of Interest as Determined by Impatience to Spend Income and Opportunity to Invest It*. Mansfield Centre, Conn: Martino Fine Books. 610 pp.

Frane, Andrew V (2015). "Are Per-Family Type I Error Rates Relevant in Social and Behavioral Science?" In: *Journal of Modern Applied Statistical Methods* 14.1 (May 1, 2015), pp. 12–23. DOI: 10.22237/jmasm/1430453040.

Frederick, Shane, George Loewenstein, and Ted O'donoghue (2002). "Time Discounting and Time Preference: A Critical Review". In: *Journal of Economic Literature* 40.2 (June 2002), pp. 351–401. DOI: 10.1257/jel.40.2.351.

Friedman, Milton (1957). *Theory of the Consumption Function*. Princeton University Press.

— (1968). "The Role of Monetary Policy". In: *The American Economic Review*, p. 17.

Fuhrer, Jeffrey (1996). "Monetary Policy Shifts and Long-Term Interest Rates". In: *The Quarterly Journal of Economics* 111.4, pp. 1183–1209.

Fuhrer, Jeffrey and George Moore (1995). "Inflation Persistence". In: *The Quarterly Journal of Economics* 110.1, pp. 127–159.

Fuhrer, Lucas Marc, Basil Guggenheim, and Silvio Schumacher (2016). "Re-Use of Collateral in the Repo Market". In: *Journal of Money, Credit and Banking* 48.6 (Sept. 2016), pp. 1169–1193. DOI: 10.1111/jmcb.12330.

Furfine, Craig H. (1999). "The Microstructure of the Federal Funds Market". In: *Financial Markets, Institutions & Instruments* 8.5 (Dec. 1999), pp. 24–44. DOI: 10.1111/1468-0416.00031.

Gabaix, X. (1999). "Zipf's Law for Cities: An Explanation". In: *The Quarterly Journal of Economics* 114.3 (Aug. 1, 1999), pp. 739–767. DOI: 10.1162/003355399556133.

Gabaix, X., P. Gopikrishnan, V. Plerou, and H. E. Stanley (2006). "Institutional Investors and Stock Market Volatility". In: *The Quarterly Journal of Economics* 121.2 (May 1, 2006), pp. 461–504. DOI: 10.1162/qjec.2006.121.2.461.

Gagnon, Joseph E., Matthew Raskin, Julie Remache, and Brian P. Sack (2011). "Large-Scale Asset Purchases by the Federal Reserve: Did They Work?" In: *Economic Policy Review* 17 (May 2011), pp. 41–59.

Galí, Jordi and Mark Gertler (1999). "Inflation Dynamics: A Structural Econometric Analysis". In: *Journal of Monetary Economics* 44.2 (Oct. 1, 1999), pp. 195–222. DOI: 10.1016/S0304-3932(99)00023-9.

Gambacorta, Leonardo and S. Iannotti (2007). "Are There Asymmetries in the Response of Bank Interest Rates to Monetary Shocks?" In: *Applied Economics* 39.19, pp. 2503–2517.

Gârleanu, Nicolae and Lasse Heje Pedersen (2016). "Dynamic Portfolio Choice with Frictions". In: *Journal of Economic Theory* 165 (Sept. 2016), pp. 487–516. DOI: 10.1016/j.jet.2016.06.001.

Gatheral, Jim (2010). "No-Dynamic-Arbitrage and Market Impact". In: *Quantitative Finance* 10.7 (Aug. 2010), pp. 749–759. DOI: 10.1080/14697680903373692.

Gatheral, Jim, Thibault Jaisson, and Mathieu Rosenbaum (2018). "Volatility Is Rough". In: *Quantitative Finance* 18.6 (June 3, 2018), pp. 933–949. DOI: 10.1080/14697688.2017.1393551.

Gatheral, Jim and Alexander Schied (2013). "Dynamical Models of Market Impact and Algorithms for Order Execution". In: *Handbook on Systemic Risk*. Ed. by Jean-Pierre Fouque and Joseph A. Langsam. 1st ed. Cambridge University Press, May 23, 2013, pp. 579–602. DOI: 10.1017/CBO9781139151184.030.

Gertler, Mark, Nobuhiro Kiyotaki, and Andrea Prestipino (2020). "A Macroeconomic Model with Financial Panics". In: *The Review of Economic Studies* 87.1 (Jan. 1, 2020), pp. 240–288. DOI: 10.1093/restud/rdz032.

Giglio, Stefano and Bryan Kelly (2018). "Excess Volatility: Beyond Discount Rates*". In: *The Quarterly Journal of Economics* 133.1 (Feb. 1, 2018), pp. 71–127. DOI: 10.1093/qje/qjx034.

Goddard, John, Hong Liu, Donal Mckillop, and John O.S. Wilson (2014). "The Size Distribution of US Banks and Credit Unions". In: *International Journal of the Economics of Business* 21.1 (Jan. 2, 2014), pp. 139–156. DOI: 10.1080/13571516.2013.835970.

Goeman, Jelle J. and Aldo Solari (2014). "Multiple Hypothesis Testing in Genomics". In: *Statistics in Medicine* 33.11 (May 20, 2014), pp. 1946–1978. DOI: 10.1002/sim.6082.

Goldstein, Robert S. (2000). "The Term Structure of Interest Rates as a Random Field". In: *Review of Financial Studies* 13.2 (Apr. 2000), pp. 365–384. DOI: 10.1093/rfs/13.2.365.

Gomber, Peter, Uwe Schweickert, and Erik Theissen (2015). "Liquidity Dynamics in an Electronic Open Limit Order Book: An Event Study Approach: Liquidity Dynamics in an Electronic Open Limit Order Book". In: *European Financial Management* 21.1 (Jan. 2015), pp. 52–78. DOI: 10.1111/j.1468-036X.2013.12006.x.

Gopikrishnan, Parameswaran, Vasiliki Plerou, Luís A. Nunes Amaral, Martin Meyer, and H. Eugene Stanley (1999). "Scaling of the Distribution of Fluctuations of Financial Market Indices". In: *Physical Review E* 60.5 (Nov. 1, 1999), pp. 5305–5316. DOI: 10.1103/PhysRevE.60.5305.

Grbac, Zorana and Wolfgang J. Runggaldier (2015). *Interest Rate Modeling: Post-Crisis Challenges and Approaches*. SpringerBriefs in Quantitative Finance. Cham: Springer International Publishing. DOI: 10.1007/978-3-319-25385-5.

Green, Leonard, Astrid F Fry, and Joel Myerson (1994). "Discounting of Delayed Rewards: A Life-Span Comparison". In: *Psychological Science* 5.1 (Jan. 1994), pp. 33–36. DOI: 10.1111/j.1467-9280.1994.tb00610.x.

Green, Leonard and Joel Myerson (2004). "A Discounting Framework for Choice With Delayed and Probabilistic Rewards." In: *Psychological Bulletin* 130.5, pp. 769–792. DOI: 10.1037/0033-2909.130.5.769.

Greenwood, Robin and Dimitri Vayanos (2010). "Price Pressure in the Government Bond Market". In: *American Economic Review* 100.2 (May 2010), pp. 585–590. DOI: 10.1257/aer.100.2.585.

— (2014). "Bond Supply and Excess Bond Returns". In: *The Review of Financial Studies* 27.3 (Mar. 1, 2014), pp. 663–713. DOI: 10.1093/rfs/hht133.

Gurgone, Andrea, Giulia Iori, and Saqib Jafarey (2018). "The Effects of Interbank Networks on Efficiency and Stability in a Macroeconomic Agent-Based Model". In: *Journal of Economic Dynamics and Control*. Special Issue in Honour of Prof. Carl Chiarella 91 (June 1, 2018), pp. 257–288. DOI: 10.1016/j.jedc.2018.03.006.

Gürkaynak, Refet S., Brian Sack, and Eric Swanson (2005). "The Sensitivity of Long-Term Interest Rates to Economic News: Evidence and Implications for Macroeconomic Models". In: *American Economic Review* 95.1 (Mar. 2005), pp. 425–436. DOI: 10.1257/0002828053828446.

Gutenkunst, Ryan N, Joshua J Waterfall, Fergal P Casey, Kevin S Brown, Christopher R Myers, and James P Sethna (2007). "Universally Sloppy Parameter Sensitivities in Systems Biology Models". In: *PLoS Computational Biology* 3.10 (Oct. 5, 2007). Ed. by Adam P Arkin, e189. DOI: 10.1371/journal.pcbi.0030189.

Halaj, Grzegorz (2018). *Agent-Based Model of System-Wide Implications of Funding Risk*. SSRN Scholarly Paper ID 3100026. Rochester, NY: European Central Bank, Jan. 10, 2018. DOI: 10.2139/ssrn.3100026.

Hamilton, James D. and Jing Cynthia Wu (2012). "Identification and Estimation of Gaussian Affine Term Structure Models". In: *Journal of Econometrics* 168.2, pp. 315–331.

— (2014). "Testable Implications of Affine Term Structure Models". In: *Journal of Econometrics* 178 (Jan. 2014), pp. 231–242. DOI: 10.1016/j.jeconom.2013.08.024.

Hansen, Lars Peter and Ravi Jagannathan (1991). "Implications of Security Market Data for Models of Dynamic Economies". In: *Journal of Political Economy* 99.2 (Apr. 1991), pp. 225–262. DOI: 10.1086/261749.

Hanson, Samuel (2014). "Mortgage Convexity". In: *Journal of Financial Economics* 113.2, pp. 270–299.

Hanson, Samuel G, David O Lucca, and Jonathan H Wright (2021). "Rate-Amplifying Demand and the Excess Sensitivity of Long-Term Rates". In: *The Quarterly Journal of Economics* 136.3 (June 30, 2021), pp. 1719–1781. DOI: 10.1093/qje/qjab011.

Hanson, Samuel G. and Jeremy C. Stein (2015). "Monetary Policy and Long-Term Real Rates". In: *Journal of Financial Economics* 115.3 (Mar. 2015), pp. 429–448. DOI: 10.1016/j.jfineco.2014.11.001.

Harford, Jarrad and Aditya Kaul (2005). "Correlated Order Flow: Pervasiveness, Sources, and Pricing Effects". In: *Journal of Financial and Quantitative Analysis* 40.1 (Mar. 2005), pp. 29–55. DOI: 10.1017/S0022109000001733.

Hasbrouck, J and Duane J. Seppi (2001). "Common Factors in Prices, Order Flows, and Liquidity". In: *Journal of Financial Economics* 59.3 (Mar. 2001), pp. 383–411. DOI: 10.1016/S0304-405X(00)00091-X.

Hasbrouck, Joel (1991). "Measuring the Information Content of Stock Trades". In: *The Journal of Finance* 46.1 (Mar. 1991), pp. 179–207. DOI: 10.1111/j.1540-6261.1991.tb03749.x.

Hayashi, Fumio (1982). "Tobin's Marginal q and Average q: A Neoclassical Interpretation". In: *Econometrica* 50.1, pp. 213–24.

He, Zhiguo and Arvind Krishnamurthy (2013). "Intermediary Asset Pricing". In: *American Economic Review* 103.2 (Apr. 1, 2013), pp. 732–770. DOI: 10.1257/aer.103.2.732.

Heath, David, Robert Jarrow, and Andrew Morton (1992). "Bond Pricing and the Term Structure of Interest Rates: A New Methodology for Contingent Claims Valuation". In: *Econometrica* 60.1, pp. 77–105. DOI: 10.2307/2951677. JSTOR: 2951677.

Heider, Florian, Marie Hoerova, and Cornelia Holthausen (2015). "Liquidity Hoarding and Interbank Market Rates: The Role of Counterparty Risk". In: *Journal of Financial Economics* 118.2 (Nov. 2015), pp. 336–354. DOI: 10.1016/j.jfineco.2015.07.002.

Heston, Steven L. (1993). "A Closed-Form Solution for Options with Stochastic Volatility with Applications to Bond and Currency Options". In: *Review of Financial Studies* 6.2 (Apr. 1993), pp. 327–343. DOI: 10.1093/rfs/6.2.327.

Hicks, J. R. (1937). "Mr. Keynes and the "Classics"; A Suggested Interpretation". In: *Econometrica* 5.2 (Apr. 1937), p. 147. DOI: 10.2307/1907242. JSTOR: 1907242.

Hicks, John (1946). *Value and Capital: An Inquiry into Some Fundamental Principles of Economic Theory*. 2. ed., reprint. Clarendon Paperbacks. Oxford: Clarendon Press. 340 pp.

Ho, Thomas S. Y. and Sang-bin Lee (1986). "Term Structure Movements and Pricing Interest Rate Contingent Claims". In: *Journal of Finance* 41.5, pp. 1011–29.

Holston, Kathryn, Thomas Laubach, and John C. Williams (2017). "Measuring the Natural Rate of Interest: International Trends and Determinants". In: *Journal of International Economics*. 39th Annual NBER International Seminar on Macroeconomics 108 (May 1, 2017), S59–S75. DOI: 10.1016/j.jinteco.2017.01.004.

Hopman, Carl (2007). "Do Supply and Demand Drive Stock Prices?" In: *Quantitative Finance* 7.1 (Feb. 2007), pp. 37–53. DOI: 10.1080/14697680600987216.

Horen, Neeltje van and Antonis Kotidis (2018). "Repo Market Functioning: The Role of Capital Regulation". In: *SSRN Electronic Journal*. DOI: 10.2139/ssrn.3225818.

Hu, Grace Xing, Jun Pan, and Jiang Wang (2013). "Noise as Information for Illiquidity". In: *The Journal of Finance* 68.6, pp. 2341–2382. DOI: 10.1111/jofi.12083.

Hudepohl, Tom, Pamina Karl, Tobias Linzert, Benoit Nguyen, Marta Skrzypińska, and Lia Vaz Cruz (2024). *How Banks Deal with Declining Excess Liquidity*. European Central Bank.

Hughston, Lane, ed. (1996). *Vasicek and beyond: Approaches to Building and Applying Interest Rate Models*. London: Risk Books. 371 pp.

Hull, John (2018). *Options, Futures, and Other Derivatives*. Tenth Edition. Chennai: Pearson. 903 pp.

Hull, John C and Alan D White (1994). "Numerical Procedures for Implementing Term Structure Models II: Two-Factor Models". In: *The Journal of Derivatives* 2.2 (Nov. 30, 1994), pp. 37–48. DOI: 10.3905/jod.1994.407908.

ISDA (2023). *Key Trends in the Size and Composition of OTC Derivatives Markets*. ISDA.

Jakab, Zoltan and Michael Kumhof (2015). *Banks Are Not Intermediaries of Loanable Funds – And Why This Matters*. SSRN Scholarly Paper ID 2612050. Rochester, NY: Bank of England, May 29, 2015. DOI: 10.2139/ssrn.2612050.

— (2018). *Banks Are Not Intermediaries of Loanable Funds — Facts, Theory and Evidence*. SSRN Scholarly Paper ID 3274706. Rochester, NY: Bank of England, Oct. 26, 2018. DOI: 10.2139/ssrn.3274706.

Janicki, Hubert P. and Edward S. Prescott (2006). "Changes in the Size Distribution of U. S. Banks: 1960 - 2005". In: *Economic Quarterly*.

Jank, Stephan, Emanuel Moench, and Michael Schneider (2021). *Safe Asset Shortage and Collateral Reuse*. Centre for Economic Policy Research.

Jiang, George and Shu Yan (2009). "Linear-Quadratic Term Structure Models – Toward the Understanding of Jumps in Interest Rates". In: *Journal of Banking & Finance* 33.3 (Mar. 1, 2009), pp. 473–485. DOI: 10.1016/j.jbankfin.2008.08.018.

Jiménez, Gabriel, Steven Ongena, José-Luis Peydró, and Jesús Saurina (2014). "Hazardous Times for Monetary Policy: What Do Twenty-Three Million Bank Loans Say About the Effects of Monetary Policy on Credit Risk-Taking?" In: *Econometrica* 82.2, pp. 463–505. DOI: 10.3982/ECTA10104.

Johannes, Michael (2004). "The Statistical and Economic Role of Jumps in Continuous-Time Interest Rate Models". In: *The Journal of Finance* 59.1, pp. 227–260. DOI: 10.1111/j.1540-6321.2004.00632.x.

Kampen, N. G. van (2007). *Stochastic Processes in Physics and Chemistry*. 3rd ed. North-Holland Personal Library. Amsterdam, The Netherlands Oxford, UK: Elsevier.

Kashyap, Anil K and Jeremy C Stein (1994). *The Impact of Monetary Policy on Bank Balance Sheets*. Working Paper 4821. National Bureau of Economic Research, Aug. 1994. DOI: 10.3386/w4821.

Keller, Joachim, Antoine Bouveret, Cristina Picillo, Zijun Liu, Julien Mazzacurati, Philippe A.M. Molitor, Jonas Söderberg, John Theal, Francesco De Rossi, and Romain Calleja (2014). "Securities Financing Transactions and the (Re)Use of Collateral in Europe – an Analysis of the First Data Collection Conducted by the Esrb from a Sample of European Banks and Agent Lenders". In: *SSRN Electronic Journal*. DOI: 10.2139/ssrn.3723337.

Kempf, Alexander and Olaf Korn (1999). "Market Depth and Order Size". In: *Journal of Financial Markets* 2.1 (Feb. 1999), pp. 29–48. DOI: 10.1016/S1386-4181(98)00007-X.

Kennedy, D. P. (1994). "The Term Structure Of Interest Rates As A Gaussian Random Field". In: *Mathematical Finance* 4.3 (July 1994), pp. 247–258. DOI: 10.1111/j.1467-9965.1994.tb00094.x.

— (1997). "Characterizing Gaussian Models of the Term Structure of Interest Rates". In: *Mathematical Finance* 7.2 (Apr. 1997), pp. 107–118. DOI: 10.1111/1467-9965.00026.

Keynes, John Maynard (1930). *A Treatise on Money: The Pure Theory of Money and The Applied Theory of Money. Complete Set.* Martino Fine Books. 816 pp.

— (1936). *The General Theory of Employment, Interest, and Money.* Harcourt Brace.

Kim, B. Kyu and Gal Zauberman (2009). "Perception of Anticipatory Time in Temporal Discounting." In: *Journal of Neuroscience, Psychology, and Economics* 2.2 (Nov. 2009), pp. 91–101. DOI: 10.1037/a0017686.

Kim, Don H. and Athanasios Orphanides (2012). "Term Structure Estimation with Survey Data on Interest Rate Forecasts". In: *Journal of Financial and Quantitative Analysis* 47.1 (Feb. 2012), pp. 241–272. DOI: 10.1017/S0022109011000627.

Kim, Don H. and Jonathan H. Wright (2005). "An Arbitrage-Free Three-Factor Term Structure Model and the Recent Behavior of Long-Term Yields and Distant-Horizon Forward Rates". In: *Finance and Economics Discussion Series of the Federal Reserve* 40, pp. 1–55. DOI: 10.17016/FEDS.2016.040.

Kishan, Ruby P and Timothy Opiela (2000). "Bank Size, Bank Capital, and the Bank Lending Channel". In: *Journal of Money, Credit and Banking* 32.1, pp. 121–41.

Kissell, Robert and Roberto Malamut (2005). "Algorithmic Decision-Making Framework". In: *The Journal of Trading* 1.1 (Dec. 31, 2005), pp. 12–21. DOI: 10.3905/jot.2006.609171.

Knicker, Max Sina, Karl Naumann-Woleske, Jean-Philippe Bouchaud, and Francesco Zamponi (2024). "Post-COVID Inflation and the Monetary Policy Dilemma: An Agent-Based Scenario Analysis". In: *Journal of Economic Interaction and Coordination* (June 24, 2024). DOI: 10.1007/s11403-024-00413-3.

Kojaku, Sadamori and Naoki Masuda (2018a). "A Generalised Significance Test for Individual Communities in Networks". In: *Scientific Reports* 8.1 (May 9, 2018), p. 7351. DOI: 10.1038/s41598-018-25560-z.

— (2018b). "Core-Periphery Structure Requires Something Else in the Network". In: *New Journal of Physics* 20.4 (Apr. 12, 2018), p. 043012. DOI: 10.1088/1367-2630/aab547.

Koopmans, Tjalling C. (1963). "On the Concept of Optimal Economic Growth". In: *Cowles Foundation Discussion Papers*. Cowles Foundation Discussion Papers 163.

Krämer, W. (1989). "On the Robustness of the F-test to Autocorrelation among Disturbances". In: *Economics Letters* 30.1 (Jan. 1989), pp. 37–40. DOI: 10.1016/0165-1765(89)90153-5.

Krishnamurthy, Arvind and Annette Vissing-Jorgensen (2011). "The Effects of Quantitative Easing on Interest Rates: Channels and Implications for Policy". In: *Brookings Papers on Economic Activity* 42 (2 (Fall) 2011), pp. 215–287.

— (2012). "The Aggregate Demand for Treasury Debt". In: *Journal of Political Economy* 120.2, pp. 233–267. DOI: 10.1086/666526. JSTOR: 10.1086/666526.

Kyle, Albert S and Anna A Obizhaeva (2023). "Large Bets and Stock Market Crashes". In: *Review of Finance* (Mar. 28, 2023), rfad008. DOI: 10.1093/rof/rfad008.

Kyle, Albert S. (1985). "Continuous Auctions and Insider Trading". In: *Econometrica* 53.6, pp. 1315–1335. DOI: 10.2307/1913210. JSTOR: 1913210.

Laubach, Thomas and John C Williams (2016). "Measuring the Natural Rate of Interest Redux". In: *Business Economics* 51.2 (Apr. 1, 2016), pp. 57–67. DOI: 10.1057/be.2016.23.

— (2003). "Measuring the Natural Rate of Interest". In: *The Review of Economics and Statistics* 85.4, pp. 1063–1070. JSTOR: 3211826.

Le Coz, Victor, Nolwenn Allaire, Michael Benzaquen, and Damien Challet (2024a). *Stylized Facts in Money Markets: An Empirical Analysis of the Eurozone Data*. Version 1. DOI: 10.48550/ARXIV.2410.16021.

Le Coz, Victor, Michael Benzaquen, and Damien Challet (2024b). *A Minimal Model of Money Creation under Regulatory Constraints*. Version 1. DOI: 10.48550/ARXIV.2410.18145.

Le Coz, Victor and Jean-Philippe Bouchaud (2024). "Revisiting Elastic String Models of Forward Interest Rates". In: *Quantitative Finance* (Sept. 25, 2024), pp. 1–18. DOI: 10.1080/14697688.2024.2401450.

Le Coz, Victor, Iacopo Mastromatteo, and Michael Benzaquen (2024c). *How Does Liquidity Shape the Yield Curve?* Version 2. DOI: 10.48550/ARXIV.2409.12282.

Le Coz, Victor, Iacopo Mastromatteo, Damien Challet, and Michael Benzaquen (2024d). "When Is Cross Impact Relevant?" In: *Quantitative Finance* 24.2 (Feb. 2024), pp. 265–279. DOI: 10.1080/14697688.2024.2302827.

Li, Canlin and Min Wei (2013). "Term Structure Modeling with Supply Factors and the Federal Reserve's Large-Scale Asset Purchase Progarms". In: *International Journal of Central Banking* 9.1, pp. 3–39.

Lillo, Fabrizio and J. Doyne Farmer (2004). "The Long Memory of the Efficient Market". In: *Studies in Nonlinear Dynamics & Econometrics* 8.3 (Jan. 16, 2004). DOI: 10.2202/1558-3708.1226.

Lillo, Fabrizio, J. Doyne Farmer, and Rosario N. Mantegna (2003). "Master Curve for Price-Impact Function". In: *Nature* 421.6919 (Jan. 2003), pp. 129–130. DOI: 10.1038/421129a.

Lip, Sean Z. W. (2011). *A Fast Algorithm for the Discrete Core/Periphery Bipartitioning Problem*. Version 1. DOI: 10.48550/ARXIV.1102.5511.

Liu, Anqi, Mark Paddrik, Steve Y. Yang, and Xingjia Zhang (2020). "Interbank Contagion: An Agent-Based Model Approach to Endogenously Formed Networks". In: *Journal of Banking & Finance*. Challenges to Global Financial Stability: Interconnections,Credit Risk, Business Cycle and the Role of Market Participants 112 (Mar. 1, 2020), p. 105191. DOI: 10.1016/j.jbankfin.2017.08.008.

Loeb, Thomas F. (1983). "Trading Cost: The Critical Link Between Investment Information and Results". In: *Financial Analysts Journal* 39.3 (May 1983), pp. 39–44. DOI: 10.2469/faj.v39.n3.39.

Long, J. Scott and Laurie H. Ervin (2000). "Using Heteroscedasticity Consistent Standard Errors in the Linear Regression Model". In: *The American Statistician* 54.3 (Aug. 2000), p. 217. DOI: 10.2307/2685594. JSTOR: 2685594.

Longstaff, Francis A. and Eduardo S. Schwartz (1992). "Interest Rate Volatility and the Term Structure: A Two-Factor General Equilibrium Model". In: *The Journal of Finance* 47.4, pp. 1259–1282. DOI: 10.1111/j.1540-6261.1992.tb04657.x.

Luca Baldo, Benoît Hallinger, Caspar Helmus, Niko Herrala, and Débora Martins (2017). *The Distribution of Excess Liquidity in the Euro Area*. LU: Publications Office.

Lucas, Robert E (1973). "Some International Evidence on Output-InflatiTornadeofs". In: *The American Economic Review* 63.3, p. 9.

Lutz, F. A. (1940). "The Structure of Interest Rates". In: *The Quarterly Journal of Economics* 55.1 (Nov. 1, 1940), pp. 36–63. DOI: 10.2307/1881665.

Lux, Thomas (2015). "Emergence of a Core-Periphery Structure in a Simple Dynamic Model of the Interbank Market". In: *Journal of Economic Dynamics and Control* 52 (Mar. 2015), A11–A23. DOI: 10.1016/j.jedc.2014.09.038.

Lynch, Paul E and Gilles O Zumbach (2003). "Market Heterogeneities and the Causal Structure of Volatility". In: *Quantitative Finance* 3.4 (Aug. 2003), pp. 320–331. DOI: 10.1088/1469-7688/3/4/308.

MacKinnon, James G and Halbert White (1985). "Some Heteroskedasticity-Consistent Covariance Matrix Estimators with Improved Finite Sample Properties". In: *Journal of Econometrics* 29.3 (Sept. 1985), pp. 305–325. DOI: 10.1016/0304-4076(85)90158-7.

Maddaloni, Angela and Jose-Luis Peydro (2011). "Bank Risk-taking, Securitization, Supervision, and Low Interest Rates: Evidence from the Euro-area and the U.S. Lending Standards". In: *The Review of Financial Studies* 24.6, pp. 2121–2165.

Mandelbrot, Benoit B., Adlai J. Fisher, and Laurent E. Calvet (1997). *A Multifractal Model of Asset Returns*. SSRN Scholarly Paper. Rochester, NY, Sept. 15, 1997.

Mankiw, N. Gregory and Lawrence H. Summers (1984). *Do Long-Term Interest Rates Overreact to Short-Term Interest Rates?* Working Paper 1345. National Bureau of Economic Research, May 1984. DOI: 10.3386/w1345.

Mantegna, Rosario N. and H. Eugene Stanley (1999). *Introduction to Econophysics: Correlations and Complexity in Finance*. Cambridge: Cambridge University Press. DOI: 10.1017/CBO9780511755767.

Marsili, Matteo, Sergei Maslov, and Yi-Cheng Zhang (1998). "Dynamical Optimization Theory of a Diversified Portfolio". In: *Physica A: Statistical Mechanics and its Applications* 253.1-4 (May 1998), pp. 403–418. DOI: 10.1016/S0378-4371(98)00075-2.

Mastromatteo, Iacopo, Bence Toth, and Jean-Philippe Bouchaud (2014). "Agent-Based Models for Latent Liquidity and Concave Price Impact". In: *Physical Review E* 89.4 (Apr. 14, 2014), p. 042805. DOI: 10.1103/PhysRevE.89.042805.

Matacz, Andrew and Jean-Philippe Bouchaud (2000a). "An Empirical Investigation Of The Forward Interest Rate Term Structure". In: *International Journal of Theoretical and Applied Finance* 03.04 (Oct. 2000), pp. 703–729. DOI: 10.1142/S0219024900000838.

— (2000b). "Explaining The Forward Interest Rate Term Structure". In: *International Journal of Theoretical and Applied Finance* 03.03 (July 2000), pp. 381–389. DOI: 10.1142/S0219024900000243.

Mehra, Rajnish and Edward C. Prescott (1985). "The Equity Premium: A Puzzle". In: *Journal of Monetary Economics* 15.2 (Mar. 1985), pp. 145–161. DOI: 10.1016/0304-3932(85)90061-3.

Mésonnier, Jean-Stéphane and Jean-Paul Renne (2007). "A Time-Varying "Natural" Rate of Interest for the Euro Area". In: *European Economic Review* 51.7 (Oct. 1, 2007), pp. 1768–1784. DOI: 10.1016/j.euroecorev.2006.11.006.

*MFI Regulation (EU) 2021/379* (2016). DOI: 10.5040/9781782258674.

Mishkin, Frederic S. (2013). *The Economics of Money, Banking and Financial Markets*. 10th ed. The Pearson Series in Economics. Boston: Pearson. 622 pp.

Mitzenmacher, Michael (2004). "A Brief History of Generative Models for Power Law and Lognormal Distributions". In: *Internet Mathematics* 1.2 (Jan. 2004), pp. 226–251. DOI: 10.1080/15427951.2004.10129088.

Mixon, Scott and Tugkan Tuzun (2018). *Price Pressure and Price Discovery in the Term Structure of Interest Rates*. 2018-065. Board of Governors of the Federal Reserve System (U.S.), Sept. 28, 2018.

*MMSR Regulation (EU) 1333/2014* (2014).

*MMSR Reporting Instructions* (2021).

Modigliani, Franco and Richard Brumberg (1955). "Utility Analysis and the Consumption Function: An Interpretation of Cross-Section Data". In: *Post-Keynesian economics*. Post-Keynesian Economics. - London : Allen and Unwin. - 1955, p. 388-436.

— (1980). "Utility Analysis and Aggregate Consumption Functions : An Attempt at Integration". In: *The life cycle hypothesis of saving*. The Life Cycle Hypothesis of Saving ; 2. - Cambridge, Mass. [u.a.] : MIT Press, ISBN 0-262-13151-X. - 1980, p. 128-197 2.

Modigliani, Franco and Richard Sutch (1966). "Innovations in Interest Rate Policy". In: *The American Economic Review* 56.1/2, pp. 178–197. JSTOR: 1821281.

Moraleda, Juan M. and Ton C.F. Vorst (1997). "Pricing American Interest Rate Claims with Humped Volatility Models". In: *Journal of Banking & Finance* 21.8 (Aug. 1997), pp. 1131–1157. DOI: 10.1016/S0378-4266(97)00019-8.

Morel, Rudy, Stéphane Mallat, and Jean-Philippe Bouchaud (2023). *Path Shadowing Monte-Carlo*. Aug. 2, 2023. arXiv: 2308.01486 [q-fin].

Moro, Esteban, Javier Vicente, Luis G. Moyano, Austin Gerig, J. Doyne Farmer, Gabriella Vaglica, Fabrizio Lillo, and Rosario N. Mantegna (2009). "Market Impact and Trading Profile of Large Trading Orders in Stock Markets". In: *Physical Review E* 80.6 (Dec. 1, 2009), p. 066102. DOI: 10.1103/PhysRevE.80.066102.

Muzy, J. F., J. Delour, and E. Bacry (2000). "Modelling Fluctuations of Financial Time Series: From Cascade Process to Stochastic Volatility Model". In: *The European Physical Journal B* 17.3 (Oct. 2000), pp. 537–548. DOI: 10.1007/s100510070131. arXiv: cond-mat/0005400.

*National Accounts Regulation (EU) 549/2013* (2013).

Neiss, Katharine and Edward Nelson (2001). *The Real Interest Rate Gap as an Inflation Indicator*. CEPR Discussion Paper 2848. C.E.P.R. Discussion Papers, June 2001.

Nelson, Charles and Andrew F. Siegel (1987). "Parsimonious Modeling of Yield Curves". In: *The Journal of Business* 60.4, pp. 473–89.

Osborne, M. F. M. (1959). "Brownian Motion in the Stock Market". In: *Operations Research* 7.2, pp. 145–173.

Pasquariello, Paolo and Clara Vega (2007). "Informed and Strategic Order Flow in the Bond Markets". In: *Review of Financial Studies* 20.6 (Nov. 2007), pp. 1975–2019. DOI: 10.1093/rfs/hhm034.

Pasquariello, Paolo and Clara Vega (2015). "Strategic Cross-Trading in the U.S. Stock Market*". In: *Review of Finance* 19.1 (Mar. 2015), pp. 229–282. DOI: 10.1093/rof/rft055.

Patzelt, Felix and Jean-Philippe Bouchaud (2017). "Nonlinear Price Impact from Linear Models". In: *Journal of Statistical Mechanics: Theory and Experiment* 2017.12 (Dec. 21, 2017), p. 123404. DOI: 10.1088/1742-5468/aa9335.

— (2018). "Universal Scaling and Nonlinearity of Aggregate Price Impact in Financial Markets". In: *Physical Review E* 97.1 (Jan. 9, 2018), p. 012304. DOI: 10.1103/PhysRevE.97.012304.

Pelizzon, Loriana, Marti G Subrahmanyam, Davide Tomio, and Jun Uno (2014). *Limits to Arbitrage in Sovereign Bonds*. Syrto working paper series, p. 44.

Pescatori, Andrea, APescatori@imf.org, Juan Sole, and JSole@imf.org (2016). "Credit, Securitization and Monetary Policy: Watch Out for Unintended Consequences". In: *IMF Working Papers* 16.76, p. 1. DOI: 10.5089/9781475522723.001.

Phillips, A. W. (1958). "The Relation Between Unemployment and the Rate of Change of Money Wage Rates in the United Kingdom, 1861–1957". In: *Economica* 25.100, pp. 283–299.

Piazzesi, Monika (2005). "Bond Yields and the Federal Reserve". In: *Journal of Political Economy* 113.2 (Apr. 2005), pp. 311–344. DOI: 10.1086/427466.

— (2010). "Chapter12 - Affine Term Structure Models". In: *Handbook of Financial Econometrics: Tools and Techniques*. Ed. by Yacine Aït-sahalia and Lars Peter Hansen. Vol. 1. Handbooks in Finance. San Diego: North-Holland, Jan. 1, 2010, pp. 691–766. DOI: 10.1016/B978-0-444-50897-3.50015-8.

Piquard, Thibaut and Dilyara Salakhova (2019). "Secured and Unsecured Interbank Markets: Monetary Policy, Substitution and the Cost of Collateral". In: *SSRN Electronic Journal*. DOI: 10.2139/ssrn.3461534.

Plerou, Vasiliki, Parameswaran Gopikrishnan, Xavier Gabaix, and H. Eugene Stanley (2002). "Quantifying Stock-Price Response to Demand Fluctuations". In: *Physical Review E* 66.2 (Aug. 26, 2002), p. 027104. DOI: 10.1103/PhysRevE.66.027104.

Plerou, Vasiliki, Parameswaran Gopikrishnan, Luís A. Nunes Amaral, Martin Meyer, and H. Eugene Stanley (1999). "Scaling of the Distribution of Price Fluctuations of Individual Companies". In: *Physical Review E* 60.6 (Dec. 1, 1999), pp. 6519–6529. DOI: 10.1103/PhysRevE.60.6519.

Plerou, Vasiliki, Parameswaran Gopikrishnan, Bernd Rosenow, Luis A.N. Amaral, and H.Eugene Stanley (2000). "Econophysics: Financial Time Series from a Statistical Physics Point of View". In: *Physica A: Statistical Mechanics and its Applications* 279.1-4 (May 2000), pp. 443–456. DOI: 10.1016/S0378-4371(00)00010-8.

Plerou, Vasiliki, H Eugene Stanley, Xavier Gabaix, and Parameswaran Gopikrishnan (2004). "On the Origin of Power-Law Fluctuations in Stock Prices". In: *Quantitative Finance* 4.1 (Feb. 2004), pp. 11–15. DOI: 10.1088/1469-7688/4/1/C02.

Poole, William (1968). "Commercial Bank Reserve Management in a Stochastic Model: Implications for Monetary Policy". In: *The Journal of Finance* 23.5 (Dec. 1968), pp. 769–791. DOI: 10.1111/j.1540-6261.1968.tb00316.x.

Poterba, James and Lawrence Summers (1988). "Mean Reversion in Stock Prices: Evidence and Implications". In: *Journal of Financial Economics* 22.1, pp. 27–59.

Potters, Marc and Jean-Philippe Bouchaud (2003). "More Statistical Properties of Order Books and Price Impact". In: *Physica A: Statistical Mechanics and its Applications* 324.1-2 (June 2003), pp. 133–140. DOI: 10.1016/S0378-4371(02)01896-4.

Ramsey, F. P. (1928). "A Mathematical Theory of Saving". In: *The Economic Journal* 38.152, pp. 543–559. DOI: 10.2307/2224098. JSTOR: 2224098.

Ray, Debajyoti and Peter Bossaerts (2011). "Positive Temporal Dependence of the Biological Clock Implies Hyperbolic Discounting". In: *Frontiers in Neuroscience* 5. DOI: 10.3389/fnins.2011.00002.

Reale, Jessica (2019). *Interbank Market and Funding Liquidity Risk in a Stock-Flow Consistent Model*. Böckler Foundation, p. 56.

Reis, Ricardo and Silvana Tenreyro (2022). "Helicopter Money: What Is It and What Does It Do?" In: *Annual Review of Economics* 14 (Volume 14, 2022 Aug. 12, 2022), pp. 313–335. DOI: 10.1146/annurev-economics-051420-020618.

Reissl, Severin (2018). "Monetary Policy and Prudential Regulation in a Hybrid AB-SFC Model with Heterogeneous Expectations". In: *SSRN Electronic Journal*. DOI: 10.2139/ssrn.3297506.

Renne, Jean-Paul (2012). *A Model of the Euro-Area Yield Curve with Discrete Policy Rates*. Working paper. Banque de France.

— (2017). "A Model of the Euro-Area Yield Curve with Discrete Policy Rates". In: *Studies in Nonlinear Dynamics & Econometrics* 21.1 (Feb. 1, 2017), pp. 99–116. DOI: 10.1515/snde-2016-0043.

Renò, Roberto (2003). "A Closer Look At The Epps Effect". In: *International Journal of Theoretical and Applied Finance* 06.01 (Feb. 2003), pp. 87–102. DOI: 10.1142/S0219024903001839.

Riefler, Winfield W. (1930). *Money Rates and Money Markets in the United States*. [1. ed.] New York [u.a.] : Harper.

Roberts, John (1997). "Is Inflation Sticky?" In: *Journal of Monetary Economics* 39.2, pp. 173–196.

Roberts, John (1998). *Inflation Expectations and the Transmission of Monetary Policy*. Finance and Economics Discussion Series 1998-43. Board of Governors of the Federal Reserve System (U.S.)

Rombach, Puck, Mason A. Porter, James H. Fowler, and Peter J. Mucha (2017). "Core-Periphery Structure in Networks (Revisited)". In: *SIAM Review* 59.3 (Jan. 2017), pp. 619–646. DOI: 10.1137/17M1130046.

Rosenbaum, Mathieu and Mehdi Tomas (2022). "A Characterisation of Cross-Impact Kernels". In: *Frontiers of Mathematical Finance* 1.4, pp. 491–523. DOI: 10.3934/fmf.2022005.

Rossa, Fabio Della, Fabio Dercole, and Carlo Piccardi (2013). "Profiling Core-Periphery Network Structure by Random Walkers". In: *Scientific Reports* 3.1 (Mar. 19, 2013), p. 1467. DOI: 10.1038/srep01467.

Rotemberg, Julio J. (1982). "Sticky Prices in the United States". In: *Journal of Political Economy* 90.6, pp. 1187–1211. JSTOR: 1830944.

Rudebusch, Glenn D. (1995). "Federal Reserve Interest Rate Targeting, Rational Expectations, and the Term Structure". In: *Journal of Monetary Economics* 35.2 (Apr. 1, 1995), pp. 245–274. DOI: 10.1016/0304-3932(95)01190-Y.

— (2001). "Is the Fed Too Timid? Monetary Policy in an Uncertain World". In: *The Review of Economics and Statistics* 83.2, pp. 203–217. JSTOR: 3211600.

Samuelson, Paul (1958). "An Exact Consumption-Loan Model of Interest with or without the Social Contrivance of Money". In: *Journal of Political Economy* 66.6.

Santa-Clara, Pedro and Didier Sornette (2001). "The Dynamics of the Forward Interest Rate Curve with Stochastic String Shocks". In: *Review of Financial Studies* 14.1 (Jan. 2001), pp. 149–185. DOI: 10.1093/rfs/14.1.149.

Sargent, Thomas (1972). "Rational Expectations and the Term Structure of Interest Rates". In: *Journal of Money, Credit and Banking* 4.1, pp. 74–97.

— (1979). "A Note on Maximum Likelihood Estimation of the Rational Expectations Model of the Term Structure". In: *Journal of Monetary Economics* 5.1, pp. 133–143.

Scaggs, Alexandra (2018). "Financial Times Article". In: *Financial times*.

Schasfoort, Joeri, Antoine Godin, Dirk Bezemer, Alessandro Caiani, and Stephen Kinsella (2017). "Monetary Policy Transmission in a Macroeconomic Agent-Based Model". In: *Advances in Complex Systems* 20.08 (Dec. 2017), p. 1850003. DOI: 10.1142/S0219525918500030.

Schmitt, François, Daniel Schertzer, and Shaun Lovejoy (1999). "Multifractal Analysis of Foreign Exchange Data". In: *Applied Stochastic Models and Data Analysis* 15.1, pp. 29–53.

Schneider, M. and F. Lillo (2019). "Cross-Impact and No-Dynamic-Arbitrage". In: *Quantitative Finance* 19.1, pp. 137–154.

Schneider, Michael (2019). "Market Microstructure, Price Impact and Liquidity in Fixed Income Markets". Scuola Normale Superiore Pisa.

Sen, Pranab Kumar (1968). "Estimates of the Regression Coefficient Based on Kendall's Tau". In: *Journal of the American Statistical Association* 63.324 (Dec. 1968), pp. 1379–1389. DOI: 10.1080/01621459.1968.10480934.

Serletis, Apostolos (2007). *The Demand for Money*. Boston, MA: Springer US. DOI: 10.1007/978-0-387-71727-2.

Sharpe, William F. (1964). "Capital Asset Prices: A Theory Of Market Equilibrium Under Conditions Of Risk". In: *The Journal of Finance* 19.3 (Sept. 1964), pp. 425–442. DOI: 10.1111/j.1540-6261.1964.tb02865.x.

Shiller, Robert J. (1979). "The Volatility of Long-Term Interest Rates and Expectations Models of the Term Structure". In: *Journal of Political Economy* 87.6 (Dec. 1979), pp. 1190–1219. DOI: 10.1086/260832.

— (1981). "Alternative Tests of Rational Expectations Models : The Case of the Term Structure". In: *Journal of Econometrics* 16.1, pp. 71–87.

Shiller, Robert J., John Y. Campbell, Kermit L. Schoenholtz, and Laurence Weiss (1983). "Forward Rates and Future Policy: Interpreting the Term Structure of Interest Rates". In: *Brookings Papers on Economic Activity* 1983.1, p. 173. DOI: 10.2307/2534355. JSTOR: 2534355.

Siegel, Andrew F. (1982). "Robust Regression Using Repeated Medians". In: *Biometrika* 69.1, pp. 242–244. DOI: 10.1093/biomet/69.1.242.

Sill, Keith (1996). "The Cyclical Volatility of Interest Rates". In: *Business Review* (Jan 1996), pp. 15–29.

Singleton, Kenneth J. (1980). "Expectations Models of the Term Structure and Implied Variance Bounds". In: *Journal of Political Economy* 88.6 (Dec. 1, 1980), pp. 1159–1176. DOI: 10.1086/260933.

Solow, Robert M. (1956). "A Contribution to the Theory of Economic Growth". In: *The Quarterly Journal of Economics* 70.1 (Feb. 1956), p. 65. DOI: 10.2307/1884513.

Sozou, P. D. (1998). "On Hyperbolic Discounting and Uncertain Hazard Rates". In: *Proceedings of the Royal Society of London. Series B: Biological Sciences* 265.1409 (Oct. 22, 1998), pp. 2015–2020. DOI: 10.1098/rspb.1998.0534.

*Statistics Reporting Regulation (EU) 2533/98* (1998).

Summers, Lawrence H. (1986). "Does the Stock Market Rationally Reflect Fundamental Values?" In: *The Journal of Finance* 41.3, pp. 591–601. DOI: 10.1111/j.1540-6261.1986.tb04519.x.

Swan, T. W. (1956). "Economic Growth And Capital Accumulation". In: *Economic Record* 32.2, pp. 334–361. DOI: 10.1111/j.1475-4932.1956.tb00434.x.

Taranto, D E, G Bormetti, and F Lillo (2014). "The Adaptive Nature of Liquidity Taking in Limit Order Books". In: *Journal of Statistical Mechanics: Theory*

*and Experiment* 2014.6 (June 9, 2014), P06002. DOI: 10.1088/1742-5468/2014/06/P06002.

Taranto, Damian Eduardo, Giacomo Bormetti, Jean-Philippe Bouchaud, Fabrizio Lillo, and Bence Tóth (2018). "Linear Models for the Impact of Order Flow on Prices. I. History Dependent Impact Models". In: *Quantitative Finance* 18.6 (June 3, 2018), pp. 903–915. DOI: 10.1080/14697688.2017.1395903.

Taylor, John B. (1993). "Discretion versus Policy Rules in Practice". In: *Carnegie-Rochester Conference Series on Public Policy* 39 (Dec. 1993), pp. 195–214. DOI: 10.1016/0167-2231(93)90009-L.

Thaler (2005). *Advances in Behavioral Finance. 2*. New York: Russell Sage Foundation [u.a.] 712 pp.

Theil, Henri (1992). "A Rank-Invariant Method of Linear and Polynomial Regression Analysis". In: *Henri Theil's Contributions to Economics and Econometrics*. Ed. by Baldev Raj and Johan Koerts. Red. by A. J. Hughes Hallet and J. Marquez. Vol. 23. Advanced Studies in Theoretical and Applied Econometrics. Dordrecht: Springer Netherlands, pp. 345–381. DOI: 10.1007/978-94-011-2546-8_20.

Tobin, James (1969). "A General Equilibrium Approach to Monetary Theory". In: *Journal of Money, Credit and Banking* 1.1, pp. 15–29.

Tomas, Mehdi, Iacopo Mastromatteo, and Michael Benzaquen (2022a). *Cross Impact in Derivative Markets*. Mar. 29, 2022. DOI: 10.48550/arXiv.2102.02834. arXiv: 2102.02834 [q-fin].

— (2022b). "How to Build a Cross-Impact Model from First Principles: Theoretical Requirements and Empirical Results". In: *Quantitative Finance* 22.6 (June 3, 2022), pp. 1017–1036. DOI: 10.1080/14697688.2021.2020328.

Tookes, Heather E. (2008). "Information, Trading, and Product Market Interactions: Cross-sectional Implications of Informed Trading". In: *The Journal of Finance* 63.1 (Feb. 2008), pp. 379–413. DOI: 10.1111/j.1540-6261.2008.01319.x.

Toth, Bence and Janos Kertesz (2009). "The Epps Effect Revisited". In: *Quantitative Finance* 9.7 (Oct. 2009), pp. 793–802. DOI: 10.1080/14697680802595668.

Toth, Bence, Yves Lemperiere, Cyril Deremble, Joachim de Lataillade, Julien Kockelkoren, and Jean-Philippe Bouchaud (2011). "Anomalous Price Impact and the Critical Nature of Liquidity in Financial Markets". In: *Physical Review X* 1.2 (Oct. 31, 2011), p. 021006. DOI: 10.1103/PhysRevX.1.021006.

Tóth, Bence, Zoltán Eisler, and Jean-Philippe Bouchaud (2017). "The Short-Term Price Impact of Trades Is Universal". In: *Market Microstructure and Liquidity* 03.02 (June 2017), p. 1850002. DOI: 10.1142/S2382626618500028.

Tóth, Bence, Imon Palit, Fabrizio Lillo, and J. Doyne Farmer (2015). "Why Is Equity Order Flow so Persistent?" In: *Journal of Economic Dynamics and Control* 51 (Feb. 2015), pp. 218–239. DOI: 10.1016/j.jedc.2014.10.007.

Uhlenbeck, G. E. and L. S. Ornstein (1930). "On the Theory of the Brownian Motion". In: *Physical Review* 36.5 (Sept. 1, 1930), pp. 823–841. DOI: 10.1103/PhysRev.36.823.

Van Binsbergen, Jules H., William F. Diamond, and Marco Grotteria (2021). "Risk-Free Interest Rates". In: *Journal of Financial Economics* (June 2021), S0304405X21002786. DOI: 10.1016/j.jfineco.2021.06.012.

Vari, Miklos (2020). "Monetary Policy Transmission with Interbank Market Fragmentation". In: *Journal of Money, Credit and Banking* 52.2-3 (Mar. 2020), pp. 409–440. DOI: 10.1111/jmcb.12604.

Vasicek, Oldrich (1977). "An Equilibrium Characterization of the Term Structure". In: *Journal of Financial Economics* 5.2 (Nov. 1, 1977), pp. 177–188. DOI: 10.1016/0304-405X(77)90016-2.

Vayanos, Dimitri and Jean-Luc Vila (2021). "A Preferred-Habitat Model of the Term Structure of Interest Rates". In: *Econometrica* 89.1, pp. 77–112. DOI: 10.3982/ECTA17440.

Verma, Vijay and Rajesh Kumar Aggarwal (2020). "A Comparative Analysis of Similarity Measures Akin to the Jaccard Index in Collaborative Recommendations: Empirical and Theoretical Perspective". In: *Social Network Analysis and Mining* 10.1 (Dec. 2020), p. 43. DOI: 10.1007/s13278-020-00660-9.

Wang, Chen (2021). *Under- and Overreaction in Yield Curve Expectations*. SSRN Scholarly Paper ID 3487602. Rochester, NY: Social Science Research Network, Oct. 5, 2021. DOI: 10.2139/ssrn.3487602.

Wang, Shanshan (2017). *Trading Strategies for Stock Pairs Regarding to the Cross-Impact Cost*. Version 3. DOI: 10.48550/ARXIV.1701.03098.

Wang, Shanshan and Thomas Guhr (2017). "Microscopic Understanding of Cross-Responses Between Stocks: A Two-Component Price Impact Model". In: *Market Microstructure and Liquidity* 03 (03n04 Dec. 2017), p. 1850009. DOI: 10.1142/S2382626618500090.

Waterfall, Joshua J., Fergal P. Casey, Ryan N. Gutenkunst, Kevin S. Brown, Christopher R. Myers, Piet W. Brouwer, Veit Elser, and James P. Sethna (2006). "Sloppy-Model Universality Class and the Vandermonde Matrix". In: *Physical Review Letters* 97.15 (Oct. 12, 2006), p. 150601. DOI: 10.1103/PhysRevLett.97.150601.

Wicksell, Knut (1898). *Interest and Prices*. Read Books. 256 pp.

Woodford, Michael (2003). *Interest and Prices: Foundations of a Theory of Monetary Policy*. Princeton, New Jersey Oxford: Princeton University Press. 785 pp.

Wu, Peng, Jean-François Muzy, and Emmanuel Bacry (2022). "From Rough to Multifractal Volatility: The Log S-fBM Model". In: *Physica A: Statistical Mechanics and its Applications* 604 (Oct. 2022), p. 127919. DOI: 10.1016/j.physa.2022.127919.

Wu, Tao L. and Shengqiang Xu (2014). "A Random Field LIBOR Market Model". In: *Journal of Futures Markets* 34.6 (June 2014), pp. 580–606. DOI: 10.1002/fut.21654.

Yamamoto, R. and B. LeBaron (2010). "Order-Splitting and Long-Memory in an Order-Driven Market". In: *The European Physical Journal B* 73.1 (Jan. 2010), pp. 51–57. DOI: 10.1140/epjb/e2009-00392-y.

Zarinelli, Elia, Michele Treccani, J. Doyne Farmer, and Fabrizio Lillo (2015). "Beyond the Square Root: Evidence for Logarithmic Dependence of Market Impact on Size and Participation Rate". In: *Market Microstructure and Liquidity* 01.02 (Dec. 2015), p. 1550004. DOI: 10.1142/S2382626615500045.

Zhou, Wei-Xing (2012). "Universal Price Impact Functions of Individual Trades in an Order-Driven Market". In: *Quantitative Finance* 12.8 (Aug. 2012), pp. 1253–1263. DOI: 10.1080/14697688.2010.504733.

Zumbach, Gilles (2010). "Volatility Conditional on Price Trends". In: *Quantitative Finance* 10.4 (Apr. 2010), pp. 431–442. DOI: 10.1080/14697680903266730.

Zumbach, Gilles and Paul Lynch (2001). "Heterogeneous Volatility Cascade in Financial Markets". In: *Physica A: Statistical Mechanics and its Applications* 298.3-4 (Sept. 2001), pp. 521–529. DOI: 10.1016/S0378-4371(01)00249-7.

# Appendices

# Résumé substantiel en français

## Contexte

La théorie macroéconomique relie la croissance de la production aux anticipations sur les taux à court terme. Ainsi, les premiers modèles de taux définissent le taux à long terme comme la moyenne des taux courts, mais les preuves empiriques montrent que les taux long sont généralement plus élevés que les prédictions de ces modèles. Cet écart a été comblé par l'introduction d'une mesure de probabilité neutre au risque, dont les fondations microéconomiques sont peu convaincantes.

Cette thèse vise à développer une théorie des taux d'intérêts utilisant des modèles d'agents et de physique statistique, en se concentrant sur les éléments influençant la fixation des taux d'intérêts par les banques : la couverture des taux à long terme par des contrats à terme et le refinancement à court terme sur le marché des repurchase agreement (repo).

## Création monétaire sur le marché des repos

Depuis la crise financière de 2008, les marchés monétaires ont subi d'importants changements réglementaires. Des excédents de réserves sont apparus et le refinancement bancaire repose de plus en plus sur les repos et la réutilisation des collatéraux.

Nous proposons un modèle minimal du réseau interbancaire des repos qui permet d'éclairer ces changements. Il montre que l'excès de liquidité peut etre généré par les chocs de paiement. L'apparition de repo evergreen et la réutilisation du collatéral apparaissent comme une réponse simple au risque de contrepartie des banques et à la réglementation. Cette réutilisation augmente avec la rareté du collatéral. Le modèle génère un réseau aux connexions stables et une structure de type cœur-périphérie. Enfin, nous montrons comment ce modèle peut être utilisé comme outil de stress test ou de conception de politique monétaire.

## Flux de liquidité sur la courbe des taux d'intérêt

Comprendre la dynamique de la courbe des taux d'intérêt à terme (FRC) est essentiel pour la gestion des risques des banques et fascinant d'un point de vue théorique. Tandis que les processus stochastiques décrivant des actifs individuels ont été bien étudiés, les objets de dimension supérieure sont beaucoup plus difficiles à modéliser.

Pour aborder ce problème, nous commençons par mesurer empiriquement comment les volumes échangés sur un actif influent le prix d'un autre, un phénomène appelé impact croisé. Nous montrons que la formation des prix se produit de manière endogène au sein des actifs hautement liquides. Ensuite, les transactions sur ces actifs influencent les prix des produits corrélés moins liquides. Notamment, nous constatons que le contrat à terme sur obligation à 10 ans sert de principal réservoir de liquidité, influençant les prix des contrats à terme sur les autres maturités. Un tel comportement remet en question la validité de la théorie en économie financière selon laquelle les taux à long terme reflètent les anticipations des agents concernant les taux courts.

En nous basant sur ces résultats, nous revisitons un modèle décrivant la courbe des taux d'intérêt à terme (FRC) comme une corde élastique où se propagent des chocs idiosyncratiques. Ce modèle capture comment les forces du marché fixent les taux de manière auto-référentielle. Le modèle est parcimonieux et reproduit précisément la structure de corrélation de la FRC. La dépendance de la corrélation aux échelles de temps (effet de Epps) est également fidèlement reproduite. Nous confirmons que le temps perçu sur les marchés des taux d'intérêt est une fonction fortement sous-linéaire du temps réel, conformément à la littérature récente en finance comportementale. Le modèle génère également des prix auto-corrélés à court terme.

Enfin, ce cadre de modélisation peut être étendu pour tenir compte de l'impact des volumes sur prix et des impacts croisés. Il permet de simuler les prix des actifs à partir des volumes échangés avec une précision proche de celle d'un modèle linéaire non contraint, mais avec beaucoup moins de paramètres.

# Appendix A

# Stylized facts in money markets

*This chapter reproduces the appendices of Le Coz et al. (2024a) as well as a more detailed description of the MMSR database.*

## A.1 Money Market Statistical Reporting database

Our empirical analyses rely on the Money Market Statistical Reporting (MMSR) database, which lists the characteristics of daily individual transactions in the Eurozone's money markets, reported by the so-called Monetary Financial Institutions (MFIs, as defined by the *Statistics Reporting Regulation (EU) 2533/98* (1998) and the *National Accounts Regulation (EU) 549/2013* (2013)). These institutions include, notably, deposit-taking corporations, consisting of (i) credit institutions and (ii) other financial intermediaries, "*whose business is to receive deposits and make investments in securities on their own account*," as defined by *Statistics Reporting Regulation (EU) 2533/98* (1998).

In line with the *MFI Regulation (EU) 2021/379* (2016), among the list of MFIs in the Eurozone, only 47 credit institutions[16] have been required since 2014 to report their money market transactions to the ECB. These banks, referred to as "reporting agents" in this section, are obligated to report the following daily:

- all borrowings with maturities up to one year from "*[...] financial corporations (except central banks where the transaction is not for investment purposes), general government, or non-financial corporations classified as wholesale according to the Basel III LCR framework*" (*Amended MMSR Regulation (EU) 2019/ 113* 2019);
- all lending to other credit institutions with maturities up to one year.

[16]The full list of reporting agents is available on the Money market statistical reporting webpage,

Table A.1 provides a sector classification of the financial corporations considered as wholesale counterparties under the Basel III LCR framework, which are covered by the MMSR database.

As shown in Table A.1, until the amended MMSR regulation was released in 2019, counterparties such as investment funds, financial auxiliaries, and captive financial institutions were excluded from the list of counterparties required to be reported, in accordance with the *MMSR Regulation (EU) 1333/2014* (2014). Transactions with central banks are reported only if they are unrelated to Eurosystem monetary policy operations and standing facilities, as specified in the *MMSR Reporting Instructions* (2021).

In both the secured and unsecured segments, the MMSR database contains information on the type of money market instrument, the dates of trade, start and termination of the contract, the interest rate, the volume, the counterparty's sector, the transaction volume, the maturity, and the trade direction (lending vs. borrowing). Additionally, the database includes identifiers for the reporting banks and their counterparties. For secured transactions, it is also possible to identify the ISIN of the collateral. Reporting banks are required to report all transactions until they mature, ensuring that any deposit recorded in the balance sheet of a bank is reported daily until the deposit is either partially or fully withdrawn.

### A.1.1 General data retreatment

We keep any interbank transactions between MMSR reporting agents for which we have non-missing reported information on the transaction volume, the LEI of the reporting agent, the LEI of the counterparty agent, the ISIN code of the collateral and the direction of the transaction (borrowing vs. lending). We remove all canceled transactions from the database - i.e. a canceled transaction corresponds to any transaction which was initially reported and was later canceled, but is not equivalent to a transaction which was approved by the bank and later matured (these are the transactions we keep for our analysis). Additionally, we make sure that the dates in our sample only correspond to official euro area trading calendar dates[17].

### A.1.2 Identification of evergreen repos

Our main data transformation consists in extracting information on the evergreen repos from the MMSR database. Evergreen repos are repos with an infinite maturity but are not flagged as such in the MMSR database. Evergreens have a notice period that usually vary between 1 to 100 days and are reported as a repo

[17] We list all calendar dates reported on the official statistical data warehouse of the ECB from the reported EONIA/ESTR rates time series.

transaction with the same maturity band everyday until the day when one or both trading counterparties decide to stop the transaction. That day, the two counterparties have to agree on a date of final maturity, which will then be reported in the database. We thus identify evergreens as any repeated transactions between the two same counterparties for at least 1 day. Specifically, we identify a unique repo as the combination of the two identifiers of the transacting counterparties (the lender and the borrower), the nominal amount and the maturity and the ISIN code of the transaction. Any repeated combination of these unique repos for more than a day are considered evergreens.

| Financial corporations | | | Definitions | Examples | Sect. | MMSR |
|---|---|---|---|---|---|---|
| Monetary Financial Institutions (MFI) | Central banks | | All financial corporations whose principal function is to issue currency, to maintain the internal and external value of the currency and to hold all or part of the international reserves of the country. | National central banks or central monetary agencies of essentially public origin. | S121 | Counter-parties |
| | Deposit-taking corporations | Credit institutions | Undertaking the business of which is to take deposits or other repayable funds from the public and to grant credits for its own account. | Commercial banks, universal banks, all-purpose banks, ect... | S122 | 47 Reporting agents |
| | | Other deposit-taking corporations | Financial intermediaries whose business is to receive deposits and make investments in securities on their own account. | Savings banks (including trustee savings banks and savings banks and loan associations), ect.. | | Counter-parties |
| | | Electronic money institutions | Other deposit-taking corporations that are principally engaged in financial intermediation in the form of issuing electronic money. | | | |
| | Money Market Funds (MMF) | | Their business is to issue investment fund shares as close substitutes for deposits, and, for their own account, to make investments primarily in money market fund shares/units, short-term debt securities, and/or deposits. | Investment funds including investment trusts, unit trusts and other collective investment schemes whose shares or units are close substitutes for deposits. | S123 | |
| Insurance corporations (IC) | | | All financial corporations engaged in financial intermediation for the pooling of risks. | Life and non-life insurance, as well as reinsurance to other insurance corporations. | S128 | |
| Pension funds (PF) | | | All financial corporations engaged in financial intermediation for the pooling of social risks. | Pension fund schemes may be organized by employers or by general government, and provide income in retirement, and often benefits for death and disability. | S129 | |
| Other financial corporations | Non-MMF investment funds | | Their business is to issue investment fund shares which are not close substitutes for deposits, and, on their own account, to make investments primarily in assets other than short-term financial assets. | Investment funds, investment funds investing in other funds ('funds of funds'), hedge funds, ect... | S124 | Excluded before 2019 |
| | Financial auxiliaries | | Financial corporations principally engaged in activities closely related to financial intermediation, but which are not financial intermediaries themselves. | Insurance/loan/securities brokers, corporations arranging derivative instruments, financial markets infrastructure compagnies, managers of pension/mutual funds, ect... | S126 | |
| | Captive financial institutions | | Financial corporations neither engaged in financial intermediation nor in providing financial auxiliary services, and where their assets or liabilities are not transacted on open markets. | Legal entities such as trusts, estates, agencies accounts and holding companies that hold controlling levels of equity of a group of subsidiary corporations, ect... | S127 | |
| | Other financial intermediaries | | financial corporations engaged in financial intermediation by incurring liabilities in forms other than currency, deposits, or investment fund shares, or in relation to insurance, pension and standardized guarantee schemes from institutional units. | Financial vehicle corporations engaged in securitization transactions (FVC), security and derivative dealers, financial leasing, factoring, venture capital companies, export/import financing companies, Central counterparties clearing houses, ect... | S125 | Counter-parties |

**Figure A.1:** Sectoral breakdown for counterparties in the MMSR database.

# Appendix B

# Model of money creation

*This section reproduces the appendices of Le Coz et al. (2024b).*

## B.1 Random growth model

We want to model money creation through positive shocks fluctuating around an average rate $g$ of new money. Such model can be formulated by

$$\begin{aligned} X_i(t+1) &= (gZ_i(t)+1)X_i(t), \\ X_i(0) &= x_0, \end{aligned} \tag{B.1}$$

where $Z_i(t) = e^{\sigma_Z \epsilon_i(t) - \frac{1}{2}\sigma_Z^2}$. We recall $(\epsilon_i(t))$ are independent normalized centered Gaussian random variables across banks and time. Taking the expectation of Eq. (B.1) yields

$$\langle X_i(t) \rangle = x_0(1+g)^t. \tag{B.2}$$

Similarly, taking the expectation of the square of Eq. (B.1) gives

$$\langle X_i^2(t) \rangle = x_0^2(g^2 e^{\sigma_Z^2} + 2g + 1)^t, \tag{B.3}$$

which shows $X(t)$ is non-stationary. For $t \gg 1$ and increments of small size $\Delta t$, by taking the logarithm of Eq. (B.1), we have

$$\ln(X_i(t)) = \sum_{t'=0}^{t} \ln(gZ_i(t')+1) + \ln(x_0). \tag{B.4}$$

Assuming $g^2 e^{\sigma_Z^2} \ll 1$ (i.e. the mean growth is small compared to fluctuations), $\ln(gZ_i + 1)$ can be approximated by $gZ_i$ which has a mean $g$ and a variance

$g^2(e^{\sigma_Z^2}-1)$ that we note $g^2v^2$. Hence, for $t$ sufficient large, by the central limit theorem, the log-returns $\ln(X_i(t+\Delta t))-\ln(X_i(t))$ behave as a Gaussian of mean $g\Delta t$ and variance $g^2v^2\Delta t$. Thus, in the limit $\Delta t \ll 1$ and $t \gg 1$, the process $X_i(t)$ reads

$$X_i(t) = x_0 e^{gt-\frac{1}{2}g^2v^2t+gvB(t)}, \tag{B.5}$$

where $B(t)$ is a Brownian motion. One can check that this expression yields the mean and variance in Eq. (B.2) and (B.3) for $g \ll 1$. The limit distribution of this type of random processes has been studied among others in Marsili et al. (1998), Gabaix (1999), and Mitzenmacher (2004). Unfortunately this process has no stationary limit unless we prevent the smallest banks to become smaller than a certain barrier. Indeed, as noticed by Mitzenmacher (2004), the logarithm of the density distribution of $X_i(t)$, noted $f_{X(t)}(x)$ reads

$$\begin{aligned}\ln(f_{X(t)}(x)) = &-\left(\frac{3}{2}-\frac{1}{gv^2}\right)\ln(x) - \frac{1}{2g^2v^2t}\ln(x)^2 \\ &- \ln(\sqrt{2\pi}g^2v^2t) - \frac{1}{2gv^2}+\frac{1}{4},\end{aligned} \tag{B.6}$$

which is clearly non stationary. We could hope solving this issue by defining a bounded variable $Y_i(t)$, the re-scaled money creation of the bank $i$ by the sum of money creation of the other banks:

$$Y_i(t) = \frac{X_i(t)}{\sum_{i=0}^{N} X_i(t)}. \tag{B.7}$$

In the limit of large $N$, the sum $\sum_{i=0}^{N} X_i(t)$ can be approximated by its mean, as long as the variance of the sum is small compared to its mean. Using Eq. (B.2), (B.3) and the central limit theorem for large $N$, this condition is meet if

$$\left(\frac{g^2e^{\sigma_Z^2}+2g+1}{(1+g)^2}\right)^t \ll N. \tag{B.8}$$

In this limit, $\sum_{i=0}^{N} X_i(t) \approx N x_0 e^{gt}$, so the density distribution function $f_{Y(t)}$ of the normalized variables $Y_i$ reads

$$\ln(f_{Y(t)}(y)) = -\frac{3}{2}\ln(y) - \frac{1}{2g^2v^2t}\ln(y)^2 - \ln(\sqrt{2\pi}g^2v^2t) + \frac{1}{4}. \tag{B.9}$$

Thus, for large $t$ and large $y$ (precisely for $\ln(y) \ll \sqrt{t}$), the quadratic term becomes negligible so the variable $Y_i$ behaves similarly to a power law of exponent 0.5. Yet, the term $-\ln(\sqrt{2\pi}g^2v^2t)$ shows that most banks have a size becoming

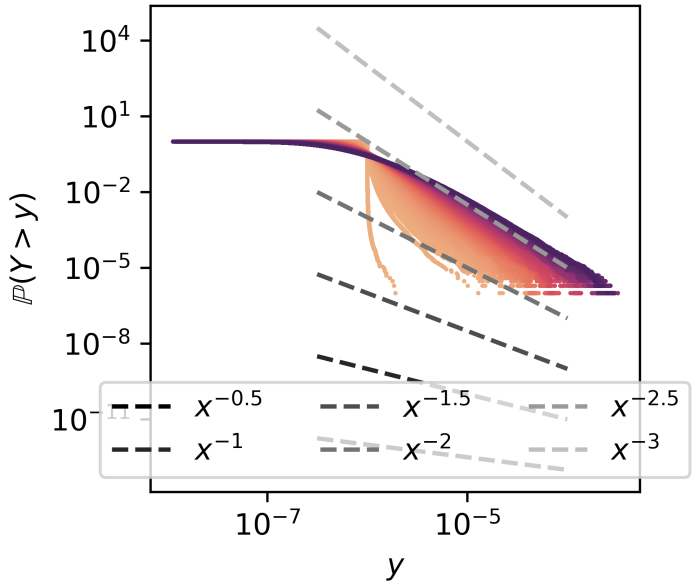


**Figure B.1:** Evolution of cumulative distribution function of the relative sizes of banks across 100 000 days with an average growth rate $g = 10\%$ and a volatility $v = 10$. Each color corresponds to a snapshot every 500 steps from the shortest (orange) to the latest (purple). Within a certain range, the measure of the tail exponent drops from infinity to around 3 in 5000 steps. This exponent is still 2.5 after 100 000 steps.

infinitely small. Correcting such behavior requires either defining a negative drift pushing bank sizes towards a barrier (Marsili et al., 1998; Gabaix, 1999) or to allow banks to exchange wealth (Bouchaud and Mézard, 2000). Both options are in contradiction with the requirements of our model. In practice, for the typical values of $g = 10\%$ per year, and $v = 10$ (i.e. some banks double their balance sheet in a year, while the median bank grows by 1%), we observe that the distribution of the $Y_i$ is almost stationary after 5000 steps (i.e. $\approx$ 20 years if we count 250 business days per year). Indeed, Fig. B.1 shows the distribution function of the relative sizes of banks moves very slowly between 5000 and 100 000 steps.

## B.2 Sensitivity analysis

As a complement to section 4.2.2, we present here the influence of several other key control parameters. Unless specified differently, all parameters are set as in the section 4.2.2. Each simulation is also conducted over 10000 steps. As previously, we simulate the same run 100 times and report the mean, excluding values outside of one standard deviation, of the stationary level of a given metric.

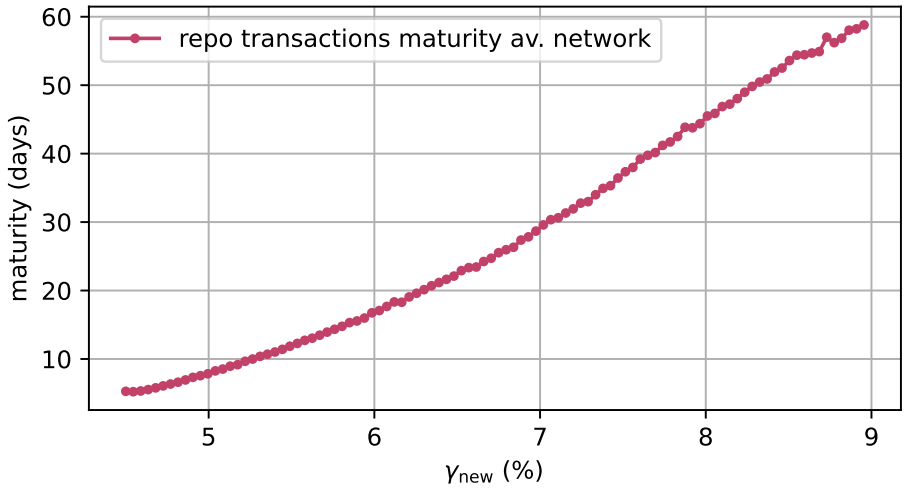


**Figure B.2:** Average maturity of repo transactions as a function of the leverage ratio equivalent of new own funds $\gamma_{new}$.

**B.2.0.0.1 The effect of new own funds** The leverage ratio is the constraint that limits the size of the balance sheet. Hence, the less binding the constraint (i.e. the higher the amount of new own funds $\gamma_{new}$ measured in leverage ratio equivalent, see section 4.1.5), the longer the maturity of repos (Fig. B.2). This results in a higher network density (Fig. B.3), a higher Jaccard network similarity index (Fig. B.4), and a higher rate of collateral re-use (Fig. B.5).

**B.2.0.0.2 The effect of the size heterogeneity** High levels of bank sizes' heterogeneity (i.e. low values of the tail exponent $\mu$) are associated to low collateral re-use rate (Fig. B.6) and network density (Fig. B.7). Indeed, when heterogeneity is high, the probability of a large positive shock to hit a large bank increases. This results in excess liquidity (Fig. B.8), which reduces the chances of subsequent shocks to generate liquidity needs, thereby reducing collateral re-use and network density.

**B.2.0.0.3 The effect of the learning coefficient** A core-periphery structure emerges if the learning coefficient $\lambda$ is above a minimum level (around 0.01 in Fig. B.9). Below this value, banks do not learn quickly enough which counterparties to trade with, resulting in a high network density (Fig. B.10).

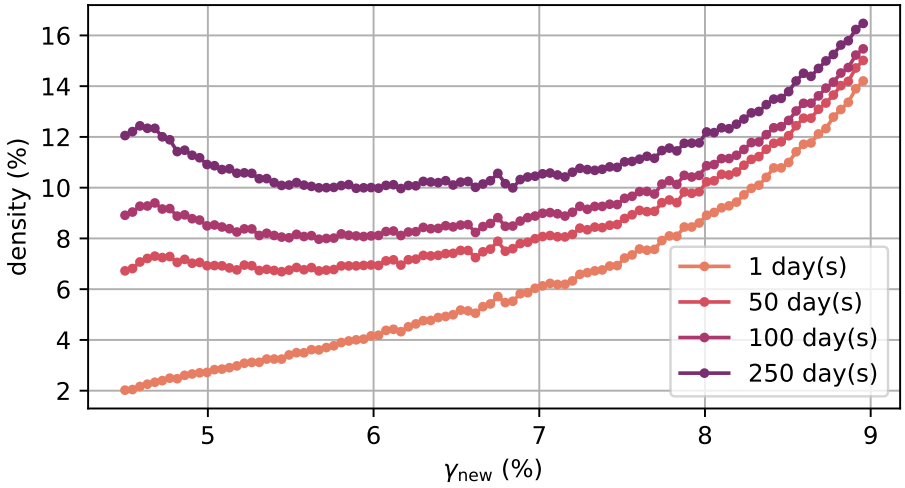


**Figure B.3:** Network density as a function of the leverage ratio equivalent of new own funds $\gamma_{\text{new}}$.

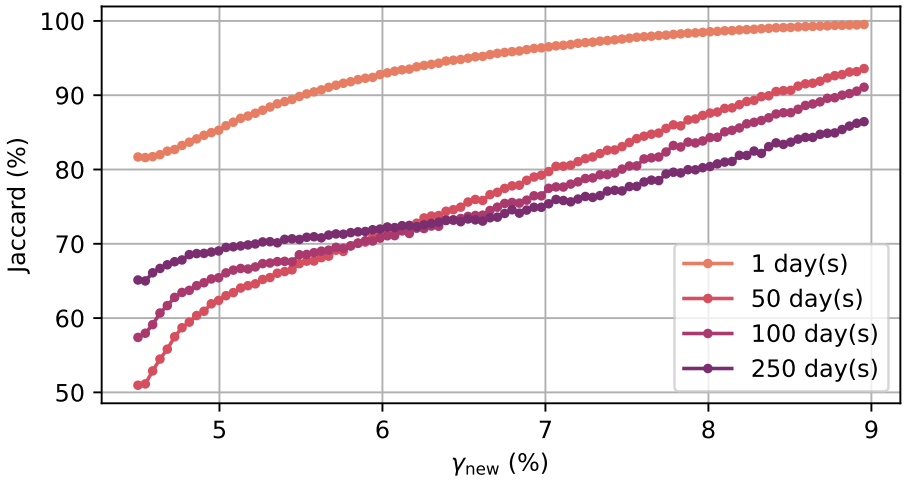


**Figure B.4:** Jaccard network similarity index as a function of the leverage ratio equivalent of new own funds $\gamma_{\text{new}}$.

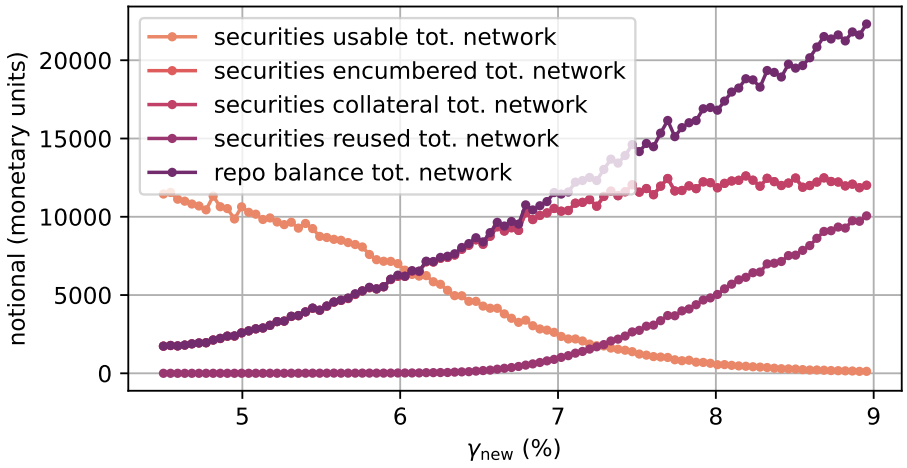


**Figure B.5:** Collateral aggregates as a function of the leverage ratio equivalent of new own funds $\gamma_{\text{new}}$.

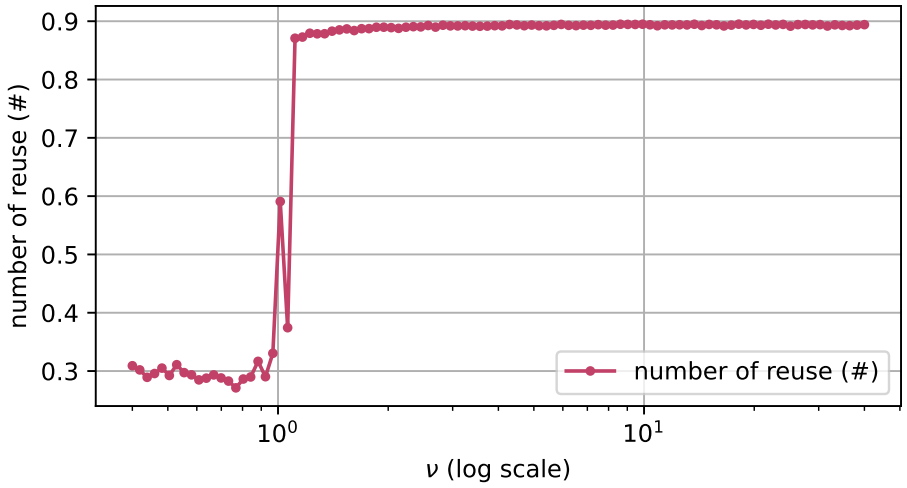


**Figure B.6:** Collateral re-use as a function of the power law exponent $\nu$ governing the distribution of bank sizes.

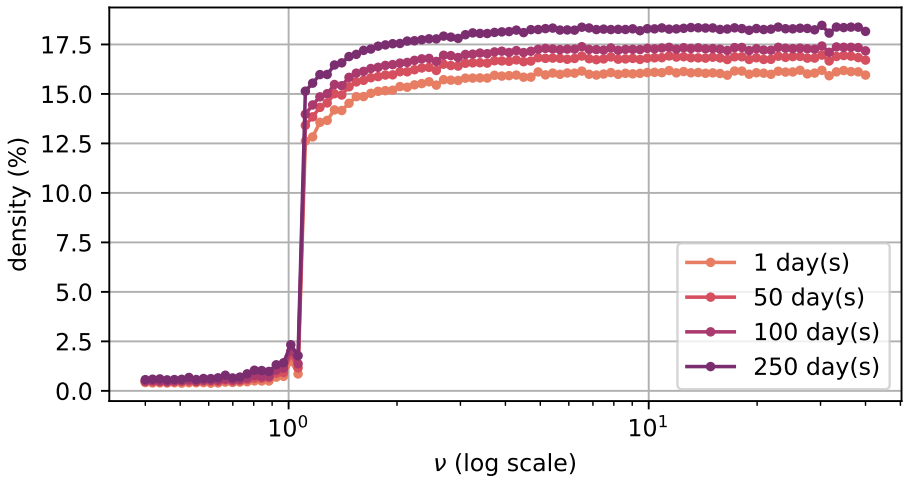


**Figure B.7:** Network density as a function of the power law exponent $\nu$ governing the distribution of bank sizes.

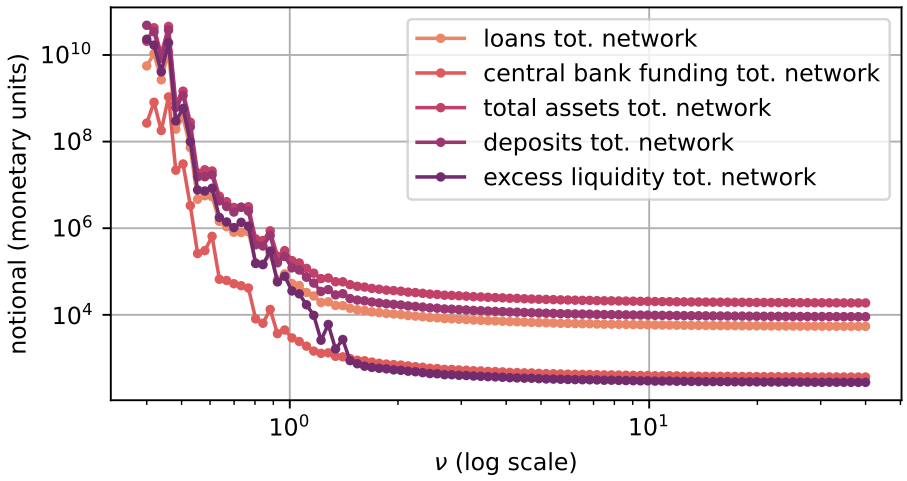


**Figure B.8:** Macro-economic aggregates as a function of the power law exponent $\nu$ governing the distribution of bank sizes.

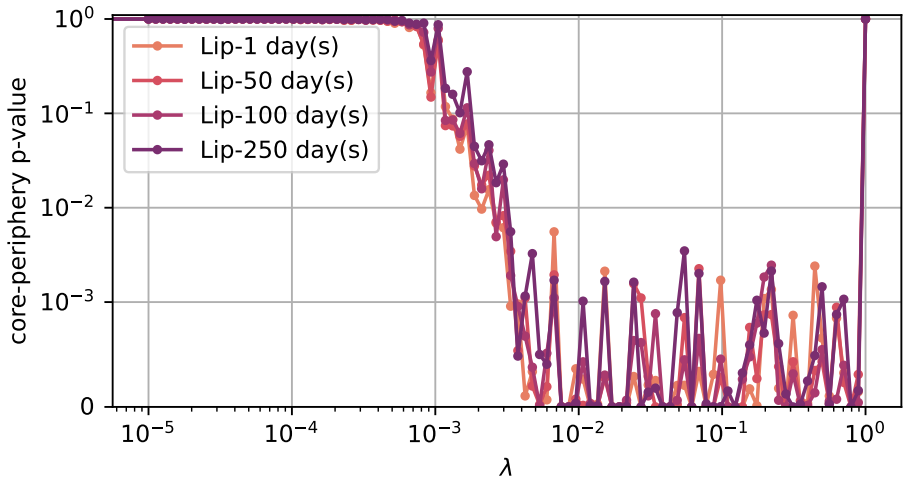


**Figure B.9:** P-values assessing the existence of a core-periphery structure according to the method proposed by Lip (2011) as a function of the learning coefficient $\lambda$.

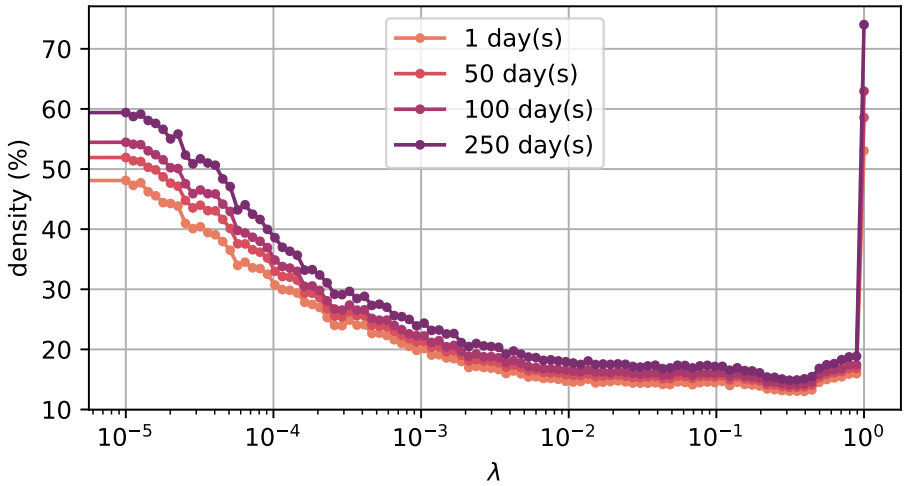


**Figure B.10:** Network density as a function of the learning coefficient $\lambda$.

# Appendix C

# Cross-impact measures

*This section reproduces the appendices of Le Coz et al. (2024d).*

## C.1 Statistical significance of the Goodness-of-fit

The main results of our analysis are expressed in terms of a generalized $\mathcal{R}^2(M)$. For a single asset $i$, the indicator $\mathcal{R}^2(I_{\sigma_i})$ is precisely the R-squared of the linear regression of its price increments over its predicted price increments in the model with no Y-ratio:

$$\Delta p_{t,i} = Y\widehat{\Delta p}_{t,i} + \eta_{t,i}, \tag{C.1}$$

where the explanatory variable $\widehat{\Delta p}_{t,i}$ is the prediction of the model with no Y-ratio.

The significance of the R-squared of the above regression can be provided by an F-test. Indeed, this latter allows us to compare two models, one model being the reduction of the other to fewer parameters. Here we compare the model with one explanatory variable to the model with only an intercept. Let $\widetilde{\xi} \in \mathbb{R}^N$ denote the vector of the errors estimated in the model with no explanatory variable, and $\widehat{\xi} \in \mathbb{R}^N$ denote the vector of the errors estimated in the cross-impact model. The F-statistic is expressed as the normalized difference between the squared errors in the two models:

$$F = \frac{\widetilde{\xi}^\top\widetilde{\xi} - \widehat{\xi}^\top\widehat{\xi}}{\widehat{\xi}^\top\widehat{\xi}}. \tag{C.2}$$

Since the errors in the parameter-free model are precisely equal to the centered explained variable, denoted as $y \in \mathbb{R}^N$, we can express this F-statistics as a function of the $\mathcal{R}^2$:

$$F = \frac{y^\top y - \widehat{\xi}^\top\widehat{\xi}}{\widehat{\xi}^\top\widehat{\xi}} = \frac{\widehat{y}^\top\widehat{y}}{\widehat{\xi}^\top\widehat{\xi}} = \frac{\mathcal{R}^2}{1-\mathcal{R}^2}. \tag{C.3}$$

Under the usual assumptions for the residuals and the explained variable, this F-statistics follows a Fisher law $F(N, N-1)$. The significance of the $\mathcal{R}^2$ can be then provided by the p-values of the F-statistics of the linear model calibrating the Y-ratio.

Yet, the residuals in the above regression are auto-correlated due to the properties of the order flows. They are also non-Gaussian (heavy tails, negative skew) and heteroskedastic, due to the properties for the price process. In fact, returns are generally conditionally heteroskedastic but unconditionally homoskedastic. Here the unconditional heteroskedasticity observed in the data might be due to some trend in the annual sample.

However, the observed levels of auto-correlation are sufficiently low (around 10% at the lag 1) to avoid compromising the robustness of the test (Krämer, 1989). This issue is further studied in the following section. Moreover, the non-Gaussianity only partially limits the robustness of the F-statistic test (Box and Watson, 1962). Yet, the heteroskedasticity issue requires using a modified F-statistic test robust to this assumption. Thus, we measure the statistical significance of the $\mathcal{R}^2$ using the approach of MacKinnon and White (1985) (implemented in the *Statsmodels* python library through the method of Long and Ervin (2000)).

These F-statistics confirm that the $\mathcal{R}^{2*}$ displayed in our study are significant. Specifically, in the single asset case, each optimal goodness-of-fit $\mathcal{R}^{2*}$ is obtained from a linear regression. The F-statistics p-values of $m \approx 10^3$ (500 assets across 5 years) statistical tests are exhibited in Fig. C.1. Notably, only few p-values are above the Bonferroni upper bound (Goeman and Solari, 2014; Frane, 2015). This upper bound is used for the identification of false positive when performing multiple hypothesis tests. Here, the rate of false positive at the confidence interval $\alpha = 10^{-2}$ is bounded by the share of p-values above $\frac{\alpha}{m} = 10^{-5}$. Figure C.1 shows that only a negligible share of these p-values are not significant (approximately 2%). The more accurate procedure from Benjamini and Hochberg (1995) yields similar results. If we compare the p-value of rank $k$ (in ascending order) to $\frac{k\alpha}{m}$, we find that 1.8% of these p-values are above this threshold.

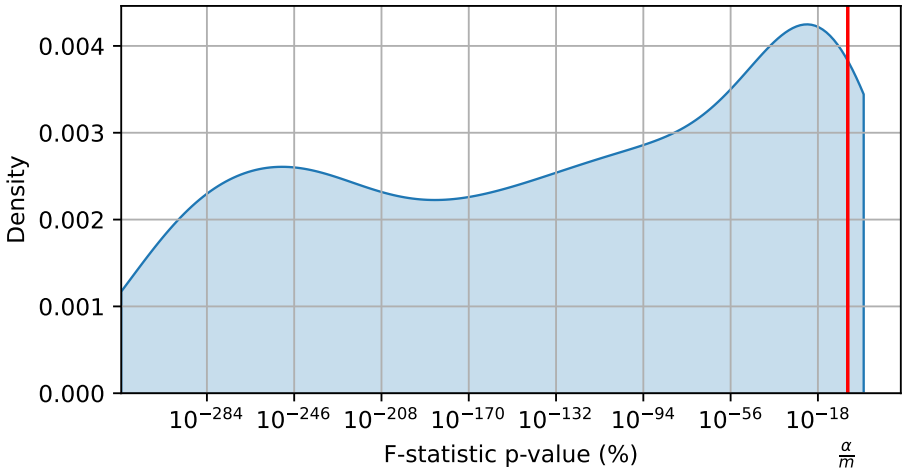


**Figure C.1:** Empirical distribution of the statistical significance of the $\mathcal{R}^{2*}(I_{\sigma_i})$ across the years and assets in our sample.

## C.2 Auto-correlation structure and comparison with the propagator model

The auto-correlation of signed order flows is a well-documented feature of financial markets (Lillo and Farmer, 2004). Using the E-mini S&P Future binned every 1 minute to calibrate the single asset model, we observe significant auto-correlation of both the signed order flows and the residuals (Fig. C.2). In contrast, the auto-correlation of prices is of the same size as the noise. If the number of data points increases, prices will become even more efficient, so the auto-correlation of the residuals will increase to compensate for the long memory of the signed order flows. Thus, the model will be invalidated.

As previously mentioned, one approach to re-conciliate the long memory of the order flows with the efficiency of prices is to define a *propagator model* (Bouchaud et al., 2006; Bouchaud, 2009; Alfonsi et al., 2016; Benzaquen et al., 2017; Bouchaud et al., 2018; Schneider and Lillo, 2019) as follow:

$$p_t = \sum_{s \leq t} G(t-s) q_s + \eta_t, \tag{C.4}$$

where $G : t \to G(t) \in \mathcal{M}_n(\mathbb{R})$ captures the dependence on past order flows and $\eta_t$ is a vector of zero-mean random variables. As shown by Tomas et al. (2022b) the calibration of the true propagator model would yield only marginal improvements in the goodness-of-fit. However, this model is significantly more

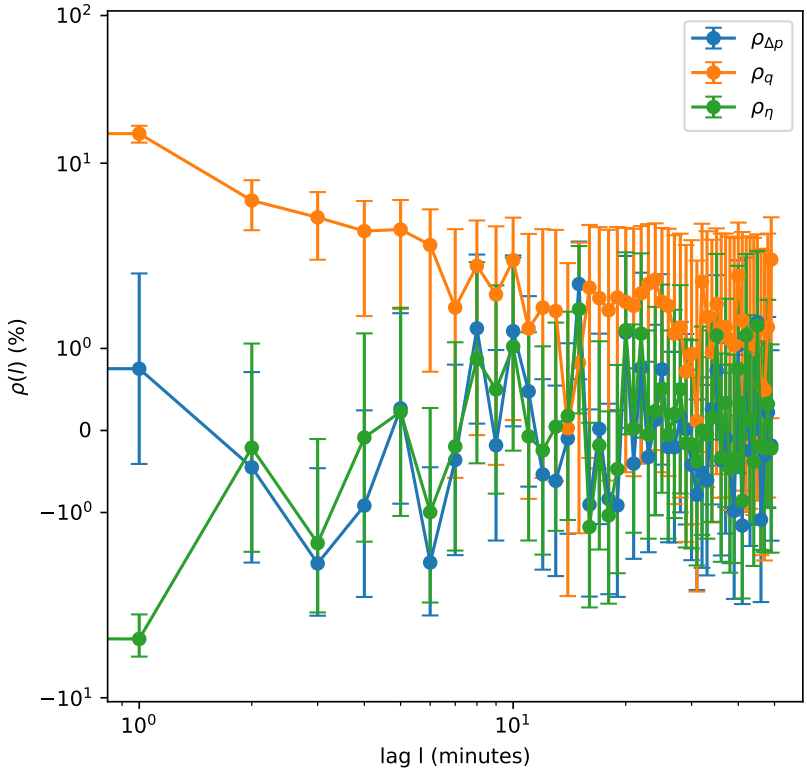


**Figure C.2:** Auto-correlation of price variations $\Delta p$, signed order flows $q$ and residuals $\eta$ for the E-mini S&P Future. Data is binned every 1 minute for the year 2021. Error bars represent one standard deviation confidence interval.

complex to calibrate, which would impede conducting this study at the same scale across time and assets.

# Appendix D

# Elastic string model

*This section reproduces the appendices of Le Coz and Bouchaud (2024).*

## D.1 Solution to the discretized Master Equation when $\psi \gg 1$

We define the *propagator* $\mathcal{G}_{\theta\theta'}(t,t')$ as the solution to

$$\frac{\partial \mathcal{G}}{\partial t} + \frac{1}{\tau}\mathcal{L}_d[\mathcal{G}] = \delta(t-t')\delta_{\theta\theta'}. \tag{D.1}$$

The linear operator in Eq. (D.1) is translation invariant as it has constant coefficients. It indicates that $\mathcal{G}_{\theta\theta'}(t,t')$ depends only on $\theta-\theta'$ and $t-t'$. The symmetry of the functions $\theta \mapsto \mathcal{L}_d[\mathcal{G}]_\theta(t)$ and $\theta \mapsto \delta_{\theta\theta'}$ further ensures that the dependence of the propagator with respect to space depends only of the absolute value of the differences $|\theta-\theta'|$. Let $H$ denote the Heaviside function. Applying discrete Fourier decomposition to the dimension $\theta-\theta'$ yields a particular solution:

$$\mathcal{F}[\mathcal{G}](\xi, t-t') = H(t-t')e^{-\frac{L_d(\xi)(t-t')}{\tau}}, \tag{D.2}$$

where $L_d(\xi) = 1 + 2\frac{(1-\cos\xi)}{\mu^2} + 4\frac{(1-\cos\xi)^2}{\nu^4}$ and $\mathcal{F}[\mathcal{G}](\xi,t-t')$ denote the spatial Fourier transform of $\mathcal{L}_d[A]_\theta(t)$ and $\mathcal{G}_{\theta\theta'}(t-t')$ respectively. These functions are continuous in $\xi$ and $t$.

Seeking a solution on $\mathbb{R}\times\mathbb{Z}$ for the discretized Eq. (7.19) without boundary

conditions, we extend the noise $\eta$ so that $\eta_\theta(t) = 0$ for $\theta \in \mathbb{Z}_-^*$. The solution is

$$\begin{aligned}\mathcal{A}_\theta(t) &= \frac{1}{\tau}\int_{\mathbb{R}} \mathrm{d}t' \sum_{\theta'=-\infty}^{+\infty} \mathcal{G}_{|\theta-\theta'|}(t-t')\eta_{\theta'}(t') \\ &= \frac{1}{\tau}\int_{-\infty}^{t} \mathrm{d}t' \sum_{\theta'=0}^{+\infty} \mathcal{G}_{|\theta-\theta'|}(t-t')\eta_{\theta'}(t'). \end{aligned} \tag{D.3}$$

Similarly, $\mathcal{A}_{-\theta}(t)$ solves the discretized Eq. (7.19) without boundary conditions when substituting $\eta_\theta(t)$ with $\eta_{-\theta}(t)$. Thus, a specific solution on $\mathbb{R}\times\mathbb{N}$ that satisfies the Neumann boundary condition is

$$A_\theta(t) := \mathcal{A}_\theta(t) + \mathcal{A}_{-\theta}(t). \tag{D.4}$$

The propagator $G_{\theta\theta'}(t-t')$ associated with this solution is defined as

$$\begin{aligned} &G_{\theta\theta'}(t-t') := \mathcal{G}_{|\theta-\theta'|}(t-t') + \mathcal{G}_{\theta+\theta'}(t-t') \\ &= \frac{1}{2\pi}\int_{-\pi}^{\pi} \mathrm{d}\xi \left(e^{i\xi(\theta-\theta')} + e^{i\xi(\theta+\theta')}\right) \mathcal{F}[\mathcal{G}](\xi, t-t'). \end{aligned} \tag{D.5}$$

For consistency with the centered discretization scheme, the inverse Fourier transform is centered on $[-\pi, +\pi]$.

## D.2 Noise correlators when $\psi \gg 1$

### D.2.1 Autocovariance of the correlated noise

For $\psi \gg 1$, the autocovariance of $A$ is defined by

$$\begin{aligned} &\mathbb{E}\left[A_\theta(t)A_{\theta'}(t')\right] := \frac{1}{\tau^2}\int_{-\infty}^{t}\mathrm{d}u\int_{-\infty}^{t'}\mathrm{d}v \\ &\sum_{(U,V)\in\mathbb{N}^2} G_{\theta U}(t-u)G_{\theta' V}(t'-v)\mathbb{E}\left[\eta_U(u)\eta_V(v)\right]. \end{aligned} \tag{D.6}$$

Recalling that

$$\mathbb{E}\left[\eta_U(u)\eta_V(v)\right] = 2D\delta(u-v)\delta_{UV}, \tag{D.7}$$

we derive

$$\begin{aligned} &\mathbb{E}\left[A_\theta(t)A_{\theta'}(t')\right] \\ &= \frac{2D}{\tau^2}\int_{-\infty}^{t\wedge t'}\mathrm{d}u \sum_{U\in\mathbb{N}} G_{\theta U}(t-u)G_{\theta' U}(t'-u). \end{aligned} \tag{D.8}$$

Substituting the propagator $G$ with its expression in Eq. (D.5) yields

$$\begin{aligned}
&\mathbb{E}\left[A_\theta(t)A_{\theta'}(t')\right] \\
&= \frac{2D}{(2\pi\tau)^2}\iint_{-\pi}^{\pi}\mathrm{d}\xi\mathrm{d}\xi'\int_{-\infty}^{t\wedge t'}\mathrm{d}u e^{-\frac{1}{\tau}\left(L_d(\xi)(t-u)+L_{q'}(t'-u)\right)} \\
&\qquad \sum_{U\in\mathbb{N}}\left(e^{i\xi(\theta-U)}+e^{i\xi(\theta+U)}\right)\left(e^{i\xi'(\theta'-U)}+e^{i\xi'(\theta'+U)}\right) \\
&= \frac{2D}{(2\pi\tau)^2}\iint_{-\pi}^{\pi}\mathrm{d}\xi\mathrm{d}\xi'\int_{-\infty}^{t\wedge t'}\mathrm{d}u e^{-\frac{1}{\tau}(L_d(\xi)(t-u)+L_d(\xi')(t'-u))} \\
&\qquad\qquad e^{i(\xi\theta+\xi'\theta')}\sum_{U\in\mathbb{Z}}\left(e^{iU(\xi+\xi')}+e^{iU(\xi-\xi')}\right) \\
&= \frac{2D}{2\pi\tau^2}\int_{-\pi}^{\pi}\mathrm{d}\xi\int_{-\infty}^{t\wedge t'}\mathrm{d}u e^{-\frac{L_d(\xi)}{\tau}(t+t'-2u)}\left(e^{i\xi(\theta-\theta')}+e^{i\xi(\theta+\theta')}\right),
\end{aligned}$$

having noted that $L_d(-\xi)=L_d(\xi)$. The computation of the integral with respect to time gives the expression of the autocovariance of $A$:

$$\mathbb{E}\left[A_\theta(t)A_{\theta'}(t')\right] = \frac{D}{2\pi\tau}\int_{-\pi}^{\pi}\mathrm{d}\xi\frac{e^{i\xi(\theta-\theta')}+e^{i\xi(\theta+\theta')}}{L_d(\xi)}e^{-\frac{L_d(\xi)}{\tau}|t-t'|}. \tag{D.9}$$

We now define the quantity $\mathcal{D}_1(\theta,\theta')$ by

$$\mathcal{D}_1(\theta,\theta') = \frac{1}{2\pi}\int_{-\pi}^{\pi}\mathrm{d}\xi\frac{e^{i\xi(\theta-\theta')}+e^{i\xi(\theta+\theta')}}{L_d(\xi)}. \tag{D.10}$$

$L_d(\xi)$ is symmetric, so one can reformulate the above quantity as

$$\mathcal{D}_1(\theta,\theta') = \frac{1}{\pi}\int_{0}^{\pi}\mathrm{d}\xi\frac{2\cos\xi\theta\cos\xi\theta'}{L_d(\xi)}. \tag{D.11}$$

Therefore, for $\tau$ close to 0, the covariance of $A$ simplifies to

$$\mathbb{E}\left[A_\theta(t)A_{\theta'}(t')\right] = \begin{cases} 0, \text{ if } t\neq t', \\ \dfrac{D}{\tau}\mathcal{D}_1(\theta,\theta'), \text{ if } t=t'. \end{cases} \tag{D.12}$$

In our case, $L_d(\xi)=1+2\frac{1-\cos\xi}{\mu^2}+4\frac{(1-\cos\xi)^2}{\nu^4}$. Hence, one can show that, for $\xi\ll 1$ and $\tau\ll 1$, the autocovariance $\mathbb{E}\left[A_\theta(t)A_{\theta'}(t')\right]$ converges to the correlator $\delta(t-t')\mathcal{D}_{BB}(\theta,\theta')$ introduced by Baaquie and Bouchaud (2004).

### D.2.2 Autocovariance of the cumulative correlated noise

We define the coarse-grained cumulative sum of $A_\theta$ over a time interval $\Delta t \gg \tau$ by

$$\Delta A_\theta = \int_{t-\Delta t/2}^{t+\Delta t/2} A_\theta(u)\mathrm{d}u. \tag{D.13}$$

We derive the autocovariance of $\Delta A$ when $\psi \gg 1$,

$$\begin{aligned}\mathbb{E}\left[\Delta A_\theta(t)\Delta A_{\theta'}(t')\right] &= \int_{t-\Delta t/2}^{t+\Delta t/2}\mathrm{d}u\int_{t'-\Delta t/2}^{t'+\Delta t/2}\mathrm{d}v\mathbb{E}\left[A_\theta(u)A_{\theta'}(v)\right],\\ &= \frac{D}{2\pi\tau}\int_{-\pi}^{\pi}\mathrm{d}\xi\int_{t-\Delta t}^{t}\mathrm{d}u\int_{t'-\Delta t}^{t'}\mathrm{d}v\frac{e^{i\xi(\theta-\theta')}+e^{i\xi(\theta+\theta')}}{L_d(\xi)}e^{-\frac{L_d(\xi)}{\tau}|u-v|}.\end{aligned} \tag{D.14}$$

We now define the quantity $\mathcal{D}_2(\theta,\theta')$ by

$$\begin{aligned}\mathcal{D}_2(\theta,\theta') &= \frac{1}{2\pi}\int_{-\pi}^{\pi}\mathrm{d}\xi\frac{e^{i\xi(\theta-\theta')}+e^{i\xi(\theta+\theta')}}{[L_d(\xi)]^2},\\ &= \frac{1}{\pi}\int_0^{\pi}\mathrm{d}\xi\frac{2\cos\xi\theta\cos\xi\theta'}{[L_d(\xi)]^2}.\end{aligned} \tag{D.15}$$

If $t=t'$, the expression of $\mathbb{E}\left[\Delta A_\theta(t)\Delta A_{\theta'}(t')\right]$ becomes

$$\begin{aligned}&\mathbb{E}\left[\Delta A_\theta(t)\Delta A_{\theta'}(t)\right]\\ &= \frac{2D}{2\pi}\int_{-\pi}^{\pi}\mathrm{d}\xi\frac{e^{i\xi(\theta-\theta')}+e^{i\xi(\theta+\theta')}}{[L_d(\xi)]^2}\left\{\Delta t+\frac{\tau}{L_d(\xi)}\left(e^{-\frac{L_d(\xi)}{\tau}\Delta t}-1\right)\right\},\\ &\xrightarrow[\tau\mapsto 0]{} 2D\Delta t\mathcal{D}_2(\theta,\theta').\end{aligned} \tag{D.16}$$

Note that in the other limit $\tau \gg 1$, one finds that

$$\mathbb{E}\left[\Delta A_\theta(t)\Delta A_{\theta'}(t)\right] \approx D\frac{\Delta t^2}{\tau}\mathcal{D}_1(\theta,\theta') \tag{D.17}$$

This encodes the Epps effect: correlations tend to zero at very small time resolutions.

Otherwise, if $|t-t'|>\Delta t$, we obtain

$$\begin{aligned}&\mathbb{E}\left[\Delta A_\theta(t)\Delta A_{\theta'}(t')\right]\\ &= -\frac{\tau D\Delta t}{\pi}\int_{-\pi}^{\pi}\mathrm{d}\xi\frac{e^{i\xi(\theta-\theta')}+e^{i\xi(\theta+\theta')}}{[L_d(\xi)]^3} \qquad \left(e^{-\frac{L_d(\xi)}{\tau}(t-t')}+e^{-\frac{L_d(\xi)}{\tau}(t-t'-\Delta t)}\right)\\ &\xrightarrow[\tau\mapsto 0]{} 0\end{aligned} \tag{D.18}$$

Hence, for $\tau$ close to 0, the covariance of $\Delta A$ can be written as

$$\mathbb{E}\left[\Delta A_\theta(t)\Delta A_{\theta'}(t')\right] = \begin{cases}0, \text{ if } |t-t'|>\Delta t,\\ 2D\Delta t\mathcal{D}_2(\theta,\theta'), \text{ if } t=t'.\end{cases} \tag{D.19}$$

## D.3 Closed formulas for the correlators when $\psi \gg 1$

We perform a rotation of the tenors $\theta$ and $\theta'$ in order to formulate our model in relation to the diagonal and anti-diagonal elements of the variance-covariance matrix.

$$\begin{cases} \theta_+ = \theta + \theta', \\ \theta_- = \theta - \theta', \end{cases} \tag{D.20}$$

For integer $\theta$'s, a second change of variable $z = e^{i\xi}$ allows us to write $\mathcal{D}_k$ as a contour integral

$$\mathcal{D}_k(\theta_+;\theta_-) = \frac{\nu^4}{2\pi}\int_{\gamma(1)} \frac{z^{|\theta_-|+1} + z^{\theta_++1}}{P(z)^k}, \tag{D.21}$$

where $P(z) = z^2 - z\left(\frac{z-1}{\mu}\right)^2 + \left(\frac{z-1}{\nu}\right)^4$ and $\gamma(1)$ is the unit circle. The residue theorem then yields

$$\begin{aligned} \mathcal{D}_1(\theta,\theta') = \nu^4 &\frac{(\beta_-^+)^{|\theta_-|+1} + (\beta_-^+)^{\theta_++1}}{(\beta_-^+ - \beta_+^+)(\beta_-^+ - \beta_+^-)(\beta_-^+ - \beta_-^-)} \\ +\nu^4 &\frac{(\beta_-^-)^{|\theta_-|+1} + (\beta_-^-)^{\theta_++1}}{(\beta_-^- - \beta_+^+)(\beta_-^- - \beta_+^-)(\beta_-^- - \beta_-^+)}, \end{aligned} \tag{D.22}$$

where,

$$\begin{aligned} \beta_\pm^+ &= 1 + \frac{\alpha_+ \pm \sqrt{\alpha_+(\alpha_+ + 4)}}{2}, \\ \beta_\pm^- &= 1 + \frac{\alpha_- \pm \sqrt{\alpha_-(\alpha_- + 4)}}{2}, \\ \alpha_\pm &= \frac{\nu^4}{2\mu^2}\left(1 \pm \sqrt{1 - 4\left(\frac{\mu}{\nu}\right)^4}\right). \end{aligned} \tag{D.23}$$

Similarly, one computes $\mathcal{D}_2(\theta,\theta')$ thanks to the residue theorem:

$$\mathcal{D}_2(\theta,\theta') = \mathrm{Res}(g,\beta_-^+) + \mathrm{Res}(g,\beta_-^-), \tag{D.24}$$

where $g(z) = \nu^8 \frac{z^{|\theta_-|+3} + z^{\theta_++3}}{P(z)^2}$ and the residuals $\mathrm{Res}(g,\beta_-^+)$ and $\mathrm{Res}(g,\beta_-^-)$ at the

poles $\beta_-^+$ and $\beta_-^-$ are given by

$$\begin{aligned}\mathrm{Res}(g,\beta_-^+) = \nu^8 &\frac{(\beta_-^+)^{|\theta_-|+2}+(\beta_-^+)^{\theta_++2}}{(\beta_-^+-\beta_+^+)^2(\beta_-^+-\beta_+^-)^2(\beta_-^+-\beta_-^-)^2}\\ &+\nu^8\frac{(\beta_-^+)^{|\theta_-|+3}+(\beta_-^+)^{\theta_++3}}{(\beta_-^+-\beta_+^+)^3(\beta_-^+-\beta_+^-)^3(\beta_-^+-\beta_-^-)^3}\\ \times\left((\beta_-^+-\beta_+^-)(\beta_-^+-\beta_-^-)\right.&+(\beta_-^+-\beta_+^+)(\beta_-^+-\beta_-^-)+\left.(\beta_-^+-\beta_+^+)(\beta_-^+-\beta_+^-)\right),\end{aligned} \tag{D.25}$$

and by

$$\begin{aligned}\mathrm{Res}(g,\beta_-^-) = \nu^8 &\frac{(\beta_-^-)^{|\theta_-|+2}+(\beta_-^-)^{\theta_++2}}{(\beta_-^--\beta_+^+)^2(\beta_-^--\beta_+^-)^2(\beta_-^--\beta_-^+)^2}\\ &+\nu^8\frac{(\beta_-^-)^{|\theta_-|+3}+(\beta_-^-)^{\theta_++3}}{(\beta_-^--\beta_+^+)^3(\beta_-^--\beta_+^-)^3(\beta_-^--\beta_-^+)^3}\\ \times\left((\beta_-^--\beta_+^-)(\beta_-^--\beta_-^+)\right.&+(\beta_-^--\beta_+^+)(\beta_-^--\beta_-^+)+\left.(\beta_-^--\beta_+^+)(\beta_-^--\beta_+^-)\right).\end{aligned} \tag{D.26}$$

## D.4 Solution to the discretized Master Equation when $\psi \ll 1$

To ensure the validity of the method of images we need $A_{-\theta}$ to be a solution of the unconstrained problem if $A_\theta$ is a solution. Therefore, we assume that $\psi \ll \theta$. As shown below, in this case, the model can be written as a function of the products $\mu\psi$ and $\nu\psi$ only. Hence, one can choose the parameter $\psi$ to be arbitrarily small to ensure that $\psi \ll 1 \leq \theta$. In this limit, the matrix $\mathcal{M}$ in Eq. (7.16) becomes:

$$\begin{aligned}\mathcal{M}_{\theta\theta'} := I_{\theta\theta'}&\\ &+\theta\left(\frac{1}{\kappa_2^4}-\frac{1}{\kappa_1^2}\right)\left(\frac{1}{2}I_1-\frac{1}{2}I_{-1}\right)_{\theta\theta'}\\ &+\theta^2\left(\frac{7}{\kappa_2^4}-\frac{1}{\kappa_1^2}\right)\left(I_1-2I+I_{-1}\right)_{\theta\theta'}\\ &+\frac{6\theta^3}{\kappa_2^4}\left(\frac{1}{2}I_2-I_1+I_{-1}-\frac{1}{2}I_{-2}\right)_{\theta\theta'}\\ &+\frac{\theta^4}{\kappa_2^4}\left(I_2-4I_1+6I-4I_{-1}+I_{-2}\right)_{\theta\theta'}.\end{aligned} \tag{D.27}$$

where we note $\kappa_1$ and $\kappa_2$ for $\mu\psi$ and $\nu\psi$ respectively, without loss of generality.

For $(\theta, \theta') \in \mathbb{Z}$ we define the *propagator matrix* $\mathcal{G}_{\theta\theta'}(t, t')$ as the solution to

$$\frac{\partial \mathcal{G}}{\partial t}(t-t') + \frac{1}{\tau}\mathcal{M}\mathcal{G}(t-t') = \delta(t-t')I. \tag{D.28}$$

The propagator reads

$$\mathcal{G}(t-t') = H(t-t')e^{-\frac{t-t'}{\tau}\mathcal{M}}. \tag{D.29}$$

Let $n$ be the number of available SOFR Futures. We assume that the matrix $\mathcal{M}$ is of size $2N+1$ with $N \gg n$. We define the indices of the lines and columns of $\mathcal{M}$ in the range $[-N, N]$.

The matrix $\mathcal{M}$ is invariant by a central symmetry with respect to the center of the matrix $\mathcal{M}_{00}$:

$$\mathcal{M} = \bar{I}\mathcal{M}\bar{I}, \tag{D.30}$$

where $\bar{I}$ is a matrix with ones only on its largest anti-diagonal. Hence, $\mathcal{F}_{\theta\theta'}(t-t') := \mathcal{G}_{-\theta\theta'}(t-t')$ is a solution for $(\theta, \theta') \in \mathbb{Z}$ of the following equation:

$$\frac{\partial \mathcal{F}}{\partial t}(t-t') + \frac{1}{\tau}\mathcal{M}\mathcal{F}(t-t') = \delta(t-t')\bar{I}. \tag{D.31}$$

It yields a solution for $(\theta, \theta') \in \mathbb{Z}$:

$$\mathcal{F}(t-t') = H(t-t')e^{-\frac{t-t'}{\tau}\mathcal{M}}\bar{I}. \tag{D.32}$$

By the method of images, the propagator $G$ for $(\theta, \theta') \in \mathbb{Z}^2$ associated to the solution that satisfies the Neumann boundary condition, is given by:

$$G(t-t') := H(t-t')e^{-\frac{t-t'}{\tau}\mathcal{M}}\left(I + \bar{I}\right). \tag{D.33}$$

As the bottom left (i.e. $\theta > 0$ and $\theta' < 0$) and top right bloc matrices (i.e. $\theta < 0$ and $\theta' > 0$) of $\mathcal{M}$ are nil, the restriction of the matrix $e^{-\frac{t-t'}{\tau}\mathcal{M}}(I + \bar{I})$ to positive $\theta$ is equal to the product of the restricted matrices $e^{-\frac{t-t'}{\tau}\mathcal{M}}$ and $I + \bar{I}$. We note $\mathcal{J}$ the restriction to positive values of $\theta$ of the matrix $I + \bar{I}$:

$$\mathcal{J}_{\theta\theta'} = \begin{cases} 2, \text{ if } \theta = \theta' = 0, \\ 1, \text{ if } \theta = \theta' > 0, \\ 0, \text{ if } \theta \neq \theta'. \end{cases} \tag{D.34}$$

Finally, for $\theta \in \mathbb{N}$, the solution $A$ to Eq. (7.16) is given by

$$\begin{aligned} A(t) &= \frac{1}{\tau}\int_{-\infty}^{t} \mathrm{d}t' G(t-t')\eta(t') \\ &= \frac{1}{\tau}\int_{-\infty}^{t} \mathrm{d}t' e^{-\frac{t-t'}{\tau}\mathcal{M}}\mathcal{J}\eta(t') \end{aligned} \tag{D.35}$$

## D.5 Noise correlators when $\psi \ll 1$

### D.5.1 Autocovariance of the correlated noise for $\tau = 0$

For $\tau \to 0$, $e^{-\frac{t-t'}{\tau}\mathcal{M}} \to \tau \mathcal{M}^{-1}\delta(t-t')$. Hence we can derive a closed formula for the noise $A$:

$$A(t) = \mathcal{M}^{-1}\mathcal{J}\eta(t) \tag{D.36}$$

Thus, the autocovariance of A is given by

$$\mathbb{E}\left[A(t)A(t')^\top\right] = 2D\delta(t-t')\mathcal{M}^{-1}\mathcal{J}^2(\mathcal{M}^{-1})^\top. \tag{D.37}$$

In this limit, the autocovariance of $\Delta A$, the coarse-grain cumulative sum of $A(t)$ over the time interval $\Delta t \gg \tau$, is given by

$$\mathbb{E}\left[\Delta A(t)\Delta A(t')^\top\right] = \begin{cases} 0, \text{ if } |t-t'| > \Delta t, \\ 2D\Delta t\mathcal{M}^{-1}\mathcal{J}^2(\mathcal{M}^{-1})^\top, \text{ if } t = t'. \end{cases} \tag{D.38}$$

Finally, the equal-time Pearson correlation coefficient among coarse-grained forward rate variations $\Delta f_\theta$ is given by

$$\rho_{\theta\theta'} = \frac{\left(\mathcal{M}^{-1}\mathcal{J}^2(\mathcal{M}^{-1})^\top\right)_{\theta\theta'}}{\sqrt{\left(\mathcal{M}^{-1}\mathcal{J}^2(\mathcal{M}^{-1})^\top\right)_{\theta\theta}\left(\mathcal{M}^{-1}\mathcal{J}^2(\mathcal{M}^{-1})^\top\right)_{\theta'\theta'}}}. \tag{D.39}$$

### D.5.2 Autocovariance of the correlated noise for $\tau > 0$

We assume $\mathcal{M}$ is diagonalizable. We define $P$ as the transformation matrix of $\mathcal{M}$, i.e.

$$\mathcal{M} := P\Lambda P^{-1} := \sum_{k\in\mathbb{N}} \lambda_k U_k V_k^\top \tag{D.40}$$

where the $U_k$ are the column vectors of the matrix $P$, $V_k^\top$ are line vectors of the matrix $P^{-1}$, and $\lambda_k$ are the eigenvalues of $\mathcal{M}$. The noise field $A$ can be expressed in this new basis as

$$A(t) = \frac{1}{\tau}\sum_{k\in\mathbb{N}} \int_{-\infty}^{t} \mathrm{d}t' e^{-\frac{t-t'}{\tau}\lambda_k}\eta(t')U_k V_k^\top \mathcal{J} \tag{D.41}$$

The autocovariance of $A$ reads

$$\begin{aligned}
&\mathbb{E}\left[A(t)A(t')^\top\right] \\
&= \frac{2D}{\tau^2}\sum_{(k,k')\in\mathbb{N}^2} U_k V_k^\top \mathcal{J}^2 V_{k'} U_{k'}^\top \int_{-\infty}^{\min(t,t')} \mathrm{d}u e^{-\frac{t-u}{\tau}\lambda_k - \frac{t'-u}{\tau}\lambda_{k'}}, \\
&= \frac{2D}{\tau}\sum_{(k,k')\in\mathbb{N}^2} \frac{K_{kk'}}{\lambda_k+\lambda_{k'}} e^{\frac{1}{\tau}(-\lambda_k t - \lambda_{k'} t' + (\lambda_k+\lambda_{k'})\min(t,t'))},
\end{aligned} \tag{D.42}$$

where the matrices $K_{kk'}$ are defined by $K_{kk'} := U_k V_k^\top \mathcal{J}^2 V_{k'} U_{k'}^\top$. We now recall the definition of the cumulative sum of $A$ over an interval of lenght $\Delta t$:

$$\Delta A(t) := \int_{t-\Delta t}^{t} \mathrm{d}u A(u) \tag{D.43}$$

Hence, the autocovariance of $\Delta A$ reads

$$\begin{aligned}
&\mathbb{E}\left[\Delta A(t)\Delta A(t')^\top\right] \\
&= \int_{t-\Delta t}^{t}\mathrm{d}u\int_{t'-\Delta t}^{t'}\mathrm{d}u'\mathbb{E}\left[A(u)A(u')^\top\right] \\
&= \frac{2D}{\tau}\sum_{(k,k')\in\mathbb{N}^2}\frac{K_{kk'}}{\lambda_k+\lambda_{k'}}\int_{t-\Delta t}^{t}\mathrm{d}u\int_{t'-\Delta t}^{t'}\mathrm{d}u' e^{\frac{1}{\tau}(-\lambda_k u - \lambda_{k'}u' + (\lambda_k+\lambda_{k'})\min(u,u'))}
\end{aligned} \tag{D.44}$$

For $t = t'$, we have,

$$\begin{aligned}
&\mathbb{E}\left[\Delta A(t)\Delta A(t)^\top\right] = 2D\sum_{(k,k')\in\mathbb{N}^2}\frac{K_{kk'}}{\lambda_k+\lambda_{k'}}\Bigg\{ \\
&\Delta t(\frac{1}{\lambda_k}+\frac{1}{\lambda_{k'}}) + \tau\left(\frac{1}{\lambda_k^2}(e^{-\frac{\Delta t}{\tau}\lambda_k}-1) + \frac{1}{\lambda_{k'}^2}(e^{-\frac{\Delta t}{\tau}\lambda_{k'}}-1)\right)\Bigg\}.
\end{aligned} \tag{D.45}$$

Notably, in the stationary limit, for $\tau$ close to zero,

$$\mathbb{E}\left[\Delta A(t)\Delta A(t)^\top\right] = 2D\sum_{(k,k')\in\mathbb{N}^2}\frac{K_{kk'}}{\lambda_k\lambda_{k'}}\Delta t \tag{D.46}$$

In the other limit $\tau \gg 1$, one finds that

$$\mathbb{E}\left[\Delta A_\theta(t)\Delta A_{\theta'}(t)\right] \approx 2D\sum_{(k,k')\in\mathbb{N}^2}\frac{K_{kk'}}{\lambda_k+\lambda_{k'}}\frac{\Delta t^2}{\tau} \tag{D.47}$$

This encodes the Epps effect: correlations tend to zero at very small time resolutions.

## D.6 The Baaquie-Bouchaud Logarithm model

The stiff propagator BB04 model (Baaquie and Bouchaud, 2004) proposed the change of variable $\bar{z}(\theta) = \theta^{\bar{\psi}}$. As mentioned in section 7.3.2, this formulation violates the constraint that for very small maturities psychological time and real time should become equivalent. In addition, this change of variable is mis-specified for $\psi$ close to zero. Indeed, for fixed $\theta$

$$\bar{z}(\theta) \xrightarrow[\psi \mapsto 0]{} 1. \tag{D.48}$$

Remediating these two limitations requires introducing two parameters, $\psi$ and $\zeta$, in the definition of the psychological time:

$$\bar{z}(\theta) = \frac{\psi}{\zeta}\left(\left(1 + \frac{\theta}{\psi}\right)^{\zeta} - 1\right), \tag{D.49}$$

where $\psi$ has dimensions of time and $\zeta$ is a pure number $\leq 1$. For this new change of variable $\bar{z}(\theta)$ is equivalent to $\theta$ for $\theta$ approaching 0, proportional to $\theta^{\zeta}$ for large values of $\theta$, and equal to $\theta$ for $\zeta = 1$. Moreover, for $\zeta$ approaching 0,

$$\bar{z}(\theta) \approx \psi \log\left(1 + \frac{\theta}{\psi}\right) = z(\theta) \tag{D.50}$$

Actually, we found that the calibration of the BB04 with the change of variable $\bar{z}$ yields an optimal value for $\zeta$ very close to 0. Hence we define a regularized version of the BB04 model by replacing $\bar{z}(\theta)$ by $z(\theta)$. For such a specification, the equal-time Pearson correlation is given by

$$\tilde{\rho}_{\theta\theta'} = \frac{\mathcal{D}_{BB}(z(\theta), z(\theta'))}{\sqrt{\mathcal{D}_{BB}(z(\theta), z(\theta))\mathcal{D}_{BB}(z(\theta'), z(\theta'))}}, \tag{D.51}$$

a result we will refer to as BBL3 model for Baaquie-Bouchaud, Logarithm, three parameters.

## D.7 Two-parameter versions

In this section, we compare the performances of the two-parameter variants of our models by assigning to the stiffness parameter $\nu$ an infinite value. This adjustment applies to: (i) the regularized version BBL3 of the continuous model from Baaquie and Bouchaud, 2004, using Eq. (D.51); (ii) our micro-founded discrete model BBD3, using Eq. (7.25). These models are denoted as BBL2 and BBD2 respectively.

| Model | $\psi^*$ (months) | $\mu^*$ |
|---|---|---|
| BBL2 | $1.27 \times 10^{-5}$ | $5.21 \times 10^4$ |
| BBD2 | 2.00 | 1.01 |

**Table D.1:** Optimal parameters obtained when fitting the tested models to empirical Pearson correlations for the period $1994 - 2023$. Two models are considered: (i) the continuous regularized model BBL2 (Eq. (D.51) with $\nu = \infty$) and our micro-founded discrete model BBD2 (Eq. (7.25) with $\nu = \infty$). While $\mu$ is dimensionless in the discrete models, this parameter is in units of 3 months$^{-1}$ in the case of the BBL2 model.

Optimal calibration parameters, obtained by fitting these models to empirical Pearson correlations for the period $1994 - 2023$, are displayed in table D.1. The BBD2 model presents plausible values for the psychological time and line tension parameters. In contrast, the BBL2 model results in improbable values for $\psi$ and $\mu$. As previously mentioned, this is primarily because the correlation surface develops a cusp around the diagonal $\theta = \theta'$, which was actually the very reason why Baaquie and Bouchaud (2004) introduced the stiffness term $\nu$.

Figure D.1 depicts the correlation coefficients along the most extended anti-diagonal for the period $1994 - 2023$ as determined by the calibration of the BBL2 and BBD2. It also illustrates the typical error across the correlation surface, underscoring the superior precision of the BBD2 model relative to the continuous variant.

## D.8 Epps effect when $\psi \gg 1$

Each colored line in Fig. D.2 represents the correlation $\rho_{\theta\theta'}$ across different time scales $\Delta t$ among pairs of forward rate variations $(\Delta f_\theta, \Delta f_{\theta'})$, as given by our model in the case $\psi \gg 1$ (see Eq. (D.16)) calibrated on daily correlations (see section 7.5.2) with the additional fitting parameter $\varepsilon$. For the pair 30-33 months, we find $\varepsilon \approx 0.026$ ($\mathcal{C}(\theta, \theta')$ is in the range of 0.14 to 0.48 when $\psi \gg 1$) and $\tau \approx 21$ minutes. Fig. D.2 demonstrates that our model is able to reproduce the whole dependence of the empirical correlations of pairs of SOFR Futures binned at different time scales.

## D.9 Curvature along the anti-diagonals

One of the most salient successes of the BB04 model is its ability, in line with observations, to reproduce the power-law decay of the curvature of forward rate correlations perpendicular to the diagonal. Fig. D.3 shows estimations of the curvatures generated by the tested models and the ones empirically observed.

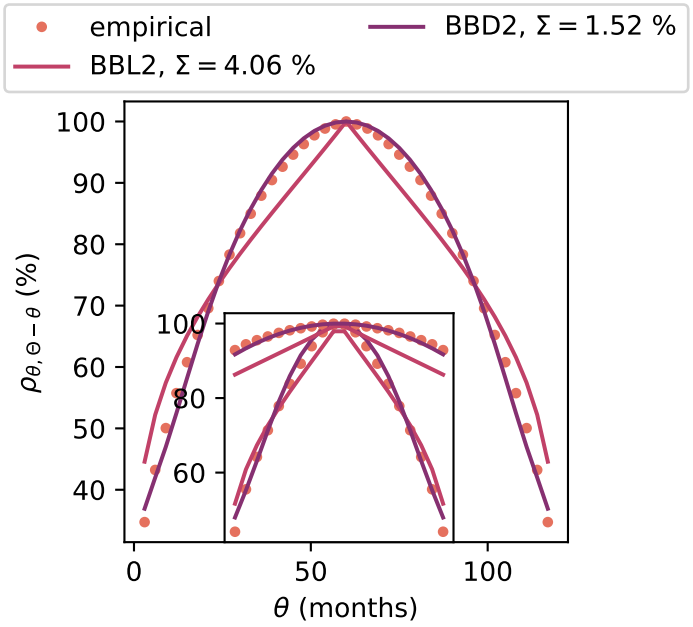


**Figure D.1:** Dots represent the empirical correlation $\rho_{\theta\theta'}$ along the longest stretch perpendicular to the diagonal, i.e. $\theta' = \Theta - \theta$ , where $\Theta$ is the maximum available maturity. The plain lines are the best fit for: (i) the regularized version BBL2 of the continuous model Baaquie and Bouchaud, 2004, using Eq. (D.51) with $\nu = \infty$; our micro-founded discrete model BBD2, using Eq. (7.25) with $\nu = \infty$.

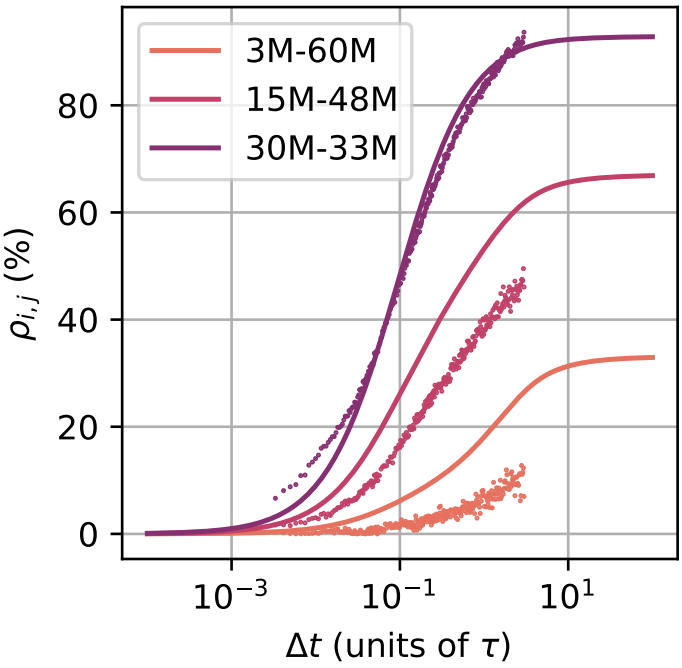


**Figure D.2:** Plain lines: theoretical Pearson correlation coefficients among three pairs of forward rate variations $(\Delta f_\theta, \Delta f_{\theta'})$ as a function of the time scale $\Delta t$ (see (D.16)). Using the empirical correlations of the pair 30-33 months, the parameter $\varepsilon$ of the idiosyncratic white noise was calibrated to 0.026, and the characteristic time of the Epps effect$\tau$ to 21 minutes. This figure also shows the theoretical correlations yielded by this set of parameters for two other pairs (15-48 and 3-60 months). Dots: empirical Pearson correlation coefficients for three pairs of SOFR Futures prices for the year 2021 at time scales ranging from 4 seconds to one hour.

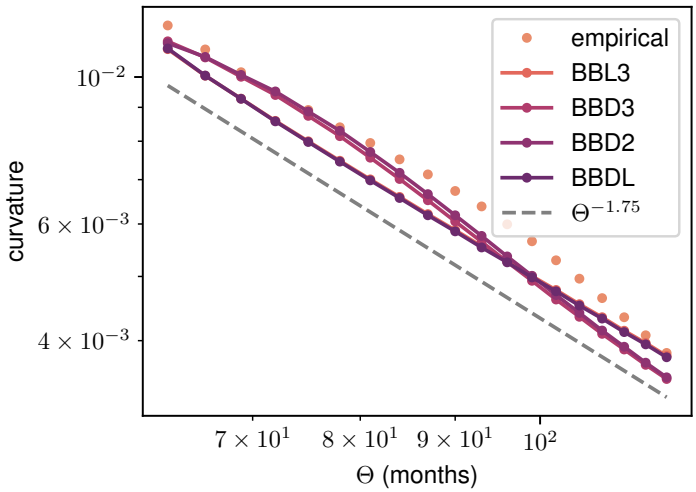


**Figure D.3:** Curvature of the correlation surface along the stretches perpendicular to the diagonal, i.e. $\theta' = \Theta - \theta$ as a function of largest tenor $\Theta$ for the $1994 - 2023$ period. Here we compare the continuous regularized model BBL3 (Eq. (D.51)) with our three micro-founded discrete models: BBD3 (Eq. (7.25)), BBD2 (Eq. (7.25) with $\nu \to \infty$), and BBDL (Eq. (7.29)).

These estimations are produced through the fitting of parabolas using 20 points around the center of each anti-diagonal of the correlation surface for the $1994 - 2023$ period. Fig. D.3 reveals the adequacy of the continuous model BBL3, and the discrete models, BBD3, BBD2, and BBDL, with the observed curvature. However, one can notice a slight change of convexity in the curvature for BBD3 and BBD2: this is probably due to the change of variable in $z(\theta)$ in Eq. 7.25.

# Appendix E

# Cross-impact field theory

*This section reproduces the appendices of Le Coz et al. (2024c).*

## E.1 Responses to the white noise for $\psi \gg 1$

### E.1.1 Covariance

We derive the covariance between $\Delta A_\theta(t)$ and $\Delta\eta_{\theta'}(t)$ in the limit $\psi \gg 1$:

$$\begin{aligned}
&\mathbb{E}\left[\Delta A_\theta(t)\Delta\eta_{\theta'}(t)\right] \\
&= \int_{t-\Delta t}^{t} \mathrm{d}u \int_{t-\Delta t}^{t} \mathrm{d}v \mathbb{E}\left[A_\theta(u)\eta_{\theta'}(v)\right] \\
&= \frac{1}{\tau}\int_{t-\Delta t}^{t} \mathrm{d}u \int_{t-\Delta t}^{u} \mathrm{d}v G_{\theta,\theta'}(u-v) \\
&= \frac{1}{2\pi\tau}\int_{-\pi}^{\pi} \mathrm{d}\xi \left(e^{i\xi(\theta-\theta')} + e^{i\xi(\theta+\theta')}\right) \int_{t-\Delta t}^{t} \mathrm{d}u \int_{t'-\Delta t}^{u} \mathrm{d}v e^{-\frac{L_d(\xi)}{\tau}(u-v)} \\
&= \frac{1}{2\pi}\int_{-\pi}^{\pi} \mathrm{d}\xi \frac{e^{i\xi(\theta-\theta')} + e^{i\xi(\theta+\theta')}}{L_d(\xi)} \int_{t-\Delta t}^{t} \mathrm{d}u \left(1 - e^{-\frac{L_d(\xi)}{\tau}(u-t+\Delta t)}\right) \\
&\xrightarrow[\tau\mapsto 0]{} \Delta t(\mathcal{D}_1)_{\theta\theta'}.
\end{aligned} \tag{E.1}$$

### E.1.2 Correlation

Using Eq. (E.1), we obtain the correlation between $\Delta A_\theta(t)$ and $\Delta\eta_{\theta'}(t)$:

$$\frac{\mathbb{E}\left[\Delta A_\theta(t)\Delta\eta_{\theta'}(t)\right]}{\sqrt{\mathbb{E}\left[\Delta A_\theta(t)^2\right]\mathbb{E}\left[\Delta\eta_{\theta'}(t)^2\right]}} = \frac{(\mathcal{D}_1)_{\theta\theta'}}{\sqrt{(\mathcal{D}_2)_{\theta\theta}}}. \tag{E.2}$$

We can show that Eq. (E.2) is well defined. For this purpose, we define the usual inner product $(f, g)$ between two integrable real-valued functions $f$ and $g$ on $[0, \pi]$ by:

$$(f, g) = \frac{1}{\pi} \int_0^\pi \mathrm{d}\xi f(\xi) g(\xi). \tag{E.3}$$

For $(\theta, \theta') \in [\![1, n]\!]^2$, having noted that $\frac{2}{\pi} \int_0^\pi \mathrm{d}\xi \cos^2 \xi\theta = 1$, we have:

$$(\mathcal{D}_1)_{\theta\theta'} = \left( \frac{\sqrt{2}\cos\xi\theta}{L_d(\xi)}, \sqrt{2}\cos\xi\theta' \right), \tag{E.4}$$

$$(\mathcal{D}_2)_{\theta\theta} = \left( \frac{\sqrt{2}\cos\xi\theta}{L_d(\xi)}, \frac{\sqrt{2}\cos\xi\theta}{L_d(\xi)} \right) \left( \sqrt{2}\cos\xi\theta', \sqrt{2}\cos\xi\theta' \right). \tag{E.5}$$

Thus, Cauchy-Schwarz's inequality ensures that

$$-1 \leq \frac{(\mathcal{D}_1)_{\theta\theta'}}{\sqrt{(\mathcal{D}_2)_{\theta\theta}}} \leq 1. \tag{E.6}$$

## E.2 Responses to the white noise for $\psi \ll 1$

### E.2.1 Covariance

We derive the covariance between $\Delta A_\theta(t)$ and $\Delta\eta_{\theta'}(t)$ in the limit $\psi \ll 1$:

$$\begin{aligned}
&\mathbb{E}\left[\Delta A(t) \Delta\eta(t)^\top\right] \\
&= \int_{t-\Delta t}^t \mathrm{d}u \int_{t-\Delta t}^t \mathrm{d}v \mathbb{E}\left[A(u)\eta(v)^\top\right] \\
&= \frac{1}{\tau} \int_{t-\Delta t}^t \mathrm{d}u \int_{t-\Delta t}^u \mathrm{d}v e^{-\frac{u-v}{\tau}\mathcal{M}} \mathcal{J} \\
&= \int_{t-\Delta t}^t \mathrm{d}u \mathcal{M}^{-1} \left(1 - e^{-\frac{u-t+\Delta t}{\tau}\mathcal{M}}\right) \mathcal{J} \\
&\xrightarrow[\tau \mapsto 0]{} \Delta t \mathcal{M}^{-1} J.
\end{aligned} \tag{E.7}$$

### E.2.2 Correlation

Using Eq. (E.7), we obtain the correlation between $\Delta A_\theta(t)$ and $\Delta\eta_{\theta'}(t)$:

$$\frac{\mathbb{E}\left[\Delta A_\theta(t) \Delta\eta_{\theta'}(t)\right]}{\sqrt{\mathbb{E}\left[\Delta A_\theta(t)^2\right] \mathbb{E}\left[\Delta\eta_{\theta'}(t)^2\right]}} = \frac{\left(\mathcal{M}^{-1}\mathcal{J}\right)_{\theta\theta'}}{\sqrt{(\mathcal{M}^{-1}\mathcal{J}^2(\mathcal{M}^{-1})^\top)_{\theta\theta}}}, \tag{E.8}$$

which is clearly well defined.

## E.3 Order flow decomposition

Let $\eta^q$ be a white noise vector such that $\mathbb{E}\left[\eta^q_\theta(t)\eta^q_{\theta'}(t')\right] = \delta_{\theta\theta'}\delta(t-t')$. We decompose the trading flow across time and space into the cumulative sum of $\eta^q$ and a kernel $K$:

$$\frac{\mathrm{d}q}{\mathrm{d}t}(t) = \int_{-\infty}^{t} \mathrm{d}t' K(t,t') O^\top \eta^q(t'), \tag{E.9}$$

where $O$ is an orthogonal matrix and the kernel $K(u,u') \in \mathbf{M}_n(\mathbb{R})$ is such that the lagged variance-covariance matrix $\Omega(t,t')$ of the infinitesimal order flow imbalance reads

$$\begin{aligned}
\Omega(t,t') :=& \mathbb{E}\left[\frac{\mathrm{d}q}{\mathrm{d}t}(t)\frac{\mathrm{d}q}{\mathrm{d}t}^\top(t')\right] \\
=& \int_{-\infty}^{t} \mathrm{d}u \int_{-\infty}^{t'} \mathrm{d}v K(t,u) O^\top \mathbb{E}\left[\eta^q(u)\eta^q(v)^\top\right] O K^\top(t',v) \\
=& \int_{-\infty}^{\min(t,t')} \mathrm{d}u K(t,u) K^\top(t',u).
\end{aligned} \tag{E.10}$$

We assume that the series of matrices $(K(t,t'))_{t\geq 0, t'\geq 0}$ can be written $K(t-t')_{t-t'\geq 0}$. Under this assumption, the lagged variance-covariance matrix $\Omega(t,t')$ is stationary and can be written as a function of the lag $\ell = t - t'$:

$$\begin{aligned}
\Omega(t, t-l) &= \int_{\mathbb{R}} \mathrm{d}u K(t-u) K^\top(t-\ell-u) \\
&= \int_{\mathbb{R}} \mathrm{d}u' K(u') K^\top(u'-\ell).
\end{aligned} \tag{E.11}$$

The Fourier transform over the lag $\ell$ of Eq. (E.11) reads

$$\mathcal{F}[\Omega](m) = \mathcal{F}[K](m)\{\mathcal{F}[K](m)\}^\top, \tag{E.12}$$

where $\mathcal{F}[K]$ and $\mathcal{F}[\Omega]$ are the Fourier transform of $\ell \to K(\ell)$ and $\ell \to \Omega(\ell)$. Thus, Eq. (E.9) is verified if and only if, each matrix $\mathcal{F}[K](m)$ is a decomposition of $\mathcal{F}[\Omega](m)$:

$$\mathcal{F}[K](m) = \{\mathcal{F}[\Omega](m)\}^{1/2}. \tag{E.13}$$

For example, we can build numerically each $\mathcal{F}[K](m)$ as the Cholesky decomposition of $\mathcal{F}[\Omega](m)$.

Still assuming stationarity, the definition of $q(t)$ in Eq. (E.9) reads as the convolution product of $K$ and $\eta$. The Fourier transform over time of Eq. (E.9) reads in matrix notations

$$\mathcal{F}\left[\frac{\mathrm{d}q}{\mathrm{d}t}\right](m) = \mathcal{F}[K](m)O^{\top}\mathcal{F}[\eta^q](m). \tag{E.14}$$

Assuming the matrix $\hat{K}(m)$ is invertible one can write Eq. (E.14) as

$$\mathcal{F}[\eta^q](m) = O\{\mathcal{F}[K](m)\}^{-1}\mathcal{F}\left[\frac{\mathrm{d}q}{\mathrm{d}t}\right](m). \tag{E.15}$$

Hence, one can also write the white noise $\eta^q$ as the convolution product:

$$\eta^q(t) = O\int_{-\infty}^{t}\mathrm{d}t' J(t-t')\frac{\mathrm{d}q}{\mathrm{d}t}(t'), \tag{E.16}$$

where the function $u \mapsto J(u)$, valued in $\mathbf{M}_n(\mathbb{R})$, is the inverse Fourier transform of $m \mapsto \{\mathcal{F}[K](m)\}^{-1}$.

## E.4 Large-bin approximation

In this section, we denote by $\bar{x}_{\Delta t}$ the observed empirical average over the time interval $[t-\Delta t, t]$ of the random process $x(t)$ (i.e., its moving average):

$$\bar{x}_{\Delta t}(t) := \frac{1}{\Delta t}\int_{t-\Delta t}^{t}\mathrm{d}t' x(t'). \tag{E.17}$$

We aim to approximate $\Delta A_\theta(t)$ as a function of coarse-grained variables $\Delta\eta$ defined over intervals of finite width $\Delta t$. For this purpose, we decompose the white noise $\eta(t')$ as the sum of its moving average and its fluctuations around this mean. Formally, we write

$$\eta(t') = \bar{\eta}_{\Delta t}(t) + \eta(t') - \bar{\eta}_{\Delta t}(t). \tag{E.18}$$

The independence and stationarity of $\eta$ across time ensures that $\bar{\eta}_{\Delta t}(t)$ is uncorrelated with $\eta(t') - \bar{\eta}_{\Delta t}(t)$:

$$\begin{aligned}
&\mathbb{E}\left[\bar{\eta}_{\Delta t}(t)\left(\eta(t') - \bar{\eta}_{\Delta t}(t)\right)\right] \\
&= \frac{1}{\Delta t}\int_{t-\Delta t}^{t}\mathrm{d}t''\mathbb{E}\left[\eta(t')\eta(t'')\right] - \frac{1}{(\Delta t)^2}\iint_{t-\Delta t}^{t}\mathrm{d}t''\mathrm{d}t'''\mathbb{E}\left[\eta(t'')\eta(t''')\right] \\
&= \frac{1}{\Delta t} - \frac{1}{\Delta t} = 0.
\end{aligned} \tag{E.19}$$

In fact, the continuous-time hypothesis, which is related to the Gaussianity of the Langevin noise $\eta$, ensures the independence between $\bar{\eta}_{\Delta t}(t)$ and $\eta(t') - \bar{\eta}_{\Delta t}(t)$ (although only an absence of correlation is needed here). It is worth mentioning that this result can also be derive by observing that the process $\int_0^t \mathrm{d}t' \eta(t') - \int_0^t \mathrm{d}t' \bar{\eta}_{\Delta t}(t')$ is a Brownian bridge.

We now define the matrix $R^\tau(t)$ by

$$R^\tau(t) = \frac{1}{\tau} \int_{-\infty}^{t} \mathrm{d}t' G(t - t'). \tag{E.20}$$

Correlations among assets appear at a time scale $\tau \ll \Delta t$ (see Epps (1979) and chapter 5) and the time decay of $G$ is very strong : $G_{\theta\theta'}(5\tau)/G_{\theta\theta'}(0) \approx 10^{-3}$ for typical values of $\kappa \approx 1$. Hence, we can approximate $R^\tau(t)$ by

$$R^\tau(t) \approx \frac{1}{\tau} \int_{t-\Delta t}^{t} \mathrm{d}t' G(t - t'). \tag{E.21}$$

Substituting $\eta$ by Eq. (E.18) in the definition (8.4) of the noise field $A(t)$ yields

$$A(t) = R^\tau(t)\, \bar{\eta}_{\Delta t}(t) + \epsilon^\tau(t), \tag{E.22}$$

where $\epsilon^\tau(t) = \frac{1}{\tau} \int_{t-\Delta t}^{t} \mathrm{d}t' G(t - t') \left(\eta(t') - \bar{\eta}_{\Delta t}(t)\right)$ is a noise independent from $\bar{\eta}_{\Delta t}(t)$. Importantly, $\epsilon^\tau$ has no temporal correlation but has a spatial structure allowing to retrieve the spatial correlations of $A(t)$. The integration of Eq. (E.22) over the interval $[t - \Delta t, t]$ yields an affine relationship between $\Delta A$ the sum of $A$ over one day, and the empirical daily means $\bar{\eta}_{\Delta t}(t)$:

$$\Delta A(t) = \left( \int_{t-\Delta t}^{t} \mathrm{d}t' R^\tau(t') \right) \bar{\eta}_{\Delta t}(t) + \int_{t-\Delta t}^{t} \mathrm{d}t' \epsilon^\tau(t'). \tag{E.23}$$

One can substitute $\eta$ with $\eta^q$ or $\eta^\top$ and $A$ with $A^q$ or $A^\top$ respectively in Eq. (E.23). Thus, having noted that $\langle \Delta A^\perp(t) \Delta \eta^q(t) \rangle = 0$, one can relate forward rate daily increments to the empirical daily means of the martingale component of the order flow:

$$\Delta f(t) = \mathrm{diag}(\sigma)\, \mathrm{diag}(\sigma_A)^{-1} \left( \int_{t-\Delta t}^{t} \mathrm{d}t' R^\tau(t') \right) \mathrm{diag}(Y) O \Omega^{-1/2} \overline{\frac{\mathrm{d}\tilde{q}}{\mathrm{d}t}}_{\Delta t}(t) + \mathcal{E}^\tau(t), \tag{E.24}$$

where the residual noise $\mathcal{E}^\tau(t)$ is independent from $\overline{\frac{\mathrm{d}\tilde{q}}{\mathrm{d}t}}_{\Delta t}(t)$. Indeed, $\mathcal{E}^\tau(t)$ reads

$$\begin{aligned} \mathcal{E}^\tau(t) = \mathrm{diag}(\sigma)\, \mathrm{diag}(\sigma_A)^{-1} \left( \int_{t-\Delta t}^{t} \mathrm{d}t' R^\tau(t') \right) \mathrm{diag}(Y^\perp) \overline{\eta^\perp}_{\Delta t}(t) \\ + \mathrm{diag}(\sigma_A)^{-1} \int_{t-\Delta t}^{t} \mathrm{d}t' \epsilon^\tau(t'). \end{aligned} \tag{E.25}$$

Moreover, by definition of the empirical mean, we have

$$\overline{\frac{\mathrm{d}\tilde{q}}{\mathrm{d}t}}_{\Delta t}(t) = \frac{1}{\Delta t}\int_{t-\Delta t}^{t} \mathrm{d}t' \frac{\mathrm{d}\tilde{q}}{\mathrm{d}t'}(t') = \frac{\Delta\tilde{q}(t)}{\Delta t}. \tag{E.26}$$

We denote $\widehat{\Delta f}$ the conditional expectancy of the forward rates increments $\Delta f$ with respect to the martingale component of the order flows $\Delta\tilde{q}(t)$:

$$\widehat{\Delta f}(t) := \mathbb{E}\left[\Delta f(t) |\, \Delta\tilde{q}(t)\right] \tag{E.27}$$

Taking the conditional expectancy of Eq. (E.24) yields

$$\widehat{\Delta f}(t) = \mathrm{diag}(\sigma)\,\mathrm{diag}(\sigma_A)^{-1}\left(\int_{t-\Delta t}^{t} \mathrm{d}t' R^{\tau}(t')\right)\mathrm{diag}(Y) O \Omega^{-1/2}\frac{\Delta\tilde{q}(t)}{\Delta t}. \tag{E.28}$$

One can choose $\tau$ arbitrarily small in the expression of $R^{\tau}(t)$. In the limit $\tau \ll 1$ we have

$$R^{\tau}(t) \xrightarrow[\tau\to 0]{} R. \tag{E.29}$$

Thus, in this limit, Eq. (E.28) reads

$$\widehat{\Delta f}(t) = \mathrm{diag}(\sigma)\,\mathrm{diag}(\sigma_A)^{-1} R\,\mathrm{diag}(Y) O \Omega^{-1/2}\Delta\tilde{q}(t). \tag{E.30}$$

In this model, the residual noise $\mathcal{E}$ in Eq. (8.31) can be seen as the limit for small $\tau$ of $\mathcal{E}^{\tau}(t)$.

## E.5 Response to order flows

In this appendix we show that

$$\mathbb{E}\left[\Delta f(t)\Delta q^{\top}(t)\right]\mathbb{E}\left[\Delta q(t)\Delta q^{\top}(t)\right]^{-1} = \mathrm{diag}(\sigma)\,\mathrm{diag}(\sigma_A)^{-1} R\,\mathrm{diag}(Y) O \Omega^{-1/2}. \tag{E.31}$$

For this purpose we first derive the expression of the covariance $\mathbb{E}\left[\Delta f(t)\Delta q(t)^{\top}\right]$. We also show that the correlation between the forward rates and the order flows is well defined.

### E.5.1 Computation of the covariance matrix

In this section we derive the expression of the covariance between forward rates and order flows.

We define the accumulated trading flows over the period $[t, t+\Delta t]$, representing a trading day, as

$$\Delta q(t) = \int_{t-\Delta t}^{t} \mathrm{d}t' \frac{\mathrm{d}q}{\mathrm{d}t}(t'). \tag{E.32}$$

The equal-time covariance between $\Delta A^q(t)$ and $\Delta q(t)$ is

$$\mathbb{E}\left[\Delta A^q(t)\Delta q^\top(t)\right] = \iint_{t-\Delta t}^{t} \mathrm{d}u\mathrm{d}v \int_{-\infty}^{v} \mathrm{d}v' \mathbb{E}\left[A^q(u)\eta^q(v')^\top\right] OK^\top(v-v'). \tag{E.33}$$

Eq. (8.24) and (8.4) imply that $\mathbb{E}\left[A^q(u)\eta^q(v')^\top\right] = \frac{1}{\tau}G(u-v')\,\mathrm{diag}\,(Y)$, so the previous expression becomes

$$\mathbb{E}\left[\Delta A^q(t)\Delta q^\top(t)\right] = \frac{1}{\tau}\iint_{t-\Delta t}^{t} \mathrm{d}u\mathrm{d}v \int_{-\infty}^{v} \mathrm{d}v' G(u-v')\,\mathrm{diag}\,(Y)OK^\top(v-v'). \tag{E.34}$$

For $\tau \ll 1$, we have $\frac{1}{\tau}G(t-t') \to R\delta(t-t')$. It yields

$$\begin{aligned}\mathbb{E}\left[\Delta A^q(t)\Delta q(t)\right] &= R\,\mathrm{diag}\,(Y)O \iint_{t-\Delta t}^{t} \mathrm{d}u\mathrm{d}v K^\top(v-u) \\ &= \Delta t R\,\mathrm{diag}(Y)O \int_0^{\Delta t} \mathrm{d}\ell K^\top(\ell).\end{aligned} \tag{E.35}$$

Thus, the covariance between the forward rates and the order flows reads

$$\mathbb{E}\left[\Delta f(t)\Delta q^\top(t)\right] = \Delta t\,\mathrm{diag}\,\sigma\,\mathrm{diag}(\sigma_A)^{-1}R\,\mathrm{diag}(Y)O\int_0^{\Delta t}\mathrm{d}\ell K^\top(\ell), \tag{E.36}$$

having noted that $\mathbb{E}\left[\Delta A^\perp(t)\Delta q^\top(t)\right] = 0$.

### E.5.2 Computation of the response matrix

We define the cross-impact matrix $\Lambda \in \mathbf{M}_n(\mathbb{R})$ as the matrix ensuring a linear relationship between forward rates increments and order flows, i.e.,

$$\Delta f(t) = \Lambda \Delta q(t) + \mathcal{E}(t), \tag{E.37}$$

where $\mathcal{E}$ is a temporally uncorrelated noise independent from $\Delta q$. One can reformulate (E.37) as

$$\mathbb{E}\left[\Delta f(t)\Delta q(t)^\top\right] = \Lambda \mathbb{E}\left[\Delta q(t)\Delta q(t)^\top\right]. \tag{E.38}$$

Yet, the variance covariance matrix of the daily trading flow imbalance reads

$$\begin{aligned}\mathbb{E}\left[\Delta q(t)\Delta q^\top(t)\right] &= \iint_{t-\Delta t}^{t} \mathrm{d}s\mathrm{d}s'\mathbb{E}\left[\frac{\mathrm{d}q}{\mathrm{d}t}(s)\frac{\mathrm{d}q}{\mathrm{d}t}^\top(s')\right] \\ &= \iint_{t-\Delta t}^{t} \mathrm{d}s\mathrm{d}s' \int_{-\infty}^{\min(s,s')} \mathrm{d}u K(s-u)K^\top(s'-u) \\ &= \Delta t \int_0^{\Delta t} \mathrm{d}l \int_{\mathbb{R}} \mathrm{d}u K(u)K^\top(u-l). \end{aligned} \tag{E.39}$$

Hence, replacing the left-hand side in (E.38) by its expression in (E.36), we have

$$\operatorname{diag}\sigma \operatorname{diag}(\sigma_A)^{-1} R \operatorname{diag}(Y) O \int_0^{\Delta t} \mathrm{d}l K^\top(l) = \Lambda \int_0^{\Delta t} \mathrm{d}l K * K^\top(l). \tag{E.40}$$

In the most general case, Eq. (E.40) requires $\Lambda$ to be time-dependent. Yet, assuming $\mathrm{d}q$ has no temporal correlation i.e., $K(u) = \delta(u)\Omega^{1/2}$, Eq. (E.40) reads

$$\Lambda = \operatorname{diag}\sigma \operatorname{diag}(\sigma_A)^{-1} R \operatorname{diag}(Y) O \Omega^{-1/2}, \tag{E.41}$$

where the equal-time variance-covariance matrix $\Omega$ is defined by $\Omega := \frac{\mathbb{E}\left[\Delta q(t)\Delta q^\top(t)\right]}{\Delta t}$.

## E.6 Correlation between forward rates and flows

In this section, we demonstrate that the correlation between the forward rate of tenor $\theta$ and the martingale component of the order flow of tenor $\theta'$, given by,

$$\rho(\Delta f_\theta(t), \Delta\tilde{q}_{\theta'}(t)) = \sum_{\theta''=1}^{n} \frac{R_{\theta\theta''}}{(\sigma_A)_\theta} Y_{\theta''} \frac{\left(\Omega^{1/2}O^\top\right)_{\theta'\theta''}}{\sqrt{\Omega_{\theta'\theta'}}}, \tag{E.42}$$

is well-defined. We assume $Y = 1$, the unit vector. In the case $\psi \ll 1$, $(\sigma_A)_\theta = \sqrt{(\mathcal{M}^{-1}\mathcal{J}^2(\mathcal{M}^{-1})^\top)_{\theta\theta}}$ and $R_{\theta\theta'} = \left(\mathcal{M}^{-1}\mathcal{J}\right)_{\theta\theta'}$. Equation (E.42) is then the canonical inner product of two normalized vectors of $\mathbb{R}^n$. Thus, the correlation $\rho(\Delta f_\theta(t), \Delta\tilde{q}_{\theta'}(t))$ is well defined.

In the case $\psi \gg 1$, one can express the numerator and the denominator in Eq. (E.42) using the inner product (E.3) on the space of integrable real-valued functions on $[0, \pi]$. For $(\theta, \theta') \in [\![1, n]\!]^2$, having noted that $(\sqrt{2}\cos\xi\theta, \sqrt{2}\cos\xi\theta') = \delta_{\theta\theta'}$, we have

$$\begin{aligned}\sum_{\theta''=1}^{n} (R)_{\theta\theta''} \left(\Omega^{1/2}O\right)_{\theta'\theta''} &= \sum_{\theta''=1}^{n} (\mathcal{D}_1)_{\theta\theta''} \left(\Omega^{1/2}O\right)_{\theta'\theta''} \\ &= \left(\frac{\sqrt{2}\cos\xi\theta}{L_d(\xi)}, \sqrt{2}\sum_{\theta''=1}^{n} \cos\xi\theta'' \left(\Omega^{1/2}O\right)_{\theta'\theta''}\right), \end{aligned} \tag{E.43}$$

and,

$$
\begin{aligned}
(\sigma_A)_\theta \Omega_{\theta'\theta'} &= (\mathcal{D}_2)_{\theta\theta} \Omega_{\theta'\theta'} \\
&= \left( \frac{\sqrt{2}\cos\xi\theta}{L_d(\xi)}, \frac{\sqrt{2}\cos\xi\theta}{L_d(\xi)} \right) \\
&\times \left( \sqrt{2} \sum_{\theta''=1}^{n} \cos\xi\theta'' \left( \Omega^{1/2} O \right)_{\theta'\theta''}, \sqrt{2} \sum_{\theta''=1}^{n} \cos\xi\theta'' \left( \Omega^{1/2} O \right)_{\theta'\theta''} \right).
\end{aligned} \tag{E.44}
$$

Thus, Cauchy-Schwarz's inequality ensures

$$
-1 \leq \frac{\sum_{\theta''=1}^{n} (\mathcal{D}_1)_{\theta\theta''} \left( \Omega^{1/2} O \right)_{\theta'\theta''}}{\sqrt{(\mathcal{D}_2)_{\theta\theta} \Omega_{\theta'\theta'}}} \leq 1. \tag{E.45}
$$

ECOLE
DOCTORALE

**Titre :** Modelisation microscopique de la courbe de taux

**Mots clés :** Théorie de champ, Microstructure de marché, Economie monetaire, Courbe de taux, Modèle d'agents, Science des réseaux

**Résumé :** La théorie macroéconomique relie la croissance de la production aux anticipations sur les taux à court terme. Ainsi, les premiers modèles de taux définissent le taux à long terme comme la moyenne des taux courts, mais les preuves empiriques montrent qu'ils sont généralement plus élevés et nécessitent l'introduction de mesures de probabilité complexes. Cette thèse utilise des modèles d'agent et de physique statistique pour développer une théorie des taux d'intérêt, se focalisant sur la fixation des prix par les banques en fonction de leurs instruments de couvertures des taux à long terme et de leurs coûts de financement à court terme sur le marché des repos.
Depuis la crise de 2008, les marchés monétaires ont subi des changements réglementaires majeurs, entraînant des excédents de réserves et un recours accru aux repos. Nous proposons un modèle minimal du réseau interbancaire des repos, montrant que l'excès de liquidité et la réutilisation des collatéraux sont des réponses aux contraintes réglementaires et aux chocs de paiement. Ce modèle apparaît comme un outil utile de stress test et de politique monétaire.
Nous explorons aussi la courbe des taux d'intérêt à terme (FRC), montrant comment la pression sur un actif affecte les prix des autres. Nous revisitons un modèle décrivant la FRC comme une corde élastique où les chocs se propagent, reproduisant avec précision sa structure de corrélation et la perception du temps sur les marchés. Le modèle permet aussi de reproduire l'impact des volumes échangés sur les prix d'autres actifs.

**Title :** Microscopic modeling of the yield curve

**Keywords :** Field theory, Market microstructure, Monetary economics, Interest rate curve, Agent-based model, Network science

**Abstract :** Macroeconomic theory links output growth to expectations about short-term interest rates. Thus, the early interest rate models define the long-term rate as the average of short-term rates, but empirical evidence shows that they are generally higher and require the introduction of complex probability measures. This thesis uses agent-based modeling to develop a theory of interest rates, focusing on how banks set prices, considering their hedging via forward rate contracts, and their liquidity costs in the repo market.
Following the 2008 financial crisis, money markets saw significant regulatory changes, leading to excess reserves and increased reliance on repos. We propose a minimal model of the repo interbank network, finding that excess liquidity and collateral re-use emerge as responses to regulatory constraints and payment shocks. The model appears to be a useful tool for stress testing and monetary policy design.
To model the forward interest rate curve (FRC), we explore how trading pressure on one asset affects another, showing endogenous price formation within liquid assets influencing less liquid ones. We then revise a model depicting the FRC as an elastic string where shocks propagate, accurately portraying its correlation structure and time perception in markets. The model also handles price and cross-impact, fitting prices to order flows with high accuracy.

**Institut Polytechnique de Paris**
91120 Palaiseau, France